

University of Alberta

A Role for Pom121 in Linking the Nuclear Pore Complex Membrane Scaffold to the
Pore Membrane Domain

by

Jana Marie Mitchell

A thesis submitted to the Faculty of Graduate Studies and Research
in partial fulfillment of the requirements for the degree of

Doctor of Philosophy

Department of Cell Biology

© Jana Marie Mitchell

Fall 2013

Edmonton, Alberta

Permission is hereby granted to the University of Alberta Libraries to reproduce single copies of this thesis and to lend or sell such copies for private, scholarly or scientific research purposes only. Where the thesis is converted to, or otherwise made available in digital form, the University of Alberta will advise potential users of the thesis of these terms.

The author reserves all other publication and other rights in association with the copyright in the thesis and, except as herein before provided, neither the thesis nor any substantial portion thereof may be printed or otherwise reproduced in any material form whatsoever without the author's prior written permission.

DEDICATION

For my parents.

ABSTRACT

A key step in the evolutionary progression from prokaryote to eukaryote was development of the endomembrane system, including encapsulation of genetic material by the impermeable nuclear envelope (NE). Trafficking of macromolecules between cytoplasmic and nuclear compartments required the concomitant evolution of nuclear pore complexes (NPCs), sophisticated transport channels embedded within the NE. NPCs are comprised of a highly specialized subset of proteins termed nucleoporins (Nups). Nups that localize to the pore membrane domain (POM) of the NE stabilize membrane curvature resulting from circumferential fusion of NE membrane leaflets to form the pore in which the NPC resides. The architecture of the membrane-scaffolding NPC coat, and importantly, how this coat interfaces the POM, is unknown. We examined the interactions between NPC scaffold proteins Nup155 and Nup160 with the POM. We show that depletion of Nup155 causes alterations in NE structure, including a dramatic decrease in NPC numbers. We describe novel interactions between β -propeller domains of Nup155 and Nup160 with the transmembrane Nup (Pom) Pom121, and suggest that these interactions are critical for NPC assembly.

To better define a role for scaffold Nups in NPC structural organization, we focused on determining atomic structures of Nups comprising the conserved Nup107-160 scaffold complex. We present the crystal structure of the *Schizosaccharomyces pombe* (Sp) Nup120¹⁻⁹⁵⁰-Nup37 heterodimer (orthologous to metazoan Nup160 and Nup37), and demonstrate that capture of Nup37 within the

scaffold coat co-evolved with the acquisition of an α -helical domain within the β -propeller of Nup160 orthologues. We demonstrated that this interaction is conserved in metazoan cells, and extended our analysis to investigate the association of additional scaffold β -propellers with Pom121. We uncovered novel interactions between Pom121 with Nup37 and Nup43, expanding the Pom121 interactome to include four β -propeller proteins of the NPC membrane coat. We envisage a model whereby Pom121 extends from the NE towards the NPC central channel, linking structural modules of the NPC through interactions with β -propeller domains of Nup37, Nup43, Nup155 and Nup160. These interactions are likely regulated during NPC assembly, and plasticity of the Pom121 interactome may facilitate the reversible dilation of the NPC transport channel in response to cellular metabolic demands.

TABLE OF CONTENT

CHAPTER I: INTRODUCTION	1
1.1 PREFACE	2
1.2 THE NUCLEAR ENVELOPE	3
1.2.1 INM PROTEINS	4
1.3 NUCLEAR PORE COMPLEXES	6
1.3.1 NUCLEOPORINS	9
1.3.1.1 <i>Core and Adaptor Scaffold Nucleoporins</i>	12
1.3.1.2 <i>Pore Membrane Proteins</i>	14
1.3.1.3 <i>FG-Repeat Nucleoporins</i>	16
1.3.2 NUCLEOCYTOPLASMIC TRANSPORT	18
1.3.2.1 <i>NTRs and Signal Sequences</i>	20
1.3.2.2 <i>Directionality of Transport</i>	23
1.4 THE STRUCTURE OF THE NUCLEAR PORE COMPLEX	26
1.4.1 NPC ARCHITECTURE REVEALED BY CRYO-ELECTRON TOMOGRAPHY	27
1.4.2 ATOMIC RESOLUTION OF NUCLEOPORINS OF THE NPC SYMMETRIC CORE	33
1.4.2.1 <i>Atomic Structures of Central Channel Nucleoporins and Model for the Dilatable Midplane Ring</i>	34
1.4.2.2 <i>Modularity of the Core Scaffold Revealed by Electron Microscopy</i>	37
1.4.2.3 <i>Atomic Structures of Core Scaffold Nucleoporins</i>	39
1.4.2.4 <i>Atomic Structures of Adaptor Scaffold Nucleoporins</i>	45
1.4.3 MODELS FOR THE NPC MEMBRANE COAT	47
1.4.3.1 <i>The 'Fence Post' Model of the Symmetric NPC Scaffold</i>	48
1.4.3.2 <i>The Lattice Model of the NPC Coat</i>	52
1.4.3.3 <i>The Computational Model of the NPC</i>	54
1.5 MECHANISMS OF NE/NPC ASSEMBLY	56
1.5.1 POST-MITOTIC NE/NPC ASSEMBLY DURING 'OPEN' MITOSIS	59
1.5.1.1 <i>NE Breakdown</i>	60
1.5.1.2 <i>Regulation of NEBD by Phosphorylation</i>	61
1.5.1.3 <i>Coordination of Post-Mitotic NE/NPC Assembly</i>	63
1.5.1.4 <i>Kinetics of Nup Recruitment to the Chromatin Surface</i>	64
1.5.1.5 <i>Models of Post-Mitotic NPC Assembly: Insertion versus Enclosure</i>	67
1.5.1.6 <i>A NE Assembly 'Checkpoint' Coordinates NPC and NE Assembly</i>	71

1.5.2	NE/NPC ASSEMBLY DURING INTERPHASE	73
1.6	THESIS FOCUS	78
CHAPTER II: EXPERIMENTAL PROCEDURES		80
<hr/>		
2.1	PLASMID CONSTRUCTION	81
2.2	PURIFICATION OF RECOMBINANT PROTEINS FROM <i>E. COLI</i>	83
2.2.1	GENERATION OF ANTI-NUP ANTIBODIES	84
2.3	SUBFRACTIONATION AND EXTRACTION OF NUCLEAR ENVELOPES	85
2.4	GST-PULLDOWN ASSAYS FROM ISOLATED NE	86
2.5	DIRECT <i>IN VITRO</i> BINDING EXPERIMENTS	87
2.6	RNA INTERFERENCE	87
2.7	WESTERN BLOTTING	89
2.7.1	SAMPLE PREPARATION	89
2.7.2	ANTIBODIES	89
2.8	IMMUNOFLUORESCENCE, IMAGE ACQUISITION, AND IMAGE PROCESSING	90
2.9	TRANSMISSION ELECTRON MICROSCOPY	92
2.10	MASS SPECTROMETRY	93
2.11	PURIFICATION OF RECOMBINANT PROTEINS FROM INSECT CELLS IN LARGE SCALE	93
2.11.1	GENERATING RECOMBINANT BACMIDS	93
2.11.2	GENERATING RECOMBINANT BACULOVIRUS	94
2.11.3	PROTEIN EXPRESSION AND PURIFICATION	95
2.11.4	AFFINITY CHROMATOGRAPHY	95
2.11.4.1	<i>Anion Exchange Chromatography</i>	96
2.11.4.2	<i>Gel Filtration Analysis</i>	97
2.12	CRYSTALLIZATION CONDITIONS	97
2.13	UV MICROSCOPY	98
2.14	STRUCTURE DETERMINATION	99

CHAPTER III: POM121 LINKS TWO ESSENTIAL SUBCOMPLEXES OF THE NUCLEAR PORE COMPLEX CORE TO THE MEMBRANE	101
<hr/>	
3.1 OVERVIEW	102
3.2 RESULTS	104
3.2.1 LOSS OF MAMMALIAN NUP155 ALTERS NUCLEAR ENVELOPE STRUCTURE	104
3.2.2 NUP155 IS ANCHORED TO THE PORE MEMBRANE BY POM121 AND NDC1	113
3.2.3 POM121 DIRECTLY INTERACTS WITH NUP160 AND NUP98	118
3.2.4 PREDICTED β -PROPELLER DOMAINS OF NUP155 AND NUP160 BIND POM121	124
3.3 DISCUSSION	128
3.3.1 NUP155 IS ESSENTIAL FOR MAMMALIAN NPC ASSEMBLY AND NUCLEAR MORPHOLOGY	130
3.3.2 THE β -PROPELLER REGIONS OF NUP155 AND NUP160 BIND DIRECTLY TO POM121	132
3.3.3 IMPLICATIONS FOR THE ROLE OF NUP155 AND NUP160 IN NPC ASSEMBLY	138
CHAPTER IV: STRUCTURAL EVOLUTION OF THE MEMBRANE COATING MODULE OF THE NUCLEAR PORE COMPLEX	143
<hr/>	
4.1 OVERVIEW	144
4.2 RESULTS	146
4.2.1 NUP37 BINDS TO NUP120 DIRECTLY	146
4.2.2 STRUCTURE DETERMINATION	146
4.2.3 NON-LIGANDED NUP37 STRUCTURE	148
4.2.4 OVERALL STRUCTURE OF THE NUP120 ¹⁻⁹⁵⁰ -NUP37 COMPLEX	151
4.2.5 NUP120 ¹⁻⁹⁵⁰ STRUCTURE	154
4.2.6 STRUCTURE OF NUP120-BOUND NUP37	160
4.2.7 NUP120-NUP37 INTERFACE	160
4.2.8 STRUCTURAL COMPARISON OF SP-NUP120 AND SC-NUP120	165
4.3 DISCUSSION	169

**CHAPTER V: BIOCHEMICAL ANALYSES OF INTERACTIONS
BETWEEN THE NPC CORE SCAFFOLD AND PORE MEMBRANE
DOMAIN 172**

5.1	OVERVIEW	173
5.2	RESULTS	175
5.2.1	BIOCHEMICAL CHARACTERIZATION OF NUP160 AND NUP37 INTERACTIONS	175
5.2.1.1	<i>Purification of Nup37</i>	175
5.2.1.2	<i>Purification of Fragments of Nup160</i>	178
5.2.1.3	<i>Nup160¹⁻⁵⁸³ does not directly interact with Nup37</i>	183
5.2.1.4	<i>Nup160³⁷⁻⁹⁵³ interacts directly with Nup37</i>	188
5.2.2	BIOCHEMICAL CHARACTERIZATION OF POM121 INTERACTIONS WITH β - PROPELLER PROTEINS OF THE NPC CORE SCAFFOLD	192
5.2.2.1	<i>Purification of Pom121²¹⁵⁻⁵⁵⁷</i>	192
5.2.2.2	<i>Purification of Complexes of Nup160¹⁻⁵⁸³-Pom121²¹⁵⁻⁵⁵⁷</i>	195
5.2.2.3	<i>Pom121²¹⁵⁻⁵⁵⁷ interacts with the β-propeller proteins Nup37 and Nup43</i>	201
5.3	DISCUSSION	204
5.3.1	THE INTERACTION BETWEEN NUP37 AND NUP160 IS CONSERVED IN METAZOAN CELLS	205
5.3.2	INTERACTIONS BETWEEN POM121 AND β -PROPELLERS LINK THE CORE SCAFFOLD TO THE POM	206
5.3.3	CONSEQUENCES OF THE UNSTRUCTURED NATURE OF POM121 ²¹⁵⁻⁵⁵⁷	208
CHAPTER VI: PERSPECTIVES		211
6.1	SYNOPSIS	212
6.2	CONSERVATION OF THE NPC-POM INTERFACE	212
6.3	CHARACTERIZING THE POM121 INTERACTOME	218
6.4	DEFINING A ROLE FOR POM121 IN NE AND NPC ASSEMBLY	221
CHAPTER VII: REFERENCES		224

LIST OF TABLES

TABLE 1-1	LIST OF NUCLEOPORIN ORTHOLOGUES ACROSS SPECIES.	11
TABLE 2-1	TABLE OF CONSTRUCTS FOR EXPRESSION IN <i>E. COLI</i> .	82
TABLE 2-2	TABLE OF CONSTRUCTS FOR EXPRESSION IN HIGH FIVE™ CELLS.	83
TABLE 2-3	TABLE OF OLIGONUCLEOTIDES USED FOR RNA INTERFERENCE.	88
TABLE 4-1	STATISTICS FROM CRYSTALLOGRAPHIC ANALYSIS.	149

LIST OF FIGURES

FIGURE 1-1	THE PROTO-COATOMER MODEL FOR THE EVOLUTION OF COATED VESICLES AND NUCLEAR PORE COMPLEXES.	8
FIGURE 1-2	MODEL OF THE HYPOTHETICAL ARRANGEMENT OF NUP SUBCOMPLEXES WITHIN THE METAZOAN NPC.	10
FIGURE 1-3	ATOMIC STRUCTURES OF KARYOPHERIN- β COMPLEXES.	22
FIGURE 1-4	MODEL FOR KARYOPHERIN-MEDIATED NUCLEOCYTOPLASMIC TRANSPORT.	24
FIGURE 1-5	ARCHITECTURE OF THE NPC FROM <i>D. DISCOIDEUM</i> , <i>X. LAEVIS</i> AND <i>H. SAPIENS</i> REVEALED BY CRYO-ELECTRON TOMOGRAPHY.	30
FIGURE 1-6	MODEL FOR THE 'RING-CYCLE' FOR DILATING AND CONSTRICTING THE NPC CENTRAL CHANNEL.	35
FIGURE 1-7	THREE-DIMENSIONAL CHARACTERIZATION OF THE HEPTAMERIC YEAST NUP84P COMPLEX BY ELECTRON MICROSCOPY.	38
FIGURE 1-8	CRYSTAL STRUCTURES OF CORE- AND ADAPTOR-SCAFFOLD NUCLEOPORINS.	40
FIGURE 1-9	MODEL OF THE 'FENCE POST' COAT FOR THE NUCLEAR PORE MEMBRANE.	50
FIGURE 1-10	'LATTICE' AND 'COMPUTATIONAL' MODELS OF THE SYMMETRIC NUCLEAR PORE COMPLEX CORE.	53
FIGURE 1-11	NUCLEAR ENVELOPE BREAKDOWN AND REASSEMBLY DURING MITOSIS IN METAZOAN CELLS.	58
FIGURE 1-12	POTENTIAL MECHANISMS OF NE/NPC ASSEMBLY POST-MITOSIS.	65
FIGURE 3-1	MULTIPLE siRNAs TARGETING DISTINCT REGIONS OF NUP155 mRNA EFFICIENTLY DEplete NUP155 AND SIMILARLY ALTER NUCLEAR MORPHOLOGY.	105
FIGURE 3-2	DEPLETION OF NUP155 ALTERS NUCLEAR MORPHOLOGY AND DECREASES NPC NUMBER.	106
FIGURE 3-3	DEPLETION OF NUP155 IN HELa CELLS LEADS TO THE MISLOCALIZATION OF NUCLEOPORINS.	109
FIGURE 3-4	NUP155 DEPLETION ALTERS TARGETING OF INM PROTEINS.	111
FIGURE 3-5	DEPLETION OF NUP155 AFFECTS THE TARGETING OF LAP2 TO THE INM.	112
FIGURE 3-6	IDENTIFICATION OF NUP155-INTERACTING PROTEINS.	114
FIGURE 3-7	BIOCHEMICAL CHARACTERIZATION OF RECOMBINANT FRAGMENTS OF POM121.	116
FIGURE 3-8	NUP155 INTERACTS DIRECTLY WITH PORE MEMBRANE PROTEINS POM121 AND NDC1.	117
FIGURE 3-9	DEPLETION OF POM121 REDUCES CELLULAR LEVELS OF NUP155.	119
FIGURE 3-10	POM121 INTERACTS WITH NUP155 AND THE NUP107-160 COMPLEX <i>IN VITRO</i> .	120
FIGURE 3-11	POM121-INTERACTING NUPS IDENTIFIED BY MASS SPECTROMETRY.	122

FIGURE 3-12	IDENTIFICATION OF NUPS THAT BIND NUP160 AND NUP98.	123
FIGURE 3-13	POM121 INTERACTS DIRECTLY N-TERMINAL DOMAINS OF NUP155 AND NUP160.	125
FIGURE 3-14	POM121 ²¹⁵⁻⁵⁵⁷ INTERACTS DIRECTLY WITH NUP98, BUT NOT SEH1 OR SEC31.	127
FIGURE 3-15	BINDING OF NUP155 TO POM121 PREVENTS THEIR INTERACTION WITH NUP160.	129
FIGURE 3-16	MODEL OF DIRECT AND INDIRECT INTERACTIONS IDENTIFIED IN THIS STUDY.	133
FIGURE 3-17	POM152P ¹⁻¹¹¹ INTERACTS WITH NUP155 AND THE NUP107-160 COMPLEX.	134
FIGURE 4-1	NUP120 OF <i>S. POMBE</i> (SP), BUT NOT OF <i>S. CEREVISIAE</i> (SC), DIMERIZES WITH NUP37.	147
FIGURE 4-2	EXPERIMENTAL PHASING.	150
FIGURE 4-3	BICYCLE-LIKE STRUCTURE OF THE NUP120 ¹⁻⁹⁵⁰ -NUP37 COMPLEX.	153
FIGURE 4-4	HELIX H2 OF 1E-1A INTERACTS WITH HELICES H6, H7, AND H9 OF THE 6D-7A INSERT OF SP-NUP120 ¹⁻⁹⁵⁰ .	156
FIGURE 4-5	BACK VIEW OF THE NUP120 ¹⁻⁹⁵⁰ -NUP37 COMPLEX.	157
FIGURE 4-6	STRUCTURAL COMPARISON OF SP-NUP120 ¹⁻⁹⁵⁰ AND SC-NUP120 ¹⁻⁷²⁹ .	159
FIGURE 4-7	STRUCTURAL COMPARISON OF THE NONLIGANDED AND NUP120-BOUND FORMS OF NUP37.	161
FIGURE 4-8	DETAILED ANALYSES OF THE NUP120 ¹⁻⁹⁵⁰ -NUP37 INTERACTOME.	162
FIGURE 4-9	SURFACE PROPERTIES OF THE NUP120 ¹⁻⁹⁵⁰ -NUP37 INTERFACE.	164
FIGURE 4-10	SUPERIMPOSED STRUCTURES OF SP-NUP120 ¹⁻⁹⁵⁰ -NUP37 AND SC-NUP120 ¹⁻⁷²⁹ .	167
FIGURE 4-11	MULTIPLE SEQUENCE ALIGNMENT OF NUP120.	168
FIGURE 5-1	PURIFICATION OF HUMAN NUP37.	176
FIGURE 5-2	DESIGN AND EXPRESSION OF NUP160 TRUNCATIONS.	179
FIGURE 5-3	STRUCTURAL COMPARISON OF SP-NUP120 ¹⁻⁹⁵⁰ AND HS-NUP160 ³⁷⁻⁹⁵³ .	182
FIGURE 5-4	PURIFICATION OF NUP160 ¹⁻⁵⁸³ .	184
FIGURE 5-5	NUP37 AND NUP160 ¹⁻⁵⁸³ DO NOT INTERACT DIRECTLY.	185
FIGURE 5-6	THE NUP160 NTE IS UNIQUE TO <i>H. SAPIENS</i> .	187
FIGURE 5-7	PURIFICATION OF NUP160 ³⁷⁻⁹⁵³ -NUP37.	189
FIGURE 5-8	CRYSTALS OF THE NUP160 ³⁷⁻⁹⁵³ -NUP37 COMPLEX.	191
FIGURE 5-9	PURIFICATION OF POM121 ²¹⁵⁻⁵⁵⁷ .	194
FIGURE 5-10	SECONDARY STRUCTURE PREDICTIONS FOR POM121 ²¹⁵⁻⁵⁵⁷ .	196
FIGURE 5-11	POM121 ²¹⁵⁻⁵⁵⁷ INTERACTS DIRECTLY WITH NUP160 ¹⁻⁵⁸³ .	198
FIGURE 5-12	MAPPING THE NUP160 BINDING DOMAIN OF POM121.	200
FIGURE 5-13	POM121 ²¹⁵⁻⁵⁵⁷ INTERACTS DIRECTLY WITH THE β -PROPELLERS OF NUP160, NUP37 AND NUP43.	203

FIGURE 6-1	MODEL FOR THE CONSERVATION OF THE NPC-POM INTERFACE IN YEAST AND METAZOA.	215
FIGURE 6-2	SECONDARY STRUCTURE PREDICTIONS FOR POM152P ¹⁻¹¹¹ .	219

LIST OF NOMENCLATURE AND ABBREVIATIONS

~	approximately
2D	two-dimensional
3D	three-dimensional
Å	angstrom
A-T	ataxia-telangiectasia
aa	amino acid residues
ACE1	ancestral coatomer element 1
ADLD	autosomal dominant leukodystrophy
ALPS	ArfGAP1 lipid packing sensor
BAF	barrier to autointegration factor
BC	lower cavity
bp	base pair
C	carboxy
CB	Coomassie blue
COP	coat protein
CPC	coat protein complex
CR	cytoplasmic ring
Cryo-ET	cryo-electron tomography
CTD	carboxy terminal domain
d	day
DIM	domain invasion motif
DNA	deoxyribonucleic acid
DNase	deoxyribonuclease
DTT	dithiothreitol
ECL	enhanced chemiluminescence
EDMD	Emery–Dreifuss muscular dystrophy
EM	electron microscopy
ER	endoplasmic reticulum
FG	phenylalanine glycine
FRAP	fluorescence recovery after photobleaching
g	gram
<i>g</i>	gravitational force
GDP	guanosine diphosphate
GSH	Glutathione
GST	glutathione-S-transferase
GTP	guanosine triphosphate
h	hour
HEAT	Huntingtin, EF3, PP2A, TOR1
HEZ	heterochromatin exclusion zone
HGPS	Hutchinson–Gilford progeria syndrome
HP1	heterochromatin protein 1
HRP	horseradish peroxidase
Hs	Homo sapiens
IBB	importin β binding
INM	inner nuclear membrane
IPTG	Isopropyl β -D-1-thiogalactopyranoside
Kap	karyopherin
KASH	Klarsicht, ANC-1, Syne Homology
kDa	kilodalton
Lap	lamina associated polypeptide
LBE	lamin B receptor
LEM	Lap2, Emerin and MAN1

LINC	linker of nucleoskeleton and cytoskeleton
LR	luminal ring
M	Molar, mega
MDa	megadalton
mg	milligram
min	minute
µg	microgram
µl	microliter
µm	micron
mRNA	messenger ribonucleic acid
mRNP	messenger ribonucleoprotein
MS	mass spectrometry
N	amino
n	nano
NE	nuclear envelope
NEBD	nuclear envelope breakdown
NET	nuclear envelope transmembrane protein
NLS	nuclear localization signal
nm	nanometer
NPC	nuclear pore complex
NR	nucleoplasmic ring
NSF	NEM-sensitive factor
nt	nucleotide
NTD	amino terminal domain
NTE	amino terminal extension
OD	optical density
NTR	nuclear transport receptor
ONM	outer nuclear membrane
ORF	open reading frame
PCR	polymerase chain reaction
PDB	protein data bank
pH	-log[H ⁺]
PMSF	phenylmethyl sulfonyl fluoride
Pom	pore membrane protein
POM	pore membrane domain
RanGAP	Ran GTPase activating protein
RanGEF	Ran guanine nucleotide exchange factor
RLNE	rat liver nuclear envelopes
RNA	Ribonucleic acid
RNAi	RNA interference
RNase	ribonuclease
RRM	RNA recognition motif
RT-PCR	reverse transcription polymerase chain reaction
SAD	single anomalous dispersion
Sc	Saccharomyces cerevisiae
SDS-PAGE	sodium dodecyl sulfate polyacrylamide gel electrophoresis
siRNA	small interfering RNA
SNARE	SNAP (Soluble NSF Attachment Protein) Receptor
Sp	Schizosaccharomyces pombe
SR	spoke ring
SS	silver stain
SUMO	small Ubiquitin-like Modifier
SUN	Sad1p, UNC-84
TCA	trichloroacetic acid
TCA	triethanolamine

TEM..... transmission electron microscopy
tRNA..... transfer ribonucleic acid
UC..... upper cavity
WB..... western blot
WD..... tryptophan-aspartic acid
WGA..... wheat germ agglutinin

CHAPTER I: INTRODUCTION

1.1 PREFACE

Nuclear pore complexes (NPCs) act as gateways that regulate the transport of macromolecules across the nuclear envelope (NE). Coupled with soluble nuclear transport receptors (NTRs), NPCs provide the sole means of communication across the otherwise impermeable nuclear envelope (NE). In addition to regulating trafficking between cytoplasmic and nuclear compartments, NPCs are positioned within the cell to participate in a myriad of essential activities, including the regulation of mitosis, gene expression, and organization of the genome (Wozniak et al., 2010; Liang and Hetzer, 2011; Van de Vosse et al., 2011). Deciphering how NPCs efficiently mediate the specific trafficking of molecules between cellular compartments, in conjunction with regulating chromatin dynamics, requires a more detailed understanding of the structural modules that comprise this sophisticated supramolecular machine.

A subset of proteins that comprise the NPC, termed nucleoporins (Nups), are specialized in stabilizing the highly curved NE membrane in the vicinity of the NPC. These Nups mimic the tertiary structure of proteins that comprise the membrane scaffolding coats of COPI, COPII and clathrin coated vesicles (Devos et al., 2004). The oligomerization of scaffold Nups into higher-order assemblies is not well understood at this time. Elucidating the molecular architecture of the NPC and understanding how Nups interface with critical effectors of associated molecular pathways will undoubtedly shed light on mechanisms of numerous cellular processes and provide key

insight into the pathophysiological progression of disease states influenced by NPC-associated processes (Liang and Hetzer, 2011). An improved understanding of the communication between NPCs and the cellular processes they influence has the potential to transform the approach to diverse areas of biomedical research, including cancer, aging, and regenerative medicine.

1.2 THE NUCLEAR ENVELOPE

The morphologically most striking change during the prokaryote-eukaryote transition of cellular evolution is the encapsulation of chromatin by a continuous double-phospholipid bilayer, resulting in the compartmentalization of DNA by the selectively permeable nuclear envelope (NE) (Blobel, 1980; Lopez-Garcia and Moreira, 1999; Dacks and Field, 2007). The surface of the NE is fenestrated by aqueous channels, formed by the fusion of outer nuclear membrane (ONM) and inner nuclear membrane (INM) leaflets (for review, see Hetzer, 2010). Within these channels reside large proteinaceous supramolecular machines termed nuclear pore complexes (NPCs), which regulate the highly selective trafficking of molecules across the otherwise impermeable NE. By physically separating, both spatially and temporarily, the unique metabolic activities of the cytoplasmic and nuclear cellular compartments, eukaryotic cells have evolved a complexity in the regulation of gene expression not achieved by prokaryotes.

Underlying the NE of metazoan cells is an intricate network of nucleus-specific filament proteins termed lamins, which collectively form the nuclear lamina. The lamina provides resistance to mechanical stress and, importantly, attachment sites for underlying chromatin (for review, see Zuleger et al., 2011; Burke and Stewart, 2012). Accordingly, lamins have been implicated in the maintenance of genomic stability, regulation of DNA damage repair, gene expression, differentiation, proliferation, and senescence. Mutations in the genes encoding lamins results in a range of disease phenotypes, including adult-onset autosomal dominant leukodystrophy (ADLD), ataxia-telangiectasia (A-T), Emery - Dreifuss muscular dystrophy (EDMD), and Hutchinson-Gilford progeria syndrome (HGPS). Furthermore, mutations in NPC components exhibit tissue-specific disease phenotypes, highlighting the critical role of the NE in the regulation of nuclear metabolism and maintenance of normal cellular physiology (for review, see Zuleger et al., 2011; Gomez-Cavazos and Hetzer, 2012).

1.2.1 INM PROTEINS

Whereas the ONM is continuous with and, therefore, biochemically and functionally similar to the endoplasmic reticulum (ER), the INM is characterized by a distinct set of integral INM proteins (alternatively referred to as nuclear envelope transmembrane (NETs) proteins) (for review, see Zuleger et al., 2011). Many of these proteins act as adaptors that establish

direct connections between the INM and underlying chromatin. While INM proteins freely diffuse throughout the ER and ONM following translation, once imported into the nucleus they are anchored in place by nucleoplasmic domains that facilitate attachment to chromatin (Burke and Ellenberg, 2002). For example, the well-characterized LEM domain (found in Lap2, Emerin, and MAN1 INM proteins) is capable of interacting with chromatin-associated barrier-to-autointegration factor (BAF), or with DNA directly (Cai et al., 2001). Large-scale proteomic analyses have uncovered numerous, previously uncharacterized transmembrane proteins specific to the INM, many of which are predicted to be able to directly bind DNA (Schirmer et al., 2003; Schirmer and Gerace, 2005; Ulbert et al., 2006b). How these novel INM proteins influence genome maintenance and expression is currently unknown, however, it has been demonstrated that ~30% map to chromosomal regions associated with 18 different human dystrophies (Schirmer et al., 2003; Schirmer and Gerace, 2005).

In addition to binding chromatin, INM proteins are intimately linked to the actin cytoskeleton by the establishment of LINC (linker of nucleoskeleton and cytoskeleton) complexes (Crisp et al., 2006; Haque et al., 2010; Rothballer et al., 2013). LINC complexes are formed by interactions between proteins containing SUN- and KASH-domains. SUN proteins are an evolutionarily conserved family of INM proteins, including SUN1, which interact directly with underlying nuclear lamina, chromatin, and DNA. These proteins traverse the luminal space of the NE where they interact with KASH

domains of proteins specific to the ONM, termed nesprins. Through the actin filament binding ability of nesprins, LINC complexes form molecular 'bridges' between cytoskeletal and nucleoskeletal networks. In this way, LINC complexes not only contribute to the mechano-structural functions of the NE, but also provide a unique link between signaling pathways in the cytoskeleton with gene regulation (for review, see Rothballer et al., 2013). Similar to proteins that compromise the nuclear lamina, components of LINC complexes, including SUN1, nesprins, and additional adaptor proteins have been linked to various dystrophies (Mejat and Misteli, 2010; Meinke et al., 2011). In summary, elucidating the complexity of the NE proteome has significant implications for human health and disease and is critical for understanding the mechanisms underlying disease pathologies.

1.3 NUCLEAR PORE COMPLEXES

NPCs are the sole means of transport of macromolecules across the NE. In addition to their roles in controlling transport, NPCs also influence gene expression, chromatin organization, chromosome inheritance, establishment of epigenetic maintenance, DNA repair, and cell cycle regulation (Therizols et al., 2006; Brickner et al., 2007; Capelson et al., 2010; Krull et al., 2010; Strambio-De-Castillia et al., 2010; Van de Vosse et al., 2011). While the double membrane of the NE was proposed to have evolved by an inward folding of chromatin-binding domains of the prokaryotic plasma membrane (the endomembrane hypothesis), the evolution of the NPC

was suggested to have begun by coating and stabilizing the loose and sharply bent ends of the infolded membrane cisternae (the proto-coatomer hypothesis) (Figure 1-1) (Blobel, 1980; Devos et al., 2004; Mans et al., 2004). The concomitant evolution of mobile transport machinery to facilitate communication between the segregated nucleoplasm and cytoplasm then led to the contemporary multimodular NPC as the stationary centerpiece of nucleocytoplasmic transport.

Since its discovery more than half a century ago, the structure and function of the NPC has been extensively investigated (Callan and Tomlin, 1950; Grossman et al., 2012). Initial observations by electron microscopy (EM) revealed striking eightfold rotational symmetry and two-fold symmetry in the plane of the NE (Unwin and Milligan, 1982; Akey, 1989; Akey and Radermacher, 1993). Importantly, observations of NPC architectures from a variety of species indicate that the structure of the NPC is generally well-conserved (Maimon et al., 2012). Proteomic analyses have estimated the molecular mass of NPCs in yeast and metazoan cells to be 66MDa and 125 MDa, respectively, thus making the NPC one of the largest proteinaceous structures in the cell (Reichelt et al., 1990; Rout and Blobel, 1993; Devos et al., 2006). While accounting for discrepancies in mass estimation due to limitations and variation of purification methodologies used in individual studies, such a difference in size suggests that although the structure of the NPC is generally well-conserved, differences must exist across species in the

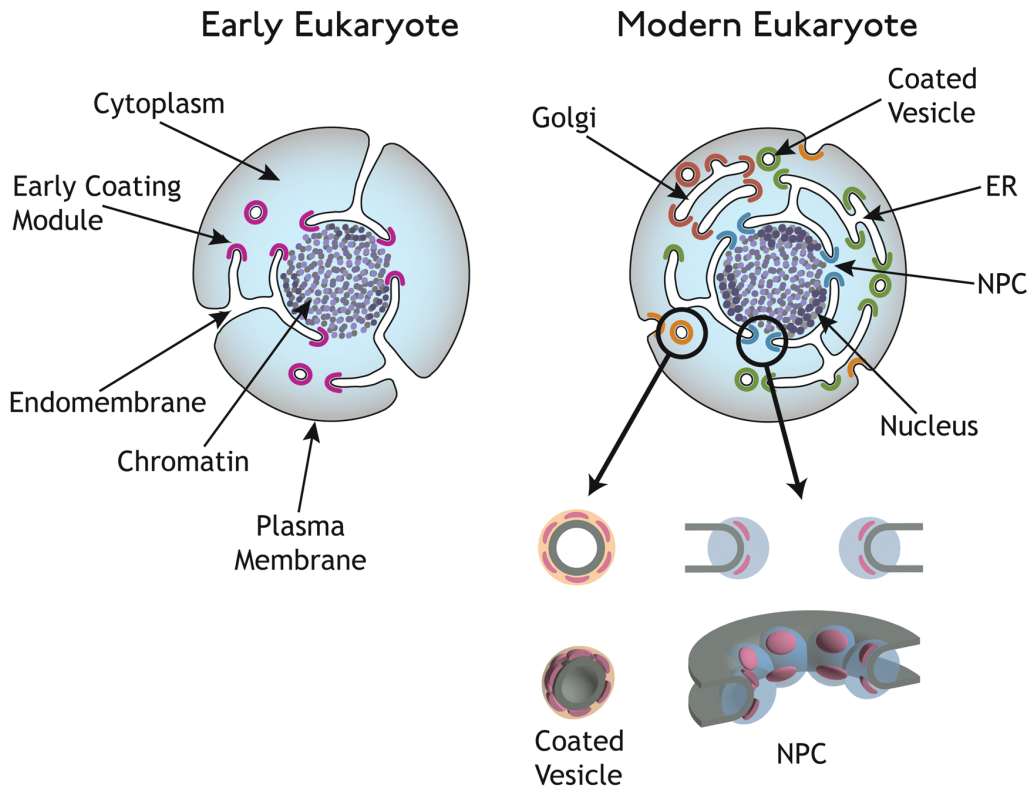


FIGURE 1-1 THE PROTO-COATOMER MODEL FOR THE EVOLUTION OF COATED VESICLES AND NUCLEAR PORE COMPLEXES.

The proto-coatomer hypothesis suggests that modern eukaryotes (right) acquired a membrane-curving protein module (purple, left) that allowed the evolution of an endomembrane system from a common eukaryotic ancestor (left) through the invagination of the plasma membrane. Over time, this protein module specialized to facilitate membrane curvature of structures involved in endocytosis (orange), ER and Golgi transport (green and brown), and NPC formation (blue). Numerous structural similarities exist between the membrane scaffolding modules of NPCs and coated vesicles (bottom right, pink), suggesting their evolution from a common eukaryotic ancestor. Adapted from Devos et al., 2004.

composition and arrangement of NPC component proteins (Grossman et al., 2012). Presumably, NPCs have been 'tailored' throughout evolution to accommodate the specific metabolic requirements of different cell types.

1.3.1 NUCLEOPORINS

The molecular components of NPCs are a generally conserved group of proteins termed nucleoporins or Nups (Figure 1-2, Table 1-1). Despite their immense molecular mass, proteomic analyses revealed that NPCs are comprised of only ~30 distinct Nups (Rout et al., 2000; Cronshaw et al., 2002). This is particularly intriguing in comparison to the mammalian ribosome, which, despite measuring only ~10% of the mass of the NPC, is assembled from ~80 distinct proteins (Wool et al., 1995). The complexity of the NPC is achieved by the repetition of each Nup in multiples of 8 copies, thus reflecting the high degree of overall internal symmetry. As a result, each NPC is a supramolecular assembly of ~500 proteins (Rout et al., 2000; Cronshaw et al., 2002; Alber et al., 2007b). Importantly, in proliferating cells of metazoa, the NPC is disassembled and rebuilt with every cell cycle. The efficient assembly of such an immense structure poses a unique challenge to the cell. The mechanisms orchestrating NPC assembly are currently unknown (Section 1.4).

Simplifying the mechanism of NPC assembly is the organization of Nups into discrete, biochemically distinct subcomplexes (2006; Tran and Wente, 2006; Hoelz et al., 2011; Grossman et al., 2012). These subcomplexes

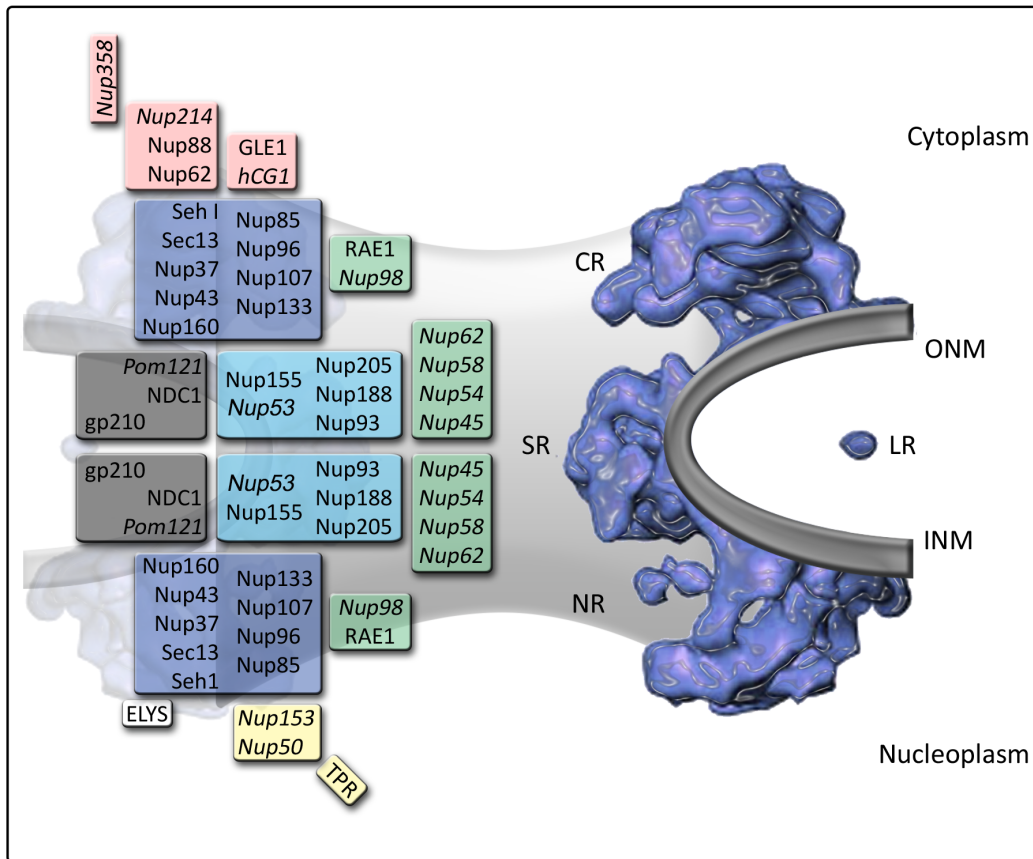


FIGURE 1-2 MODEL OF THE HYPOTHETICAL ARRANGEMENT OF NUP SUBCOMPLEXES WITHIN THE METAZOAN NPC.

Schematic representation of a cross-section of the metazoan NPC embedded in the nuclear envelope. Nups are indicated as components of distinct subcomplexes (left), and localized based on positional information obtained from immunofluorescence, electron microscopy, and biochemical analyses. Members of the core scaffold Nup107-160 complex are in purple, the adaptor scaffold Nup53-93 complex in blue, and barrier Nups in green. Asymmetrically localized Nups of the cytoplasmic filaments and nuclear basket are in orange and yellow, respectively. Nups that contain FG-repeats are italicized. The positions of various Nup subcomplexes mirror their potential positions within the structure of the Human NPC obtained by cryo-electron tomography (right). Positions of the cytoplasmic ring (CR), spoke ring (SR), nucleoplasmic ring (NR), luminal ring (LR), outer nuclear membrane (ONM) and inner nuclear membrane (INM) are indicated. Adapted from Maimon et al., 2012; Rothballer and Kutay, 2012a.

TABLE 1-1 LIST OF NUCLEOPORIN ORTHOLOGUES ACROSS SPECIES.

	<i>H. sapiens</i>	<i>D. melanogaster</i>	<i>C. elegans</i>	<i>S. pombe</i>	<i>S. cerevisiae</i>
Cytoplasmic Filaments	Nup358 (RanBP2)	Nup358	NPP-9	-	-
Cytoplasmic Ring and Associate factors	Nup214 (CAN)	Nup214	NPP-14	Nup146	Nup159p
	Nup88	Nup88	-	Nup82	Nup82p
	GLE1	GLE1	-	Gle1	Gle1p
	hCG1	CG18789	-	Amo1	Nup42p
Nup98 Complex	Nup98	Nup98	NPP-10N	Nup189N	Nup145N, Nup100, Nup116
	RAE1 (GLE2)	RAE1	NPP-17	Rae1	Gle2p
Channel Nups (Nup62 Complex)	Nup54	Nup54	NPP-1	Nup44	Nup57p
	Nup58				
	Nup45	Nup58	NPP-4	Nup45	Nup49p
	Nup62	Nup62	NPP-11	Nsp1	Nsp1p
Core Scaffold (Nup107-160 Complex)	Nup37	CG11875	-	Nup37	-
	Nup43	Nup43	C09G9.2	-	-
	Nup85	Nup75	NPP-2	Nup85	Nup85p
	Nup96	Nup96	NPP-10C	Nup189C	Nup145Cp
	Nup107	Nup107	NPP-5	Nup107	Nup84p
	Nup133	Nup133	NPP-15	Nup132, Nup131	Nup133p
	Nup160	Nup160	NPP-6	Nup120	Nup120p
	Sec13	Sec13	NPP-20	Sec13	Sec13p
SEH1	Nup44A	NPP-18	Seh1	Seh1p	
Adaptor Scaffold (Nup53-93 Complex)	Nup53 (Nup35)	CG6540	NPP-19	Nup40	Nup53p, Nup59p
	Nup93	CG7262	NPP-13	Nup97, Nup106	Nic96p
	Nup155	Nup154	NPP-8	SPAC890.06	Nup170p, Nup157p
	Nup188	CG8771	-	Nup184	Nup188p
	Nup205	CG11943	NPP-3	Nup186	Nup192p
Nucleoplasmic Ring and Associated Factors	Nup153	Nup153	NPP-7	Nup124	Nup1p
	Nup50	Nup50	NPP-16	Nup61	Nup2p
	-	-	-	Nup60	Nup60p
Nuclear Basket	TPR	Mtor	NPP-21	Nup211	Mlp1p, Mlp2p
Trnasmembrane Nups	Pom121	-	-	-	-
	NDC1	Ndc1	NPP-22	Cut11	Ndc1p
	GP210	Gp210	NPP-12	-	-
	TMEM33	Kr-h2	Y37D8A.17	Tts1	Pom33p
	-	-	-	Po152	Pom152p
	-	-	-	Mug31	Pom34p
Associated Nups	ELYS	Elys	MEL-28	-	-
	Centrin	CG174931, CG318021	R08D7.51	-	-
	Aladin	CG16892, CG13137	-	-	-

Adapted from Rothballer and Kutay 2012b.

are comprised of structurally related Nups that function as molecular building blocks, which, owing to its inherent symmetry, may be rapidly assembled to form the NPC. Based on the structural motifs they comprise, Nup subcomplexes are localized to specific domains to the NPC (for review, see Devos et al., 2006; Grossman et al., 2012). These domains are generally categorized as the pore membrane domain (POM) of the NE, the scaffold domain that stabilizes the POM, and the central channel that facilitates nuclear transport. Nups that comprise the POM contain transmembrane domains that presumably, through interactions with surrounding scaffold Nups, anchor the NPC within the NE (Devos et al., 2006). Nups that form the scaffold modules of the NPC are structurally specialized to stabilize the sharply curved NE membrane in the vicinity of the POM (Devos et al., 2004; Devos et al., 2006). Finally, Nups that line the NPC central channel are characterized by phenylalanine-glycine (FG) repeats that are critical for establishing the NPC permeability barrier (Finlay et al., 1991; Strawn et al., 2004; Wentz and Rout, 2010).

1.3.1.1 CORE AND ADAPTOR SCAFFOLD NUCLEOPORINS

The cylindrical core of the NPC forms the molecular framework on which the asymmetric and FG-Nups are organized. By analogy to their yeast counterparts, components of two conserved vertebrate subcomplexes, the Nup107–160 complex (containing Nup37, Nup43, Nup85, Nup96, Nup107, Nup133, Nup160, Sec13, and Seh1, termed Nup84p complex in yeast) and the

Nup53–Nup93 complex (including Nup53, Nup93, Nup155, Nup188, and Nup205), comprise the NPC symmetric core and adaptor scaffold, respectively (Figure 1-2)(Grandi et al., 1997; Belgareh et al., 2001; Loiodice et al., 2004; Hawryluk-Gara et al., 2005, for review see Hetzer and Wentz, 2009). The arrangement of Nups in the conserved Nup107-160 complex has been well defined (Section 1.3) (Lutzmann et al., 2002; Kampmann and Blobel, 2009). Importantly, Nup37 and Nup43 are evolutionarily recent additions to the Nup107-160 complex, such that they are absent from the budding yeast *S. cerevisiae* (Loiodice et al., 2004). Presumably, organisms acquired either one, or both while progressing towards more complexity (Table 1-1). For example, the fission yeast *S. pombe* acquired Nup37, but not Nup43. This has important implications for the assembly of the membrane-scaffolding coat and suggests that the oligomerization of orthologous Nup107-160 subcomplexes into the elaborate, lattice-like NPC membrane scaffold may differ across species (Chapter IV).

Among the core scaffold Nups, Nup155 and several members of the Nup107–160 complex are predicted to contain two distinct fold types, an N-terminal β -propeller and a C-terminal α -solenoid domain (Berke et al., 2004; Devos et al., 2004; Schwartz, 2005; Devos et al., 2006; Brohawn et al., 2008). This organization is analogous to the molecular architecture of coat protein complexes (CPCs) that stabilize the sharp, convex curvature of COPI-, COPII-, and clathrin-coated vesicles, and has led to the hypothesis that β -propeller/ α -solenoid Nups function similarly to induce curvature of the pore

membrane (Devos et al., 2004; Devos et al., 2006; Stagg et al., 2007; DeGrasse et al., 2009; for review see Onischenko and Weis, 2011). Importantly, both Sec13p and Seh1p are *bone fide* components of COPII coated vesicles, strengthening the idea that the Nup107-160 complex similarly assembles a membrane coat for the POM (Devos et al., 2004).

1.3.1.2 PORE MEMBRANE PROTEINS

Several Poms are associated with the NPC and are predicted to both contribute to the core scaffold as well as anchor it to the pore membrane. In vertebrates, three Poms have been identified: gp210, NDC1, and Pom121 (Gerace et al., 1982; Hallberg et al., 1993; Mansfeld et al., 2006; Stavru et al., 2006a). Gp210 contains a single transmembrane domain with a short N-terminal region extending into the pore and available to bind the core scaffold (Wozniak et al., 1989; Greber et al., 1990). Pom121 also contains a single transmembrane segment but has a much larger, ~120 kDa domain extending towards the NPC interior (Hallberg et al., 1993; Soderqvist and Hallberg, 1994). Finally, NDC1 is a multi-membrane spanning protein with an ~45 kDa C-terminal domain positioned within the pore (Lau et al., 2006; Mansfeld et al., 2006; Stavru et al., 2006a). Although these proteins are likely to play an important role in NPC structure, how they interact with other Nups is largely unknown (see Chapter III) (Table 1-1) (for review see Suntharalingam and Wentz, 2003). Recently, an additional potential Pom has been identified in yeast, termed Pom33p (Chadrin et al., 2010). Unlike other

Poms characterized, a pool of Pom33p localizes to the ER in addition to the fraction which resides at the NPC. Depletion of Pom33p suggests it may play important, yet undefined role in NPC assembly. However, depletion of TMEM33, the human orthologue of Pom33p, displayed no such phenotype (Chadrin et al., 2010). Thus the overall contribution of Pom33p and TMEM33 to NPC biogenesis remains to be established.

Deciphering the conservation of Poms across species has been precluded by the lack of identity in primary sequence composition and tertiary structure arrangement (DeGrasse et al., 2009). Based on both limited sequence identity of C-terminal domains and topology of N-terminal transmembrane domains, NDC1 orthologues were identified in numerous species from yeast through metazoa (Mansfeld et al., 2006; Stavru et al., 2006a). The assignment of orthologues for metazoan Pom121 and gp210, however, has been more challenging. Mimicking the domain topology of gp210, yeast Pom152p is a single-pass transmembrane Nup comprised of a large luminal domain and a small NPC-facing domain. Moreover, it has recently been suggested that the luminal domains of both gp210 and Pom152p share similarity with membrane cargo proteins of CPCs (intimins and cadherins, respectively), strengthening the idea of the common evolutionary origins of NPC and CPC structural proteins (Mans et al., 2004; Devos et al., 2006; Onischenko and Weis, 2011). Functional evaluation, however, has failed to uncover any significant similarity between these two proteins. While it has been demonstrated that Pom152p plays an important

role in NPC assembly in yeast, gp210 is dispensable for NPC in metazoan cells (Madrid et al., 2006; Stavru et al., 2006b; Onischenko et al., 2009). Intriguingly, although they display markedly different membrane topologies, a fragment of the large NPC-facing domain of Pom121 has been shown to display significant sequence similarity to a region of the NPC-facing domain of Pom152p (Wozniak et al., 1994). The function of this region remains to be investigated. Based on data accumulated from experiments described within this thesis, we discuss the potential orthology between Pom152p and Pom121 in Chapters III and VI.

1.3.1.3 FG-REPEAT NUCLEOPORINS

Nups that line the central channel of the NPC are specialized to interact with soluble nuclear transport receptors (NTRs), which shuttle cargo through the NPC (for review, see Wentz and Rout, 2010). These Nups are characterized by the presence of between four and forty-eight FG-repeats dispersed throughout long, natively unfolded domains (Zeitler and Weis, 2004). By occupying the NPC transport channel, FG-repeats play a critical role in establishing the permeability barrier while simultaneously preserving the distinct cytoplasmic and nucleoplasmic proteomes.

FG-Nups emanating from the NPC core towards the cytoplasmic and nuclear compartments form the cytoplasmic filaments and nuclear basket, respectively (Rout et al., 2000; Strawn et al., 2004). These asymmetrically localized Nups are in key position to provide docking sites for specific

nuclear transport events (Walde and Kehlenbach, 2010). Intriguingly, studies in yeast have demonstrated that the entire subset of asymmetric FG-Nups could be depleted without significantly affecting nuclear transport efficiency or cell survival (Strawn et al., 2004). Instead, FG-Nups that localize to the interior of the NPC transport channel were shown to be essential for normal NPC function (Finlay et al., 1991; Guan et al., 1995; Hu et al., 1996; Strawn et al., 2004). In metazoan cells, it was shown that these 'channel' FG-Nups form a symmetric complex containing Nup54, Nup58, and Nup62 (the Nup62 complex) (Finlay et al., 1991). Together with Nups of the core and adaptor scaffold domains, these Nups comprise the NPC 'symmetric core' (Hoelz et al., 2011). It has recently been proposed that FG-repeat domains of channel Nups function as molecular sensors that regulate the reversible dilation of the NPC transport channel in response to cargo-bound NTRs (section 1.4.2.1) (Melcak et al., 2007; Solmaz et al., 2011; Solmaz et al., 2013). In this way, the transport status of the NPC, and transitions between active and inactive conformations, would be intimately linked to the metabolic demands of the cell (Solmaz et al., 2013).

While most FG-Nups line the translocation channel, FG-repeats have been identified in two Nups associated with the pore membrane domain. The transmembrane Nup Pom121 contains ~25 conserved FG-repeats clustering near its C-terminus (Hallberg et al., 1993). While Pom121 is anchored to the pore membrane through its N-terminal transmembrane domain, it is conceivable that its long, unstructured C-terminal domain extends towards

the translocation channel to participate in nuclear transport. Alternatively, interactions between Pom121 and surrounding scaffolding Nups might trigger conformational changes within Pom121 that preclude its extension towards the central channel, restricting the mobility of the C-terminus and sequestering FG-repeats within the central scaffold. In summary, the potential role for Pom121 in nuclear transport remains to be evaluated.

In addition, several conserved FG-repeats have been identified in the adaptor-scaffold Nup53 (Marelli et al., 1998; Hawryluk-Gara et al., 2005). Through a conserved C-terminal amphipathic helix, Nup53 is intimately associated with the pore membrane (Marelli et al., 2001; Hawryluk-Gara et al., 2005; Vollmer et al., 2012). As the FG-repeats of Nup53 are located adjacent to its membrane-binding domain, it is unlikely they extend towards the central channel. Furthermore, contrary to the predicted disordered conformation of canonical FG-repeat domains, structural analysis of Nup53 revealed the localization of FG-repeats within distinct structural domains that mediate homo-dimerization of Nup53 polypeptides (Handa et al., 2006). Accordingly, Nup53 is unable to physically interact with NTRs, as FG-repeats are buried within the interaction interface (Handa et al., 2006). Together, these data suggest that a role for Nup53 in nuclear transport is unlikely.

1.3.2 NUCLEOCYTOPLASMIC TRANSPORT

While implicated in a host of cellular activities, the principle function of the NPC is the orchestration of nucleocytoplasmic transport. This includes

bi-directional shuttling of cargoes such as transcription factors, ribosomal proteins, mRNPs, transfer RNAs (tRNAs), ribosomal subunits and viral capsids (Tetenbaum-Novatt and Rout, 2010). While transport of small ions and molecules (<40 kDa, < 5 nm) through the NPC may occur by passive diffusion, transport of larger macromolecules and protein complexes requires interactions with NTRs that permeate the FG-meshwork lining the NPC translocation channel. It has been estimated that an individual NPC facilitates the selective transport of ~1000 macromolecules each second (Ribbeck and Gorlich, 2001). This translates into ~1 million translocation events per second for the nucleus of a typical mammalian cell. As an extension of this, it is predicted that the collective efforts of NPCs within the entire human body may transport ~1 kg of material each minute (Weis, 2007). Therefore, cells have evolved a sophisticated transport system to accomplish this enormous biological feat. In metazoan cells, this machinery comprises > 80 individual factors that may be categorized as stationary components of the NPC that facilitate transport (the FG-Nups), mobile NTRs that specifically recognize cargoes destined for transport and interact with FG-Nups, and finally, components that supply metabolic energy to relieve entropic restraints imposed by facilitated transport (the RanGTP system) (Guttler and Gorlich, 2011). Despite extensive efforts in this area, a unified model of the mechanisms orchestrating nuclear transport has not been achieved.

1.3.2.1 NTRs AND SIGNAL SEQUENCES

Cargos destined for transport across the NPC contain nuclear localization signals (NLS) or nuclear export signals (NES) that specify the directionality of transport as either nuclear import or export, respectively. The majority of NTRs that mediate transport belong to the karyopherin- β superfamily (Kap β), termed import-Kaps or export-Kaps (alternatively referred to as importins and exportins) (Strom and Weis, 2001; Mosammaparast and Pemberton, 2004; Stewart, 2007). Individual cargos destined for transport may be recognized by numerous Kap β s. The promiscuity observed in Kap β -cargo recognition presumably ensures that redundant transport pathways exist for essential cargos (Chook and Suel, 2011). Of all the components of the nuclear transport system, NTRs are unique in that they interact with each facet of the transport machinery; NTRs interact directly with cargoes, FG-repeats of FG-Nups, and with RanGTP (Chook and Blobel, 1999; Cingolani et al., 1999; Bayliss et al., 2000a; Lee et al., 2000). Accordingly, the structures of NTRs have been extensively studied, and numerous NTR-complexes, including many for the Kap β superfamily, have been described (Cook et al., 2007; Cook and Conti, 2010; Chook and Suel, 2011; Guttler and Gorlich, 2011).

While members of the Kap β family have relatively low sequence identity (10-20%), their overall structure is conserved (Chook and Suel, 2011). Kap β s are α -helical proteins that are comprised of \sim 20 HEAT-repeats. The \sim 40 amino acid residues that compose the HEAT motif are arranged as a

series of antiparallel α -helices, stacked against one another in tandem to form a right-handed superhelical domain. In general, FxFG residues of FG-Nups intercalate neighboring helices on the outer concave surface of the Kap β solenoid (Figure 1-3A) (Bayliss et al., 2000a; Bayliss et al., 2002). The paucity of this interaction interface helps to explain the low-affinity nature of interactions between FG-Nups and Kap β s. It can be envisaged that as Kap β -cargo complexes traverse the transport channel, multiple transient interactions between Kap β s and FG-repeats of neighboring Nups facilitate their translocation through the pore.

Crystal structures of Kap β -cargo complexes demonstrate marked differences in the way in which Kap β s recognize substrates destined for import (Cingolani et al., 1999; Cingolani et al., 2002; Lee et al., 2003; Lee et al., 2005). This inherent flexibility in cargo recognition presumably allows for the import of a broad range of different cargos (Lee et al., 2005). The interaction between Kap β and the importin- β binding domain (IBB) of the adaptor protein Kap α has been well described at the atomic level (Cingolani et al., 1999). The use of the Kap α as an adaptor in cargo recognition defines what has been termed the 'classical' nuclear import system (for review, see (Lange et al., 2007). The IBB domain of Kap α is comprised of a short sequence of basic amino acid residues, thus resembling the classical monopartite NLS (Gorlich et al., 1996). Evaluation of the atomic structure of Kap β bound to the IBB of Kap α demonstrates that the IBB domain is nestled within the inner concave C-terminal arch of Kap β (Figure 1-3B).

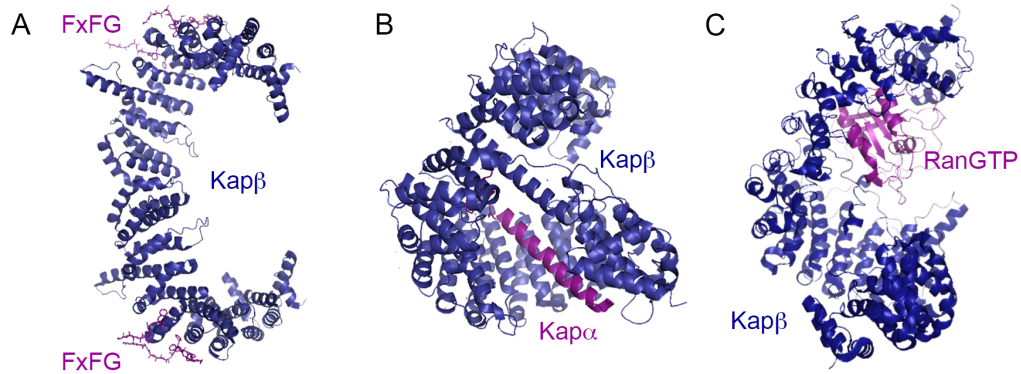


FIGURE 1-3 ATOMIC STRUCTURES OF KARYOPHERIN- β COMPLEXES.

Crystal structures of (A) karyopherin- β in complex with FxFG repeats from Nsp1p (Protein Data Bank code (PDB) 1F59) (Bayliss et al., 2000b), (B) karyopherin- β in complex with the importin- β binding domain (IBB) of karyopherin- α (1QGK; Cingolani et al., 1999), and (C) karyopherin- β 2 in complex with the non-hydrolysable GTP analogue GppNHp (1QBK; Chook et al., 1999). For simplicity, karyopherins are colored blue and ligands are colored purple. Adapted from Hoelz et al., 2011.

Only a small fraction of cargos recognized by Kap β s have been elucidated (Chook and Suel, 2011). Complicating the identification of Kap β substrates is the mode of NLS recognition. Kap β s may recognize a linear sequence of specific amino acid residues, or instead recognize the tertiary structure adopted by a conformational NLS, whose overall structural would dictate binding specificity. In this regard, the flexibility of the Kap β solenoid could allow for binding to a number of substrates that adopt various conformations (Fried and Kutay, 2003). Therefore, an overall model describing the interactions of Kap β s with subsets of cargos awaits a more comprehensive repertoire of substrates.

1.3.2.2 DIRECTIONALITY OF TRANSPORT

Import of cargo through the NPC is thought to be a passive process, with energy expenditure being required solely for the dissociation of NTR-cargo complexes in the nucleus (for review, see Stewart, 2007; Guttler and Gorlich, 2011). In this way, nuclear transport has been referred to as facilitated, rather than active transport. In the classical model of nuclear transport, the vectorial movement of Kap α/β -cargo complexes through the NPC is driven by the affinity of Kap β for the nucleotide-bound state of Ran, which cycles between GDP- and GTP-bound forms (Figure 1-4). RanGDP is converted to RanGTP by the action of guanine

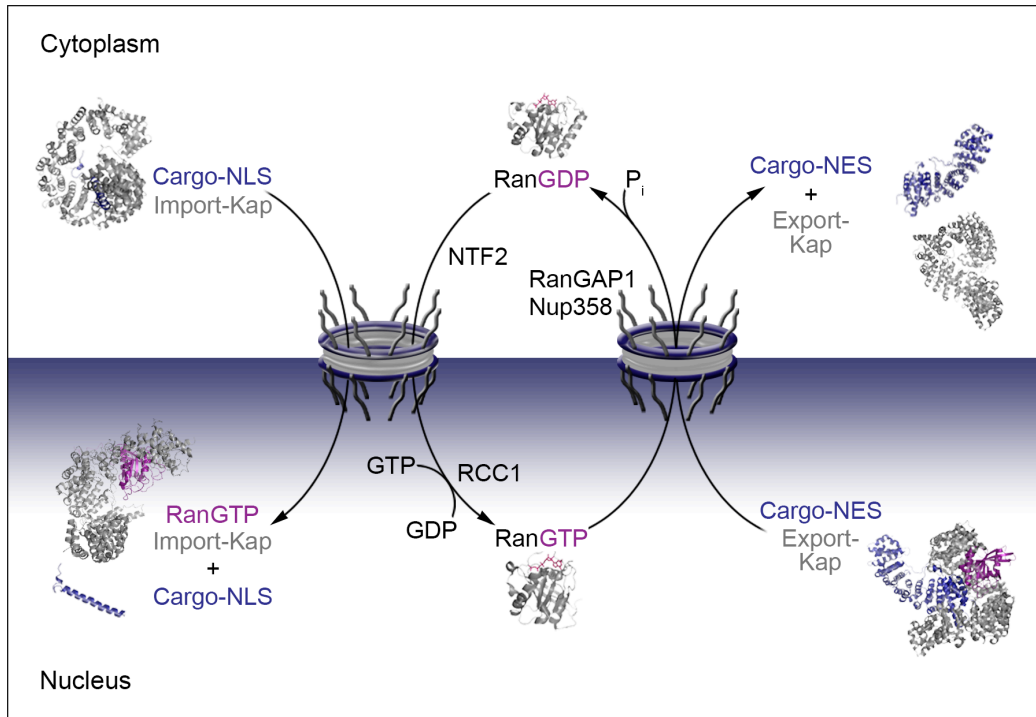


FIGURE 1-4 MODEL FOR KARYOPHERIN-MEDIATED NUCLEOCYTOPLASMIC TRANSPORT.

The nuclear localization sequence (NLS) of cargo destined for import (blue, left) is recognized by an import karyopherin in the cytoplasm. The import complex traverses the NPC and is dissociated by RanGTP in the nucleoplasm. Export karyopherins recognize nuclear export sequences (NES) of cargo destined for export in the nucleus (right). In complex with RanGTP, the export complex is transported through the NPC to the cytoplasm, where GTP hydrolysis by the cytoplasmic filament-bound RanGAP1 dissociates the complex. RanGDP is imported into the nucleus by the karyopherin NTF2, and is converted to RanGTP by chromatin bound guanine nucleotide exchange factor RCC1, replenishing the RanGTP gradient. Crystal structures used to depict import and export complexes include: import kap-cargo-NLS (importin- β + importin- α IBB, protein data bank code (PDB) 1QGK; Cingolani et al., 1999), import Kap-RanGTP (importin β -RanGTP, 1QBK; Chook and Blobel, 1999), cargo-NLS (importin α IBB, 1QGK; Cingolani et al., 1999), export kap-cargo-NES-RanGTP (Cse1p + Kap60p + RanGTP, 1WA5; Matsuura and Stewart, 2004), export kap (cytoplasmic Cse1p, 1Z3H; Cook et al., 2005), cargo-NES (Kap60p, 1WA5; Lee et al., 2005), RanGDP (3GJ0; Partridge and Schwartz, 2009) and RanGTP (2BKU; Lee et al., 2005).

nucleotide-exchange factor (RanGEF) RCC1, which catalyzes the exchange of GDP for GTP. RCC1 is physically tethered to chromatin through interactions with histones H2A and H2B, therefore restricting the localization of RanGTP to the nuclear interior (Ohtsubo et al., 1989; Bischoff and Ponstingl, 1991; Nemergut et al., 2001). Conversely, hydrolysis of Ran-bound GTP to GDP is restricted to the cytoplasm, where Ran GTPase activating protein (RanGAP1) is physically tethered to Nup358 of the NPC cytoplasmic filaments (Matunis et al., 1996; Mahajan et al., 1997; Saitoh et al., 1997). By physically separating the activities of RanGEF and RanGAP, a gradient of RanGTP is established that is 100 – 1000 fold higher in the nucleus (Gorlich et al., 1996; Izaurralde et al., 1997).

The RanGTP gradient is harnessed by the differential affinities of cargo-bound import- and export-Kaps for RanGTP. Import-Kaps bind cargo in the GDP-rich environment of the cytoplasm (Figure 1-4). Import-Kap-cargo complexes traverse the NPC where they encounter a surplus of RanGTP. Import-Kaps have a ~1000 higher affinity for Ran in its GTP- versus GDP-bound state, thus driving the dissociation of the import-Kap complex, releasing cargo into the nucleus (Rexach and Blobel, 1995; Gorlich et al., 1996; Bischoff and Gorlich, 1997; Gilchrist et al., 2002; Timney et al., 2006). The mechanism underlying the change in affinity of Kap β s for cargo following translocation was suggested by the crystal structures of GTP-bound import-Kaps, including human Kap β 2 and the yeast orthologue Kap95p (Chook and Blobel, 1999; Lee et al., 2005). As depicted in Figure 1-

3C, RanGTP binds the inner concave surface of the conserved N-terminal domain of Kap β 2, inducing a conformational shift in the Kap β 2 solenoid that dislodges cargo from the C-terminal binding pocket, presumably facilitating dissociation of the transport complex at the culmination of import (Chook and Blobel, 1999). A similar mechanism has been proposed for the RanGTP-mediated release of cargo from Kap95p in yeast (Lee et al., 2005). GTP-bound Kap β is shuttled back to the cytoplasm, where it is recycled by the activity of RanGAP1 for future rounds of transport.

Nuclear export occurs in nearly the opposite way, where export-Kaps bind cargo synergistically with RanGTP (Wente and Rout, 2010). This ternary complex traverses the pore, and GTP hydrolysis by RanGAP1 dissociates the complex to release cargo into the cytoplasm. To compensate for the loss of nuclear GTP, RanGDP is transported into the nucleus by the nuclear transporter NTF2 and converted to RanGTP by RCC1, thereby replenishing the pool of RanGTP that coordinates transport (Ribbeck et al., 1998; Smith et al., 1998). In summary, by combining the affinities of Kaps for the nucleotide-bound states of Ran with the compartmentalization of Ran nucleotide effectors, the cell has established an elegant mechanism that ultimately orchestrates the directionality of protein transport.

1.4 THE STRUCTURE OF THE NUCLEAR PORE COMPLEX

Since its discovery more than half a century ago, resolution of the structure of the NPC has been actively pursued using a variety of

methodologies (Callan and Tomlin, 1950; Hoelz et al., 2011; Grossman et al., 2012). Initial observations by electron microscopy (EM) revealed the conserved octagonal symmetry of the NPC and identified the cytoplasmic filaments and nuclear basket (Gall, 1967; Maul, 1971). However, progress towards a high-resolution model of the NPC has been precluded by its unprecedented size and dynamic nature. Resolution of the NPC at the atomic level is inhibited by difficulty in obtaining large amounts of homogenous material, while observations of native NPCs by EM are confounded by its inherent flexibility (Grossman et al., 2012). Thus, a 'divide and conquer' strategy has been adopted to resolve the atomic structure of the NPC, where X-ray crystallographic analyses of individual Nups, Nup hetero-dimers and hetero-trimers, and eventually entire subcomplexes can be combined with 3D-reconstructions of native NPCs recapitulated using cryo-electron tomography (Cryo-ET) to achieve a high-resolution structural model of the entire NPC (Hoelz et al., 2011; Grossman et al., 2012). Recent advances in 3D reconstructions of native NPCs by cryo-ET as well as atomic-level structural characterizations of the symmetric NPC core are discussed below.

1.4.1 NPC ARCHITECTURE REVEALED BY CRYO-ELECTRON TOMOGRAPHY

The canonical features of the NPC have been revealed by Cryo-ET of isolated and often detergent-extracted material. These studies identified the central framework of the NPC symmetric core embedded within the NE (Unwin and Milligan, 1982). 3D reconstructions at ~ 90 Å resolution revealed

the NPC core to be comprised of two concentric rings, anchored within either the cytoplasmic or nucleoplasmic half of the NPC (Unwin and Milligan, 1982; Jarnik and Aebi, 1991; Stoffler et al., 2003). These were termed the cytoplasmic ring (CR) and nucleoplasmic ring (NR) (Figure 1-5C). The CR and NR are connected by elongated spoke-like structures, termed the spoke ring (SR). Examination of the periphery of the NPC revealed distinct lateral channels of ~10 nm, which were proposed to allow passage of membrane-bound INM proteins through the NPC during nucleocytoplasmic transport (Hinshaw et al., 1992). Circumscribing the NPC core is a ring of proteinaceous material within the NE lumen, termed the luminal ring (LR), presumably comprised of transmembrane Poms (Akey and Radermacher, 1993). Connections between the LR and surrounding symmetric core anchor the NPC within the NE. Importantly, all studies described the NPC as displaying intrinsic plasticity. This was attributed to conformational flexibility of the spoke ring, and is proposed to be a critical aspect of the function of the NPC in mediating transport of large macromolecules (Grossman et al., 2012; Solmaz et al., 2013).

Advances in imaging techniques and computational processing led to 3D reconstructions of NPCs from *D. discoideum*, *X. laevis*, and *H. sapiens* at resolutions of 58, 64, and 66 Å, respectively (see below; Figure 1-5B) (Beck et al., 2004; Frenkiel-Krispin et al., 2010; Maimon et al., 2012). While the averaging of tomograms and generation of 3D structures used in previous studies assumed the NPC to be perfectly symmetrical around the octad axis,

FIGURE 1-5 ARCHITECTURE OF THE NPC FROM *D. DISCOIDEUM*, *X. LAEVIS* AND *H. SAPIENS* REVEALED BY CRYO-ELECTRON TOMOGRAPHY.

(A) Schematic representation of the NE and NPC density of *Dictyostelium discoideum* (yellow), *Homo sapiens* fibroblasts (orange), and *Xenopus laevis* oocytes (green). Size ratios between the different nuclei are depicted; R represents the average radius of a nucleus. NPC distribution and density (NPCs/ μm^2) is depicted in $1 \mu\text{m}^2$. (B) A comparison of the three average structures derived from the cells of corresponding organisms in native conditions by Cryo-electron tomography (Cryo-ET). Average heights and widths of each structure are provided in nm, and the resolution of each structure is provided in angstroms (\AA). (C) Cross-section of the structure of the NPC from *H. sapiens*. Key dimensions are indicated in \AA , including the height of the NE lumen and NPC, and width of the peripheral channels, NPC transport channel and NPC (including luminal connections). Positions of the cytoplasmic ring (CR), spoke ring (SR), nuclear ring (NR), luminal ring (LR), outer nuclear membrane (ONM) and inner nuclear membrane (INM) are indicated. Adapted from Maimon et al., 2010, and Maimon et al., 2012.

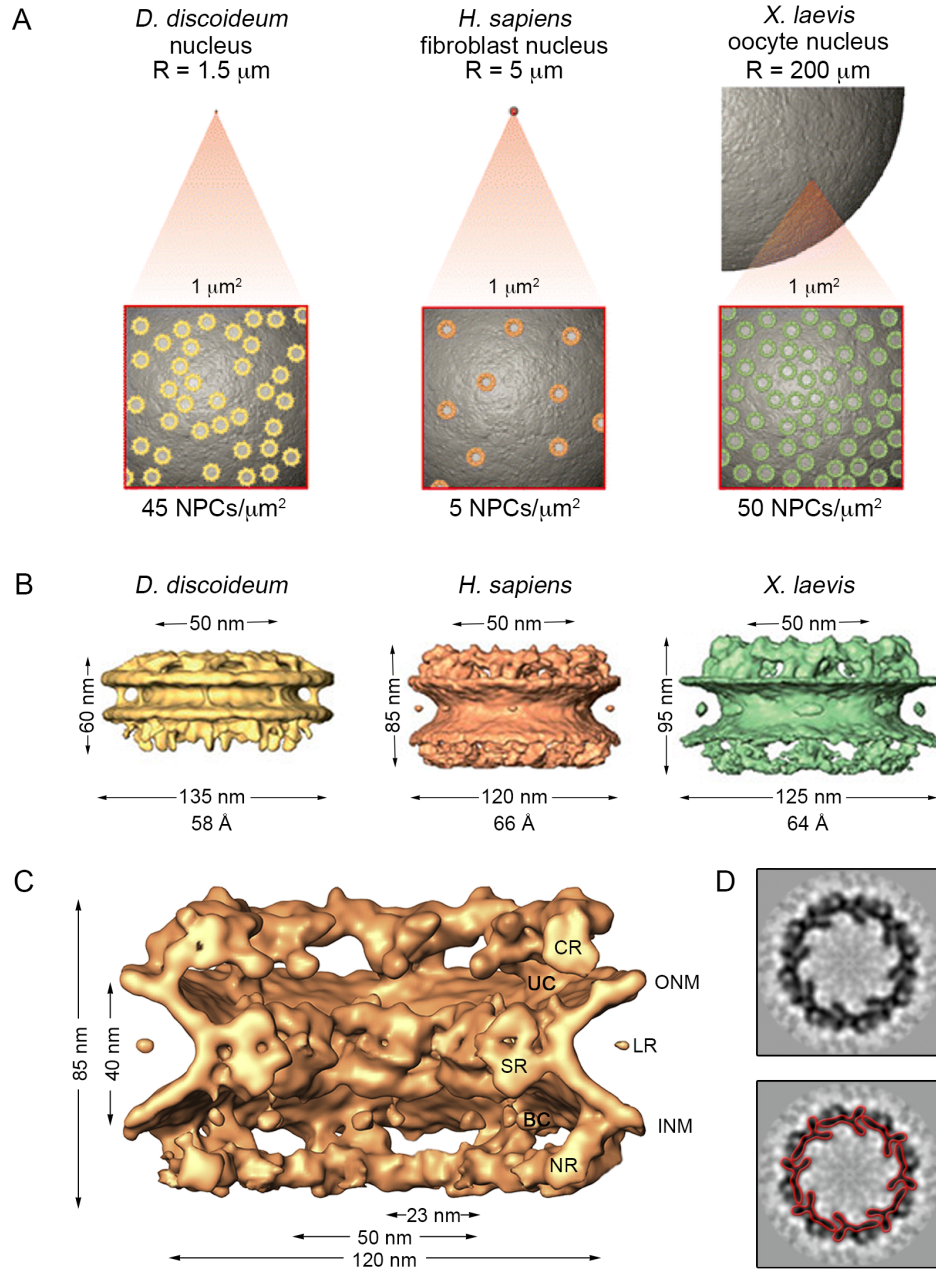


FIGURE 1-5 ARCHITECTURE OF THE NPC FROM *D. DISCOIDEUM*, *X. LAEVIS* AND *H. SAPIENS* REVEALED BY CRYO-ELECTRON TOMOGRAPHY.

Medalia and colleagues employed new computational algorithms to compensate for the inherent dynamicity of individual NPCs (Forster et al., 2005; Yahav et al., 2011). In these studies, each NPC was dissected *in silico* into 8 distinct protomers. The averaging of individual protomers allowed for marked enhancement of resolution and improved signal-to-noise ratio of resulting models. This methodology, termed symmetry-independent averaging, has the important advantage of imaging NPCs in their near-native state; non-purified intact NPCs were imaged within the NE, and for *D. discoideum* and *H. sapiens*, within an intact, functional nucleus. Refined models obtained using this methodology both confirm and extend previous observations, and revealed a wealth of novel features of the NPC. In general, while the overall architecture of the NPC is well conserved between species, important similarities and differences were revealed upon structural comparison.

NPCs from all species demonstrate canonical 8-fold rotational symmetry and 2-fold symmetry in the plane of the NE. Intriguingly, the diameter of the central channel, measuring 50 Å, is highly conserved (Figure 1-5B) (Beck et al., 2004; Frenkiel-Krispin et al., 2010; Maimon et al., 2012). This has important implications when considering the mechanism of dilation of the central channel to accommodate transport of large macromolecules, and suggests the dynamicity of interactions between Nups of the symmetric core might be conserved across species (i.e. Nup54 and Nup58) (see section 1.4.2.1) (Melcak et al., 2007; Solmaz et al., 2011; Solmaz et al., 2013).

Additionally, the CR from all species is remarkably well conserved. In models of the Human NPC, Maimon and colleagues suggest the CR resembles a series of linked Y-shaped structures, arranged head-to-tail around the pore (Figure 1-5D) (Maimon et al., 2012). This observation has important implications with respect to the higher-order arrangement of Nup subcomplexes within the NPC (see below).

While the architecture of the CR is conserved, differences are observed in the connections between the CR and SR, as well as SR and NR. In the Human NPC, this is accomplished by a series of delicate tubular connections, which delineate large, low-density regions termed the upper and lower cavities (UC and BC, respectively) (Figure 1-5C). It was postulated that these hollow regions allow for conformational changes within the NPC that occur in response to metabolic activity (Maimon et al., 2012). These connections are not well defined in yeast or *D. discoideum*. Major differences also exist in the height of the NPC as it envelops the POM. This is presumably a result of differences in height of the luminal space of the NE across species; the thickness of the NE ranges from ~ 300 Å in yeast to ~ 600 Å in metazoan cells (Akey and Radermacher, 1993; Yang et al., 1998). Thus, owing to the conservation of NPC composition and homology of Nup subcomplex organization, a similar set of Nups must compensate for an almost doubling of NE/NPC height. How this is achieved is currently unknown. It is conceivable that transmembrane proteins within the nuclear membrane in the vicinity of the POM aid in bridging the increased luminal space (Maimon

et al., 2012). Specifically, Poms may play an important role in expanding the NPC coat, as they are among the most degenerate NPC proteins. Additionally, structural rearrangements of Nups comprising the NPC core scaffold, including changes in inter- and intra-subcomplex associations, and perhaps differences in stoichiometry, might allow for the construction of a membrane coat specifically tailored for an extended POM (Maimon et al., 2012). Together, NPCs of all organisms display a similar architecture with unique overall dimensions, reflecting differences in protein composition, organization, and divergence of Nups at the amino acid sequence level (Maimon and Medalia, 2010; Maimon et al., 2012).

1.4.2 ATOMIC RESOLUTION OF NUCLEOPORINS OF THE NPC SYMMETRIC CORE

However informative, 3D models of intact NPCs obtained through Cryo-ET are unable to recapitulate the intricacies of Nup interactions at the atomic level. While the obstacles impeding crystallographic analyses of entire NPCs remain insurmountable, the focus has been to evaluate the structures of individual Nups and Nup subcomplexes, such that they may be pieced together like building blocks to assemble a model that would reveal the architecture of the plenary NPC (Hoelz et al., 2011; Grossman et al., 2012). Aiding this process is the inherent modularity of the NPC. The observations that Nups are composed of relatively few structural motifs (including β -propellers and α -solenoids) and are organized in discrete subcomplexes that are ordered with 8-fold rotational symmetry around the NPC markedly

simplifies efforts of structural determination (Devos et al., 2006; Brohawn et al., 2009). Recent progress in deciphering the atomic structures of individual Nups of the symmetric NPC core and the subcomplexes they comprise is discussed below.

1.4.2.1 ATOMIC STRUCTURES OF CENTRAL CHANNEL NUCLEOPORINS AND MODEL FOR THE DILATABLE MIDPLANE RING

Recent crystallographic analyses of FG-Nups that comprise the symmetric NPC central channel (Nup54, Nup58, and Nup62) have led to the proposal of a model for the reversible expansion and contraction of the NPC midplane ring (Figure 1-6) (Melcak et al., 2007; Solmaz et al., 2011; Solmaz et al., 2013). Structural analysis of Nup54 and Nup58 revealed their homotetramerization in solution, as well as the formation of an elaborate heterododecamer, comprised of eight molecules of Nup54 and four molecules of Nup58. The crystal structure of the Nup54-Nup58 hetero-dodecamer revealed oligomerization of Nup54-Nup58 modules into an extended helical structure (Solmaz et al., 2011). Computational manipulation of this helix allowed the formation of a ring-like structure comprised of eight Nup54-Nup58 hetero-dodecamers, with symmetry and dimensions remarkably similar to those observed for the NPC central channel by cryo-EM (Figure 1-6D) (i.e. 50 nm diameter) (Solmaz et al., 2011; Maimon et al., 2012). Similarly, the *in silico* placement of Nup54 and Nup58 homo-tetramers around the NPC channel revealed the formation of a constricted symmetrical ring with a diameter of ~10-20 nm (Figure 1-6E). Importantly, a central

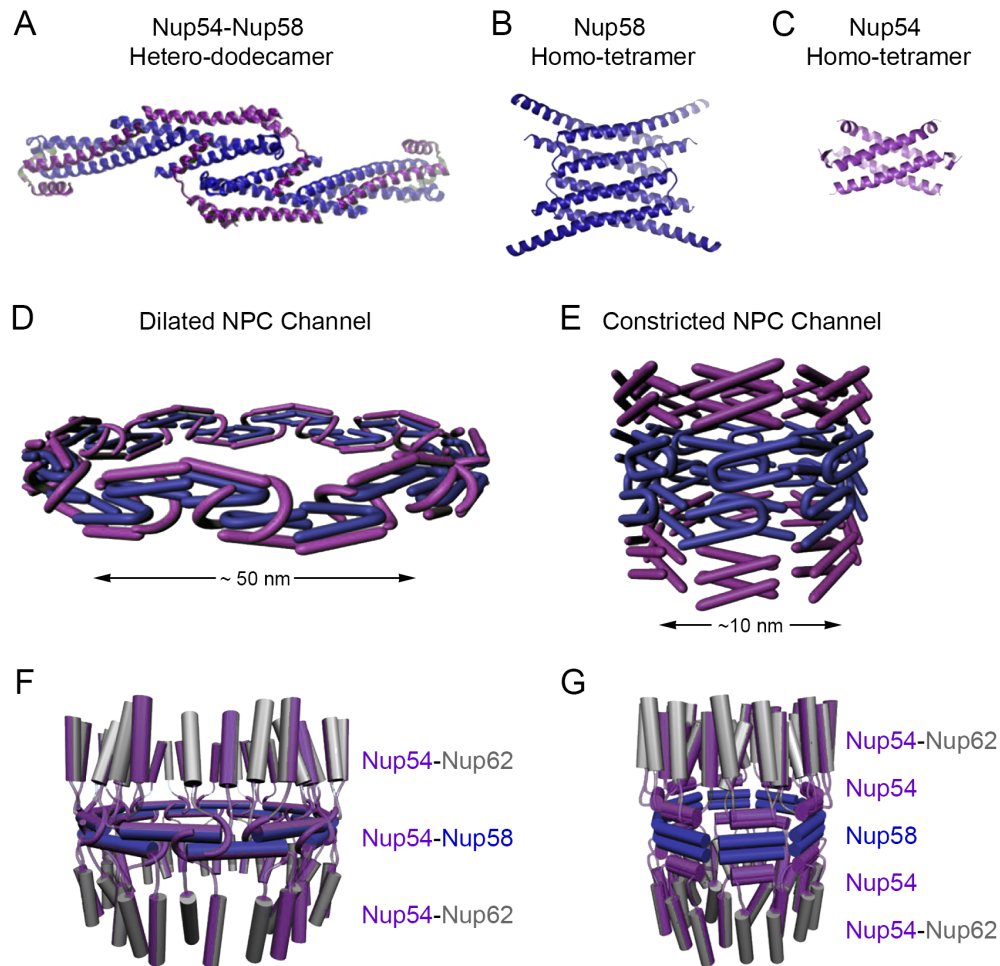


FIGURE 1-6 MODEL FOR THE 'RING-CYCLE' FOR DILATING AND CONSTRICTING THE NPC CENTRAL CHANNEL.

(A) Nup54-Nup58 hetero-dodecamer consisting of eight copies of Nup54 (purple) and four copies of Nup58 (blue). (B) Homo-tetramer of Nup58. Each Nup58 polypeptide consists of a helical hairpin. (C) Homo-tetramerization of Nup54 α -helices. (D) Model for the dilated NPC midplane ring, comprised of eight Nup54-Nup58 dodecamers. (E) Model for the constriction of the NPC midplane ring; homo-oligomerization of Nup54 and Nup58 results in the formation of three concentric rings. Homo-oligomers of Nup58 form the centre ring, while Nup54 homo-oligomers are tentatively placed above and below. (F, G) Finger-like projections of Nup62 (gray) to the dilated (F) and constricted (G) transport channel, connected to the midplane ring by flexible extensions of Nup54. Cycling from a dilated to a constricted state (F to G) increases crowding of fingers. Adapted from Solmaz et al., 2013.

feature of all Nup54 and Nup58 structures is the inherent instability of their oligomerization interfaces. Thus, it was proposed that transitioning between homo- and hetero-oligomerization states would allow for the reversible dilation and constriction of the transport channel, akin to open and closed, or active and inactive NPCs (Solmaz et al., 2011; Solmaz et al., 2013).

This model was expanded by the addition of vertical, finger-like projections of Nup62 to either side of the midplane ring through heterodimerization with Nup54 (Figure 1-6F) (Solmaz et al., 2011; Solmaz et al., 2013). While coiled regions of Nup62 and Nup54 mediate the heterodimerization interface, the FG-repeat domains of each protein are free to extend towards the cytoplasmic and nucleoplasmic boundaries of the NPC. The FG-repeat domain of centrally localized Nup58 is predicted to extend towards the NPC interior. A central tenant of this model is the regulation of midplane ring deformation by NTR-cargo complexes as they traverse the NPC transport channel (Solmaz et al., 2013). It is proposed that in the constricted state, inter-molecular cohesion of FG-repeat domains of neighboring Nups maintains the NPC in a closed conformation. Interactions between FG-Nups with NTR-cargo complexes would disrupt the FG network, allowing the transition towards Nup54-Nup58 hetero-oligomerization and subsequent dilation of the midplane ring. In this model, FG-Nups act as molecular sensors that regulate the overall activity of the NPC, facilitating the dilation of the NPC midplane ring in the presence of NTR-cargo complexes destined for transport, and constricting the ring in their absence. In this way,

the conformation of the NPC, and the transitioning between active and inactive states, would be intimately linked to the transport requirements of the cell.

1.4.2.2 MODULARITY OF THE CORE SCAFFOLD REVEALED BY ELECTRON MICROSCOPY

To date, the majority of NPC structures resolved at the atomic level represent Nups from the core scaffold, in particular from the heptameric Nup84p complex of *S. cerevisiae*. This complex is orthologous to the metazoan Nup107-160 complex, and is comprised of seven Nups including Nup84p, Nup85p, Nup120p, Nup133p, Nup145C, Sec13p, and Seh1p (Table 1-1, Figure 1-7). Early studies by 2D EM revealed the modular self-assembly of the complex into a characteristic Y-shape (Figure 1-7A)(Lutzmann et al., 2002). Biochemical analyses characterized Nup hetero-dimeric and heterotrimeric complexes that comprise the molecular building blocks of the Y (Lutzmann et al., 2002). EM analysis of each of these complexes revealed their specific shapes, allowing them to be pieced together to build a structural model of the Y. In this model, the β -propeller/ α -solenoid Nup120p forms one arm of the Y; the other is composed of the β -propeller Seh1p and the α -solenoid Nup85p. Completing the triskelion-like connection at the hub of the Y is a complex of the β -propeller Sec13p and α -solenoid Nup145Cp. The stalk of the Y is extended by the α -solenoid Nup84p and concludes with the β -propeller/ α -solenoid Nup133p (Figure 1-7B) (Lutzmann et al., 2002).

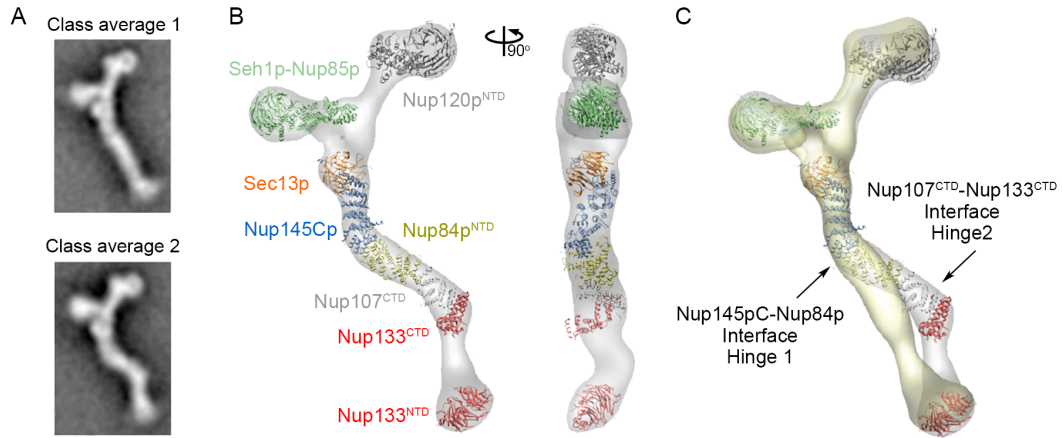


FIGURE 1-7 THREE-DIMENSIONAL CHARACTERIZATION OF THE HEPTAMERIC YEAST NUP84P COMPLEX BY ELECTRON MICROSCOPY.

(A) Imaging of 9,082 particles revealed two distinct structural classes of heptamer conformations. The averages obtained from 497 and 608 images are shown for the class average 1 and 2 conformations, respectively. (B, C) Docking of available crystal structures into the 3D projection map of the heptamer. A view of the heptamer rotated 90° around the vertical axis is shown. (C) Superposition of heptamer conformations. The hinge regions of the interfaces of Nup84p (Nup107) complexes are indicated. Adapted from (Kampmann and Blobel, 2009; Hoelz et al., 2011).

Recent 3-dimensional EM analysis has confirmed this arrangement, and revealed additional features of the Y-complex (Kampmann and Blobel, 2009). Immunogold labeling using specific anti-Nup antibodies experimentally confirmed the positioning of Nups, and extended the model to include the localization of β -propellers to the peripheral surface of the Y-complex, with α -solenoids forming the connecting segments. This arrangement was likened to the architecture of the clathrin triskelion (Kampmann and Blobel, 2009). Analysis of the stalk of the Y-complex revealed two hinge-like regions at either end of Nup84p, at the Nup84p-Nup145C and Nup84p-Nup133p interfaces (the metazoan orthologue of Nup84p is Nup107, Figure 1-7C). These hinges were proposed to allow movement within the Y-complex to allow circumferential adjustments in response to transport requirements of the cell (Kampmann and Blobel, 2009). Thus, dynamicity has emerged as an overarching theme for the architecture of the NPC, and is a hallmark of intra-subcomplex interactions as well as those that comprise the entire structure.

1.4.2.3 ATOMIC STRUCTURES OF CORE SCAFFOLD NUCLEOPORINS

The first atomic structures of components of the heptameric Y-complex were provided by metazoan orthologues of Nup84p and Nup133p (Nup107 and Nup133, respectively, Figure 1-8D, E) (Berke et al., 2004; Boehmer et al., 2008; Whittle and Schwartz, 2009). The N-terminal domain

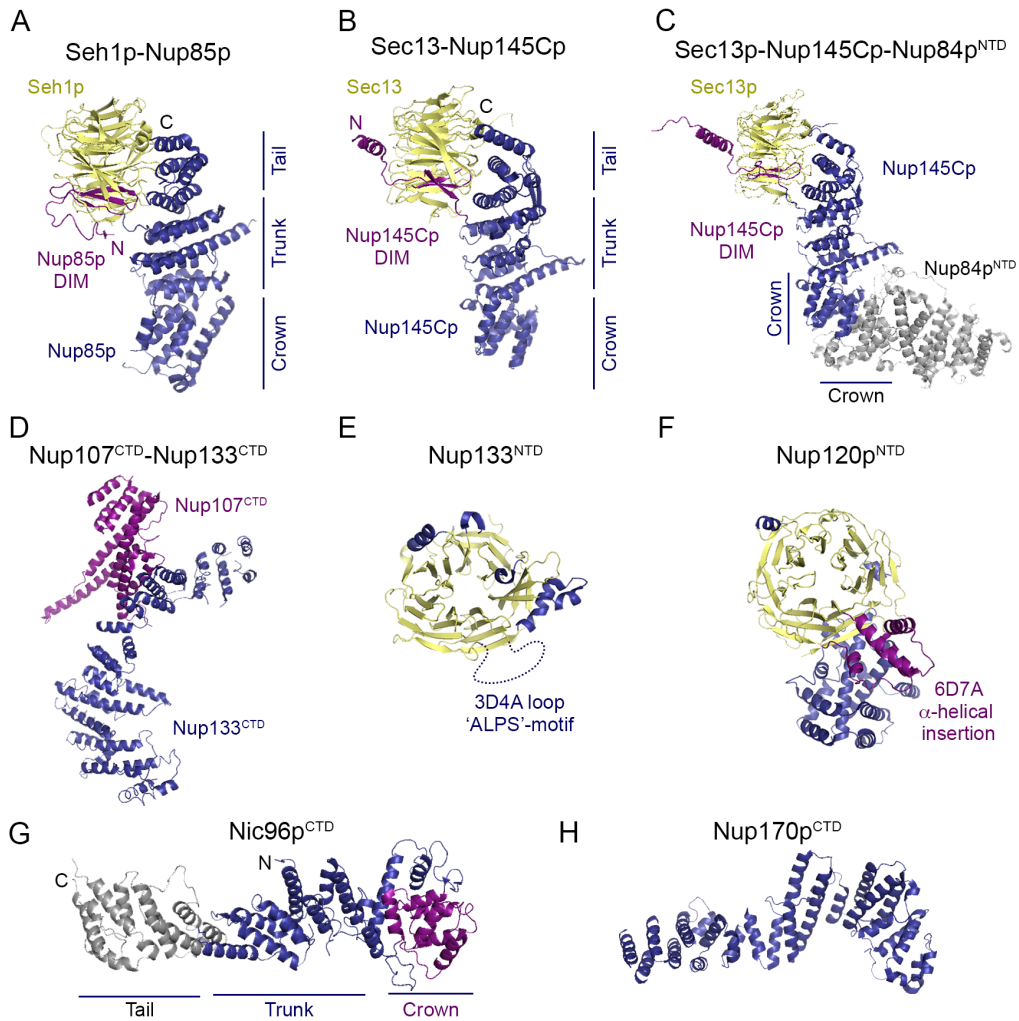


FIGURE 1-8 CRYSTAL STRUCTURES OF CORE- AND ADAPTOR-SCAFFOLD NUCLEOPORINS.

(A-F) Crystal structures of core scaffold Nups and complexes thereof: A) Seh1p-Nup85p (Protein Data Bank (pdb) code 3F3F; Debler et al., 2008), B) Sec13-Nup145Cp (3BG1; Hsia et al., 2007), C) Sec13p-Nup145Cp-Nup84p^{NTD} (amino-terminal domain) (3IKO; Nagy et al., 2009), D) Nup107^{CTD}-Nup133^{CTD} (carboxy terminal domain) (3I4R; Whittle and Schwartz, 2009), E) Nup133^{NTD} (1XKS; Berke et al., 2004), and F) Nup120p^{NTD} (3F7F; Seo et al., 2009). A dashed line indicates the 'ALPS' -motif of the Nup133^{NTD}. The 6D7A α -helical insert of Nup120p is indicated in purple. (G, H) Crystal structures of adaptor scaffold Nups, including G) Nic96p^{CTD} (2RFO; Schrader et al., 2008) and H) Nup170p^{CTD} (3I5P; Whittle and Schwartz, 2009). Structures of Nup107, Nup133, and Sec13 (within the Sec13-Nup145Cp complex) are from human recombinant proteins, all others are from *S. cerevisiae* (indicated by a p). DIM refers to domain invasion motif, where the seventh blade of the β -propellers of Seh1p and Sec13p are provided *in trans* by Nup85p and Nup145Cp, respectively. The amino-termini (N) and carboxy-termini (C) of Nup85p, Nup145Cp, and Nip96p^{CTD} are indicated. The trunk, crown and tail regions of Nups containing ACE1 motifs are indicated. Adapted from Hoelz et al., 2011.

(NTD, residues 76-478) of Nup133 folds into a canonical 7-bladed β -propeller, containing a unique disordered extension protruding from blades 3 and 4, termed the 3D-4A loop (Figure 1-8E) (Berke et al., 2004). Bioinformatic analysis revealed that this region contains an amphipathic α -helix termed ArfGAP1 lipid packing sensor (ALPS) motif. While initially unstructured in solution, this disordered motif of \sim 25 amino acids forms an amphipathic α -helix in the presence of curved membranes (Berke et al., 2004; Drin et al., 2007). Serine and threonine residues demarcate the polar face of the helix, while bulky, hydrophobic residues line the membrane-interacting interface. The presence of this domain suggests that Nup133 is positioned close to the POM where it may facilitate stabilization of membrane curvature. The structure of the C-terminal domain (CTD, 517-1156) of Nup133 was solved in a complex with the CTD of Nup107 (658-925) (Figure 1-8D) (Boehmer et al., 2008; Whittle and Schwartz, 2009). Both fragments form extended, irregularly stacked α -helices that comprise unique α -helical domains with no significant similarity to canonical α -helical folds. Nup133 and Nup107 are positioned head-to-tail within the Y-complex, and this interaction has been demonstrated to be essential for targeting Nup133p to the NPC *in vivo* (Boehmer et al., 2008).

A novel α -helical domain was also revealed in the structure of Nup120p (Figure 1-8F) (Seo et al., 2009). The crystal structure of the Nup120p NTD (residues 1-729) displays a 7-bladed β -propeller characterized by several insertions, followed by a unique α -helical domain.

An important feature of the β -propeller domain of Nup120p is the extension of a unique α -helical bundle from between blades 6 and 7, termed the 6D-7A insert (Figure 1-8F). This helical bundle sits atop the α -helical domain and is one of the highest conserved regions of the Nup120p NTD. While no apparent function has been described for the Nup120p 6D-7A α -helical insert, the conservation of this domain in *S. pombe* is discussed in Chapter IV.

The α -helical domain of Nup120p NTD is characterized by two long α -helices connected by a sharp hairpin loop, reminiscent of a leucine-zipper motif. The remaining α -helices wrap around the entirety of the leucine zipper-like hydrophobic core. Biochemical analyses revealed that the hairpin loop harbors a specific binding site for Nup133p. The binding site within Nup133p was mapped to its N-terminal ~15 amino acid residue unstructured domain, termed the N-terminal extension (NTE). NTEs are common motifs of Nup β -propellers, and it has been proposed that they provide flexible connections that allow changes in NPC circumference during transport (Seo et al., 2009). Additionally, NTEs have been shown to be sites of phosphorylation that disrupt Nup interactions, triggering NPC disassembly during mitosis (see section 1.5.1.2) (Glavy et al., 2007). The physiological relevance of Nup120p-Nup133p hetero-dimerization was supported by mutagenesis experiments *in vivo* that demonstrated defects in nuclear transport when this interaction was abolished (Seo et al., 2009). Because Nup120p and Nup133p are localized to opposite poles of the Y-complex, it was proposed that the interaction of these Nups would require the head-to-

tail arrangement of Y complexes to assemble a ring-like structure delineating the POM (Seo et al., 2009). This prediction is a central tenet of the ‘fence post’ model of the NPC membrane coat (discussed in section 1.4.3.1).

The next major advance came with the resolution of complexes of Seh1p-Nup85p and Sec13p-Nup145Cp, leading to the proposal of two diametrically opposed models for the architecture of the NPC symmetric core (Figure 1-8A, B; see section 1.4.3) (Hsia et al., 2007; Brohawn et al., 2008; Debler et al., 2008; Brohawn and Schwartz, 2009b). As suggested by previous tertiary structure predictions, Seh1p (1-180) and Sec13p (1-322) form β -propellers (Devos et al., 2004; Devos et al., 2006). A unique feature of these β -propellers was uncovered, however, that was unexpected; the seventh blade of Seh1p and Sec13p β -propellers is provided *in trans* by extensions from Nup85p and Nup145Cp α -helical domains, respectively (Figure 1-8A, B). The complementation of a β -propeller domain in this way was termed the domain invasion motif (DIM), and has so far been restricted to complexes of Nups and coat proteins comprised of Seh1p and Sec13p (Fath et al., 2007; Hsia et al., 2007; Brohawn et al., 2008; Debler et al., 2008; Brohawn and Schwartz, 2009b; Nagy et al., 2009; Whittle and Schwartz, 2010).

The α -helical domains of Nup85p (1-570) and Nup145Cp (125-555) similarly displayed unique folds; both proteins are comprised of a series of extended, irregularly packed α -helices that fold back on themselves to form a rigid, J-shaped α -helical domain (Hsia et al., 2007; Brohawn et al., 2008; Debler et al., 2008). This type of fold architecture is again restricted to NPC

and vesicle coat proteins, and has since been observed in crystal structures of Nup84p of the Y-complex, Nic96p of the adaptor scaffold, and within Sec16p and Sec31p of the COPII vesicle coat (Jeudy and Schwartz, 2007; Brohawn et al., 2008; Brohawn and Schwartz, 2009b; Whittle and Schwartz, 2010). Restriction of this domain to Nups and vesicle coat proteins prompted the terminology ancestral coatomer element 1 (ACE1) (Brohawn et al., 2008). Structural analysis of the ACE1 motif revealed its inherent tripartite composition; the N-terminal and middle regions of ACE1 elements fold together to constitute the 'trunk' of the domain, connected by a U-turn of α -helices that comprise the 'crown' (Figure 1-8A, B, and G) (Brohawn et al., 2008). Nups containing ACE1 elements are typified by an additional extension termed the 'tail' that is not present in Sec16p or Sec31p (Whittle and Schwartz, 2010). The discovery of this conserved domain architecture within scaffolding components of NPCs and coated vesicles is the founding principle of the 'lattice' model of the NPC membrane coat (discussed in section 1.4.3.2) (Brohawn and Schwartz, 2009a).

The most recent crystal structure described for Nups of the heptamer is the hetero-trimeric complex of Sec13p-Nup145C-Nup84p (Figure 1-8C) (Brohawn and Schwartz, 2009b; Nagy et al., 2009). Together, these Nups form the stalk of the Y-complex. As mentioned previously, both Nup145Cp and Nup84p fold into J-shaped α -solenoids that contain ACE1 motifs (Brohawn et al., 2008; Brohawn and Schwartz, 2009b). Analysis of the binding interface between Nup145Cp and Nup84p revealed their interaction

through the hydrophobic linkage of the highly curved base of their ACE1 'crown' domains. Structures of hetero-trimers from independent laboratories revealed the arrangement of Sec13p-Nup145Cp-Nup84p into a distinct elongated Z-shaped structure (Brohawn and Schwartz, 2009b; Nagy et al., 2009). Intriguingly, this structure, along with other crystal structures of Nups of the heptameric Y-complex could be fit into the 3D spatial map of the heptamer previously generated by EM, providing the first glimpse of the Y-complex at atomic resolution (Figure 1-7B) (Nagy et al., 2009). It is predicted that structural rearrangements at the Nup145Cp-Nup84p interface allow transitions between distinct heptamer conformations. Specifically, the Z-shaped Sec13p-Nup145Cp-Nup84p hetero-trimer fits into EM models of the Y-complex with a zigzag shaped stalk (Figure 1-7C) (Nagy et al., 2009).

1.4.2.4 ATOMIC STRUCTURES OF ADAPTOR SCAFFOLD NUCLEOPORINS

While structures of Nups comprising the heptamer of the core scaffold have been actively pursued, few structures of adaptor scaffold Nups have been solved at the atomic level. Structural predictions suggest that members of this complex (termed the Nup53-93 complex), including Nup93, Nup155, Nup188, and Nup205, are composed mainly of α -solenoid domains (Devos et al., 2006). Like other Nups comprising the symmetric core, Nic96p, the *S. cerevisiae* orthologue of Nup93, was revealed to fold into an α -solenoid containing the tripartite ACE1 domain (Figure 1-8G) (Jeudy and Schwartz, 2007). Similarly, Nup155 architecturally resembles coat proteins, being

comprised of an N-terminal β -propeller followed by a C-terminal α -solenoid. However, analysis of the crystal structure of the CTD of Nup170p, the orthologue of Nup155 in *S. cerevisiae*, revealed a novel bipartite stacked α -solenoid domain connected by flexible hinges (Figure 1-8H) (Whittle and Schwartz, 2009). Structural analysis of the Nup170p CTD (979-1502) revealed remote homology to the α -solenoid domain of Nup133p, as well as Human Nup133 (Whittle and Schwartz, 2009). While the overall consequence of this domain homology is unclear at present, it has been shown that α -solenoid domains of both Nup133p and Nup170p are required for targeting to the NPC (Boehmer et al., 2008; Flemming et al., 2009).

Nup53, an additional member of the adaptor scaffold, is structurally distinct from other scaffold Nups in that it folds into an atypical RNA recognition motif (RRM) (Handa et al., 2006). Analysis of the crystal structure of *Mus musculus* Nup53 (173-252) suggests that while the general architecture of this motif is conserved, specific amino acid residues of the β -sheet surface have diverged from the canonical RRM sequence. It was revealed that this unique hydrophobic interface allows homo-dimerization of Nup53 polypeptides, a novel function for this fold not previously observed. It was proposed that Nup53 homo-dimerization might facilitate inter-subcomplex interactions that contribute to oligomerization of structural modules around the POM (Handa et al., 2006). Although not resolved in the crystal structure, Nup53 contains a conserved amphipathic helix at its C-terminus (Marelli et al., 2001; Hawryluk-Gara et al., 2005; Vollmer et al.,

2012). This helix has been proposed to anchor Nup53 within the NE membrane and is critical for NPC assembly (see section 1.5.2) (Marelli et al., 2001; Vollmer et al., 2012).

Resolution of the remaining structures of Nups of Nup53-93 complex will undoubtedly provide important structural information of both the assembly of the adaptor scaffold complex and formation of the symmetric NPC core scaffold as a whole. It will be intriguing to discern the topology of α -solenoids of Nup188 and Nup205, and evaluate their respective fold architecture. Resolution of the atomic structures of Nups has so far revealed a wealth of new structural domains, including the novel snake-like coil of the Nup120p NTD, the irregularly stacked α -helices of Nup170p and Nup133p, as well as DIMs and ACE1 motifs common to both NPCs and coated vesicles. Elucidating the structural architecture of core and adaptor scaffold complexes, and the interaction interfaces that link them, is of critical importance for arriving at a unified, high-resolution model of the NPC. Current models predicting the higher-order assembly of the core and adaptor scaffold Nups into a membrane coat specifically tailored for the NPC pore membrane are discussed below.

1.4.3 MODELS FOR THE NPC MEMBRANE COAT

Several models of the NPC symmetric core scaffold have recently been proposed. While each model differs with respect to orientation and stoichiometry of Nups and Nup subcomplexes, the feasibility of each model is

actively debated. Analyses of crystal structures of the heptameric Nup84p complex led to the proposal of the 'fence post' and 'lattice' models of the NPC membrane scaffold, with each model suggesting ring formation by heptamers in distinct and mutually exclusive arrangements. A third model, the 'computational' model, arrived at a third arrangement of Nups by combining a series of proteomic data with computational algorithms, in the absence of structural data. Features of these models are discussed below.

1.4.3.1 THE 'FENCE POST' MODEL OF THE SYMMETRIC NPC SCAFFOLD

Analyses of Nup145Cp - Sec13p and Nup85p - Seh1p pairs in solution revealed that both complexes exist in dynamic equilibrium between heterodimer, hetero-tetramer, and, to a much lesser extent, hetero-octameric assemblies (Hsia et al., 2007). Interactions that might facilitate the oligomerization of these higher-order structures were inferred by analyzing crystal contact sites within crystals of each complex (Hsia et al., 2007; Debler et al., 2008). For both complexes, analyses of multiple crystals revealed striking similarities in the structure of hetero-octameric assemblies; homo-dimerization between α -solenoid domains allows formation of hetero-tetramers, which oligomerize into hetero-octamers by homo-dimerization between β -propeller domains (Figure 1-9A). As the higher-order assemblies are remarkably similar in their overall symmetry, curvature, and dimension, it was proposed that each complex acts to form a vertical pole of the

FIGURE 1-9 MODEL OF THE 'FENCE POST' COAT FOR THE NUCLEAR PORE MEMBRANE.

A) Comparison of the structures of Seh1p-Nup85p and Sec13-Nup145Cp hetero-octamers (Protein Data Bank (PDB) codes 3BG1 and 3F3F, respectively) (Hsia et al., 2007; Debler et al., 2008). β -propellers are colored yellow, α -solenoids in blue, and domain invasion motifs (DIMs) in purple. (B) Schematic representation of the higher-order assembly of heptamers that comprise the coat cylinder predicted by the fence post model. Four rings formed by heptamers arranged head-to-tail are stacked in an antiparallel manner at the pore membrane domain. The position of Sec13p-Nup145Cp and Seh1p-Nup85p hetero-octamer 'fence posts' are indicated in dark and light blue, respectively. Measurements of the predicted coat cylinder are in accordance with the width and height of the yeast NPC as revealed by electron microscopy. The arrangement of heptamers in this manner forms a cylinder that conforms to the 8-fold rotational and 2-fold lateral symmetry observed for NPCs. (C) Predicted inter-subcomplex interaction conformations dictated by the promiscuity of Nup interactions observed in crystal structures (see text). Red lines indicate interactions described as promiscuous; black lines indicate interactions that have not previously been described as promiscuous. Nup145Cp-Nup84p hetero-dimerization contributes to one vertical pole of the coat cylinder (top panel, shaded light blue). Nup145Cp homo-dimerization is predicted to contribute two additional vertical poles (bottom panel, shaded dark blue). Adapted from Hoelz et al., 2011.

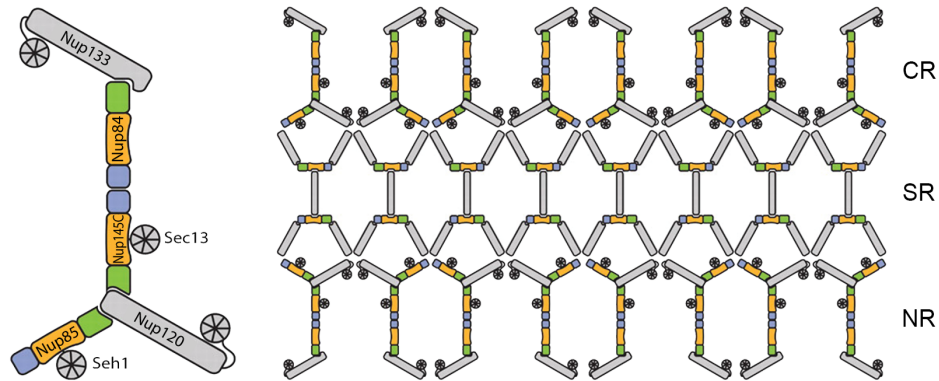
cylindrical NPC coat (Hsia et al., 2007; Debler et al., 2008). Horizontal connections between adjacent heptamers in a head-to-tail manner were proposed based on interactions observed between Nup120p and Nup133p (Seo et al., 2009). Thus, a model was proposed where Y-shaped heptamers assemble into ring-like structures that circumscribe the pore membrane. Four rings, each composed of eight heptamers, are stacked on top of each other in an antiparallel fashion to form a coat cylinder (Figure 1-9B). Homodimers of Nup145Cp or Nup85p link the inner and outer rings, whereas homo-dimerization of Sec13p or Seh1p connect the center rings (Figure 1-9C) (Hsia et al., 2007; Debler et al., 2008).

Recent analyses of the hetero-trimer of Sec13p-Nup145Cp-Nup84p revealed what at first appeared to be an inconsistency of this model. The binding interface observed between Nup145Cp and Nup84p overlaps with the proposed Nup145Cp homo-dimerization interface, thus precluding homo-dimerization into higher-order assemblies (Brohawn and Schwartz, 2009b; Nagy et al., 2009). However, the authors suggest that apparent switching from homo- to hetero-modality is consistent with the overall plasticity observed within the NPC general architecture, and may be a key component to the functioning of the NPC in the transport of large macromolecules (Figure 1-9C) (Hoelz et al., 2011).

1.4.3.2 THE LATTICE MODEL OF THE NPC COAT

The 'lattice' model for the NPC scaffold proposed by Schwartz and colleagues centers around the observations that Nups and vesicle coat proteins share similar domain architectures that facilitate membrane curvature (Figure 1-10) (Brohawn et al., 2008; Brohawn and Schwartz, 2009a). Evaluation of crystal structures of numerous Nups and coat proteins, including Nup85p, Nup145Cp, Nup84p, Nic96p, Sec13p, and Sec16p, revealed the conservation of their unique ACE1 domains. In this model, the vertical arrangement of Nup84p heptamers would position the ACE1 domains of Nups along the pore membrane, analogous to the arrangement of coat proteins along membranes of vesicle coats (Brohawn et al., 2008; Brohawn and Schwartz, 2009a). Oligomerization of vertical heptamers, through as yet unidentified contacts, would allow the formation of a lattice-like membrane coat for the NPC (Figure 1-10A). Due to similarities in the domain architectures of Nups and vesicle coat proteins, including β -propellers, α -solenoids, and ACE1 motifs, the arrangement of Nups in such a way would mimic the higher-order assemblies of coat proteins of COPI, COPII, and clathrin-coated vesicles. Nups containing α -solenoids would provide the main frame of the heptamer, while interactions between β -propellers would provide links between individual heptamers and between heptamers and surrounding Nups (Brohawn and Schwartz, 2009a; Kampmann and Blobel, 2009; Leksa and Schwartz, 2010).

A Lattice Model



B Computational Model



FIGURE 1-10 'LATTICE' AND 'COMPUTATIONAL' MODELS OF THE SYMMETRIC NUCLEAR PORE COMPLEX CORE.

(A) Arrangement of Nup84p heptamers to form a putative lattice structure that coats the NPC pore membrane domain. ACE1 motifs are highlighted within Nups of the heptamer (left panel, crown domain colored blue, stalk in yellow and tail in green). A schematic of the lattice model (right panel) depicts the vertical arrangement of heptamers to potentially form what is observed by electron microscopy to be cytoplasmic and nuclear rings (CR and NR). The putative arrangement of Nups with the adaptor scaffold is indicated. The inner ring formed by the adaptor scaffold Nups would contribute to the spoke ring (SR). (B) Localization of the core and adaptor scaffold Nups as determined in the 'computational' model of the NPC symmetric core. Nups are represented by their predicted localization volumes and colored according to subcomplex association (core scaffold heptamer in yellow, adaptor scaffold Nups in purple). The nuclear envelope is indicated in grey. The right panel depicts all 456 Nups included in the analysis for an overall model of the NPC. The luminal ring is colored orange; barrier Nups are divided into linker Nups (pink/blue) and FG-Nups (green). Adapted from Alber et al., 2007b; Brohawn and Schwartz, 2009a.

An extension of this model postulates the positioning of members of the adaptor scaffold as being sandwiched between the core scaffold lattice in the midplane of the NPC (Brohawn and Schwartz, 2009a). The overall height of such an assembly is consistent with the observed height of the *S. cerevisiae* NPC resolved by Cryo-EM (Yang et al., 1998; Kiseleva et al., 2004). While this model draws exciting parallels between the organizational principles of NPCs and coat proteins, much more information is required to validate this model, primarily to resolve how vertically arranged heptamers would interact with one another, and with the underlying adaptor scaffold. Resolution of additional scaffold Nup hetero-dimers and hetero-trimers will presumably shed light on how these interactions might occur.

1.4.3.3 THE COMPUTATIONAL MODEL OF THE NPC

In the absence of structural information provided by analyses of crystal structures of Nups at the atomic level, Rout and colleagues generated a computational model of the entire NPC by integrating numerous proteomic data (Figure 1-10B) (Alber et al., 2007a; Alber et al., 2007b). Data included in the model describe protein shape, stoichiometry, localization as determined by immuno-EM, protein interaction networks, and overall symmetry of the NPC. These data were translated into a series of spatial restraints that were then refined to derive a model for the NPC. This approach was particularly ambitious in that it sought to determine the respective localizations of the ~456 Nups that comprise the yeast NPC. The resulting model described the

concentric ring architecture of the NPC scaffold, with 2 outer rings comprised of the heptameric Nup84p complex sandwiching 2 inner rings comprised of the Nup53-93 adaptor scaffold complex. FG-Nups were appropriately positioned adjacent to the central channel. This model also evaluated the potential positioning of Poms, and predicted the formation of a luminal proteinaceous ring within the NE that circumscribes the NPC. Importantly, this model suggests the horizontal arrangement of scaffold heptamers around the NPC, analogous to that suggested in the fence post model. While the resolution of the resulting computational model is limited to ~50 nm, a detailed analysis of Nup interactions within and between subcomplexes is not possible. It will be interesting to see how future structural models based on atomic-resolution data compare to this structural NPC model generated *in silico*.

Although the composition and higher-order structure of the NPC coat cylinder remain uncertain, all models agree that multiple copies of the Y-shaped heptameric complex are located in the periphery of the NPC core and serve as a coating module (Strambio-De-Castillia et al., 2010; Hoelz et al., 2011; Grossman et al., 2012). Discrepancies between models include the alignment of heptamers and their overall stoichiometry. Resolving these issues will require multidisciplinary approaches to unambiguously define the structure of the NPC coat. For example, visualizing the NPC by Cryo-EM has revealed horizontally positioned Y-shaped structures that might represent the head-to-tail arrangement of heptamers proposed by the fence post and

computational models. Further support for this arrangement has been provided by recent experiments evaluating the orientation of fluorescently tagged Nups of the heptamer (Kampmann et al., 2011). In these experiments, a GFP moiety was rigidly attached to Nup107 and Nup133, and visualized using polarized fluorescence microscopy in live cells. The anisotropy of the resulting fluorescence was then used to determine the orientation of heptamers within the NPC. Results from this experiment unambiguously suggest that the long arm of the heptamer, comprised of Nup107 and Nup133, lies horizontally within the plane of the NE, thus providing the first experimental evidence in support of the fence post and computational models (Kampmann et al., 2011). Intriguingly, similar results were obtained in the evaluation of the orientation of Nic96p of the adaptor scaffold, and suggest that it is arranged horizontally along the NPC perimeter (Kampmann et al., 2011). In general, it will be important to evaluate further data from a multitude of experimental approaches before the architecture of the NPC membrane coat may be conclusively determined.

1.5 MECHANISMS OF NE/NPC ASSEMBLY

While NPCs are generally structurally conserved across species, the dynamics of the NPC life cycle vary markedly. For example, the density of NPCs within the NE varies according to species, cell cycle stage, and differentiation state (Grossman et al., 2012). A typical yeast nucleus contains ~100 NPCs, while the oocytes of *X. laevis* may contain in excess of 5×10^7

NPCs per nucleus (Winey et al., 1997; Frenkiel-Krispin et al., 2010). However, in general, regardless of species or cell type, proliferating cells display a burst of NPC synthesis during S-phase of the cell cycle, such that the total number of NPCs has doubled in preparation for cell division and redistribution of contents to daughter cell nuclei (Maul et al., 1972). Thus, there exists a conserved, sophisticated mechanism linking the rate of NPC biogenesis to the metabolic activity of the cell (Doucet et al., 2010).

The dynamics of the NE and embedded NPCs during the cell cycle differ dramatically between 'lower' unicellular eukaryotes (e.g. yeast and filamentous fungi) and 'higher' eukaryotes (e.g. metazoan cells) (Heath, 1980; De Souza and Osmani, 2009). During mitosis in *S. cerevisiae*, the NE remains intact and spindle microtubules assemble inside the nucleus to facilitate segregation of chromatin. Newly assembled NPCs must be inserted into the continuous double lipid bilayer of the NE. Because of similarities in NE topology (e.g. a sealed NE), the insertion of nascent NPCs formed during interphase of metazoan cells might employ a similar mechanism (discussed below).

In contrast, distribution of heritable material in proliferating cells of metazoa requires disruption of the NE to allow the mitotic spindle access to underlying chromatin (termed 'open' mitosis, summarized in Figure 1-11). Following chromosome segregation, NPCs begin to reassemble on expanding chromatin concomitant with recruitment of NE membranes. It can be

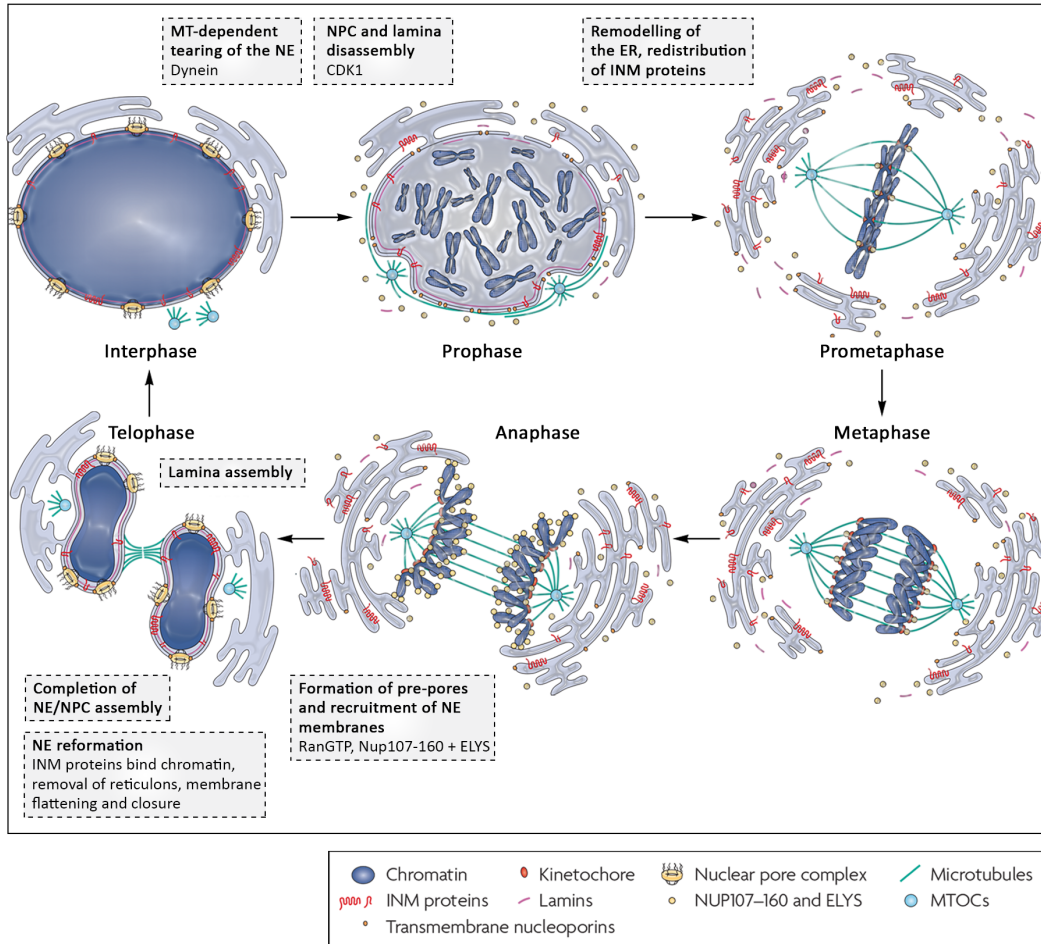


FIGURE 1-11 NUCLEAR ENVELOPE BREAKDOWN AND REASSEMBLY DURING MITOSIS IN METAZOAN CELLS.

The activation of mitotic kinases, including the master mitotic regulator CDK1, triggers entry into prophase. Microtubules that are attached to the nuclear envelope (NE) in conjunction with the minus-end-directed motor dynein lead to NE invaginations around centrosomes and to the formation of holes on the opposing site of the NE. Phosphorylation of Nups triggers NPC disassembly. The transition into prometaphase is marked by the loss of the NE permeability barrier. Phosphorylation of nuclear lamins and INM proteins by CDK1 and other mitotic kinases results in lamina disassembly and allows for the retraction of NE membranes into the mitotic ER network. In metaphase, most soluble components of the NE are dispersed throughout the cytoplasm, whereas INM proteins reside in the tubular mitotic ER. NPC assembly is initiated during anaphase by the recruitment of Nup107-160 complexes to chromatin through ELYS, resulting in the formation of chromatin-bound 'pre-pores'. Binding of INM proteins to DNA/chromatin supports the recruitment of membranes to chromatin. NPC formation is completed by the step-wise recruitment of further NPC constituents and the NE is sealed. Finally, transport-competent NPCs allow for the nuclear import of lamins to complete the assembly of the nuclear lamina. Adapted from Güttinger et al., 2009.

envisaged that the topology of the re-forming NE membrane necessitated the evolution of a unique NE/NPC assembly mechanism to coordinate the assembly of NPCs within the reforming NE. Thus, for organisms undergoing 'open' mitosis, distinct mechanisms likely exist that mediate NPC assembly in different cell cycle stages (Schooley et al., 2012).

1.5.1 POST-MITOTIC NE/NPC ASSEMBLY DURING 'OPEN' MITOSIS

The mechanisms underlying NE/NPC breakdown and subsequent reassembly during mitosis in cells that undergo 'open' mitosis are intimately linked with progression of the cell cycle, and are regulated both spatially and temporally by the actions of mitotic regulators (Guttinger et al., 2009). Mitotic kinases, including the master mitotic regulator Cdk1/CycB, act to modify a myriad of NE associated proteins, including Nups, INM proteins and lamins. This modification initiates a cascade of events during early prophase that leads to complete disruption of the NE and reorganization of its contents, including depolymerization of the nuclear lamina, dispersal of soluble Nups, and redistribution of NE membranes and INM proteins (including Poms) into the mitotic ER network (Figure 1-11). Biochemical evidence suggests that soluble Nups remain associated in mitotically stable subcomplexes, facilitating their efficient reassembly at the resolution of mitosis (Miller and Forbes, 2000; Harel et al., 2003; Walther et al., 2003). Following chromosome segregation in late anaphase, membranes are

recruited to decondensing chromatin, NPCs begin to reassemble within the expanding NE, and nuclear compartmentalization is restored.

Intriguingly, it is becoming clear that many NPC components themselves are critical regulators of cell cycle progression. Mounting evidence has demonstrated that Nups, Importin β , and RanGTP engage in transport-independent roles during mitosis, and are essential effectors of spindle assembly and kinetochore function (for review, see Imamoto and Funakoshi, 2012). The mechanisms underlying mitotic progression have presumably co-evolved with those regulating post-mitotic NE/NPC assembly to coordinate faithful transmission of hereditary material with reestablishment of the permeability barrier.

1.5.1.1 NE BREAKDOWN

The rapid disassembly of the NE during prophase allows for a massive influx of cytoplasmic proteins that orchestrate the myriad of events underlying formation of the mitotic spindle and subsequent mitotic events (for review, see Hetzer, 2010). The dissolution of NE integrity occurs concomitantly with the disassembly of NPCs, culminating at the transition from prophase to prometaphase. A combination of evidence obtained by EM, indirect immunofluorescence, and live-cell confocal imaging has demonstrated that the initiation of NE breakdown (NEBD) is dependent on the actions of mitotic microtubules and the NE associated microtubule motor complex dynein-dynactin (Beaudouin et al., 2002; Salina et al., 2002). This

has led to the proposal of a model of NEBD whereby tension created by the minus-end directed movement of dynein on microtubules creates mechanical stress that results in physical tearing of the NE and underlying nuclear lamina.

1.5.1.2 REGULATION OF NEBD BY PHOSPHORYLATION

The mitotic fates of NE and NPC components in cells undergoing 'open' mitosis are regulated by the actions of mitotic kinases. Phosphorylation sites of a multitude of Nups and NE proteins have been reported by individual studies and large-scale proteomic analyses (Nousiainen et al., 2006; Glavy et al., 2007; Blethrow et al., 2008; Daub et al., 2008; Dephoure et al., 2008; Guttinger et al., 2009). These studies identified consensus sites for mitotic kinases, most often Cdk1, on Nups from virtually all subcomplexes of the NPC, including members of the Nup107-160 complex, the Nup53-93 complex, Nup98, Pom121 and gp210. Importantly, it has been demonstrated that depletion of Cdk1 inhibits NEBD *in vitro*, highlighting the crucial role for this mitotic kinase in regulating NE dynamics (Muhlhauser and Kutay, 2007).

At this time, however, the consequences of such modifications remain largely unknown. In general, protein modification by phosphorylation is thought to interrupt protein-protein interactions, either directly by sterically inhibiting interaction sites, or indirectly by inducing conformational changes within protein structure (Johnson and Barford,

1993). In this way it can be envisaged that phosphorylation would contribute to the dismantling of the NE by leading to the disassembly of NPCs, depolymerization of the lamina, and disruption of INM protein contacts. Indeed, it has been shown that phosphorylation of lamins leads to depolymerization of the lamina network and dispersal of monomeric lamins throughout the mitotic cytoplasm (Gerace and Blobel, 1980; Heald and McKeon, 1990; Nigg, 1992; Hocevar et al., 1993). Phosphorylation of INM proteins triggers the dissociation of intranuclear contacts, allowing their translocation to the ER periphery (Yang et al., 1997; Worman and Courvalin, 2000; Guttinger et al., 2009). Finally, through a less well-understood mechanism, phosphorylation of Nups has been proposed to dissolve the FG-meshwork of the central channel and disrupt interactions between Nup subcomplexes (Macaulay et al., 1995; Favreau et al., 1996; Laurell and Kutay, 2011).

A model has recently developed for the role of phosphorylated Nup98 in the early events of NEBD. Live-cell imaging of GFP-tagged Nups during mitosis has revealed that Nup98 is specifically released from NPCs at the onset of NEBD (Dultz et al., 2008). This is followed by the synchronous disassembly of the NPC central framework. It has since been demonstrated that release of Nup98 from the NPC is dependent on the concerted efforts of multiple mitotic kinases that act to hyperphosphorylate the Nup98 GLFG-repeat domain (Laurell et al., 2011). Presumably, the redundancy provided by requiring the actions of multiple kinases in the initial steps of NEBD

provides a molecular fail-safe to ensure that NPC disassembly is restricted to cells that are fully committed to enter mitosis (Laurell and Kutay, 2011). Further analysis demonstrated that the collective mutation of phosphorylation sites within the Nup98 GLFG domain markedly delayed the onset of NEBD (Laurell et al., 2011). The consequence of hyperphosphorylation of Nup98 GLFG-repeats is not yet fully understood at a molecular level, however it is presumed that this modification aids in disrupting intermolecular cohesion between Nup98 GLFG-repeats within the NPC central channel (Laurell and Kutay, 2011). In this way, the loss of Nup98 would be a critical first step in dissolving the tangled FG-meshwork of the NPC interior. The overall permeability of the NE would be compromised by the resulting 'leaky' pores, allowing for the influx of mitotic regulators required for the completion of NEBD and subsequent mitotic events.

1.5.1.3 COORDINATION OF POST-MITOTIC NE/NPC ASSEMBLY

Reconstructing the nucleus at the end of mitosis requires a dramatic restructuring of the mitotic ER network to form the continuous NE bilayer and establish nuclear compartmentalization with each cell division. NE membranes and INM proteins must be sequestered from the ER reservoir and targeted to the surface of decondensing chromatin. Similarly, Nup subcomplexes, lamins, and other soluble NE components are recruited from the mitotic cytoplasm and assembled into the reforming NE. While a timeline for the recruitment of Nups to the chromatin surface during post-mitotic

NE/NPC assembly has been well established, models describing the recruitment of NE membranes are actively debated (Dultz et al., 2008; Dultz and Ellenberg, 2010; Schooley et al., 2012). At this time, the architecture of the mitotic ER, specifically the local morphology of the ER-chromatin interface during membrane recruitment, remains to be elucidated (Schooley et al., 2012). Approaching a unified model of NE recruitment and membrane expansion is critical, as the topology of the assembling NE directly affects the mechanisms underlying NPC biogenesis.

1.5.1.4 KINETICS OF NUP RECRUITMENT TO THE CHROMATIN SURFACE

The recruitment of Nups to the chromatin surface during post-mitotic NE/NPC assembly has been well documented (Figure 1-12). In a key study, Ellenberg and colleagues (2008) compiled a comprehensive series of GFP-tagged Nups and followed their localization throughout mitosis. From this, a model was proposed that delineated the ordered step-wise recruitment of Nups to the expanding chromatin surface during late anaphase. Importantly, these observations are consistent with previous data obtained using indirect immunofluorescence of cultured mammalian cells and from *X. laevis* nuclear reconstitution assays *in vitro* (Chaudhary and Courvalin, 1993; Bodoor et al., 1999; Belgareh et al., 2001; Daigle et al., 2001; Hetzer et al., 2005).

Post-mitotic NPC assembly is initiated by the recruitment of the

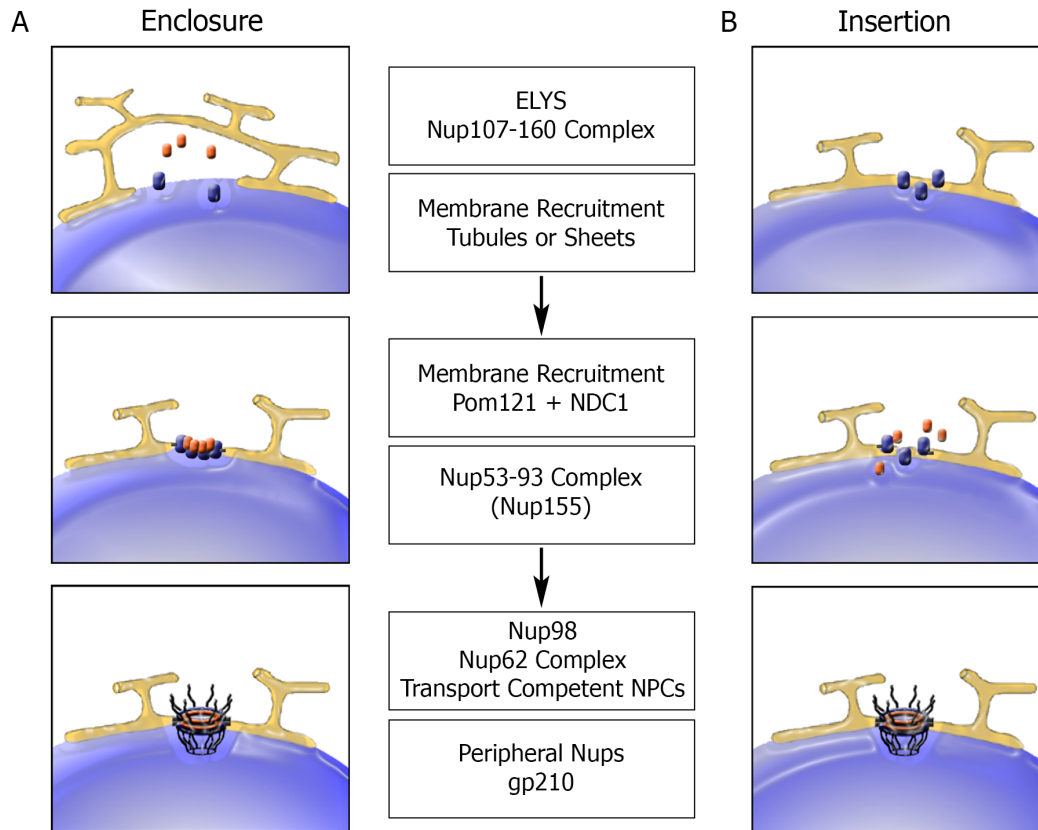


FIGURE 1-12 POTENTIAL MECHANISMS OF NE/NPC ASSEMBLY POST-MITOSIS.

Models depicting either A) enclosure of an NPC pre-pore by lateral expansion of membrane tubules, or B) insertion of nascent NPCs within flattened membrane cisternae. Importantly, in both modes of assembly, the order of recruitment of Nups is the same. The Nup107-160 complex is recruited to the chromatin surface by the AT-hook DNA-binding protein ELYS. Following INM protein-mediated membrane recruitment in the form of membrane tubules (enclosure model) or sheets (insertion model), Pom121 and NDC1 are incorporated into the NPC pre-pore. The recruitment of the Nup53-93 complex is mediated by membrane-associated Nups, Nup53 and Nup155, which interact with Poms at the nascent pore membrane domain. This is followed closely by the addition of FG-Nups including Nup98 and the Nup64 complex, the incorporation of peripheral Nups and remaining transmembrane Nup gp210. Importantly, the insertion of NPCs into an intact NE membrane requires sophisticated, as-yet-unidentified fusion machinery. It should be noted that the order of events is the same for both the enclosure and insertion modes of NPC assembly. Modified from Burke et al., 2002.

Nup107-160 complex to the chromatin surface, where it is anchored in place by the association with DNA-binding protein ELYS (Belgareh et al., 2001; Harel et al., 2003; Walther et al., 2003; Franz et al., 2007). ELYS contains an AT-hook motif at its C-terminus, which facilitates binding to AT-rich chromatin (Rasala et al., 2008). It has been proposed that the Nup107-160 complex forms a 'pre-pore' structure on chromatin, onto which other subcomplexes are assembled (Harel et al., 2003; Walther et al., 2003). As an extension of this, it was suggested that the Nup107-160 pre-pore might self-assemble to form ring-like structures, reminiscent of the cytoplasmic and nucleoplasmic rings of the mature NPC. However, quantitative analyses measuring the fluorescence of GFP-tagged Nup107-160 complex members at the chromatin surface suggest they exist as a monomeric subcomplex until the addition of membranes, and presumably, membrane associated proteins (Lu et al., 2011). This is in agreement with observations by scanning EM that demonstrate structures displaying canonical 8-fold symmetry are not formed until the recruitment of membranes (Maul, 1977; Sheehan et al., 1988; Drummond et al., 2006; Rotem et al., 2009; Lu et al., 2011). Thus, the molecular architecture of the chromatin associated pre-pore remains to be defined.

The establishment of the Nup107-160 pre-pore is followed closely by the recruitment of membranes containing Pom121 and NDC1, and by the association of Nups of the adaptor scaffold. Importantly, depletion of members of the Nup107-160 complex, the Nup53-93 complex, and Pom121

or NDC1 have been shown to inhibit NE/NPC assembly, both *in vitro* and *in vivo*, highlighting their critical role in the early steps in the assembly process (Boehmer et al., 2003; Harel et al., 2003; Antonin et al., 2005; Stavru et al., 2006a; Stavru et al., 2006b; Funakoshi et al., 2007; Hawryluk-Gara et al., 2008; Funakoshi et al., 2011; Shaulov et al., 2011; Talamas and Hetzer, 2011). The FG-repeat containing Nup98 and Nup62 complex are next incorporated into the assembling NPC. At this time, nascent NPCs are capable of mediating selective transport (Dultz et al., 2009). Finally, during expansion of the NE and into G1 of the cell cycle, peripheral Nups comprising the cytoplasmic filaments and nuclear basket are recruited, in addition to the remaining Pomgp210 (Chaudhary and Courvalin, 1993; Bodoor et al., 1999; Burke and Ellenberg, 2002). It should be emphasized that due to the timing of its arrival at the NE, gp210 is not likely to play an important role in the initial stages of post-mitotic NE/NPC assembly.

1.5.1.5 MODELS OF POST-MITOTIC NPC ASSEMBLY: INSERTION VERSUS ENCLOSURE

While the recruitment of Nups to the reforming NE has been well established, it remains unclear how Nups interface with the surrounding NE membranes during NPC assembly, and how this is coordinated with the formation of a sealed NE. Current models of NE/NPC assembly describe either the 'enclosure' of nascent NPCs by NE membranes as they migrate across the chromatin surface, or the 'insertion' of NPCs into an intact NE, much the same way as NPCs are assembled into the continuous NE during

interphase (Figure 1-12). The 'insertion' model is particularly attractive in that it proposes a unifying model for NE/NPC assembly that is applicable to different cell cycle stages and may be conserved across all eukaryotes (Schooley et al., 2012).

A central tenet of the insertion model of NE/NPC biogenesis is the requirement for fusion of ONM and INM leaflets to establish a pore into which the NPC may be inserted. Indeed, the requirement of fusion machinery for nuclear reconstitution *in vitro* has been observed (Hetzer et al., 2001; Baur et al., 2007). These experiments led to a model whereby the hexameric ATPase p97, a component of fusion machinery employed by the ER and golgi organelles during interphase, is required for distinct fusion steps during NPC assembly; first, in a complex with the adaptors Udf1-Npl4, p97 would mediate annular fusion that would resolve gaps in the NE as it is sealed, and second, in a complex with the adaptor protein p47, p97 would mediate point fusion of membranes as they are incorporated into the expanding NE (Hetzer et al., 2001; Kondo et al., 2004). Additional evidence suggested a role for the hexameric ATPase NSF (NEM-sensitive factor). A model was proposed that suggested dimerization of soluble NSF attachment protein receptors (SNAREs) would juxtapose the ONM and INM leaflets to trigger NSF-mediated membrane fusion during NE reformation (Baur et al., 2007).

However, it has since been demonstrated that NE/NPC assembly *in vitro* can occur in the presence of fusion inhibitors, negating a role for p97- or NSF-mediated membrane fusion (Anderson and Hetzer, 2007). It should be

noted that membrane fractions used during *in vitro* NE/NPC assembly assays are highly fragmented as a result of centrifugation, and do not resemble the flattened membrane cisternae characteristic of the mitotic ER of intact cultured cells (Anderson and Hetzer, 2007; Lu et al., 2009). In this regard, it was subsequently demonstrated that membrane fusion during NE/NPC assembly *in vitro* could be circumvented if extracts were incubated in the presence of pre-formed, intact ER cisternae (Anderson and Hetzer, 2007). Instead, it was proposed that the requirement for fusion machinery observed in previous assays represented the reconstitution and maintenance of ER cisternae from membrane vesicles. In summary, potential fusion machinery required for the proposed insertion of nascent NPCs into the NE during post-mitotic NE/NPC assembly remains to be identified.

Alternatively, it has been suggested that NPCs are assembled into the reforming NE by the 'enclosure' of membranes as they spread across the chromatin surface. Importantly, NE/NPC assembly by this model would have necessitated the evolution of a mechanism distinct from that used during interphase. It can be envisaged that membranes recruited to the chromatin surface would engulf Nup107-160 pre-pore structures, which would then, by the addition of Pom121 and NDC1, trigger further NPC assembly within the NE. As membranes spread across the chromatin surface, small gaps would remain that must be sealed to efficiently re-establish the permeability barrier (Burke and Ellenberg, 2002). Several mechanisms have been proposed to mediate this process. First, annular fusion has been suggested as a

mechanism that would seal residual gaps in the NE surface, using as yet unidentified fusion machinery (Burke and Ellenberg, 2002). Second, it has been suggested that reshaping of the NE membrane by interactions between INM proteins and chromatin might facilitate the formation of a sealed NE. In this model, tension generated by the accumulation of INM proteins within the NE would trigger the spontaneous closure of remaining NE gaps (Anderson and Hetzer, 2008). Finally, it has been proposed that residual NE holes might be targeted to sites of NPC assembly. As NE membranes stretch across the surface of expanding chromatin, assembling NPCs would fill remaining gaps formed by the convergence of neighboring cisternae. In this model, resident pore membrane proteins would subsequently recruit membrane scaffold Nups, and NPC assembly would commence within the pre-established pore (Antonin and Mattaj, 2005). In summary, NPC incorporation into the assembling NE via 'enclosure' would require a mechanism distinct from that used for assembly of NPCs into an intact NE.

Several lines of evidence tend toward the enclosure model, without directly supporting it. First, the kinetics of interphase and post-mitotic NPC assembly differ by an order of magnitude, likely reflecting the nuclear environment characteristic of each cell cycle stage (Dultz and Ellenberg, 2010). While the number of NPCs doubles throughout interphase of the cell cycle, NPCs are assembled *en masse* into the rapidly forming NE to efficiently reestablish nuclear compartmentalization following mitosis (Maul et al., 1972; Dultz et al., 2009; Dultz and Ellenberg, 2010). In general, NPCs are

inserted into the intact NE gradually over S-phase of the cell cycle, while a burst of NPC synthesis into the reforming NE is required at the resolution of mitosis. Second, the order of recruitment of Nups to the chromatin surface differs between interphase and post-mitotic assembly. As discussed, post-mitotic NPC assembly is initiated by the binding of Nup107-160 followed by the addition of Pom121 and NDC1, whereas during interphase assembly, Pom121 recruitment clearly precedes incorporation of Nup107-160 (see below) (Doucet et al., 2010; Dultz and Ellenberg, 2010). Finally, cell cycle differences exist in the requirement of different Nups for NPC assembly. For example, chromatin-bound ELYS is essential for post-mitotic NPC assembly, while is dispensable for assembly during interphase (Franz et al., 2007). Alternatively, interphase-specific roles have been described for Nup53 and Nup133, which have been implicated in mediating membrane curvature (discussed below) (Doucet et al., 2010; Vollmer et al., 2012). Based on this evidence, it seems that post-mitotic NPC assembly must employ a mechanism distinct from that used during interphase. Further evidence must be accumulated, however, to unambiguously clarify the mechanism coordinating the post-mitotic assembly of NPCs into the reforming NE.

1.5.1.6 A NE ASSEMBLY 'CHECKPOINT' COORDINATES NPC AND NE ASSEMBLY

A number of important studies have revealed key roles for pore membrane proteins and components of the NPC scaffold in NE/NPC biogenesis in metazoan cells post-mitosis (for review see Hetzer and Wentz,

2009). Using nuclear reconstitution assays *in vitro*, both Pom121 and NDC1 have been shown to be essential for this process (Antonin et al., 2005; Mansfeld et al., 2006; Shaulov et al., 2011). Similarly, Nup53, Nup155, and components of the Nup107–160 complex are also required for NE/NPC assembly. Importantly, they appear to function at distinct assembly steps. While the Nup107–160 complex binds to chromatin in an early step of NPC assembly, Nup53 and Nup155 function later at a step required for the fusion of NE vesicles and the formation of the double membrane NE (Belgareh et al., 2001; Harel et al., 2003; Walther et al., 2003; Franz et al., 2005; Rasala et al., 2006; Franz et al., 2007; Gillespie et al., 2007; Dultz et al., 2008; Hawryluk-Gara et al., 2008; Rasala et al., 2008). Their roles also seem to be linked to those of Pom121 and NDC1, both of which have been proposed to function at a similar point in NE/NPC assembly. Furthermore, the loss of Nup53, Nup155, Pom121, or NDC1 appears to activate a NE assembly checkpoint, which arrests NE assembly after binding of membrane vesicles to chromatin and before formation of the double membrane NE (Antonin et al., 2005; Franz et al., 2005). Importantly, a functional NE assembly checkpoint requires the Nup107–160 complex. Therefore, it seems reasonable to assume that termination of the checkpoint is linked to interactions of the Nup107–160 complex with pore membrane proteins and other members of the NPC scaffold. Investigations aimed towards deciphering these interactions are described in detail in Chapter III and V.

1.5.2 NE/NPC ASSEMBLY DURING INTERPHASE

In preparation for cell division and distribution of NPCs to daughter cells, the number of NPCs doubles during S-phase of the cell cycle (Maul et al., 1971; Maul et al., 1972). In addition, NPC numbers in non-proliferating cells vary according to metabolic demand and during differentiation (Maul et al., 1971; Doucet et al., 2010). This requires the insertion of nascent NPCs into the continuous NE lipid bilayer, necessitating the fusion of ONM and INM leaflets. This mode of NPC assembly is conserved across all eukaryotes, regardless of the assembly mechanism used during open or closed mitosis. As discussed, while it is theoretically possible that mechanisms employed by metazoan cells during interphase and post-mitotic NPC assembly are the same, recent evidence highlights important differences between the two and suggests that they occur through distinct pathways (Doucet and Hetzer, 2010; Doucet et al., 2010). In general, it is thought that the juxtaposition of ONM and INM leaflets during NPC assembly during interphase might require the use of a specific subset of Nups able to facilitate specific membrane curvature events, distinct from those used post-mitosis. While little is known about the mechanism underlying interphase NPC assembly in metazoan cells, the ease of genetic manipulation of *S. cerevisiae* has allowed the identification of several key players in the assembly process. Integrating information obtained from studies in yeast and metazoan cells is beginning to reveal an overarching, conserved model for interphase NPC assembly.

Observations made by several groups have implicated roles for Poms Ndc1p, Pom152p, and Pom34p, as well as Nup53p, Nup59p, Nup157p, and Nup170p of the adaptor scaffold complex during NPC assembly of *S. cerevisiae* (Flemming et al., 2009; Makio et al., 2009; Onischenko et al., 2009; Rexach, 2009). The mechanism whereby these Poms and Nups likely contribute to NPC assembly was elegantly deciphered by integrating information obtained through biochemical and phenotypic analyses of combinations of genetic defects. In general, NPC numbers are reduced upon deletion of specific combinations of Poms and/or scaffold Nups (Makio et al., 2009; Onischenko et al., 2009). Intriguingly, visualization of the NE in these cells by EM revealed the formation of specific nuclear and cytoplasmic NPC assembly intermediates, suggesting a role for these proteins in the insertion of nascent NPCs into the intact NE. Importantly, these NPC assembly intermediates remained functional, and could be used to initiate NPC assembly following reversal of the specific genetic block (Onischenko et al., 2009). Together, these studies established important connections between Poms and adaptor scaffold Nups and highlight their critical roles in NPC assembly. These results led to the proposal of a model that describes the initial recruitment of Ndc1p, Pom152p, and Pom34p to sites of NPC assembly (Rexach, 2009). This is followed by recruitment of lipophilic Nup53p/Nup59p due to the association of its amphipathic C-terminal helix with NE membranes, and direct interactions with Ndc1p (Marelli et al., 2001; Onischenko et al., 2009). Next, the scaffolding Nup170p/Nup57p is recruited

through interactions with Pom152p, where it is proposed to participate in stabilizing membrane curvature (Makio et al., 2009; Rexach, 2009). Together, the Poms and adaptor scaffold Nups establish a platform within the NE onto which further Nups are assembled.

It has been demonstrated that the temporal recruitment of Nups during interphase assembly in metazoan cells occurs in a similar order as in yeast. In metazoa, interphase NPC assembly initiates with the gradual accumulation of Pom121 at sites of future assembly (Doucet et al., 2010; Dultz and Ellenberg, 2010; Funakoshi et al., 2011; Talamas and Hetzer, 2011). This is followed by the rapid, synchronous recruitment of the scaffolding Nup107-160 and Nup53-93 complexes (Dultz and Ellenberg, 2010). Importantly, essential roles for members of each scaffolding complex during interphase NPC assembly have been defined (Doucet et al., 2010; Vollmer et al., 2012).

It was recently revealed that Nup133, a member of the Nup107-160 complex, contains a membrane-binding ALPS motif within its N-terminal β -propeller (Drin et al., 2007). ALPS motifs are characterized by their ability to target membranes with strong positive curvature. Intriguingly, the ALPS motif of Nup133 is unique to metazoan cells, and is absent from Nup133p of *S. cerevisiae*. Instead, ALPS motifs have been predicted in other members of yeast scaffolding complexes, including Nup85p, Nup120p, and Nup170p (Drin et al., 2007). Whether these motifs represent *bone fide* membrane curvature-sensing domains remains to be established. It has been

demonstrated, however, that the ALPS motif of metazoan Nup133 is capable of sensing membranes of high curvature both *in vitro* and *in vivo* (Drin et al., 2007; Doucet et al., 2010). Furthermore, in experiments where depletion of endogenous Nup133 was supplemented with either wild-type or ALPS-mutant GFP-Nup133, it was revealed that the Nup133 ALPS motif is required specifically for NPC assembly during interphase (Doucet et al., 2010). Together, it was proposed that Nup133 targets the Nup107-160 scaffolding complex specifically to fusion sites at the ONM and INM junction. In this way, Nup133 ALPS would aid in stabilizing the highly curved pore membrane domain during membrane fusion events that occur specifically during interphase NPC assembly.

An interphase-specific NPC assembly role has additionally been described for Nup53. It has been demonstrated previously that Nup53 is intimately linked to the pore membrane domain through an interaction with Lamin B and NDC1, and is essential for NPC assembly *in vivo* (Hawryluk-Gara et al., 2005; Hawryluk-Gara et al., 2008). Depletion of Nup53 using siRNA causes a decrease in cellular levels of Nup53-interacting proteins, including Nup93, Nup155, and Nup205, and a reduction in the number of NPCs (Hawryluk-Gara et al., 2005). Conversely, overexpression of Nup53p in *S. cerevisiae* has been demonstrated to cause massive proliferation of the NE (Marelli et al., 2001). Recent investigations have uncovered the molecular elements that may contribute to these phenotypes (Vollmer et al., 2012). Nup53 is comprised of two membrane-binding domains, separated by an

RNA-recognition motif (RRM) (Handa et al., 2006; Vollmer et al., 2012). While it is theoretically possible the Nup53 RRM mediates interactions with oligonucleotides, a role for this domain has been demonstrated in mediating Nup53 dimerization (Handa et al., 2006; Vollmer et al., 2012). Furthermore, dimerization markedly increases the avidity of Nup53 for membranes. Molecular dissection of the function of Nup53 domains demonstrated that while either membrane-binding domain is sufficient for post-mitotic NPC assembly, NPC assembly during interphase specifically requires the C-terminal membrane-binding α -helix (Vollmer et al., 2012). This is in contrast to previous work that established a role for the Nup155-binding domain of Nup53 during post-mitotic NPC assembly *in vitro* (Hawryluk-Gara et al., 2008). Together, it has been proposed that Nup53 binds and distorts NE membranes in the vicinity of NPC assembly intermediates, thereby linking members of the Nup53-93 complex to the pore membrane domain. These membrane distortions may contribute to the formation of the pore membrane domain, which would be stabilized by the downstream recruitment of scaffolding Nups (Vollmer et al., 2012).

Finally, an interphase-specific role has been described for Pom121 in NPC assembly (Doucet et al., 2010; Funakoshi et al., 2011; Talamas and Hetzer, 2011). Using *X. laevis* nuclear reconstitution assays, it was demonstrated that in the absence of Pom121, NPCs failed to assemble into the expanding, intact NE (Doucet et al., 2010). This was supported by observations that suggested the complete inhibition of NPC assembly

following Pom121 depletion during interphase of synchronized cells *in vivo* (Doucet et al., 2010). Intriguingly, overexpression of Pom121 in U2OS cells markedly affected NE structure, causing an increase in the juxtaposition of INM and ONM leaflets. This suggested that Pom121 is able to influence the architecture of the NE in such a way that might be utilized during NPC assembly into an intact NE (Talamas and Hetzer, 2011). The mechanism whereby Pom121 mediates interphase NPC assembly has not yet been determined. To better define a role for Pom121 in NPC assembly, both during interphase and post-mitosis, requires an understanding of the way in which this transmembrane Nup interacts with the surrounding scaffold NPC core. Experiments aimed toward deciphering the Pom121 interaction network are described in Chapter III and V.

1.6 THESIS FOCUS

NPC assembly within the surrounding NE is dependent on a specialized subset of structural proteins that polymerize into a membrane-coating scaffold that stabilizes the energetically unfavorable membrane curvature of the POM. We characterized a role for one such scaffold Nup, Nup155, in NPC assembly through a mechanism that likely involves its association with surrounding Poms NDC1 and Pom121. We extended our analysis to investigate Pom121 interactions with additional scaffold Nups, and expanded the repertoire of Pom121 interactors to include members of the conserved Nup107-160 core scaffold complex: Nup37, Nup43, and

Nup160. To better understand the evolution of the NPC membrane scaffold, we solved the atomic structure of a complex between orthologues of Nup160 and Nup37 from *S. pombe*. Our data are consistent with a model whereby Pom121 links key structural modules of the NPC to the surrounding pore membrane through interactions with β -propeller domains of Nup37, Nup43, Nup155 and Nup160, and that these interactions are critical for the assembly of the NPC within the NE.

CHAPTER II: EXPERIMENTAL PROCEDURES

2.1 PLASMID CONSTRUCTION

The open reading frames (ORFs) of proteins, or fragments thereof, described in Tables 2.1 and 2.2 were amplified using the Phusion® High-Fidelity PCR Kit (New England BioLabs Inc., Ipswich, MA). cDNA of Nup155 (1-509) was generated and subsequently amplified using the SuperScript™ One-Step RT-PCR System with Platinum® Taq DNA Polymerase (Invitrogen™, Burlington, ON). PCR products were purified using the QIAquick PCR Purification kit (QIAGEN, Mississauga, ON). Purified DNA was digested with 10U of restriction endonuclease, as outlined in Tables 2.1 and 2.2 (NEB), for 24 hours at 37 °C. Digested DNA was purified using the QIAquick Gel Extraction kit (QIAGEN), and ligated into the indicated vectors at a 3:1 molar ratio using the Quick Ligation™ kit (NEB). Ligated constructs were transformed into Subcloning Efficiency™ DH5α™ Competent Cells (Life Technologies, Grand Island, NY). Successful ligations were determined by colony PCR using Taq DNA Polymerase (NEB) with gene-specific forward DNA primers and vector-specific reverse DNA primers. Positive constructs were isolated from overnight cultures of DH5α cells using the QIAprep Spin Miniprep kit (QIAGEN). The presence and orientation of cDNAs within the indicated vector was further confirmed by sequence analysis performed by GENEWIZ, Inc. (South Plainfield, NJ) and Biotic Solutions (MCLAB, San Francisco, CA).

Of note, the cDNA clone used to generate Nup160^{37-1327ΔC} contains small deletions of the both the N- and C-termini, corresponding to amino acid

residues 1-36, 1328-1402, and 1410-1420 of full length Nup160 (1436 amino acid residues in length; NCBI reference sequence NP_056046.1). The Nup160 construct created using this cDNA as a template is referred to as Nup160^{37-1327ΔC} throughout this thesis.

KIAA cDNA clones were obtained from the Kazusa DNA Research Institute (Japan). The Human Fetal Kidney (HFK) cDNA library was obtained from BD Biosciences (San Jose, CA). IMAGE cDNA clone MGC:150678 (Clone Id 40124592) encoding the ORF of Human Nup160 was obtained from Thermo Fisher Scientific Inc. (Waltham, MA). Additional cDNAs encoding Human Nup37 and Nup160 were obtained from A. Hoelz.

TABLE 2-1 TABLE OF CONSTRUCTS FOR EXPRESSION IN *E. COLI*.

Vector	Protein	Insert		Tag		RE		Template
		aa Start	aa Stop	N-Term	C-Term	N-Term	C-Term	
pGEX-6P1	Nup155	1	509	GST	-	EcoRI	NotI	HeLa RNA
pGEX-6P1	Nup155	60	1391	GST	-	EcoRI	EcoRI	KIAA0791
pGEX-6P1	Nup155	510	1391	GST	-	EcoRI	NotI	KIAA0791
pGEX-6P1	Nup155	757	1391	GST	-	EcoRI	NotI	KIAA0791
pGEX-6P1	Pom121	215	557	GST	-	NotI	NotI	KIAA0618
pGEX-6P1	Pom121	215	1249	GST	-	NotI	NotI	KIAA0618
pGEX-6P1	Pom121	558	1249	GST	-	NotI	NotI	KIAA0618
pGEX-6P1	Pom121	364	458	GST	-	NotI	NotI	KIAA0618
pGEX-6P1	Nup160	37	444	GST	-	BamHI	NotI	KIAA0197
pGEX-6P1	Nup160	37	490	GST	-	BamHI	NotI	KIAA0197
pGEX-6P1	Nup160	37	1327ΔC	GST	-	BamHI	NotI	KIAA0197
pGEX-6P1	Nup160	1	1436	GST	-	BamHI	NotI	MGC:150678
pGEX-6P1	Nup160	491	1436	GST	-	BamHI	NotI	MGC:150678
pGEX-6P1	Nup160	968	1436	GST	-	BamHI	NotI	MGC:150678
pGEX-6P1	Nup98	316	920	GST	-	BamHI	NotI	HFK cDNA Lib.
pGEX-6P1	NDC1	292	674	GST	-	EcoRI	NotI	HFK cDNA Lib.
pGEX-6P1	Sec13	1	322	GST	-	EcoRI	NotI	HFK cDNA Lib.
pGEX-6P1	Seh1	1	421	GST	-	BamHI	NotI	HFK cDNA Lib.
pGEX-6P1	Sec31	1	560	GST	-	EcoRI	NotI	HFK cDNA Lib.
pGEX-6P1	Nup53	1	326	GST	-	Hawryluk-Gara et al., 2005		
pGEX-6P1	Pom152p	1	111	GST	-	Makio et al., 2009		
pGEX-4T1	Nup170p	1	1502	GST	-	Makio et al., 2009		

TABLE 2-2 TABLE OF CONSTRUCTS FOR EXPRESSION IN HIGH FIVE™ CELLS.

Vector	Protein	Insert		Tag		RE		Template
		aa Start	aa Stop	N-Term	C-Term	N-Term	C-Term	
pFastBac-HT	ScNup120	1	729	His ₆	-			Seo et al., 2009
pFastBac-HT	SpNup120	1	1136	His ₆	-	EcoRI	NotI	Sp Genomic DNA
pFastBac-HT	SpNup120	1	950	His ₆	-	EcoRI	NotI	Sp Genomic DNA
pFastBacDualMCSII	SpNup37	1	391	-	-	EcoRI	NotI	Sp Genomic DNA
pFastBacDualMCSII	Nup37	1	326	-	-	EcoRI	NotI	Nup37 cDNA
pFastBacDualMCSI	Pom121	215	557	His ₆	-	BamHI	NotI	KIAA0618
pFastBac-HT	Nup160	1	485	His ₆	FLAG	BamHI	XhoI	Nup160 cDNA
pFastBac-HT	Nup160	1	514	His ₆	FLAG	BamHI	XhoI	Nup160 cDNA
pFastBac-HT	Nup160	1	553	His ₆	FLAG	BamHI	XhoI	Nup160 cDNA
pFastBac-HT	Nup160	1	562	His ₆	FLAG	BamHI	XhoI	Nup160 cDNA
pFastBac-HT	Nup160	1	583	His ₆	FLAG	BamHI	XhoI	Nup160 cDNA
pFastBac-HT	Nup160	1	633	His ₆	FLAG	BamHI	XhoI	Nup160 cDNA
pFastBac-HT	Nup160	1	666	His ₆	FLAG	BamHI	XhoI	Nup160 cDNA
pFastBac-HT	Nup160	1	751	His ₆	FLAG	BamHI	XhoI	Nup160 cDNA
pFastBac-HT	Nup160	1	786	His ₆	FLAG	BamHI	XhoI	Nup160 cDNA
pFastBac-HT	Nup160	1	872	His ₆	FLAG	BamHI	XhoI	Nup160 cDNA
pFastBac-HT	Nup160	1	885	His ₆	FLAG	BamHI	XhoI	Nup160 cDNA
pFastBac-HT	Nup160	1	905	His ₆	FLAG	BamHI	XhoI	Nup160 cDNA
pFastBac-HT	Nup160	1	921	His ₆	FLAG	BamHI	XhoI	Nup160 cDNA
pFastBac-HT	Nup160	1	953	His ₆	FLAG	BamHI	XhoI	Nup160 cDNA
pFastBac-HT	Nup160	1	974	His ₆	FLAG	BamHI	XhoI	Nup160 cDNA
pFastBac-HT	Nup160	1	992	His ₆	FLAG	BamHI	XhoI	Nup160 cDNA
pFastBac-HT	Nup160	1	1012	His ₆	FLAG	BamHI	XhoI	Nup160 cDNA
pFastBac-HT	Nup160	1	1074	His ₆	FLAG	BamHI	XhoI	Nup160 cDNA
pFastBac-HT	Nup160	1	1136	His ₆	FLAG	BamHI	XhoI	Nup160 cDNA
pFastBac-HT	Nup160	1	1208	His ₆	FLAG	BamHI	XhoI	Nup160 cDNA
pFastBac-HT	Nup160	1	1256	His ₆	FLAG	BamHI	XhoI	Nup160 cDNA
pFastBac-HT	Nup160	1	1281	His ₆	FLAG	BamHI	XhoI	Nup160 cDNA
pFastBac-HT	Nup160	1	1303	His ₆	FLAG	BamHI	XhoI	Nup160 cDNA
pFastBac-HT	Nup160	1	1318	His ₆	FLAG	BamHI	XhoI	Nup160 cDNA
pFastBac-HT	Nup160	1	1333	His ₆	FLAG	BamHI	XhoI	Nup160 cDNA
pFastBac-HT	Nup160	1	1400	His ₆	FLAG	BamHI	XhoI	Nup160 cDNA
pFastBac-HT	Nup160	1	953	His ₆	-	BamHI	XhoI	Nup160 cDNA

2.2 PURIFICATION OF RECOMBINANT PROTEINS FROM *E. COLI*

pGEX based plasmids were transformed into *E. coli* BL21-CodonPlus(DE3)-RIL competent cells (Agilent Technologies Inc., La Jolla, CA). Cells were grown to an OD₂₆₀ of 0.8, and production of GST-fusion proteins was induced using 1 mM IPTG for 4 hrs at 20 °C. Cells were collected by centrifugation and resuspended in lysis buffer consisting of 50 mM Tris, pH

7.5, 300 mM NaCl, 150 mM KOAc, 2 mM MgOAc, 10% glycerol, 0.1% Igepal (Sigma-Aldrich Inc., St. Louis, MO), 1 mM DTT and Complete Protease Inhibitor Cocktail tablets (Roche Applied Science) (60 ml of buffer/g pellet). Cell suspensions were sonicated and then clarified by centrifugation at 27 000 x *g* for 20 min. GST-fusion proteins were isolated using Glutathione (GSH) Sepharose™ 4B Media (GE Healthcare, Baie d'Urfe, QC). Following repeated washing, bead-bound recombinant proteins were incubated with lysis buffer supplemented with 2 mM ATP and 10 mM MgSO₄ for 10 min at 37 °C. Protein yield was estimated using SDS-PAGE followed by staining with Bio-Safe Coomassie (Bio-Rad Laboratories Inc., Mississauga, ON). Bead-bound recombinant proteins were used directly in pulldown assays with NE extracts or for binding purified recombinant proteins (see below). Pom121²¹⁵⁻⁵⁵⁷ and NDC1²⁹²⁻⁶⁷⁴ were released from beads using PreScission Protease (GE Healthcare) for 16 hrs at 4 °C, and subsequently used in direct *in vitro* binding experiments (see below).

2.2.1 GENERATION OF ANTI-NUP ANTIBODIES

Recombinant proteins used for the purpose of eliciting antibodies in rabbits (including Nup98⁴⁹⁶⁻⁸⁵⁵, Nup155¹⁻⁵⁰⁹, Nup155⁷⁵⁷⁻¹³⁹¹, Nup160³⁷⁻⁴⁹⁰, Ndc1²⁹²⁻⁴⁴⁹, and Pom121²¹⁵⁻⁵⁵⁷) were released from GSH Sepharose media by proteolysis using PreScission Protease (GE Healthcare) for 16 hrs at 4 °C. After repeated washing of the beads, pooled eluates were concentrated to 0.1 mg of protein/ml. Approximately 100 mg of purified protein was injected

into rabbits concomitantly with Freund's adjuvant (Sigma-Aldrich Inc., St. Louis, MO), and sera were subsequently collected at four-week intervals .

2.3 SUBFRACTIONATION AND EXTRACTION OF NUCLEAR ENVELOPES

Subfractionation of rat liver nuclei was performed as previously described (Blobel and Potter, 1966; Wozniak et al., 1989). Livers harvested from Sprague-Dawley rats were washed in 0.25 M STEAKM (0.25 M sucrose, 50 mM triethanolamine, 25 mM KCl, 5 mM MgCl₂, 0.5 mM PMSF and 1 mM DTT), and minced using ethanol-washed razor blades. The triturate was further homogenized in 2 x 0.25 M STEAKM (v/w) using a chilled Potter homogenizer, and filtered through cheesecloth prior to centrifugation for at 4 °C for 10 min at 800 x *g*. Pellet fractions were collected, briefly homogenized and diluted with 2 x 2.3 M STEAKM (v/v) (2.3 M sucrose, 50 mM triethanolamine, 25 mM KCl, 5 mM MgCl₂, 0.5 mM PMSF, 1 mM DTT). The diluted homogenate was layered over a cushion of 2.3 M STEAKM and centrifuged at 4 °C for 75 min at 140 000 x *g*. Nuclei in the pellet fraction were harvested, resuspended in 0.25 M STEAKM, and stored at -80 °C.

Nuclei were ruptured by successive rounds of nuclease digestion (Dwyer and Blobel, 1976). NEs obtained from this procedure were pelleted in 100 A₂₆₀ unit fractions (1 A₂₆₀ unit represents the amount of material derived from ~3 x 10⁶ nuclei (Aaronson and Blobel, 1974), and proteins were extracted from membranes as previously described (Radu et al., 1993). Briefly, NEs were extracted with 1% Triton X-100, 400 mM NaCl, 20 mM Tris,

pH 7.5, 1 mM DTT, and Complete Protease Inhibitor Cocktail tablets. Insoluble material was pelleted by centrifugation at 20 000 x *g* for 20 min at 4 °C. The supernatant fraction was further clarified by syringe filtration using a 0.22 mm filter (Millipore Corp., Billerica, MA), diluted 3.75 fold in 20 mM Tris, pH 7.5, and supplemented with Tween20 (final concentration: 20 mM Tris, pH 7.5, 106 mM NaCl, 0.3% Triton X-100, 0.1% Tween20, 66 A₂₆₀ of NE/ml). These NE extracts were used immediately in GST-pulldown assays.

The handling and exsanguination of rats used in this study was performed in accordance with guidelines appointed by the Animal Care & Use Committee for Biosciences, University of Alberta.

2.4 GST-PULLDOWN ASSAYS FROM ISOLATED NE

NE extracts derived from ~30 A₂₆₀ units of nuclei were incubated with bead-bound recombinant proteins (~5-10 mg) for 4 hrs at 4 °C. Following binding, beads were extensively washed in a buffer containing 20 mM Tris, pH 7.5, 106 mM NaCl, 0.3% Triton X-100, 0.1% Tween20, 1 mM DTT, and Complete Protease Inhibitor Cocktail tablets. Bound proteins were eluted from beads using SDS-sample buffer and resolved by SDS-PAGE. Proteins were visualized using Bio-Safe coomassie blue stain (Bio-Rad), silver staining, or were transferred to nitrocellulose for western blot analysis (see below).

2.5 DIRECT *IN VITRO* BINDING EXPERIMENTS

To assess direct protein-protein interactions using recombinant proteins, ~1-5 μg of purified recombinant protein was incubated with ~ 1 mg of the bead-bound GST-fusion protein for 30 min at 4 °C. After repeated washing with lysis buffer, proteins were eluted from beads using SDS-sample buffer and resolved by SDS-PAGE. Proteins were visualized using Bio-Safe coomassie blue stain (Bio-Rad). Bound proteins were transferred to nitrocellulose following SDS-PAGE and detected using specific polyclonal antibodies.

2.6 RNA INTERFERENCE

The sequences of siRNA oligonucleotides used for experiments described within this thesis are provided in Table 2.3. *Silencer*® Pre-designed siRNAs targeting exon 2 (catalogue #138652), the exon 8/9 junction (catalogue #110275), and exon 27 (catalogue #110276) of Nup155 mRNA were obtained from Ambion Inc. (Austin, TX). siRNAs were additionally designed to target the Nup155 exon 4/5 junction, Pom121, NDC1 and gp210 (QIAGEN). Non-specific siRNAs used as controls in siRNA experiments were designated nonsense and control (QIAGEN).

TABLE 2-3 **TABLE OF OLIGONUCLEOTIDES USED FOR RNA INTERFERENCE.**

Target	Sequence
Nup155 exon 2	5'-r[CCGUUUCUGGCAUGUCAGA]dT-3'
Nup155 exon 4/5	5'-r[GCAGGCAUCUUUCAACCUC]dT-3'
Nup155 exon 8/9	5'-r[GGAGUAAUACAGGUGUAUG]dT-3'
Nup155 exon 27	5'-r[GGAUGAGCUCUUUAGUAUU]dT-3'
Pom121	5'-r[CAGUGG CAGUGGACAUUCA]dT-3'
NDC1	5'-r[CUGCACCACAGUAUUUAUU]dT-3'
gp210	5'-r[GAACCUCCAUUCACUACA A]dT-3'
Nonsense	5'-r[AAAGCGCAUUGCGCAUACG]dT-3'
Control	5'-r[CUGUGCAAGCCG UUGUGUA]dT-3'

To deplete Nup155, HeLa cells were transfected with 480 nM siRNA using Oligofectamine (Invitrogen). Cells were harvested at 24, 48, and 72 hr time points and analyzed by immunofluorescence or western blot analysis (see below). As a control, cells were incubated with nonsense siRNA or with transfection reagent alone. This protocol was additionally used to deplete Nup155 from HeLa cells expressing ectopic GST-GST-cNLS (Erkman et al., 2005) and from HeLa cells stably expressing Pom121-EGFP3 (Rabut et al., 2004).

To deplete the pore membrane proteins Pom121, NDC1, and gp210, HeLa cells were transfected with 35 nM of the indicated siRNAs using Oligofectamine (Invitrogen). As a control, cells were alternatively left untreated or incubated with control siRNA. Seventy-two hrs after transfection, cells were analyzed by immunofluorescence or western blot analysis (see below).

2.7 WESTERN BLOTTING

2.7.1 SAMPLE PREPARATION

Prior to western blotting, HeLa cells grown in 35 mm dishes were detached using 0.05% Trypsin-EDTA (Invitrogen) and then washed with PBS. Cell pellets were resuspended in SDS-sample buffer at a concentration of $\sim 10^4$ cells/ml, yielding a total protein concentration of ~ 1 mg/ml. Samples were briefly sonicated and denatured at 95 °C for 2 min. Approximately 10 μ g of total protein was resolved by SDS-PAGE and transferred to nitrocellulose. Proteins extracted from NEs were precipitated in 10 % TCA and resuspended in SDS-sample buffer (0.1 A_{260} units/ml). 1 A_{260} unit was resolved by SDS-PAGE and transferred to nitrocellulose (Load fractions). Membranes were blocked with 5% skim milk powder in PBS-T (PBS containing 0.1% Tween20).

2.7.2 ANTIBODIES

Membranes were incubated overnight at 4 °C with anti-sera diluted in 5% milk-PBS-T. Antibodies directed against Nup155, NDC1, Pom121 and Nup98 are described above. Antibodies directed against Nup53 (Hawryluk-Gara et al., 2005), Nup107 (kindly provided by V. Doye; Belgareh et al., 2001), Nup205 (kindly provided by U. Kutay; Mansfeld et al., 2006), gp210 (IQ294; ImmuQuest Ltd., North Yorkshire, UK), and Lamin B (Chaudhary and Courvalin, 1993), Lem2 (kindly provided by I. Mattaj, (Ulbert et al., 2006a)

and LBR (kindly provided by H. Herrmanns, (Buendia and Courvalin, 1997) were previously described. Polyclonal guinea pig antibodies directed against Nup93 were kindly provided by V. Cordes. Commercially available monoclonal antibodies were used to detect Nup62, Nup153, Nup214 and Nup358 (using mAb414 MMS-120p; Covance Inc., Laval, QC), Tubulin (T9026; Sigma-Aldrich), Lap2 (611000; BD Biosciences), and HuR (3A2; Santa Cruz Biotechnology). HRP-conjugated secondary antibodies used to detect primary antibodies included goat anti-guinea pig IgG (Sigma-Aldrich), donkey anti-rabbit IgG, and sheep anti-mouse IgG (GE Healthcare). Chemiluminescence was initiated using ECL detection reagent (GE Healthcare) and the signal was detected using Fuji RX film (FUJIFILM Canada Inc., Mississauga, ON).

2.8 IMMUNOFLUORESCENCE, IMAGE ACQUISITION, AND IMAGE PROCESSING

HeLa cells grown on coverslips were rinsed with PBS and then treated with 0.2 % Triton X-100 in PBS for 2 min. Coverslips were gently washed to remove detergent and fixed with 3.75 % formaldehyde in PBS for 10 min. Following a PBS wash, coverslips were incubated with 2 % skim milk powder in PBS-T for 30 min, followed by incubation with primary antibodies diluted in 2 % milk-PBS-T for 2 hr at room temperature. Primary antibodies used for immunofluorescent detection are listed above. Primary antibody binding was detected with fluorophore-conjugated secondary

antibodies, including Cy3-conjugated donkey anti-mouse IgG, Cy3-conjugated donkey anti-guinea pig IgG (Jackson ImmunoResearch Laboratories, Westgrove, PA), and Alexa Fluor® 488 donkey anti-rabbit IgG (Invitrogen). Secondary antibodies were diluted in PBS-T containing the nuclear DNA stain DRAQ5™ (1 mM, Biostatus Ltd., Leicestershire, UK). Coverslips were mounted on glass slides using Fluoromount-G (Electron Microscopy Sciences, Hatfield, PA).

Some deviations from the protocol outlined above were used. 1) For the results presented in Figure 3-2E, HeLa cells expressing ectopic GST-GFP-cNLS were first fixed with 3.75 % formaldehyde in PBS and then permeabilized with 0.2 % Triton X-100 in PBS. 2) For the results presented in Figure 3-9, 1 % paraformaldehyde in PBS was used in place of formaldehyde, and 2 % BSA was used in place of skim milk powder. 3) To further investigate the localization of Lap2 following Nup155 depletion (Figure 3-5), 0.005 % Digitonin (EMD Chemicals Inc., Darmstadt, Germany) was used in place of Triton X-100, and PBS was used in place of PBS-T (Joseph et al., 2002).

Micrographs were obtained using a Zeiss LSM510 laser scanning system coupled with a Zeiss Axiovert 100M and 63X plan-apochromat objective (Carl Zeiss MicroImaging Inc., Thornwood, NY). Images were acquired using LSM 5 software (Carl Zeiss MicroImaging) and processed using ImageJ 1.42q software (National Institutes of Health, Bethesda, MD; Abramoff, 2004).

For visualization of the GST-GFP-cNLS reporter protein following Nup155 depletion, images were obtained using a Zeiss Observer Z1 coupled with an AxioCam MRm (Carl Zeiss MicroImaging). Images were acquired as a series of Z-stacks (~ 15 sections), and were deconvolved using Axiovision software (Carl Zeiss MicroImaging). Subsequent image processing was performed using ImageJ software (Abramoff, 2004). Z-series are displayed as average intensity Z-projections.

2.9 TRANSMISSION ELECTRON MICROSCOPY

HeLa cells analyzed by transmission electron microscopy were released from culture dishes using 0.05 % Trypsin, pelleted, and then washed with PBS. Cell pellets were fixed with 2.5 % Gluteraldehyde, 0.1 M Cacodylate, pH 7.4 for 24 hr. Pellets were washed repeatedly with 0.1 M Cacodylate, followed by staining with 1 % OsO₄ in 0.1 M Cacodylate for 1 hr. Pellets were rinsed with distilled water and dehydrated through progressive ethanol washes of increasing concentration (10 min each; 60 %, 80 %, 95 %, 100 % ethanol). Pellets were further treated with 100 % Propylene Oxide (3 x 10 min washes), incubated in Propylene Oxide containing Epon (1:1), and finally embedded in 100 % Epon at 65°C for 24 hr. Once cured, blocks were sectioned. These resulting sections were examined using a Philips 410 transmission electron microscope (Philips/FEI Corporation, Eindhoven, Holland) and images were acquired using a Megaview III CCD camera (Soft Imaging System/Olympus, Lakewood, CO) and AnalySIS software (Soft

Imaging System). Images were subsequently processed using ImageJ. The number of NPCs per mm of distance along the NE was manually counted and data presented using Excel. Data from three independent experiments were statistically analyzed using InStat (GraphPad Software Inc., La Jolla, CA).

2.10 MASS SPECTROMETRY

Proteins detected by Coomassie Blue staining in pulldown experiments using GST-Pom121³⁶⁴⁻⁴⁵⁸ or GST-Pom152p¹⁻¹¹¹ were excised from SDS-polyacrylamide gels and subjected to in-gel trypsin digestion followed by LC-MS/MS using a Q-TOF Premier mass spectrometer (Waters Corp., Milford, MA). Protein identification was performed by peptide mass fingerprinting using PEAKS mass spectrometry software (Bioinformatics Solutions Inc., Waterloo, ON).

2.11 PURIFICATION OF RECOMBINANT PROTEINS FROM INSECT CELLS IN LARGE SCALE

2.11.1 GENERATING RECOMBINANT BACMIDS

Approximately 100 ng of pFastBac constructs generated as outlined in Table 2.2 were incubated with 100 μ l of MAX Efficiency[®] DH10Bac[™] chemically competent cells (Life Technologies Inc.). Following heat shock at 42 °C for 60 s, cells were mixed with 1 ml of SOC media, and allowed to recover for 5 hr at 37 °C, with rotation at 225 rpm. Cells were serially diluted

and plated on LB agar containing 50 mg/ml kanamycin, 7 mg/ml gentamicin, 10 mg/ml tetracycline, 100 mg/ml Bluo-gal, and 40 mg/ml IPTG. Following 48 hr incubation at 37 °C, white colonies were isolated and used to inoculate overnight cultures. Genomic DNA from overnight cultures was isolated using the QIAGEN Genomic Tip genomic DNA isolation kit. Bacmid transposition was confirmed by PCR of genomic DNA using gene-specific forward DNA primers and bacmid-specific (T7) reverse DNA primers. Positive bacmids were additionally confirmed by sequencing.

2.11.2 GENERATING RECOMBINANT BACULOVIRUS

Recombinant baculovirus was produced in Sf9 cells cultured in Sf-900™ II media (Life Technologies Inc.) supplemented with 10 % FBS and 1 x antibiotics-antimycotics (Life Technologies Inc.) at 27 °C. Prior to transfection, cells were plated in 35 mm dishes at a density of 8×10^5 cells per dish, in unsupplemented media in the absence of antibiotics. Five µg of bacmid DNA was incubated with 20 µl Cellfectin® II transfection reagent (Life Technologies Inc.) for 30 min at room temperature prior to addition to cell culture media. Following incubation for 5 hours at 27 °C, media was replaced with SF-900™ II supplemented with 10 % FBS and 1 x antibiotics-antimycotics. Cell culture media contain P0 virus was harvested 72 hr following transfection.

Initial low-titer viral stocks were amplified to P1 and P2 high-titer stocks using the following protocol. 9×10^6 cells were plated in 150 mm

dishes containing 30 ml SF-900™ II media supplemented with 10 % FBS and 1 x antibiotics-antimycotics. 1 ml of P0 virus was added to cell culture media, and incubated for 48 hr at 27 °C. Media was harvested and stored at 4 °C. Using the same procedure, 1 ml of P1 virus was used to infect 9×10^6 cells for production of P2 virus. P2 virus was harvested following 48 hr incubation at 27 °C, and used immediately to elicit protein production in High Five™ suspension cells.

2.11.3 PROTEIN EXPRESSION AND PURIFICATION

Approximately 100 ml of P2 virus was used to infect 1 L of High Five™ cells grown in suspension to a density of 2×10^6 cells/L in SF-900™ II supplemented with 1 x antibiotics-antimycotics. Cells were harvested 48 hr following infection by centrifugation at $100 \times g$ for 5 min. Cells were lysed in buffer containing 20 mM HEPES, pH 7.5 and 500 mM NaCl, 0.1 % TX-100, supplemented with Protease Inhibitor Cocktail tablets, by sonication for 1.5 min. Lysate was clarified by centrifugation at $40\,000 \times g$ for 1 hr at 4 °C.

2.11.4 AFFINITY CHROMATOGRAPHY

Clarified lysates were incubated with 15 ml Ni-NTA Agarose (QIAGEN) or GSH Sepharose™ 4B Media (GE Healthcare) equilibrated in buffer containing 20 mM HEPES, pH 7.5 and 500 mM NaCl, 0.1 % TX-100, for 30 min at 4 °C. Beads were isolated by centrifugation at $100 \times g$ for 5 min at 4

°C, and washed 3 x in 50 ml of lysis buffer. Samples containing Ni-NTA Agarose were additionally washed in 50 ml lysis buffer supplemented with 20 mM Imidazole (Sigma). Bound proteins were eluted from Ni-NTA Agarose or GSH Sepharose media using 3 x 20 ml of 20 mM Hepes, pH 7.5, supplemented with 200 mM Imidazole or 20 mM GSH, respectively. Eluate was immediately supplemented with 5 mM DTT.

2.11.4.1 ANION EXCHANGE CHROMATOGRAPHY

Eluate from affinity purifications was loaded onto a 5 ml HiTrap column containing high performance Q Sepharose at 5 ml/min. The column was washed in 10 column volumes (CVs) of 20 mM Hepes, pH 7.5, and bound proteins were eluted using a linear gradient of 20 mM Hepes, pH 7.5 and 1 M NaCl, over 4 CVs in 2 ml fractions. Protein-containing fractions were sampled, resolved by SDS-PAGE and stained with Coomassie blue stain. Fractions containing the recombinant protein of interest were either flash frozen in liquid nitrogen, or incubated with 1:100 (w/w) TEV protease for 16 hr at 4 °C to remove affinity tags.

Separation of Human Nup37 from GST was accomplished by tandem affinity-ion exchange chromatography using a 5 ml GStap™ Fast Flow column (GE Healthcare) coupled with a HiTrap™ Q Sepharose column (GE Healthcare). In this purification scenario, GST is immobilized by GSH Sepharose, and Q Sepharose retains Nup37. After sample loading, columns were disconnected and eluted individually.

2.11.4.2 GEL FILTRATION ANALYSIS

Purified proteins in isolation or mixtures of approximately equal molar ratios of the designated proteins were incubated for 10 min on ice before injection into a Superdex 200 10/300 GL gel filtration column (GE Healthcare) equilibrated in a buffer containing 10 mM Hepes (pH 7.4), 200 mM NaCl, and 5 mM DTT. Complex formation was confirmed by SDS/PAGE analysis of the designated eluted fractions, followed by Coomassie brilliant blue staining.

2.12 CRYSTALLIZATION CONDITIONS

Crystals of Sp-Nup37 were grown at 30 °C using the hanging-drop vapor-diffusion method by mixing 1 μ L of the purified protein and 1 μ L of crystallization buffer containing 100 mM Hepes (pH 7.4), 0.5 M lithium sulfate, 10% (vol/vol) 1,4-Butanediol, and 10 mM DTT. The crystals belong to space group $P4_12_12$, with $a = 131 \text{ \AA}$, $b = 131 \text{ \AA}$, $c = 117 \text{ \AA}$, $\alpha = 90^\circ$, $\beta = 90^\circ$, and $\gamma = 90^\circ$, and they contain one molecule in one asymmetry unit.

Crystals of the Sp-Nup120¹⁻⁹⁵⁰-Nup37 complex were grown by the hanging-drop vapor-diffusion method at 16 °C by mixing 1 μ L of the purified protein (15mg/ml) and 1 μ L of crystallization buffer containing 10% (wt/vol) Peg3350, 0.1 M Bis-Tris (pH 5.5), 0.2 M ammonium acetate. The crystals belong to space group $P2_12_12_1$, with $a = 70 \text{ \AA}$, $b = 123 \text{ \AA}$, $c = 172 \text{ \AA}$, α

= 90°, β = 90°, and γ = 90°, and they contain one copy of the hetero-dimeric complex in one asymmetry unit.

Crystals of Human Nup37 were grown by the hanging-drop vapor-diffusion method at 30 °C by mixing 1 μ L of the purified protein and 1 μ L of crystallization buffer containing 100 mM Hepes, pH 7.4, 0.5 M lithium sulfate, 10% (vol/vol) 1,4-Butanediol, 10% (wt/vol) PEG 3350, and 10 mM DTT. Crystals of Nup160³⁷⁻⁹⁵³-Nup37 were grown by the hanging-drop vapor-diffusion method at 16 °C by mixing 1 μ L of the purified protein and 1 μ L of crystallization buffer containing 0.1 M Bis-Tris, pH 6.5, 0.1 M NaCl and 1.5 M Ammonium Sulfate, and 1 mM TCEP. Amorphous crystals of Nup160¹⁻⁵⁸³-Pom121²¹⁵⁻⁵⁵⁷ were grown by the hanging-drop vapor-diffusion method at 16 °C by mixing 1 μ L of the purified protein and 1 μ L of crystallization buffer containing 0.1 M Bis-Tris, pH 8.5, 0.2 M NaCl, and 10 mM TCEP.

2.13 UV MICROSCOPY

To ensure crystals formed were comprised of protein, UV microscopy was used to visualize the intrinsic fluorescence of tyrosine and tryptophan amino acid residues. Plates containing crystals grown in hanging-drop format were imaged directly using a [JANSi](#) UVEX microscope with UV excitation at 400 nm (JAN Scientific Inc., Seattle WA). Micrographs were processed using Photoshop CS6 software (Adobe Systems Incorporated).

2.14 STRUCTURE DETERMINATION

All X-ray diffraction data were collected at the National Synchrotron Light Source at Brookhaven National Laboratory, beamline X29. Data were collected at $-170\text{ }^{\circ}\text{C}$ with crystals flash frozen in crystallization buffer supplemented with 25% (vol/vol) ethylene glycol. All data collected in this study were processed using the HKL2000 suite (Otwinowski Z, 1997). Phases of nonliganded Nup37 were calculated using anomalous differences of a heavy atom derivative dataset from 1 mM thimerosal-soaked crystals in crystallization well solution lacking DTT using the single-anomalous dispersion (SAD) suite of the PHENIX program (Adams et al., 2010). The phases were improved using solvent flattening with the PHENIX program. The initial model was built using the PHENIX Autobuild suite aided by manual correction of the coordinates in the Coot program (Emsley et al., 2010) and refined with REFMAC5 (Collaborative Computational Project, 1994).

The initial phases for the Sp-Nup120¹⁻⁹⁵⁰-Nup37 complex were obtained by molecular replacement using the structure of the nonliganded Nup37 as the search model with the Phaser program (Collaborative Computational Project, 1994). The phases were improved by the MR SAD suite of the PHENIX program using Hg- and Au-derivative crystals (Adams et al., 2010). Iterative cycles of model building and refinement were performed with the Coot (Emsley et al., 2010) and REFMAC (Collaborative Computational Project, 1994) programs. The unambiguous assignment of the

protein sequence was achieved with the help of the mercury and gold positions. The final refined model contains residues 1–949 of Nup120 and residues 6–386 of Nup37. Residues 35–43, 220–226, 318–320, 385–387, 399–404, 446–450, and 746–758 of Nup120 and residues 84–94 of Nup37 are disordered.

The stereochemical quality of the final model was assessed with PROCHECK (Laskowski RA, 1993). There were no residues in the disallowed region of the Ramachandran plot. Details of the data collection, phasing, and refinement statistics are provided in Table 4-1.

**CHAPTER III: POM121 LINKS TWO ESSENTIAL SUBCOMPLEXES OF THE
NUCLEAR PORE COMPLEX CORE TO THE MEMBRANE**

A version of this chapter has been previously published in: Mitchell, J.M., J. Mansfeld, J. Capitanio, U. Kutay, and R.W. Wozniak. 2010. Pom121 links two essential subcomplexes of the nuclear pore complex core to the membrane. *The Journal of Cell Biology*. 191:505-521. J. Mansfeld contributed the data presented in Figure 3-9, and J. Capitanio independently confirmed the localization of Nup98 following Nup155 depletion.

3.1 OVERVIEW

Nuclear pore complexes (NPCs) act as gateways that regulate the transport of macromolecules across the nuclear envelope (NE). In addition to their roles in controlling transport, NPCs also influence gene expression, chromatin organization, and chromosome inheritance. Although approaching ~100 MDa in mass in vertebrate cells, NPCs are composed of only ~30 distinct proteins termed nucleoporins (Nups). Nups are categorized into discrete subcomplexes in accordance with their structural composition and function within the NPC. Barrier Nups line the central channel of the NPC and regulate trafficking of macromolecules. Scaffold Nups, which topologically mimic the tertiary structure of proteins comprising coated vesicles, stabilize the curvature of the NE within the vicinity of the NPC. Interactions between scaffold Nups with transmembrane Nups (Poms) embedded within the pore membrane domain (POM) presumably anchor the NPC within the NE. However, at this time, no such interactions have been reported. We investigated the molecular interactions that exist at the interface between the NPC scaffold and the POM, and show that key players mediating these interactions in mammalian cells are the scaffold Nups Nup155 and Nup160. Depletion of Nup155 massively alters NE structure, causing a dramatic decrease in NPC numbers and the improper targeting of membrane proteins to the inner nuclear membrane (INM). The role of Nup155 in NPC assembly is likely closely linked to events at the POM, as we show that Nup155 interacts with the Poms NDC1 and Pom121. Furthermore,

we demonstrate that the N-terminus of Pom121 directly binds the β -propeller regions of Nup155 and Nup160. We propose a model in which the interactions of Pom121 with Nup155 and Nup160 are predicted to assist in the formation of the nuclear pore and the anchoring of the NPC to the pore membrane.

3.2 RESULTS

3.2.1 LOSS OF MAMMALIAN NUP155 ALTERS NUCLEAR ENVELOPE STRUCTURE

Studies in *C. elegans* and *X. laevis* suggest that Nup155 plays an essential role in NE and NPC assembly (Franz et al., 2005). Here we have used a variety of tools to investigate the function of mammalian Nup155 in establishing and maintaining the structure of the NE and NPC, with the goal of defining the mechanistic basis for the role of Nup155 in these processes. First, we examined the consequences of depleting Nup155 on the structure of HeLa cell nuclei. Several siRNAs directed against distinct regions of Nup155 mRNA were tested for their ability to deplete Nup155. Each of the siRNAs produced similar phenotypes (Figure 3-1 and 3-2). By 72 hours post siRNA transfection, the cellular levels of Nup155 were greatly reduced as determined by western blotting (Figure 3-1). Immunofluorescence analysis using anti-Nup155 antibodies showed that ~50-70% of Nup155-specific siRNA treated cells exhibited a decrease in Nup155 staining at the NE (Figure 3-1A and 3-2).

The loss of Nup155 was accompanied by a decrease in the number of NPCs. Transmission electron microscopy (TEM) revealed a decrease in the number of NPCs per μm of sectioned NE, from ~ 1.31 NPCs/ μm in mock treated samples to ~ 0.31 NPCs/ μm in Nup155 depleted cells (Figure 3-2B and 3-2C). This decrease in NPCs was also revealed by immunofluorescence microscopy using the monoclonal antibody mAb414, which binds several FG-Nups, including Nup62, Nup153, Nup214, and Nup358. In cells treated with

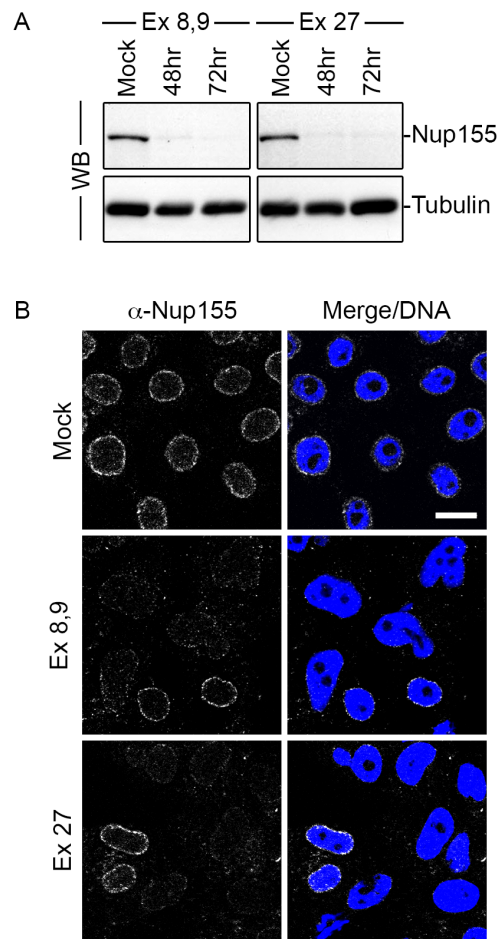


FIGURE 3-1 MULTIPLE siRNAs TARGETING DISTINCT REGIONS OF NUP155 mRNA EFFICIENTLY DEplete NUP155 AND SIMILARLY ALTER NUCLEAR MORPHOLOGY.

HeLa cells were incubated in the presence of siRNAs targeting exon 8/9 or exon 27 of Nup155 for 72 h. As a control, cells were incubated with transfection reagent alone. (A) After 72 h, cells were treated with SDS-sample buffer and polypeptides were resolved by SDS-PAGE. Western blots (WB) were used to evaluate the levels of Nup155 and an α -tubulin loading control. (B) Alternatively, 72 h after transfection, cells were processed for immunofluorescence and probed with antibodies directed against Nup155. DNA was visualized using DRAQ5 (Merge/DNA). Bar, 10 μ m.

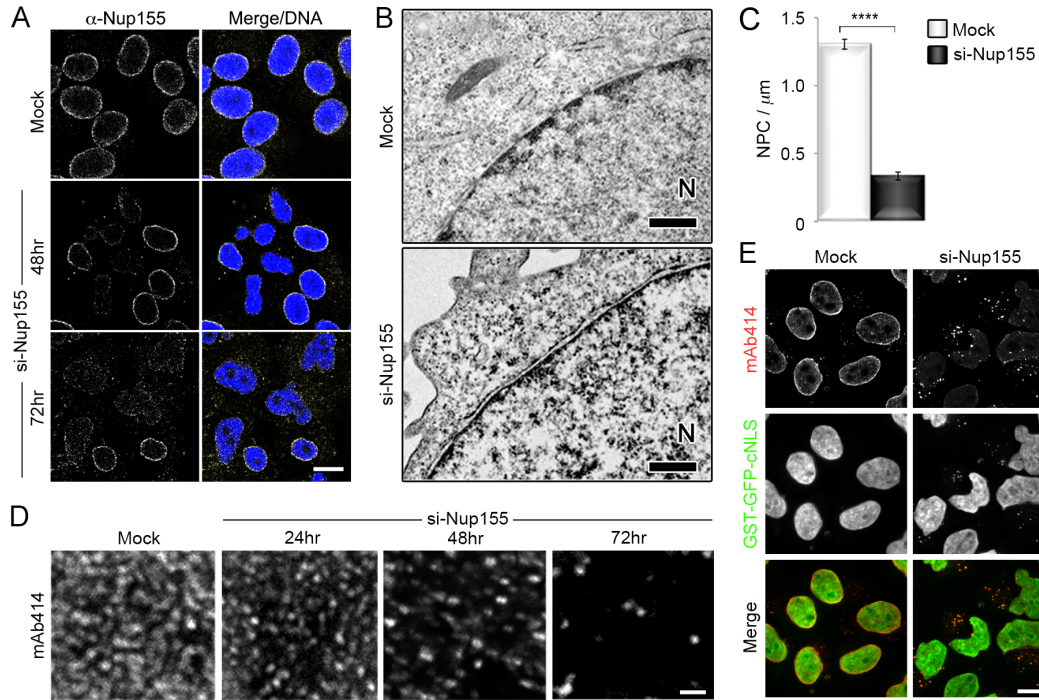


FIGURE 3-2 DEPLETION OF NUP155 ALTERS NUCLEAR MORPHOLOGY AND DECREASES NPC NUMBER.

HeLa cells were treated with transfection reagent alone (Mock) or the Nup155-specific siRNA-targeting exon 27 (si-Nup155) as indicated. (A) Nup155 levels were assayed by indirect immunofluorescence using anti-Nup155 antibodies at the indicated times and DNA visualized with DRAQ5 (Merge/DNA). Bar, 10 μm . (B and C) Mock- or Nup155-depleted HeLa cells were processed for transmission electron microscopy 72 h after transfection. The position of the nucleoplasm is indicated (N). Bar, 0.5 μm . (C) The number of NPCs per micron of NE was determined by examining individual nuclear sections ($n > 48$ sections per condition). The average number of NPCs per micron of NE is shown. The P value ($P < 0.0001$, represented by asterisks) was calculated using a Welch corrected unpaired t test. Error bars indicate standard error. (D) NPCs at the nuclear surface of Nup155-depleted cells were visualized by indirect immunofluorescence using mAb414 at the indicated times after siRNA treatment. Bar, 1 μm . (E) HeLa cells expressing GST-GFP-cNLS were incubated in the presence of transfection reagent alone (Mock) or with Nup155-specific siRNAs. 72 h after transfection, GST-GFP-cNLS was visualized together with mAb414-reactive Nups detected by immunofluorescence. Bar, 10 μm . To obtain the results presented in (C), the number of NPCs was determined from ~ 30 nuclei from mock and si-Nup155 depleted cells in each of three independent experiments. Representative images of the nuclear surface are presented in (D).

Nup155 siRNA, the number of foci recognized by mAb414 at the NE progressively decreased during the time course of the experiment (Figure 3-2D). Those NPCs that remained, even after 72 hr of Nup155-specific siRNA treatment, appeared to be functional, as a GST-GFP-cNLS import reporter continued to accumulate in the nucleus (Figure 3-2E).

While Nup155 depletion causes a decrease in the number of NPCs, we detected little or no change in the cellular levels of various Nups including Nup62, Nup93, Nup107, and NDC1 by western blot analysis (Figure 3-3A). Moreover, Nup53, a binding partner of Nup155 (see below), showed only a slight decrease in cellular levels. The apparent discrepancy between the decrease in NPC numbers and the unchanged levels of Nups in Nup155-depleted cells was explained by immunofluorescence analysis. All of the Nups examined, including Nup53, Nup93, Nup98, Nup107, Nup153, Nup358, and the pore membrane protein Pom121 accumulated within cytoplasm foci concomitant with a decrease in their levels at the NE (Figure 3-3B-G). Moreover, co-immunofluorescence analysis revealed overlapping signals between the mAb414 antibody and that produced by the anti-Nup53, -Nup93, -Nup98, -Nup358 or -Nup107 antibodies or Pom121-EGFP3, suggesting that each individual focus contains multiple Nups.

Accompanying the loss of NPCs, essentially all cells depleted of Nup155 exhibited alterations in the morphology of the nucleus after 72 hr of

FIGURE 3-3 DEPLETION OF NUP155 IN HELA CELLS LEADS TO THE MISLOCALIZATION OF NUCLEOPORINS.

HeLa cells were incubated in the presence of transfection reagent alone (Mock) or Nup155-specific siRNA (si-Nup155) for 72 h. (A) Total cell extracts from Mock- and Nup155-depleted cells were assayed by Western blot (WB) analysis using antibodies directed against the indicated proteins. Note: the bottom blot panels are from separate experiments. (B–F) The cellular distribution of various Nups was visualized by indirect immunofluorescence using the indicated polyclonal anti-Nup antibodies and the mouse monoclonal mAb414 (mAb414 detects Nup62, Nup153, Nup214, and Nup358) or mouse monoclonal anti-Nup153. (G) In Mock- or Nup155-specific siRNA-transfected cells, Pom121-EGFP3 was visualized directly and compared with mAb414-reactive Nups detected by immunofluorescence. In all panels merged fluorescence images and DNA visualized with DRAQ5 are shown (Merge/DNA). Bar, 10 μ m.

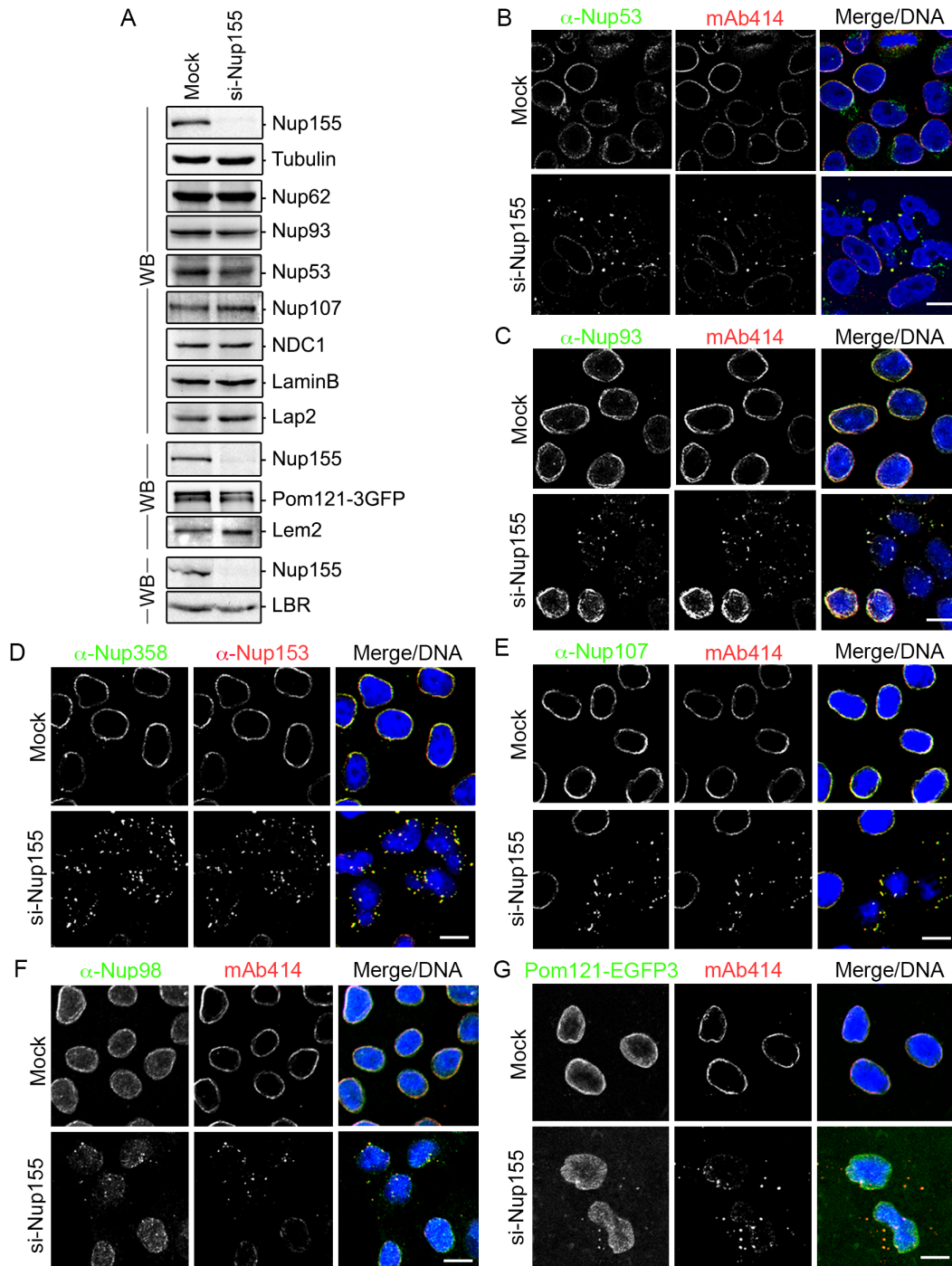


FIGURE 3-3 DEPLETION OF NUP155 IN HELA CELLS LEADS TO THE MISLOCALIZATION OF NUCLEOPORINS.

siRNA treatment. Nuclei were observed that were kidney-shaped or contained multiple lobes connected by bridges of NE membrane (Figures 3-1 to 3-5). These changes in the contour of depleted nuclei did not appear to be due to an overt change in the structure of the lamina, as both Lamin B and Lamins A/C retained their normal peripheral nuclear localization in these cells (Figure 3-4). This abnormal nuclear morphology also prompted us to examine the distribution of several INM proteins including Lap2 (lamina-associated polypeptide 2), Lem2 (lamina-associated polypeptide–emerin–MAN1), and LBR (lamin B receptor) (for review see Schirmer and Gerace, 2005). Depleting Nup155 did not affect total cellular levels of these proteins (Figure 3-3A), however NE levels of all three proteins were decreased (Figure 3-4), with Lap2 also accumulating in multiple foci adjacent to the surface of the NE (Figure 3-4 and 3-5). This latter observation prompted us to examine the localization of Lap2 in cells permeabilized with digitonin. This detergent perforates the plasma membrane but leaves the NE intact. In mock treated cells, anti-Lap2 antibodies failed to detect Lap2, as the NE blocked their accessibility to Lap2 in the inner nuclear membrane (Figure 3-5). However, in Nup155 depleted cells, Lap2 was detected in the ER-like structures and the outer nuclear membrane, suggesting that it failed to efficiently target to the INM. On the basis of these results, we conclude that, in addition to its role in NPC assembly, Nup155 is likely required for the targeting of at least some integral membrane proteins to the INM. This function appears to be specific for Nup155, as depletion of its interacting

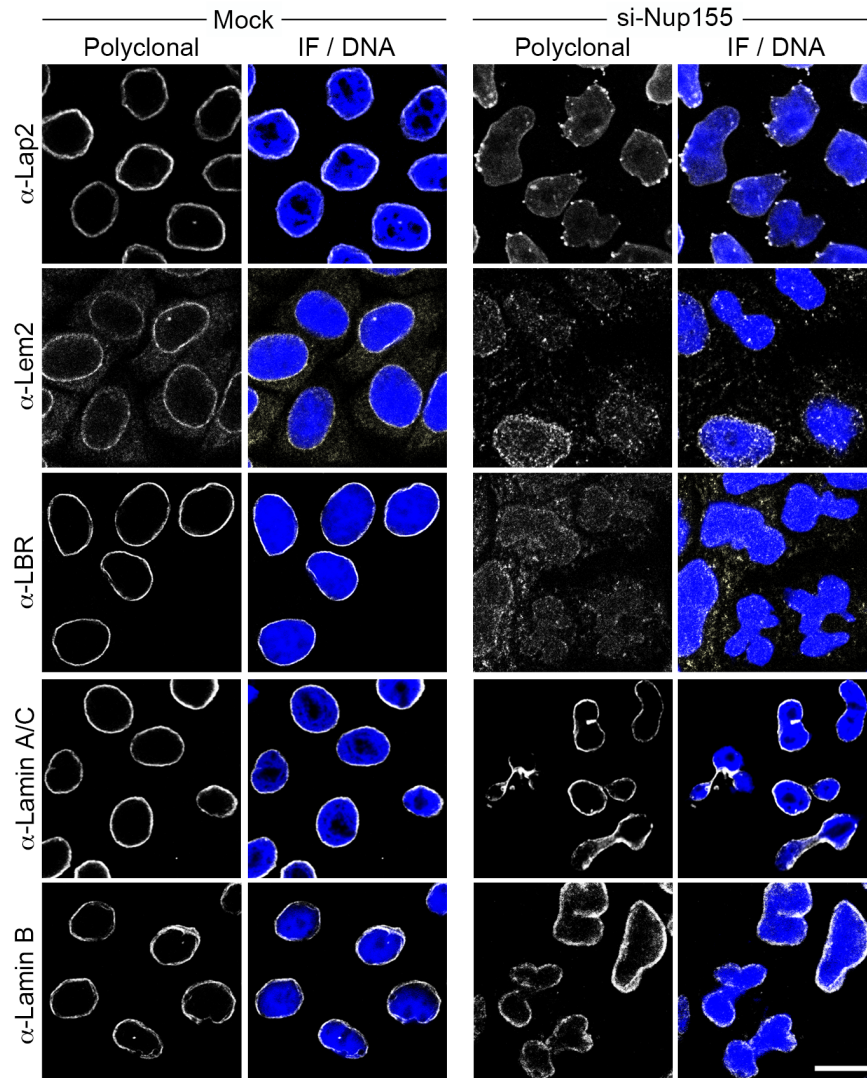


FIGURE 3-4 NUP155 DEPLETION ALTERS TARGETING OF INM PROTEINS.

HeLa cells were incubated in the presence of transfection reagent alone (Mock) or Nup155-specific siRNA (si-Nup155) for 72 h and then processed for immunofluorescence microscopy. The indicated INM proteins and lamin B were visualized using specific polyclonal antibodies and DNA was visualized using DRAQ5 (Merge/DNA). Bar, 10 μ m.

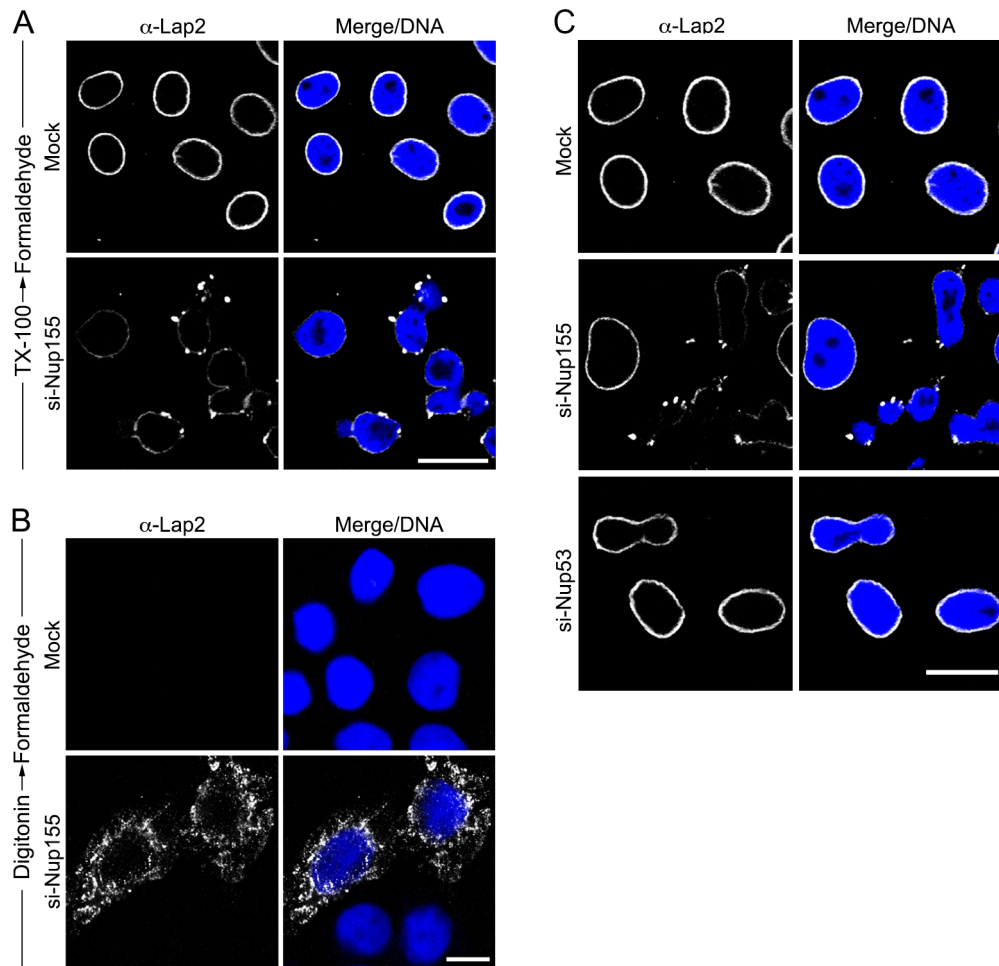


FIGURE 3-5 DEPLETION OF NUP155 AFFECTS THE TARGETING OF LAP2 TO THE INM.

HeLa cells grown on coverslips were incubated for 72 h in the presence of siRNAs targeting Nup155 or Nup53, or with transfection reagent alone, as indicated. Cells were pre-extracted with 0.2% Triton X-100 (A and C) or 0.005% digitonin (B) followed by formaldehyde fixation. Digitonin permeabilizes the plasma membrane but leaves the NE intact. Under these conditions antibodies have access to ER and outer nuclear membrane proteins, but not to inner nuclear membrane proteins. The localization of Lap2 was examined by immunofluorescence using a specific monoclonal antibody. DNA was visualized using DRAQ5 nuclear stain (Merge/DNA). Bar, 10 μ m.

partner, Nup53, did not alter the INM localization of Lap2 (Figure 3-5, panel C) or emerin (Hawryluk-Gara et al., 2005).

3.2.2 NUP155 IS ANCHORED TO THE PORE MEMBRANE BY POM121 AND NDC1

To further understand the mechanistic basis for the requirement of Nup155 in NPC and NE structure, we used GST-pulldown assays to define its interacting partners. To facilitate this analysis, purified rat liver NEs were used as an abundant source of mammalian proteins. During extract preparation, conditions were used that disrupt the NE and solubilize most Nups, lamins, and integral membrane proteins. These extracts were then incubated with GST-Nup155 immobilized on glutathione-Sepharose beads. Bound protein species were analyzed by SDS-PAGE and western blotting (Figure 3-6). Our results show that many Nups failed to bind Nup155 and were absent from the bound fraction, including Nup93 and Nup62. However, as anticipated based on previous studies (Hawryluk-Gara et al., 2005), Nup53 was detected bound to GST-Nup155 but not GST alone. In addition, Nup153 was also detected bound to Nup155. Bound and unbound fractions were also probed with antibodies directed against each of the three known mammalian pore membrane proteins, gp210, NDC1, and Pom121. As shown in Figure 3-6, both NDC1 and Pom121 bound Nup155, while gp210 was absent from the bound fraction. To extend these results, pulldown experiments were performed using GST-fusion proteins containing the pore-facing domain of

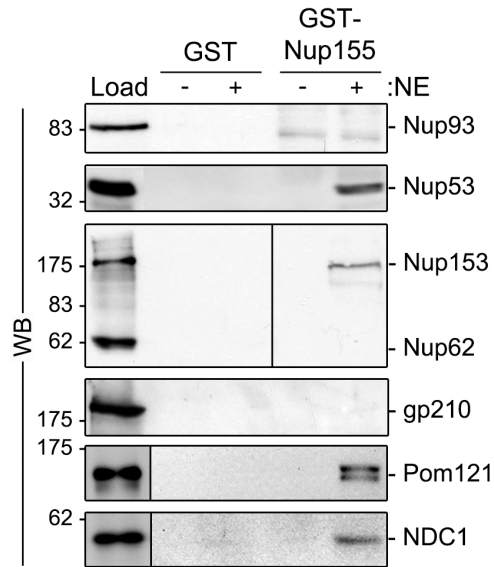


FIGURE 3-6 IDENTIFICATION OF NUP155-INTERACTING PROTEINS.

GST-Nup155 or GST alone were bound to glutathione-Sepharose beads and then incubated in the presence (+) or absence (-) of solubilized rat liver NE extracts. Bound proteins were eluted from beads using SDS-sample buffer. Interacting Nups were detected by Western blot (WB) using antibodies directed against the indicated proteins. mAb414 was used to detect Nup62 and Nup153. Approximately 5% of the NE extract loaded on each column was resolved in the lane marked Load.

Pom121. GST-fusions to the entire pore-exposed region of Pom121 were largely insoluble and heavily degraded after expression in *E. coli* (Figure 3-7A), necessitating the construction of smaller, more stable GST-truncations. Using hydrophobicity profiles and secondary structure predictions, fragments of Pom121 were designed in an effort to improve protein solubility and stability (see section 2.1, Table 2.1). As shown in Figure 3-7, a GST-Pom121 fusion containing amino acid residues 215-557 (Pom121²¹⁵⁻⁵⁵⁷) was capable of binding Nup155 in rat liver NE extracts, while more C-terminal pore-exposed regions, including residues 558-1218 and 835-1218 (Pom121⁵⁵⁸⁻¹²¹⁸ and Pom121⁸³⁵⁻¹²¹⁸), did not. Of note, the Pom121²¹⁵⁻⁵⁵⁷ construct lacks FG-repeats.

It was unclear from our pulldown experiments whether Nup155 directly bound Pom121 and NDC1, or instead their interactions were mediated by other Nups. To test for direct interactions, GST-Nup155 was immobilized on glutathione-Sepharose beads and then incubated with purified recombinant Pom121²¹⁵⁻⁵⁵⁷ or a fragment of NDC1 consisting of its C-terminal residues 292-674 positioned on the cytoplasmic face of the pore membrane. As shown in Figure 3-8A, Pom121²¹⁵⁻⁵⁵⁷ binds to GST-Nup155 but not GST alone. Similarly, the NDC1²⁹²⁻⁶⁷⁴ fragment was also capable of binding GST-Nup155 while failing to bind GST or GST-Nup53 (Figure 3-8B).

On the basis of our results, we conclude that Nup155 directly interacts with both Pom121 and NDC1 near the pore membrane. We infer

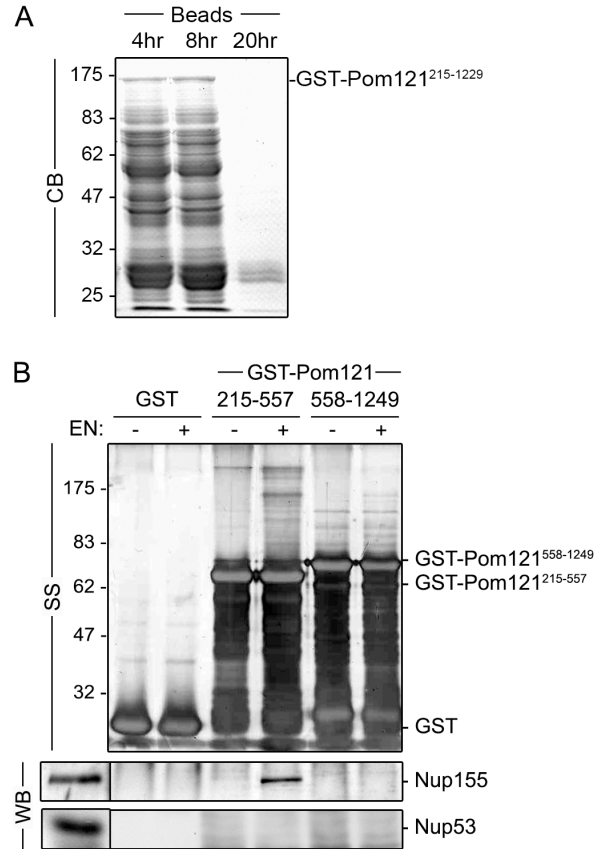


FIGURE 3-7 BIOCHEMICAL CHARACTERIZATION OF RECOMBINANT FRAGMENTS OF POM121.

(A) The pore-facing domain of Pom121 (215-1229) was expressed as a GST-tagged recombinant protein in *E. coli*. After induction with IPTG, cells were harvested at the indicated time points. Clarified lysates were incubated with Glutathione Sepharose, and proteins eluted with SDS-sample buffer were resolved by SDS-PAGE and stained with Coomassie blue (CB). (B) GST-tagged truncations of the pore-facing domain of Pom121 (amino acid residues 215-557 or 558-1218) were incubated with (+) or without (-) rat liver NE extracts. Interacting proteins were eluted with SDS-sample buffer. Polypeptides were resolved by SDS-PAGE and analyzed by Western blotting (WB) using a Nup155-specific polyclonal antibody. Approximately 5% of the NE extract loaded on each column was resolved in the lane marked Load. To the right of each panel, the point at which the named recombinant protein migrates in the appropriate lane is indicated. Mass markers are in kilodaltons.

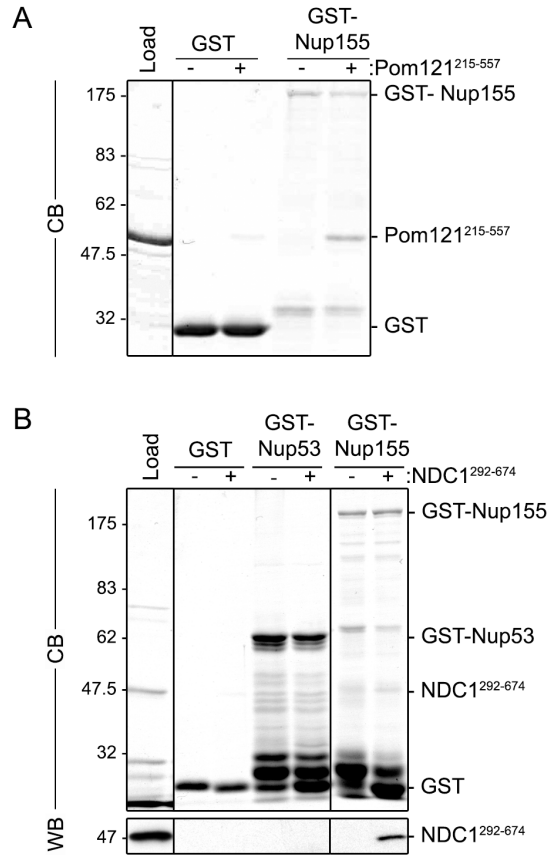


FIGURE 3-8 NUP155 INTERACTS DIRECTLY WITH PORE MEMBRANE PROTEINS POM121 AND NDC1.

Glutathione–Sepharose beads with attached GST-Nup155, GST-Nup53, or GST alone were incubated with (+) or without (-) purified recombinant Pom121²¹⁵⁻⁵⁵⁷ (A) or Ndc1²⁹²⁻⁶⁷⁴ (B). Bound proteins were eluted using SDS sample buffer, and polypeptides were detected using Coomassie blue staining (CB) (A, B) or Western blot (WB) using anti-NDC1 antibodies (B). The lanes marked Load contain 50% of the total purified Pom121²¹⁵⁻⁵⁵⁷ loaded on the beads. To the right of each panel, the point at which the named recombinant protein migrates in the appropriate lane is indicated. Mass markers are in kilodaltons.

from these data that Pom121 and NDC1 may function in the assembly and anchoring of Nup155 at the NPC. To test this idea, we used siRNAs to deplete NDC1, Pom121, or gp210 in HeLa cells and then examined the levels and localization of Nup155 and other Nups. Western blot analysis revealed that each of these membrane proteins could be efficiently depleted (Figure 3-9A). The depletion of gp210 or NDC1 had little effect on cellular levels of Nup155 or other Nups examined (Figure 3-9A). Moreover, the NE association of Nup155 was unaffected by depletion of gp210 (Figure 3-9C). Nup155 was also detected at the NE of cells depleted of NDC1, albeit at reduced levels relative to untreated cells. The most striking effects on Nup155 were seen in cells depleted of Pom121, where both the NE localization and total cellular levels of Nup155 were greatly reduced as detected by western blotting and immunofluorescence microscopy. We also observed that depletion of Pom121 caused slight reductions in total cellular levels and reduced NE association of Nup53, Nup93, and Nup107 (Figure 3-9B).

3.2.3 POM121 DIRECTLY INTERACTS WITH NUP160 AND NUP98

In addition to Nup155, further analysis of GST-Pom121²¹⁵⁻⁵⁵⁷ interacting partners revealed a more complex set of interacting Nups. Several abundant polypeptides with masses ranging from approximately 90 to 160 kDa bound GST-Pom121²¹⁵⁻⁵⁵⁷, but not GST alone (Figure 3-10). Less abundant, but specific, interactors were also detected at higher and lower

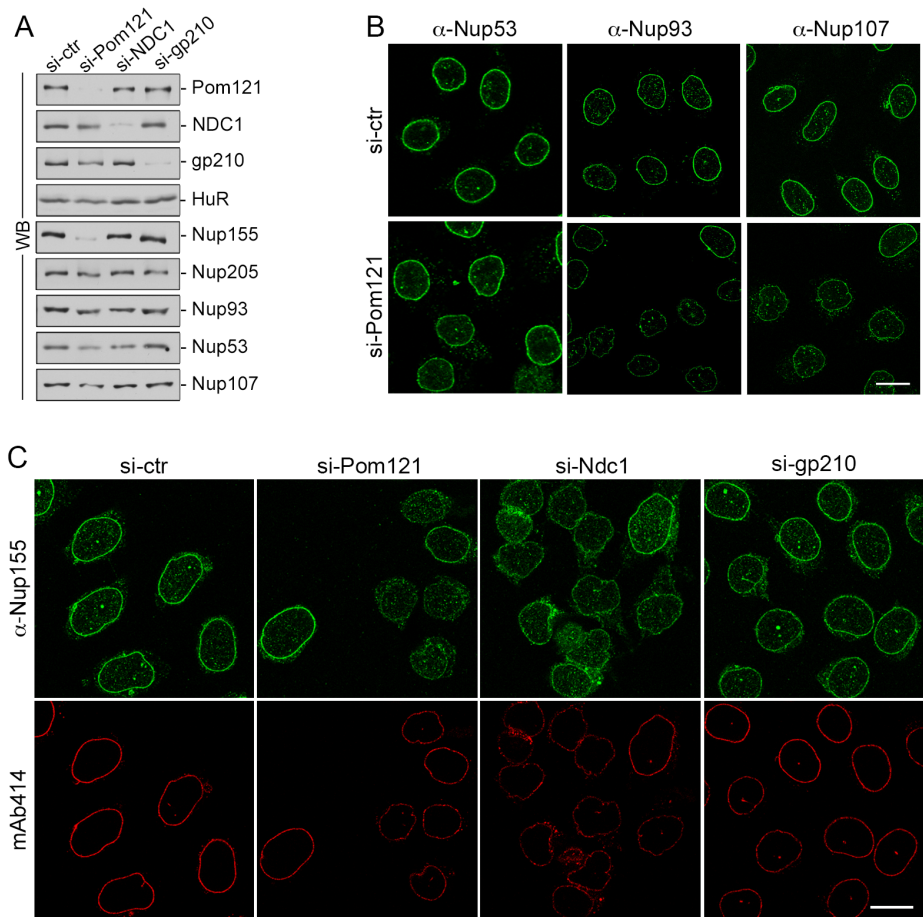


FIGURE 3-9 DEPLETION OF POM121 REDUCES CELLULAR LEVELS OF NUP155.

HeLa cells were incubated in the presence of control siRNAs (si-ctr) or siRNAs targeting Pom121, NDC1, or gp210 as indicated. (A) Cells were harvested and analyzed by Western blotting (WB) using antibodies directed against the indicated proteins. α -HuR was used as a loading control. (B) HeLa cells were processed for immunofluorescence microscopy using anti-Nup53, anti-Nup93, or anti-Nup107 polyclonal antibodies. Bar, 10 μ m. (C) Cells were processed for immunofluorescence microscopy and interrogated using anti-Nup155 or mAb414 antibodies. Bar, 10 μ m. Experiments presented in this figure were performed by J. Mansfeld in the laboratory of U. Kutay at ETH, Zurich.

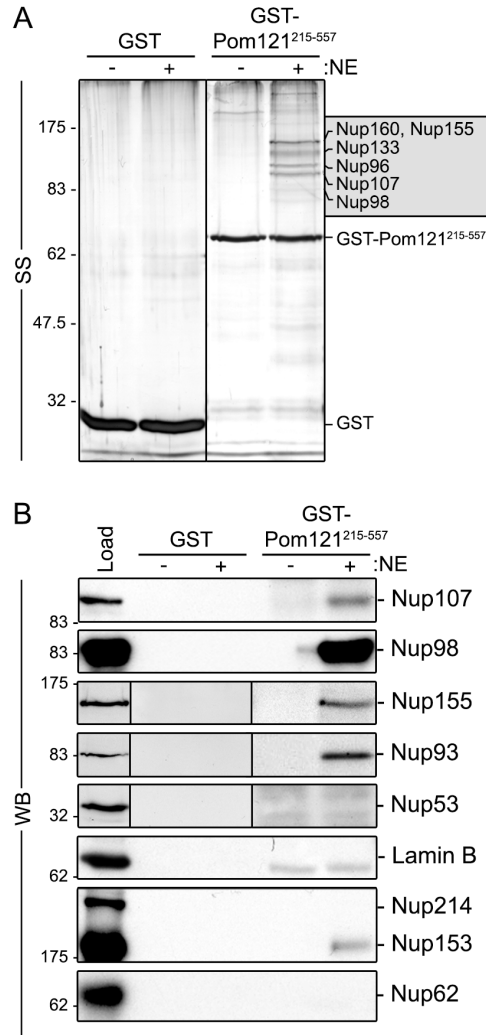


FIGURE 3-10 POM121 INTERACTS WITH NUP155 AND THE NUP107-160 COMPLEX *IN VITRO* .

Bead-bound GST-Pom121²¹⁵⁻⁵⁵⁷ or GST alone was incubated with (+) or without (-) rat liver NE extracts. Interacting proteins were eluted with SDS-sample buffer. Polypeptides were resolved by SDS-PAGE and visualized by silver staining (SS; A) or analyzed by Western blotting (WB; B) using antibodies directed against the indicated proteins. mAb414 was used to detect Nup62, Nup153, and Nup214. Approximately 5% of the NE extract loaded on each column was resolved in the lane marked Load. Prominent bands were analyzed by mass spectrometry (see Figure 3-11) and the predominant species identified in the 90–160-kD range are indicated in the shaded box. Molecular mass markers are indicated in kilodaltons.

molecular masses. Mass spectrometry (MS) analysis of five of the most abundant polypeptides identified peptides derived from Nup155, Nup98, Nup96, Nup107, Nup133, and Nup160, the latter four being members of the Nup107-160 complex (Figure 3-10A and 3-11). The presence of Nup107 and Nup98 in the GST-Pom121²¹⁵⁻⁵⁵⁷ bound fraction was further confirmed by western blotting (Figure 3-10B). The identities of several less intensely staining species were also determined by MS analysis or western blotting, including the interacting Nups Nup93 and Nup205, additional members of the Nup107-160 complex (Nup85/75, Nup43), Nup153, Nup358, and ELYS (Figure 3-10 and 3-11). Western blotting failed to detect various other Nups including Nup53, Nup62, and Nup214.

Members of the Nup107-160 complex and Nup98 represent the abundant species in Pom121 pulldowns, and as such were strong candidates for directly binding Pom121. Thus, we further investigated these interactions in pulldown experiments using recombinant GST-Nup160 and GST-Nup98 (Figure 3-12). For Nup98, a truncation lacking most of the N-terminal FG repeats (amino-acid residues 316-920; Nup98³¹⁶⁻⁹²⁰) was tested, as full length Nup98 was largely insoluble. Similar to the experiments described above for GST-Nup155 and GST-Pom121²¹⁵⁻⁵⁵⁷, GST-Nup160 and GST-Nup98 were incubated with NE extract and proteins in the bound fraction were interrogated by western blot analysis. As predicted, GST-Nup160 bound to Nup107. Furthermore, we detected Nup53, Nup153, and,

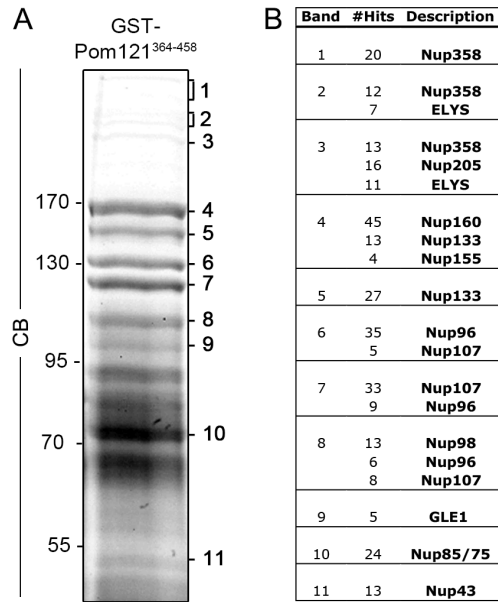


FIGURE 3-11 POM121-INTERACTING NUPS IDENTIFIED BY MASS SPECTROMETRY.

(A) Bead-bound GST-Pom121³⁶⁴⁻⁴⁵⁸ was incubated with rat liver NE extracts. Interacting proteins were eluted with SDS-sample buffer. Polypeptides were resolved by SDS-PAGE and visualized by Coomassie blue staining (CB). Both GST-Pom121³⁶⁴⁻⁴⁵⁸ and GST-Pom121²¹⁵⁻⁵⁵⁷ (shown in Figure 3-10) exhibit a similar pattern of bound Nups. Prominent bands that bound GST- Pom121³⁶⁴⁻⁴⁵⁸ but not GST alone (not depicted) are labeled 1–11. These species were excised from the gel and analyzed by mass spectrometry. The table in B lists the most abundant proteins detected in each of the excised regions and the number of peptides identified of the corresponding polypeptide.

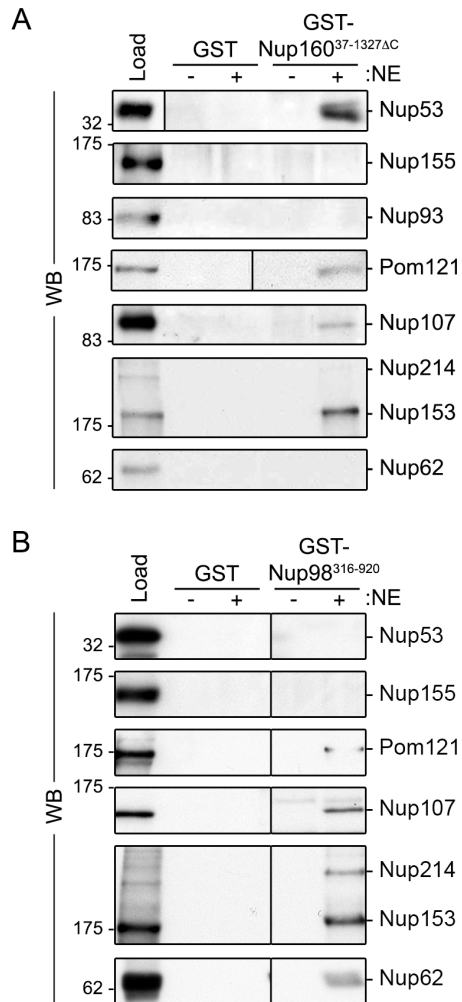


FIGURE 3-12 IDENTIFICATION OF NUPS THAT BIND NUP160 AND NUP98.

GST-Nup160^{37-1327ΔC} (A), GST-Nup98³¹⁶⁻⁹²⁰ (B), or GST alone were bound to glutathione-Sepharose beads and incubated in the presence (+) or absence (-) of solubilized rat liver NE extracts. Bound proteins were eluted from beads using SDS-sample buffer. Interacting Nups were detected by Western blot (WB) using antibodies directed against the indicated proteins. mAb414 was used to detect Nup62, Nup153, and Nup214. Approximately 5% of the NE extract loaded on each column was resolved in the lane marked Load. Molecular mass markers are indicated in kilodaltons.

importantly, Pom121 bound to GST-Nup160. These interactions appeared to be specific as various other Nups examined, including Nup155, Nup93, and Nup62, failed to bind GST-Nup160. Similar experiments using GST-Nup98³¹⁶⁻⁹²⁰ also detected a subset of bound NPC proteins, including Pom121, Nup107, and various other Nups (Nup214, Nup153, and p62), but not Nup155 or Nup53.

To understand the molecular basis for these interactions, we tested whether Nup160 and Nup98³¹⁶⁻⁹²⁰ were capable of directly binding Pom121²¹⁵⁻⁵⁵⁷. Using recombinant proteins and *in vitro* binding assays, we observed that both GST-Nup160 and GST-Nup98³¹⁶⁻⁹²⁰ bound to Pom121²¹⁵⁻⁵⁵⁷ (Figure 3-13B and 3-14A, respectively). These data, and those discussed above, suggest that at least three Nups, Nup98, Nup155, and Nup160, are capable of directly binding Pom121.

3.2.4 PREDICTED β -PROPELLER DOMAINS OF NUP155 AND NUP160 BIND POM121

Nup155 and Nup160 are predicted to share a similar structural organization consisting of an N-terminal β -propeller and C-terminal α -solenoid domain (Berke et al., 2004; Devos et al., 2004; Schwartz, 2005; Devos et al., 2006). We investigated the role of these domains in binding to Pom121 using *in vitro* binding assays with GST-fusions containing the β -propeller or α -solenoid domains of Nup155 or Nup160 (Figure 3-13). Similar

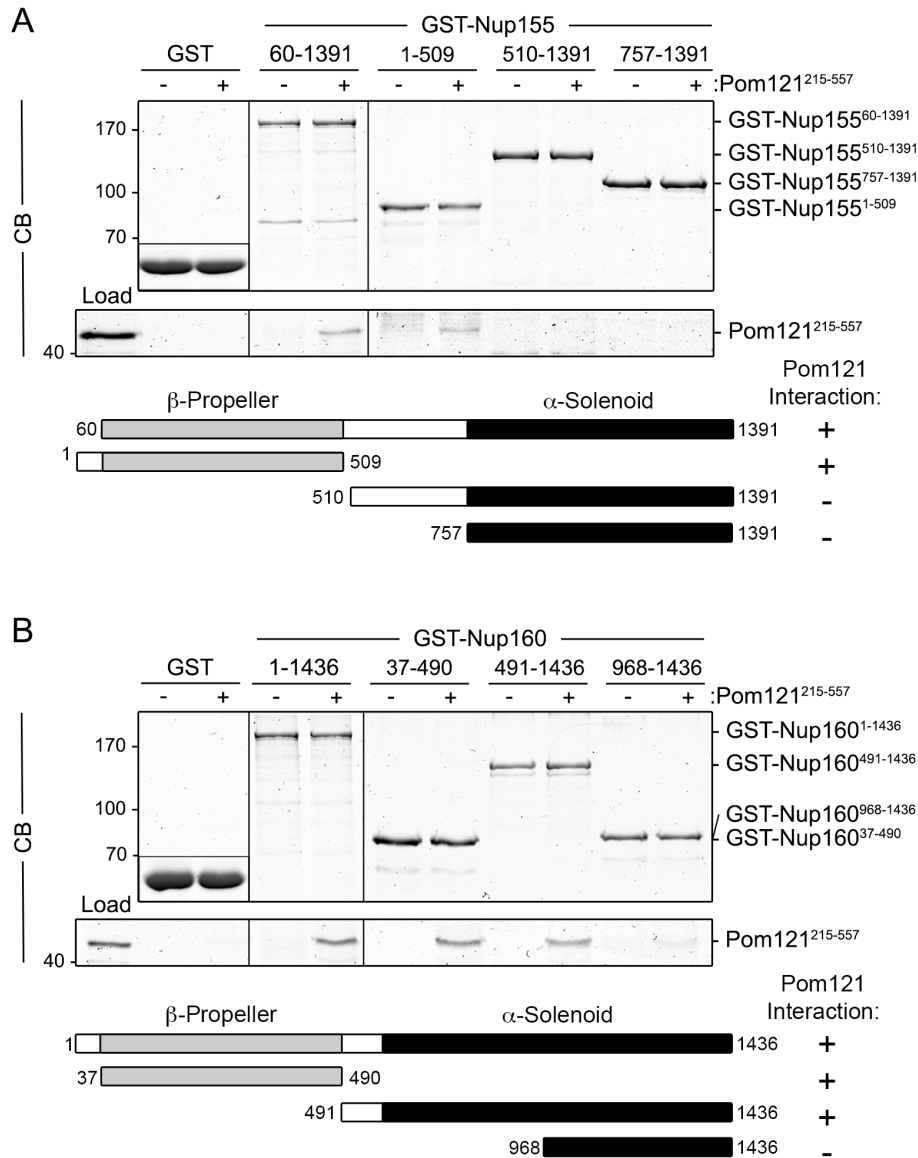


FIGURE 3-13 POM121 INTERACTS DIRECTLY N-TERMINAL DOMAINS OF NUP155 AND NUP160.

Purified Pom121²¹⁵⁻⁵⁵⁷ was incubated with bead-bound (A) GST-Nup155⁶⁰⁻¹³⁹¹, GST-Nup155¹⁻⁵⁰⁹, GST-Nup155⁵¹⁰⁻¹³⁹¹, and GST-Nup155⁷⁵⁷⁻¹³⁹¹, or (B) GST-Nup160¹⁻¹⁴³⁶, GST-Nup160³⁷⁻⁴⁹⁰, GST-Nup160⁴⁹¹⁻¹⁴³⁶, and GST-Nup160⁹⁶⁸⁻¹⁴³⁶. Shown in each panel are controls where Pom121²¹⁵⁻⁵⁵⁷ was incubated with GST alone (shown as inset). To obtain the results shown in each panel, bead-bound proteins were eluted using SDS-sample buffer, resolved by SDS-PAGE, and visualized by Coomassie blue (CB) staining. The lane marked Load contains 10% of the total purified Pom121²¹⁵⁻⁵⁵⁷ loaded on the beads. To the right of each panel, the point at which the named protein migrates in the appropriate lane is indicated. Schematic representations of Nup155 (A) and Nup160 (B) fragments and their observed binding to Pom121²¹⁵⁻⁵⁵⁷ are summarized. Mass markers are in kilodaltons.

to full length Nup155, a GST-fusion containing the Nup155 β -propeller region (GST-Nup155¹⁻⁵⁰⁹) bound to Pom121²¹⁵⁻⁵⁵⁷ (Figure 3-13A), however, no interaction was observed with truncations of the α -solenoid domain (GST-Nup155⁵¹⁰⁻¹³⁹¹ and GST-Nup155⁷⁵⁷⁻¹³⁹¹). The interaction of Nup160 with Pom121 was more complex. The predicted β -propeller of Nup160 (GST-Nup160³⁷⁻⁴⁹⁰) also interacted with Pom121²¹⁵⁻⁵⁵⁷ (Figure 3-13B). However, unlike Nup155, a GST-fusion containing a portion of the α -solenoid region of Nup160 (residues 491-1436) also bound Pom121. Further truncation of this fragment suggested the binding activity is likely contained within residues 491-967, as GST-Nup160⁹⁶⁸⁻¹⁴³⁶ showed only trace levels of bound Pom121²¹⁵⁻⁵⁵⁷. Together, these results suggest that Pom121 binds the β -propeller domains of Nup155 and Nup160, with Nup160 containing additional Pom121 interacting determinants. These former interactions appear to be specific for the β -propeller regions of Nup155 and Nup160, as the β -propeller domains of two other Nup107-160 complex subunits, Sec13 and Seh1, did not significantly bind Pom121²¹⁵⁻⁵⁵⁷ (Figure 3-14B).

The ability of similarly structured regions of Nup155 and Nup160 to bind to Pom121²¹⁵⁻⁵⁵⁷ raised the question of whether their β -propeller domains can bind simultaneously to Pom121 or whether their binding is mutually exclusive. To test this, we examined the ability of a preformed complex of purified, recombinant Pom121²¹⁵⁻⁵⁵⁷ and the β -propeller region of Nup155 (Nup155¹⁻⁵⁰⁹) to bind full length Nup160. Individually, Pom121²¹⁵⁻

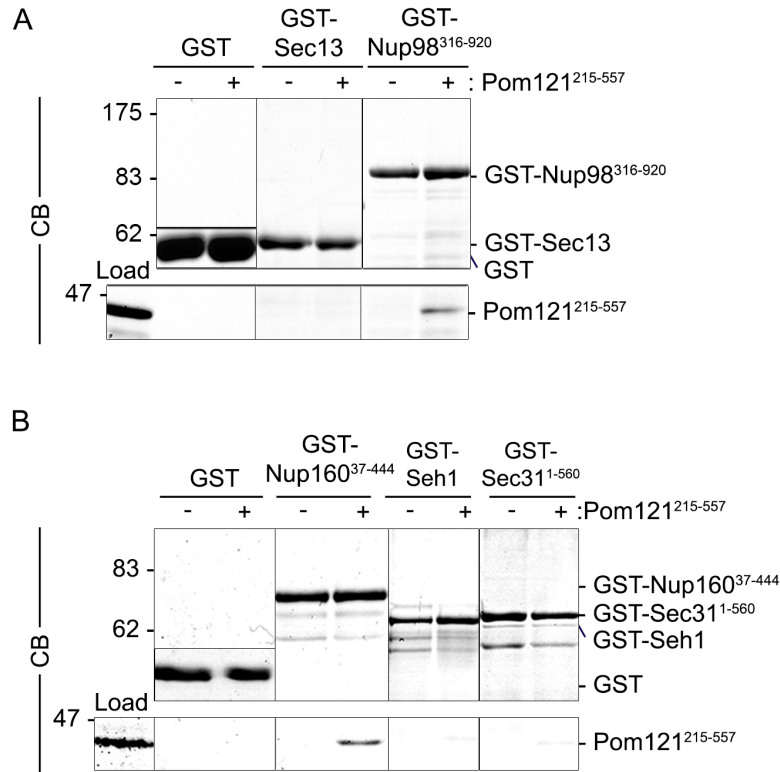


FIGURE 3-14 POM121²¹⁵⁻⁵⁵⁷ INTERACTS DIRECTLY WITH NUP98, BUT NOT SEH1 OR SEC31.

(A) Purified Pom121²¹⁵⁻⁵⁵⁷ was incubated with bead-bound GST-Sec13, GST-Nup98³¹⁶⁻⁹²⁰, or GST alone. Interacting proteins were eluted with SDS-sample buffer. Polypeptides were resolved by SDS-PAGE and visualized by Coomassie blue staining (CB). Approximately 10% of purified Pom121²¹⁵⁻⁵⁵⁷ incubated with each sample is indicated in the lane marked Load. (B) Purified Pom121²¹⁵⁻⁵⁵⁷ was incubated with bead-bound GST-Nup160³⁷⁻⁴⁴⁴, GST-Seh1, GST-Sec31 or GST alone (shown as inset). Bead-bound proteins were eluted using SDS-sample buffer, resolved by SDS-PAGE, and visualized by Coomassie blue (CB) staining. The lane marked Load contains 5% of the total purified Pom121²¹⁵⁻⁵⁵⁷ loaded on the beads. To the right of each panel, the point at which the named protein migrates in the appropriate lane is indicated. Mass markers are in kilodaltons.

⁵⁵⁷ or Nup155¹⁻⁵⁰⁹ was capable of binding bead-bound GST-Nup160 (Figure 3-13B, 3-15A, and 3-15C). However, when Pom121²¹⁵⁻⁵⁵⁷ was first incubated with Nup155¹⁻⁵⁰⁹, and the two proteins allowed to interact, the binding of these proteins to Nup160 was greatly inhibited (Figure 3-15C). These results suggest that the binding of Pom121²¹⁵⁻⁵⁵⁷ to Nup155¹⁻⁵⁰⁹ inhibits their interactions with Nup160.

3.3 DISCUSSION

We have demonstrated that Nup155 plays an essential role in the assembly of the mammalian NPC and is required for normal nuclear morphology. Depletion of Nup155 from HeLa cells results in a dramatic reduction in NPC number and the accumulation of Nups in cytoplasmic foci. Loss of Nup155 is also accompanied by massive changes in NE structure and the improper targeting of several integral membrane proteins to the INM. The critical role of Nup155 in NPC assembly and NE structure is likely played at the nuclear pore membrane domain where it interacts directly with the membrane Nups Pom121 and NDC1. We show that the N-terminal β -propeller region of Nup155 binds to the N-terminal third of Pom121. This same region of Pom121 also binds directly to the Nup107-160 complex through an interaction with the β -propeller region of Nup160. These results support a model in which the N-terminus of Pom121 anchors the NPC core through its binding to the β -propeller regions of Nup155 and Nup160. These

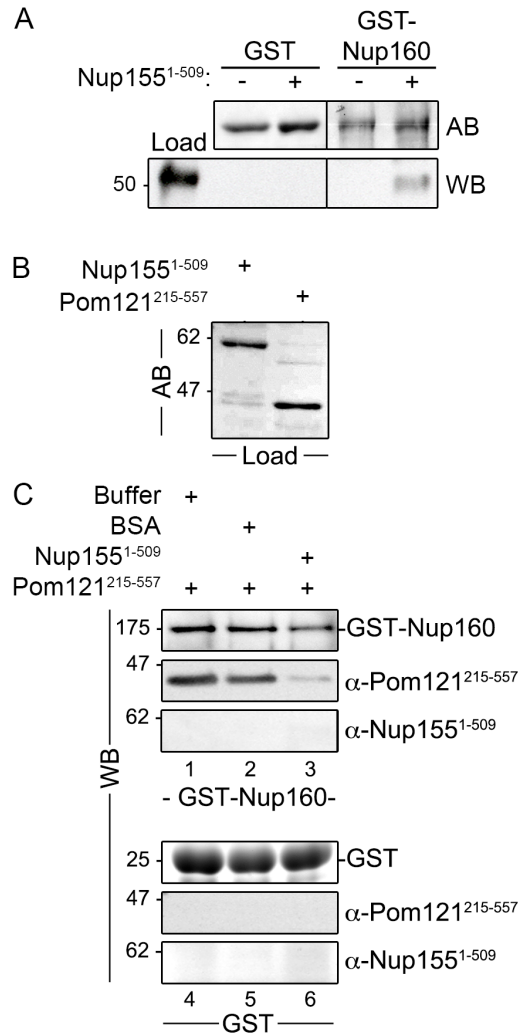


FIGURE 3-15 BINDING OF NUP155 TO POM121 PREVENTS THEIR INTERACTION WITH NUP160.

(A) Bead-bound GST-Nup160 or GST alone was incubated with purified Nup155¹⁻⁵⁰⁹. Bound proteins were eluted using SDS-sample buffer and resolved by SDS PAGE. Levels of GST and GST-Nup160 were visualized using amido black (AB). Nup155¹⁻⁵⁰⁹ was detected using a Nup155-specific polyclonal antibody. The lane marked Load contains 6% of the total purified Nup155¹⁻⁵⁰⁹ loaded on the beads. (B and C) Purified Pom121²¹⁵⁻⁵⁵⁷ and Nup155¹⁻⁵⁰⁹ (25% of the total Load protein is shown in B after amido black [AB] staining) were mixed and allowed to interact for 30 min before addition to bead-bound GST-Nup160 or GST alone (lanes 3 and 6). Note: to perform the binding reactions under similar conditions, Pom121²¹⁵⁻⁵⁵⁷ was supplemented with BSA to a total protein concentration similar to that of combined Pom121²¹⁵⁻⁵⁵⁷-Nup155¹⁻⁵⁰⁹. Bound proteins were eluted using SDS-sample buffer and resolved by SDS- PAGE. Western blotting (WB) using anti-Pom121, anti-Nup155, or anti-GST-Nup160 antibodies was used to detect the presence of each protein. Mass markers are indicated in kilodaltons.

interactions are likely to play an important role in the formation of the pore membrane and the assembly of the NPC core.

3.3.1 NUP155 IS ESSENTIAL FOR MAMMALIAN NPC ASSEMBLY AND NUCLEAR MORPHOLOGY

Through the use of siRNA-mediated depletion assays in human HeLa cells, we have shown that reducing cellular levels of Nup155 causes a drastic decrease in the number of NPCs and massive changes in nuclear structure (Figures 3-1 to 3-5). Changes in nuclear morphology in response to the loss of an individual Nup have been documented in various organisms, most notably in yeast (for review, see Doye and Hurt, 1995; Hetzer and Wentz, 2009). While the underlying cause of this general phenotype is unclear, its occurrence in response to different mutations suggests that it likely reflects a systemic response to the loss of NPC numbers or function that includes an increase in nuclear surface area and, perhaps, an attempt to increase total NPC numbers.

The depletion of Nup155 also causes a general decrease in the NE association of at least three INM proteins, LBR, Lem2, and Lap2, and a corresponding increase in the cytoplasmic pool of these proteins, presumably within the ER or other endomembranes (Figure 3-4 and 3-5). Moreover, Lap2 appears to concentrate in numerous foci along the NE, which are most clear in cells extracted with detergent prior to fixation (Figure 3-5). In cells permeabilized with digitonin, where the NE remains intact, these

Lap2 foci appear to accumulate in the ONM, as they are accessible to 'cytoplasmically positioned' antibodies that are excluded from the nuclear interior (Figure 3-5A). The ability of Lap2 to accumulate in the ONM would suggest binding sites for Lap2 are present there. One possibility is that Lap2, like another INM protein emerin, can interact with LINC complexes, macromolecular assemblies that span the double membrane of the NE (Haque et al., 2010).

The inhibition of membrane protein targeting to the INM appears to be a phenotype specific to the depletion of Nup155. Depletion of several other Nups, including Nup53 (Hawryluk-Gara et al., 2005); Figure 3-5), ELYS (Franz et al., 2007), or the adaptor scaffold Nup Nup188 (Theerthagiri et al., 2010) does not inhibit access of membrane proteins to the INM. In contrast, *X. laevis* nuclei assembled *in vitro* in the absence of Nup188 showed increased accessibility of membrane proteins to the INM (Theerthagiri et al., 2010). Furthermore, as depletion of Nup53 or ELYS inhibits NPC formation, merely reducing the number of NPCs is unlikely to limit the movement of membrane proteins to the INM. Instead, Nup155 may play a more direct role as suggested for its counterpart, Nup170p, in *S. cerevisiae* (King et al., 2006). In yeast, karyopherins have been shown to play an active role in the targeting of at least a subset of membrane proteins to the INM. These studies also showed that INM protein targeting is compromised by the loss of Nup170p. While the mechanistic basis for these observations is unclear, our data are consistent with a similar pathway functioning in higher eukaryotes.

3.3.2 THE β -PROPELLER REGIONS OF NUP155 AND NUP160 BIND DIRECTLY TO POM121

On the basis of several observations, we conclude that Nup155 is positioned in close proximity to the pore membrane. Our pulldown analysis using GST-Nup155 revealed binding to Pom121 and NDC1, and, importantly, direct interactions between domains of these membrane proteins and Nup155 could be reconstituted *in vitro* using recombinant proteins (Figure 3-6, 3-8, and summarized in Figure 3-16). Our proposed localization of Nup155 adjacent to the pore membrane is similar to that suggested for its yeast counterparts, Nup157p and Nup170p (Tcheperegine et al., 1999; Alber et al., 2007b; Flemming et al., 2009; Makio et al., 2009; Onischenko et al., 2009). Nup170p directly interacts with the yeast pore membrane protein Pom152p (Makio et al., 2009) and is positioned in the vicinity of Ndc1p in architectural models of the yeast NPC (Alber et al., 2007a; Alber et al., 2007b). However, no direct interaction has been reported between Nup170p and Ndc1p.

The ability of Pom121 and Pom152p to bind Nup155 and Nup170p, respectively, would suggest they share similar functions in the NPC. In support of this idea, we also observed that the Nup155 binding region of Pom121 (residues 215-557) can directly bind yeast Nup170p (Figure 3-17E). Similarly, a pore-exposed region of Pom152p (residues 1-111) can bind Nup155, as well as members of the Nup107-160 complex, in pulldown assays (Figure 3-17A-D). Thus, while Pom121 and Pom152p fail to exhibit any

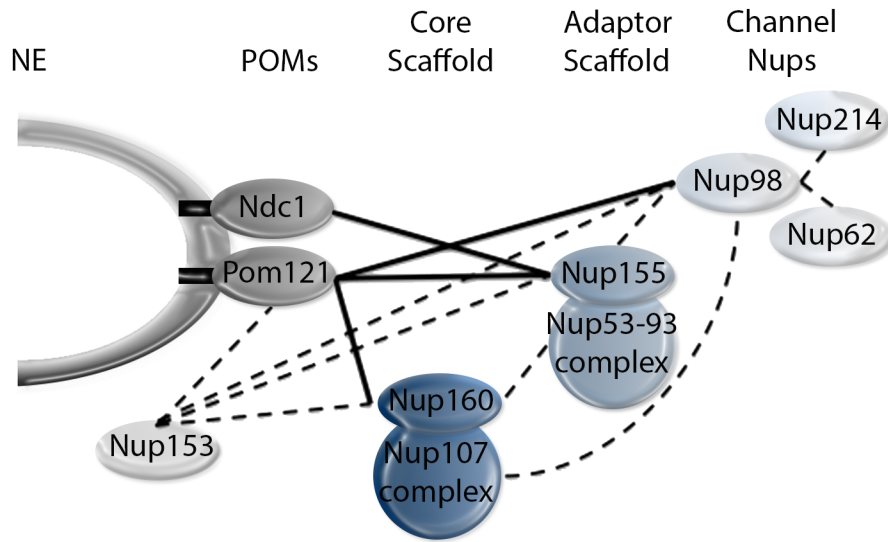


FIGURE 3-16 MODEL OF DIRECT AND INDIRECT INTERACTIONS IDENTIFIED IN THIS STUDY.

Solid lines depict direct interactions identified using *in vitro* binding assays. Dashed lines represent interactions identified from pulldown experiments using rat liver nuclear envelopes and recombinant GST-tagged Nups as bait (see Figures 3-6, 3-8, 3-10, 3-12 and 3-14). The transmembrane domains of Pom121 and NDC1 within the pore membrane domain of the nuclear envelope (NE) are indicated by black rectangles.

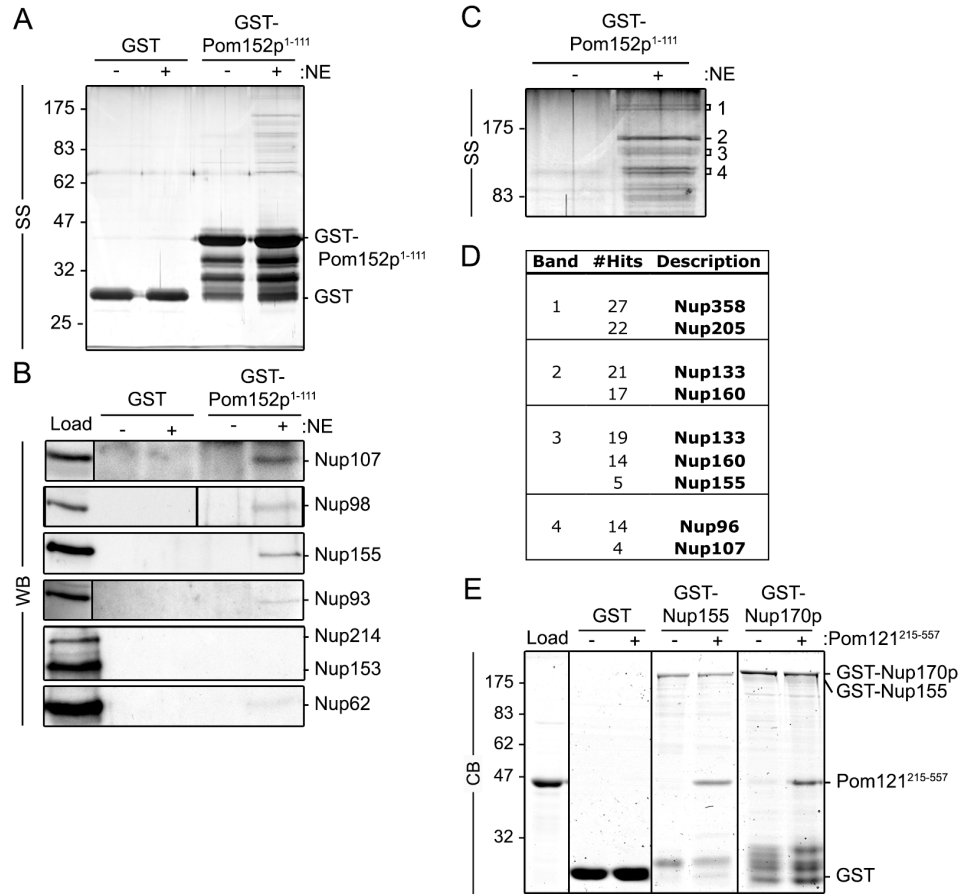


FIGURE 3-17 POM152P¹⁻¹¹¹ INTERACTS WITH NUP155 AND THE NUP107-160 COMPLEX.

(A–D) Bead-bound GST-Pom152p1-111 or GST alone were incubated with (+) or without (-) rat liver NE extracts. Interacting proteins were eluted with SDS-sample buffer. Polypeptides were resolved by SDS-PAGE and visualized by silver staining (SS; A and C) or were detected by Western blot (WB; B) using antibodies directed against the indicated proteins. mAb414 was used to detect Nup62, Nup153, and Nup214. Approximately 5% of the NE extract loaded on each column was resolved in the lane marked Load. (C) Shown is a magnification of a region of the gel from A, including labeled sections of the gel that were analyzed by mass spectrometry (labeled 1–4). (D) Proteins detected by MS in each of the excised gel regions and the numbers of peptides identified in the corresponding polypeptide are indicated. (E) Purified Pom121215–557 was incubated with bead-bound GST-Nup155, GST-Nup170p, or GST alone. Bead-bound proteins were eluted using SDS-sample buffer, resolved by SDS-PAGE, and visualized by Coomassie blue (CB) staining. The lane marked Load contains 25% of the total purified Pom121215–557 loaded on the beads. To the right of each panel, the point at which the named protein migrates in the appropriate lane is indicated. Mass markers are in kilodaltons.

extensive sequence similarity, their ability to bind similar Nups across species lead us to conclude that they contain conserved Nup binding regions. However, these domains remain difficult to pinpoint. They may be small, or contained within uncharacterized secondary or tertiary structural features.

In addition to Nup155, our GST-Pom121 pulldown experiments also detected components of the Nup53-Nup93 complex, the Nup107-160 complex, and EYLS (a binding partner of the Nup107-160 complex) (Figure 3-10 and 3-11). These results are in agreement with previously reported data obtained from pulldown experiments using *X. laevis* Pom121 and egg cytosol (Rasala et al., 2008). Importantly, we have now shed light on the molecular basis of these associations by establishing the nature of these interactions, most notably the identification of Nup160 as a direct binding partner of Pom121 within the Nup107-160 complex (Figure 3-13 and 3-15). Through further analysis of the interactions of Pom121 with Nup160 and Nup155, we have determined that the primary Pom121 binding region in each Nup is contained within an N-terminal β -strand-rich region predicted to form a β -propeller (Berke et al., 2004). This structural feature is known to mediate many protein-protein interactions (Hudson and Cooley, 2008).

Within the NPC, β -propeller motifs are most prevalent in the core scaffold Nups. In particular, six of the nine members of the Nup107-160 complex contain predicted β -propeller structures. However, little is known about their interacting partners or their functions. In the yeast counterpart of the Nup107-160 complex (the Nup84p complex), binding partners for two

β -propeller proteins, Seh1p and Sec13p, have been identified as Nup85p and Nup145Cp (Hsia et al., 2007; Brohawn et al., 2008; Debler et al., 2008), both of which are components of the Nup84p complex. Our studies now establish the β -propeller regions of Nup160 and Nup155, but not Seh1 or Sec13, as key structural elements in linking their respective protein complexes to Pom121.

A role for Nup160 in positioning the Nup107-160 complex near the pore membrane is also inferred by studies of its yeast counterpart, Nup120p. Like Nup160, Nup120p has been proposed to lie adjacent to the pore membrane (Alber et al., 2007a; Alber et al., 2007b). Moreover, other observations suggest Nup120p is strategically positioned to influence the structure and oligomeric state of the Nup84p complex. Elegant studies have shown that Nup120p contributes one arm to the Y-shaped Nup84p complex (Siniosoglou et al., 2000; Lutzmann et al., 2002; Kampmann and Blobel, 2009). Recently, it has also been proposed that Nup120p may link consecutive Nup84p complexes by binding Nup133p, positioned at the foot of the Y complex, to form rings consisting of eight Nup84p complexes arranged head-to-tail (Seo et al., 2009). The C-terminal, α -helical region of Nup120p mediates binding to Nup133p. This would position the N-terminal β -propeller of Nup120p near the junction between Nup84p complexes but free to interact with other binding partners, including membrane proteins such as Pom152p. It is intriguing to consider that this conformation of Nup120p molecules, established by the formation of a ring of Nup84p complexes, may facilitate their membrane association. By analogy, Nup160

could contribute to the interactions of similar higher-order structures to Pom121.

We also observe that Pom121 binds to the predicted β -propeller region of Nup155. These results lead us to conclude that the N-terminal region of Pom121 (within residues 215-557) contains one or more binding sites for the β -propeller regions of at least two Nups (Nup155 and Nup160). The extent to which Pom121 binds other β -propeller containing Nups has not been fully explored. However, in examining a subset of these Nups, we have observed specificity for Nup155 and Nup160, as the β -propeller proteins Sec13 and Seh1, as well as the COPII protein Sec31, show only negligible binding to Pom121 (Figure 3-14). Importantly, our analysis has also led us to conclude that, while Pom121 can bind the β -propeller regions of both Nup155 and Nup160, it cannot interact with them both simultaneously (Figure 3-15). This could be explained by direct competition between these Nups for a single site on Pom121 or by one β -propeller inducing a conformational change in Pom121 that blocks a second β -propeller binding site.

Our results may reflect the presence of separate Pom121-Nup155 and Pom121-Nup160 complexes within the NPC. A single Nup in two distinct complexes is not unprecedented. For example, yeast Nsp1p appears to be part of two distinct complexes (Grandi et al., 1993; Grandi et al., 1995a; Grandi et al., 1995b; Bailer et al., 2001). Another possibility is that the interactions between individual β -propeller proteins and Pom121 are

dynamic and change under different conditions. For instance, interactions between Pom121 and a specific Nup could be established and later broken during the course of NPC assembly or be altered in response to changes in the transport properties of the NPC (Feldherr, 1998; Feldherr et al., 2002; Makhnevych et al., 2003). Plasticity in molecular interactions between Nups and Pom121 is supported by our experiments showing that full length Nup160 can bind to Pom121 and the β -propeller of Nup155 if each is presented individually (Figure 5-13 and 5-15). However, Nup160 does not bind a preformed Nup155-Pom121 complex (Figure 5-15). These results would suggest that conditions that disrupt the interactions of Nup155 and Pom121 could facilitate their interactions with Nup160.

3.3.3 IMPLICATIONS FOR THE ROLE OF NUP155 AND NUP160 IN NPC ASSEMBLY

The molecular architecture of Nup155 and Nup160, consisting of an N-terminal β -propeller and a C-terminal α -solenoid, is similar to the outer cage components of CPCs functioning in vesicular transport, including clathrin and Sec31 (Berke et al., 2004; Schwartz, 2005; Stagg et al., 2007). Based on this similarity, it has been hypothesized that the β -propeller- α -solenoid Nups play a role at the pore membrane similar to their counterparts in the CPC (Devos et al., 2004; Schwartz, 2005; Devos et al., 2006), including inducing and maintaining membrane curvature during and following NPC formation. How Nups such as Nup155 and Nup160 might perform these functions, and the degree to which they are similar to those performed by

CPCs, is unclear. Based on our data, we believe that these Nups play a more direct role in interfacing with membranes and membrane proteins than clathrin or Sec31. For instance, clathrin and Sec31 do not bind directly to membranes and both require adaptor proteins to bridge their interactions with integral membrane cargo proteins (Gurkan et al., 2007; Pucadyil and Schmid, 2009). By contrast, our data indicate that Nup155 and Nup160 directly interact with membrane proteins, which could be viewed analogously to 'cargo' proteins of CPCs. Moreover, certain β -propeller- α -solenoid Nups also contain predicted amphipathic ALPS motifs, including Nup133, Nup120p, and Nup170p (Drin et al., 2007) that may allow them to directly bind the pore membrane. In fact, *in vitro* binding studies have demonstrated that the ALPS motif of Nup133 is capable of directly binding vesicles with a defined membrane curvature (Drin et al., 2007). ALPS motifs and other amphipathic features are present in some components of the adaptor layer of CPCs but have not been detected in clathrin or Sec31. In addition to their ability to interface with the membrane, members of β -propeller- α -solenoid Nups also interact with other Nups that appear capable of inducing and/or stabilizing membrane curvature. Nup155 interacts with Nup53 (Figure 3-6; Hawryluk-Gara et al., 2005) and both Nup155 and the Nup107-160 complex bind Nup153 (Figure 3-6, 3-10 and 3-11; Vasu et al., 2001). The overproduction of both Nup153 and the yeast counterpart of Nup53 induce membrane proliferation and the formation of tubular membranes (Bastos et al., 1996; Marelli et al., 2001). Thus, the Pom121-

mediated juxtaposition of Nup155 and Nup160, as well as Nup98, to the membrane may aid in the association of additional Nups with the POM.

We envisage a model in which the pore-exposed region of Pom121 extends toward the central axis of the NPC with its N-terminal region positioned nearest the membrane and functioning as a binding site for Nup155 and Nup160 and their respective complexes. As is the case in yeast, how these complexes are configured relative to one another and the membrane is open to speculation (Alber et al., 2007b; Hsia et al., 2007; Brohawn and Schwartz, 2009a). More C-terminal regions of Pom121 containing its FG-repeat domain are predicted to extend beyond this coat into the central channel of the NPC where it would join other FG-Nups to facilitate the movement of transport factors through the NPC.

The interactions of Pom121 with Nup155 and Nup160 and their juxtaposition to the pore membrane are consistent with several observations that place these proteins at critical, and temporally related, steps in NPC assembly. As we have shown here, siRNA depletion of Nup155 in HeLa cells leads to a reduction of NPCs and the mislocalization of all Nups examined, including Pom121, into cytoplasmic foci (Figure 3-3). These phenotypes are consistent with those observed upon depletion of the orthologues of human Nup155 in *C. elegans* and *S. cerevisiae* (Franz et al., 2005; Flemming et al., 2009; Makio et al., 2009; Onischenko et al., 2009). Efficient depletion of Pom121 also leads to a decrease in NPC numbers and an accompanying decline in the NE association of several Nups including Nup155 (Figure 3-9;

Mansfeld et al., 2006; Funakoshi et al., 2007). Consistent with these data, several observations indicate that Pom121 and Nup155 may function at a similar step in NPC assembly that is closely linked to formation and stabilization of the pore membrane. Beyond the afore mentioned physical relationship to the membrane, studies examining the effects of depleting these proteins on NE and NPC assembly in *X. laevis* egg extracts point to a similar role for these proteins in the membrane dynamics required for NE and NPC assembly (Antonin et al., 2005; Franz et al., 2005). In fact, depletion of either Nup155 or Pom121 appears to activate a NE assembly checkpoint, which inhibits the formation of the double membrane NE (Antonin et al., 2005; Franz et al., 2005). Interestingly, NE assembly arrest is dependent on the Nup107-160 complex, suggesting that this complex plays a key role in sensing the completion of critical NE and NPC assembly steps necessary to inactivate the checkpoint. Among these steps may be the interactions of Pom121 and/or Nup155 with Nup160.

Since the initial publication of this manuscript (2010), several groups have independently examined the NPC-binding domain of Pom121 described here (Pom121²¹⁵⁻⁵⁵⁷) to more clearly define a role for Pom121 in NE/NPC biogenesis (Doucet et al., 2010; Yavuz et al., 2010; Funakoshi et al., 2011; Shaulov et al., 2011). Intriguingly, two distinct bipartite NLS regions within the NPC-binding domain of *X. laevis* Pom121 have been defined (Doucet et al., 2010; Yavuz et al., 2010; Shaulov et al., 2011). Five distinct NLS regions within the same domain of the human Pom121 orthologue have

similarly been uncovered (Funakoshi et al., 2011). These NLS regions have been demonstrated to bind to the importins Kap β and Kap α , and are required for the efficient targeting of Pom121 to the NE during interphase (Yavuz et al., 2010; Funakoshi et al., 2011). Correspondingly, mutations of Pom121 NLSs inhibit Pom121 recruitment to the NE, and specifically inhibit NPC assembly during interphase (see section 1.5.2) (Doucet et al., 2010; Funakoshi et al., 2011).

Importantly, binding of the Nup107-160 complex at 'seeding sites' of future NPC assembly is unaffected in the absence of Pom121. While it has been shown that recruitment of the Nup107-160 complex to chromatin requires the AT-hook binding domain of ELYS (section 1.5.1.4), binding of Pom121 to chromatin has been mapped to two distinct regions of the NPC-binding domain (Shaulov et al., 2011). These results suggest a model whereby Pom121 and Nup107-160 complex members are recruited independently to sites of future NPC assembly at the NE. According to the data presented here, a critical next step in NPC assembly would be the establishment of interactions between Pom121 with the scaffold Nups Nup155 and Nup160, ultimately leading to fusion of INM and ONM leaflets and completion of NPC assembly.

CHAPTER IV: STRUCTURAL EVOLUTION OF THE MEMBRANE COATING MODULE OF THE NUCLEAR PORE COMPLEX

A version of this chapter has been previously published in: X. Liu†, J.M. Mitchell†, R.W. Wozniak, G. Blobel, and J. Fan. 2012. Structural evolution of the membrane-coating module of the nuclear pore complex. *Proceedings of the National Academy of Sciences of the United States of America*. 109:16498-16503. †X. Liu, and J.M. Mitchell contributed equally to this work.

The division of labor that resulted in data presented in the following chapter was as follows: X. L. produced viral bacmids, amplified viral stocks, elicited protein production and performed affinity purifications. J. M. M. performed affinity purifications, anion exchange chromatography, gel filtration chromatography, crystallization trials and optimization, and evaluated crystal quality by initial diffraction analyses. J. F. assisted in optimization of crystal conditions, collected x-ray diffraction data, and solved the structures of Sp-Nup37 and the Sp-Nup120¹⁻⁹⁵⁰-Nup37 complex. Structural analyses were performed by J. F. with assistance in interpretation from G. B. and J. M. M. Figures presented in the manuscript and in the following chapter were produced by J. F. and J. M. M.

4.1 OVERVIEW

The coatomer module of the nuclear pore complex borders the cylinder-like nuclear pore membrane domain of the nuclear envelope. In evolution, a single coatomer module increases in size from hetero-heptamer (*S. cerevisiae*, *Sc*) to hetero-octamer (*S. pombe*, *Sp*) to hetero-nonamer (metazoan cells). Notably, the heptamer-octamer transition proceeds through acquisition of the nucleoporin Nup37. How Nup37 contacts the heptamer was unknown. Using recombinant nucleoporins, we show that Sp-Nup37 binds the Sp-Nup120 member of the hetero-heptamer, but does not bind an Sc-Nup120 homolog. To elucidate the Nup37-Nup120 interaction at the atomic level, we carried out crystallographic analyses, either of Sp-Nup37 alone or in a complex with an N-terminal, ~110 kDa fragment of Sp-Nup120, comprising residues 1-950. Corroborating structural predictions, we determined that Nup37 folds into a 7-bladed β -propeller. Several disordered surface regions of the Nup37 β -propeller assume structure when bound to Sp-Nup120. The N-terminal domain of Sp-Nup120¹⁻⁹⁵⁰ also folds into a 7-bladed propeller with a markedly protruding 6D-7A insert, and is followed by a contorted helical domain. Conspicuously, this 6D-7A insert contains an extension of 50 residues, which is highly conserved also in metazoan cells, but is absent in Sc-Nup120. Strikingly, it is this extension of the 6D-7A insert where numerous contacts to the Nup37 β -propeller are localized. Another contact region is situated toward the end of the helical region of Sp-Nup120¹⁻

⁹⁵⁰. Our findings inform on the evolution and the assembly of the coatomer module of the nuclear pore complex.

4.2 RESULTS

4.2.1 NUP37 BINDS TO NUP120 DIRECTLY

Nup37 and Nup43 were detected as additional members of the Y-shaped complex isolated from vertebrate cells (Fontoura et al., 1999; Loiodice et al., 2004). To determine which member of the Sp Y-shaped complex interacts with Nup37, we performed gel filtration analysis using various combinations of recombinant proteins. We found that full-length Sp-Nup37 bound to full-length Sp-Nup120 (referred to as Nup37 and Nup120 in the following text unless otherwise indicated). But as Sc lacks a counterpart of Nup37, Nup37 failed to bind to full-length Sc-Nup120 (Figure 4-1A-C). SDS-PAGE analysis revealed that full-length Nup120 was partially proteolyzed into a ~110 kDa fragment (indicated by an asterisk in Figure 4-1B, left panel), which remained competent to bind Nup37. Guided by secondary structure predictions, we made several C-terminally truncated forms of Nup120 and identified a stable fragment Nup120¹⁻⁹⁵⁰ that could be co-crystallized with full-length Nup37 (J. Fan, personal communication).

4.2.2 STRUCTURE DETERMINATION

We crystallized Nup37 protein by itself or in complex with Nup120¹⁻⁹⁵⁰. Non-liganded Nup37 was crystallized in space group P4₁2₁2 with one molecule in one asymmetric unit. The structure was solved by single-anomalous dispersion (SAD) using anomalous X-ray diffraction data obtained

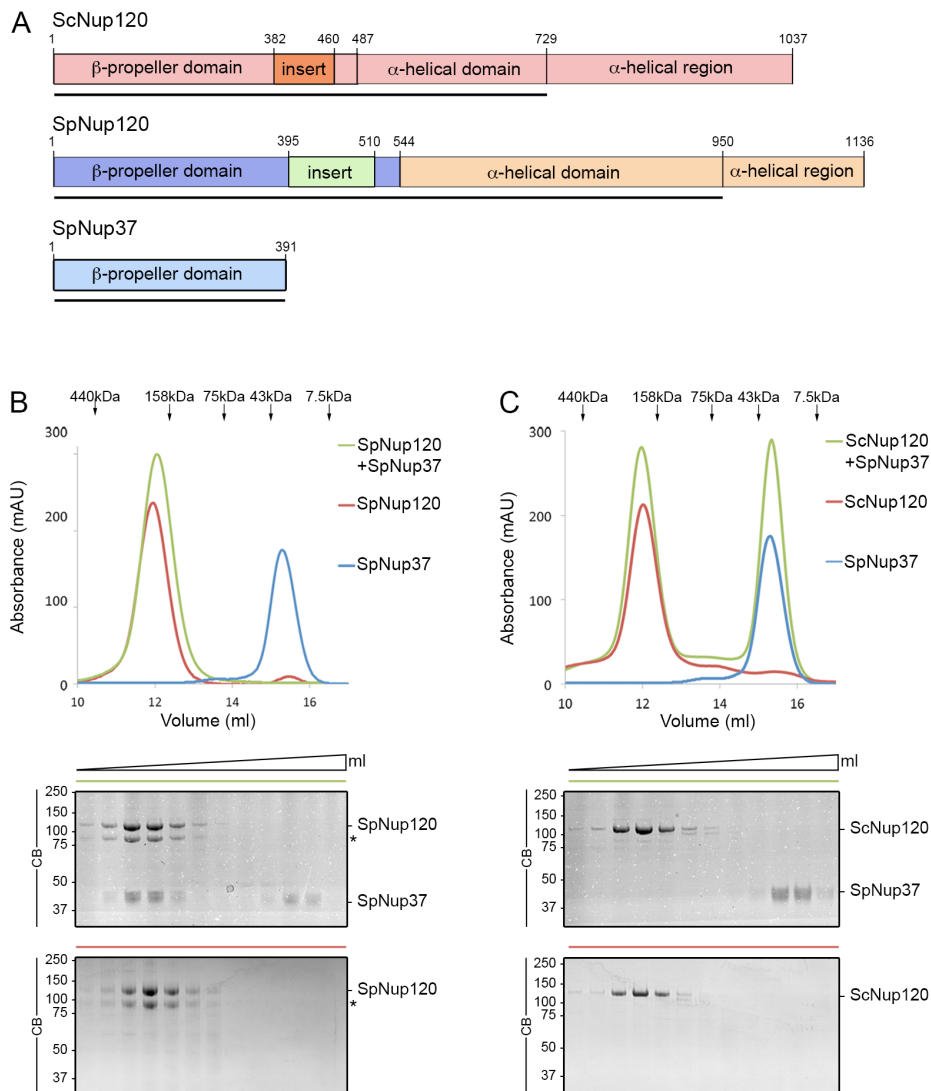


FIGURE 4-1 NUP120 OF *S. POMBE* (SP), BUT NOT OF *S. CEREVISIAE* (SC), DIMERIZES WITH NUP37.

(A) Domain structures of Sc-Nup120, Sp-Nup120, and Sp-Nup37 are indicated by various colors; residue numbers indicate boundaries for each domain, and bars depict crystallized domains. (B and C) Full-length Sp-Nup120, but not Sc-Nup120, forms a complex with Sp-Nup37, as detected by gel filtration (top) and SDS/PAGE analysis of indicated fractions (bottom). Colored lines above CB-stained gels correspond to gel filtration legend. Asterisk in B indicates major degradation product of Sp-Nup120.

from a Hg-derivative crystal. The structure was refined to 2.4 Å resolution with R_{work} and R_{free} values of 20% and 22% (for details of crystallographic statistics, see Table 4-1). The structure of Nup37 provided the initial phases for the structure determination of the Nup120¹⁻⁹⁵⁰-Nup37 complex.

The Nup120¹⁻⁹⁵⁰-Nup37 complex crystallized in space group of $P2_12_12_1$ with one copy of the hetero-dimer in the asymmetric unit. The structure was solved by combining phase information from the non-liganded Nup37 structure and isomorphous anomalous signal from Hg and Au using MR-SAD method by PHENIX (Adams et al., 2010). The assignment of residues during model building was aided by the heavy atom positions (Figure 4-2), and the structure was refined to 2.5 Å resolution with R_{work} and R_{free} values of 21% and 25%, respectively (Table 4-1).

4.2.3 NON-LIGANDED NUP37 STRUCTURE

Nup37 folds into a seven-blade donut-shaped β -propeller domain, with an outer dimension of 50 Å wide and 30 Å high (Figure 4-3A). The seven radially arranged blades enclose a central water-rich tunnel ~10 Å in diameter. The WD-40 repeats in Nup37 lack the typical Trp-Asp (WD) sequence for known classes of WD-40 repeats, which supports the notion that WD-40 repeats are highly degenerated repeats (van der Voorn and Ploegh, 1992). Common to most β -propellers, the 7th blade of the Nup37 β -propeller is characterized by “Velcro” arrangement, for which, the interaction

TABLE 4-1 STATISTICS FROM CRYSTALLOGRAPHIC ANALYSIS.

Dataset	Nup120 ¹⁻⁹⁵⁰ .Nup37 native	Nup120 ¹⁻⁹⁵⁰ .Nup37 Au	Nup120 ¹⁻⁹⁵⁰ .Nup37 Hg
Wavelength	1.075	1.039	1.009
Space group	P2 ₁ 2 ₁ 2 ₁	P2 ₁ 2 ₁ 2 ₁	P2 ₁ 2 ₁ 2 ₁
Cell dimensions			
<i>a</i> , <i>b</i> , <i>c</i> (Å)	70, 123, 172	69.7, 122.9, 172.1	69.7, 122.7, 172.8
α, β, γ (°)	90, 90, 90	90, 90, 90	90, 90, 90
Resolution (Å)	35.0–2.4 (2.5–2.4)	35–3.3 (3.4–3.3)	50–3.1 (3.2–3.1)
R _{sym} (%)	7 (91.4)	13.7 (80)	10.1 (94.5)
I/σI	34 (2.6)	25 (3.2)	32.3 (2.4)
Completeness (%)	99.5 (99.4)	100 (100)	100 (100)
Redundancy	7.2 (7.6)	6.8 (7.0)	6.5 (6.5)
Refinement			
Resolution (Å)	35.0–2.4 (2.46–2.4)		
Reflections (F >0σ)	56346		
Total atoms	10231		
R factor (%)	21 (32.6)		
R _{free} (%)	25.8 (41)		
rmsd			
Bond lengths (Å)	0.006		
Bond angles (°)	1.1		
B factors (Å ²)	62.1		
Ramachandran plot			
Favored/allowed (%)	88/12		

Dataset	Nup37 native	Nup37 Hg
Wavelength	1.075	1.009
Space group	P4 ₁ 2 ₁ 2	P4 ₁ 2 ₁ 2
Cell dimensions		
<i>a</i> , <i>b</i> , <i>c</i> (Å)	131, 131, 117	131, 131, 117
α, β, γ (°)	90, 90, 90	90, 90, 90
Resolution (Å)	45–2.4 (2.5–2.4)	35.0–3.2 (3.3–3.2)
R _{sym} (%)	7.2 (76)	13.4 (78.5)
I/σI	31.3 (3.0)	35.1 (5.6)
Completeness (%)	99.7 (100)	92.3 (94.5)
Redundancy	4.8 (5.0)	12 (10.7)
Refinement		
Resolution (Å)	35–2.4 (2.5–2.4)	
Reflections (F >0σ)	38275	
Total atoms	2777	
R factor (%)	20.7 (28.2)	
R _{free} (%)	21.9 (31)	
rmsd		
Bond lengths (Å)	0.009	
Bond angles (°)	1.4	
B factors (Å ²)	55.6	
Ramachandran plot		
Favored/allowed (%)	95.5/4.5	

$R_{sym} = \frac{\sum_h \sum_i |I_{hi} - I_h|}{\sum_h \sum_i I_{hi}}$ for the intensity (*I*) of *i* observations of reflection *h*. R factor = $\frac{\sum ||F_{obs}| - |F_{calc}||}{\sum |F_{obs}|}$, where *F*_{obs} and *F*_{calc} are the observed and calculated structure factors, respectively. Numbers in parentheses indicate the highest resolution shell and their statistics. R_{free}, R factor calculated using reflection data chosen randomly (5% of data) and omitted from the start of refinement.

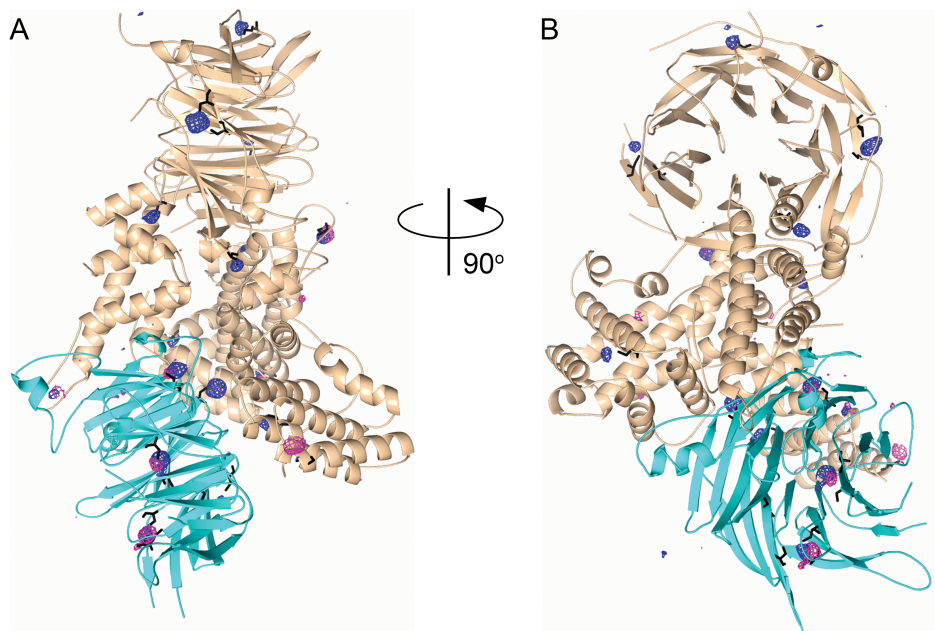


FIGURE 4-2 EXPERIMENTAL PHASING.

(A and B) Two views of the anomalous difference Fourier maps, contoured at the $4\text{-}\sigma$ level, illustrating mercury (blue) and gold (pink) modification sites. Cysteine residues (black) in the close vicinity are shown as sticks.

between D-strand from the N-terminus and C- strand from the C-terminus marks the closure site of the propeller (marked by an asterisk in Figure 4-3A). This “Velcro” closure is thought to provide extra structural stability to the propeller (Chaudhuri et al., 2008). The top surface of the β -propeller is decorated by short DA and BC loops and the bottom surface by longer AB and CD loops. Compared to the top short loops, which have a mean B-factor of $\sim 50 \text{ \AA}^2$, most of the bottom long loops exhibit higher flexibility as indicated by their higher B-factor (average B-factor of $\sim 80 \text{ \AA}^2$). In particular, the bottom 2AB, 4CD, and 5CD loops are not visible in non-liganded state.

4.2.4 OVERALL STRUCTURE OF THE NUP120¹⁻⁹⁵⁰-NUP37 COMPLEX

The Nup120¹⁻⁹⁵⁰-Nup37 hetero-dimer, composed of ~ 110 kDa Nup120¹⁻⁹⁵⁰ and ~ 40 kDa Nup37, forms a compact structure with an overall dimension of $80 \text{ \AA} \times 75 \text{ \AA} \times 130 \text{ \AA}$. Nup120¹⁻⁹⁵⁰ is folded into an N-terminal seven-bladed β -propeller domain with a large α -helical insert between the 6th and 7th blade, followed by a contorted α -helical domain (Figure 4-3B). Its β -propeller domain and C-terminal α -helical domain were packed in a plane whereas its 6D-7A insert and the captured Nup37 β -propeller projected from the surface of this plane. Moreover, the 6D-7A insert and the C-terminal α -helical domain are organized like a pair of clamps, with one end opening up wider than the other, fastening two β -propeller domains in both ends (Figure 4-3B, right panel). The Nup120 β -propeller sits at the narrower

FIGURE 4-3 BICYCLE-LIKE STRUCTURE OF THE NUP120¹⁻⁹⁵⁰·NUP37 COMPLEX.

(A) Cartoon representation of the non-liganded (upper) and bound (lower) forms of Nup37 showing the bottom of the β -propeller. Of the four disordered regions (dotted lines, Upper), three assume structure in the bound form (Lower). (B) Ribbon representation from two angles; blue, β -propeller domain of Nup120; green, 6D-7A insert of β -propeller; wheat, helical domain of Nup120; cyan, β -propeller of Nup37. The blades of the two β -propeller structures (note their opposite orientation) and some prominent α -helices are labeled. Note that the helical domain of Nup120 (wheat) provides much of the bicycle frame including one side of each of the two prongs for mounting the two wheels, with the other side provided by the β -propeller insert (green); the “front” wheel is the Nup120 β -propeller; the “rear” wheel is the Nup37 β -propeller. (C) Schematic tracing of polypeptide chains of Nup120¹⁻⁹⁵⁰ and full-length Nup37; β -strands of β -propellers (A-E) are indicated by thick arrows; α -helices (h1-h30) are indicated by rectangles and are numbered in order of their occurrence from the N to the C terminus; loops are indicated by lines, and disordered regions are indicated by dotted lines; a dotted outline indicates a portion of β -propeller insert that is absent in Sc-Nup120.

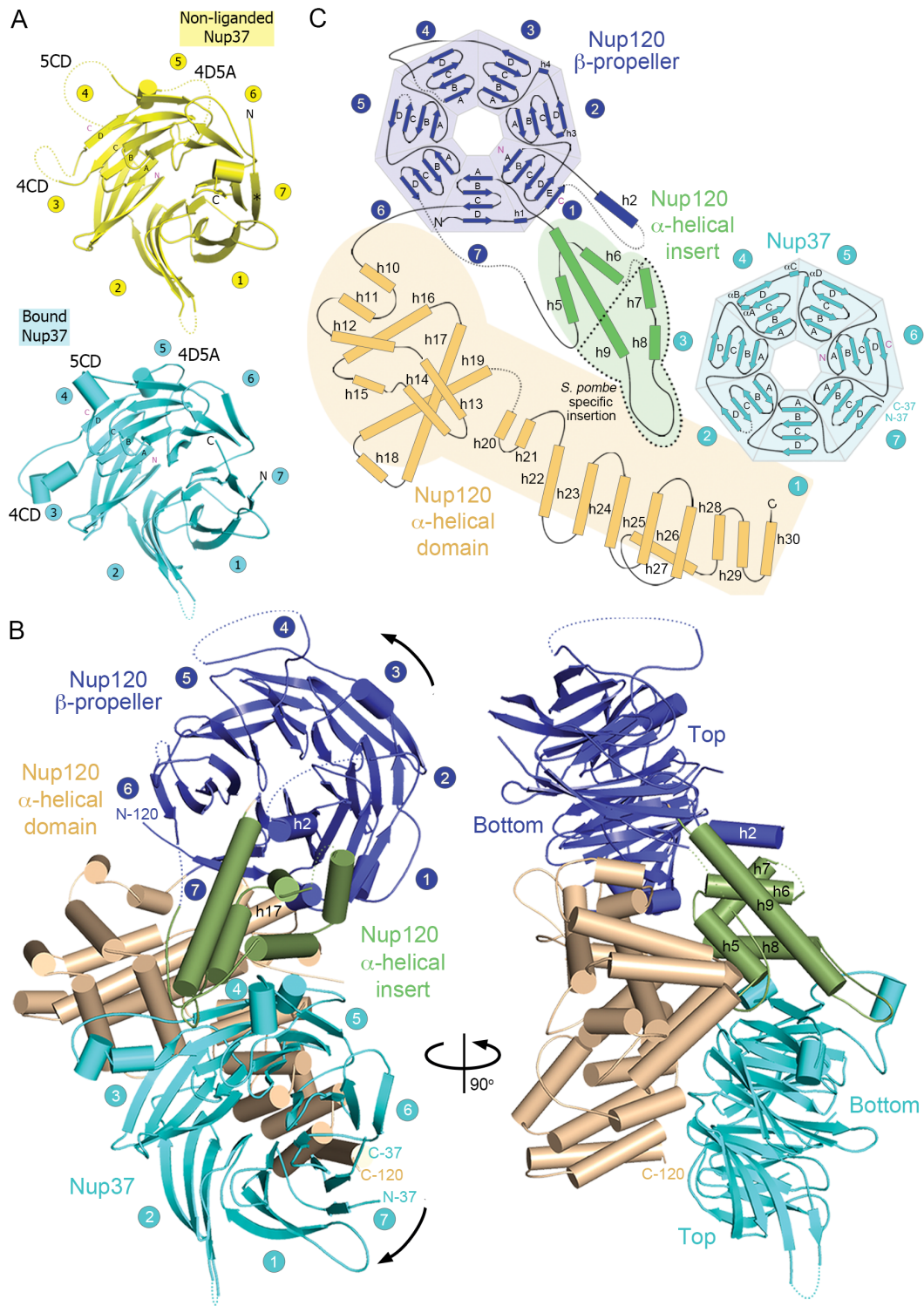


FIGURE 4-3 BICYCLE-LIKE STRUCTURE OF THE NUP120¹⁻⁹⁵⁰-NUP37 COMPLEX.

end while Nup37 β -propeller snugly fits into the wider cleft at the opposite end. With the top surfaces inclined at an $\sim 30^\circ$ angle, the two β -propellers are organized in opposite orientations (Figure 4-3B, left panel).

When viewed along the central axis of the two β -propellers, the overall architecture of Nup120¹⁻⁹⁵⁰-Nup37 can be compared to a bicycle, in which Nup120¹⁻⁹⁵⁰ supplies a “front” wheel (its β -propeller) and the main frame plus the prongs for the “rear” wheel (Figure 4-3B, left panel). The “rear” wheel is furnished by Nup37. Schematic tracings of the polypeptide chains of Nup120¹⁻⁹⁵⁰ and of full-length Nup37 are shown in Figure 4-3C.

4.2.5 NUP120¹⁻⁹⁵⁰ STRUCTURE

Compared to the 4-strand-per-blade arrangement seen in conventional β -propeller domains, the first blade of the Nup120 β -propeller is uniquely characterized by an extra β strand ($\beta 1E$) running parallel to the $\beta 1D$ strand at the outer surface. This feature is also present in the Sc-Nup120 propeller (Leksa et al., 2009; Seo et al., 2009). Following this $\beta 1E$ strand, helix h2 (spanning residue 44-55, labeled in Figure 4-3B) protrudes out of the top surface, running roughly parallel to the central axis of the β -propeller.

Another distinct feature for Nup120 is a prominent insert comprising helices h5-h9 (spanning residues 395-510) between the 6th and 7th blade of its β -propeller domain (Figures 4-3B and 4-3C). Notably, the 1E-1A helix h2 runs anti-parallel to h6 of the 6D-7A insert (Figure 4-3B, right panel) and is closely embraced by helices h6, h7 and h9. As a result, helix h2,

together with the 5-helix-insert, fold into a distinct helical bundle domain (Figures 4-3B and 4-4).

The C-terminal α -helical domain (spanning residues 544-950) adopts an “L” shape structure composed of 21 α -helices (h10-h30), with a bulging arm comprising helices h10-h22 (residues 548-800) and a slender arm furnished by helices h23-h30 (residues 810-950) (Figure 4-5). The bulging arm is centered on a prominent hydrophobic helix hairpin, helices h17 and h19, with a length of ~ 50 Å and ~ 34 Å, respectively. Helices h10-h16 coil like a snake around the base of the helix hairpin, distal to the Nup120 β -propeller domain, whereas the upper half of the helix hairpin closely packs against helices h20-h22. As a result, this helix hairpin is almost fully buried and forms a prominent hydrophobic core (Figures 4-3B and 4-5).

The slender arm of the “L” is formed by helices h23-h30 (Figures 4-3B, 4-3C and 4-5). This region represents an extension of the helical region compared to the previously reported Sc-Nup120¹⁻⁷²⁹ structure (Figure 4-6). Helices h23-h30 are roughly organized into four antiparallel pairs with h27 off pitch, stacking with h28 at a 45° angle. As a result, helices h23-h30 forms a crescent shape with its convex surface contacting Nup37 and the concave side surface largely occupied by helix h27. Overall, these eight helices extend ~ 45 Å in the direction perpendicular to h17 (Figure 4-5).

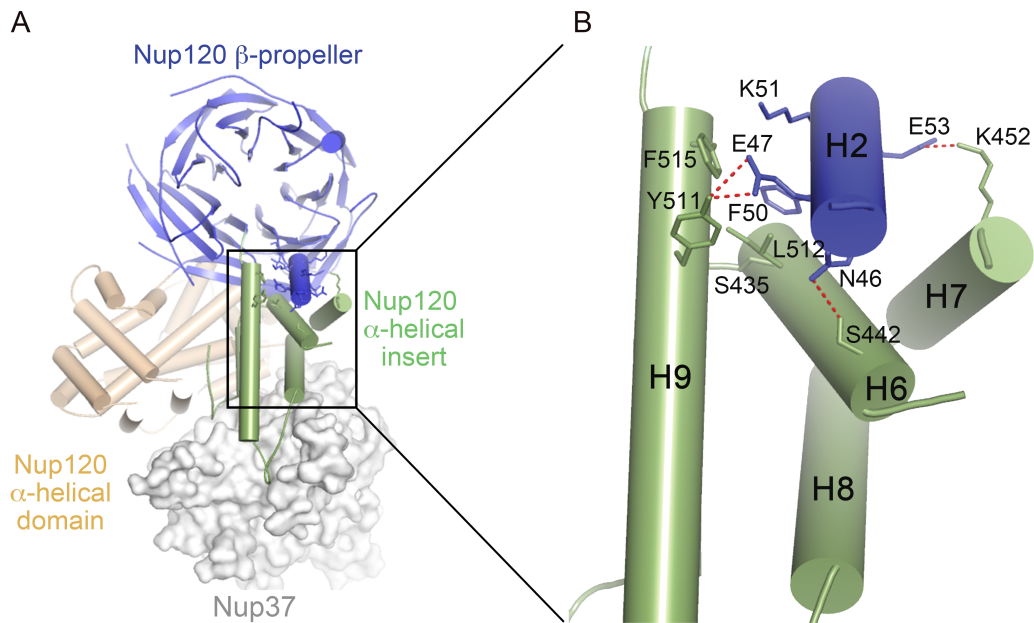


FIGURE 4-4 HELIX H2 OF 1E-1A INTERACTS WITH HELICES H6, H7, AND H9 OF THE 6D-7A INSERT OF SP-NUP120¹⁻⁹⁵⁰.

(A) Sp-Nup120¹⁻⁹⁵⁰ is depicted in a cartoon model, and Nup37 is shown in a surface model. Models are color coded as in Fig. 5. (B) Close-up view of the boxed region in A. Helices h2 (in blue) and h6, h7, h8, and h9 (in green) are labeled. Residues involved in the direct interactions between h2 and the 6D-7A insert are shown as sticks and are labeled. Hydrogen bonds of the interface are shown as red dashed lines. In addition, F50 of helix h2 stacks with L512 of h6, and K51 of helix h2 makes van der Waals interactions with F515 of helix h9.

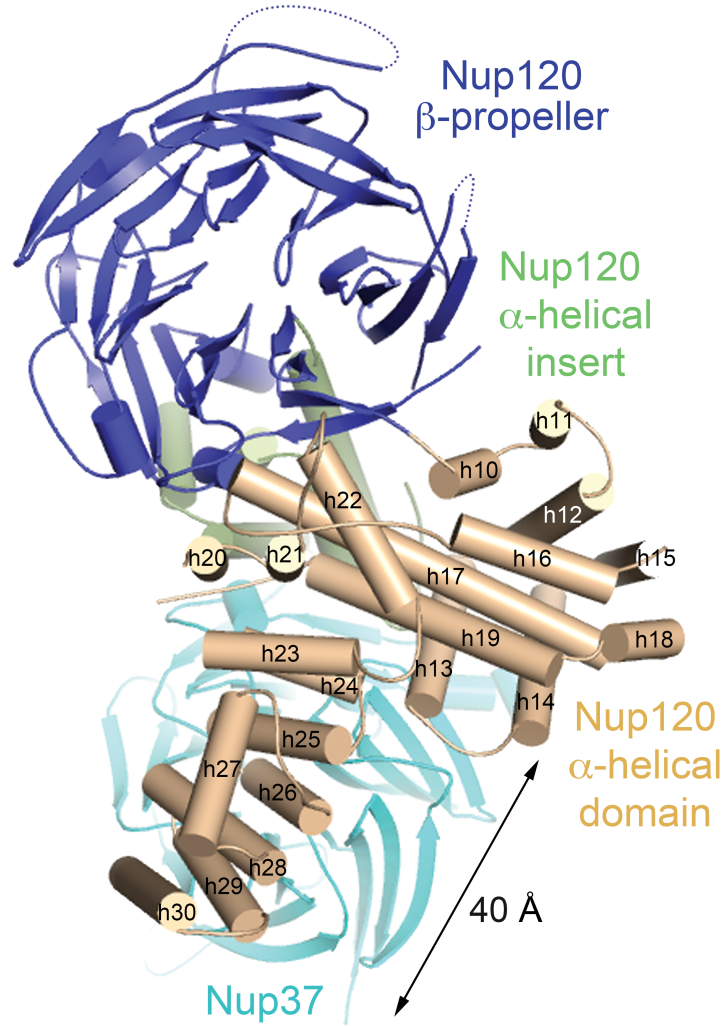


FIGURE 4-5 BACK VIEW OF THE NUP120¹⁻⁹⁵⁰-NUP37 COMPLEX.

The Nup120¹⁻⁹⁵⁰-Nup37 complex is depicted as a cartoon model. Twenty-one α-helices (h10–30) of the L-shaped α-helical domain of Sp-Nup120¹⁻⁹⁵⁰ are labeled.

FIGURE 4-6 **STRUCTURAL COMPARISON OF SP-NUP120¹⁻⁹⁵⁰ AND SC-NUP120¹⁻⁷²⁹.**

The two sequences were aligned according to their secondary structures; residue numbers are indicated. Identical residues are shaded in blue; an inserted stretch of about 50 residues in Sp-Nup120 is shaded in pink. Indicated secondary structural elements for Sc-Nup120 are based on the crystal structure determined at 2.6-Å resolution [PDB ID:3F7F (Seo et al., 2009)]. Color codes are as in Figure 4-1A. Secondary structural elements are indicated: Arrows indicate β -strands numbered according to their location in the seven-bladed β -propeller; boxes indicate α -helices numbered in order from the N terminus to the C terminus; lines indicate loops, and dotted lines indicate disordered regions. The locations of residues of Sp-Nup120 interacting with Nup37 are indicated by green asterisks in the insert domain of the β -propeller and by wheat-colored circles in α -helical domain.

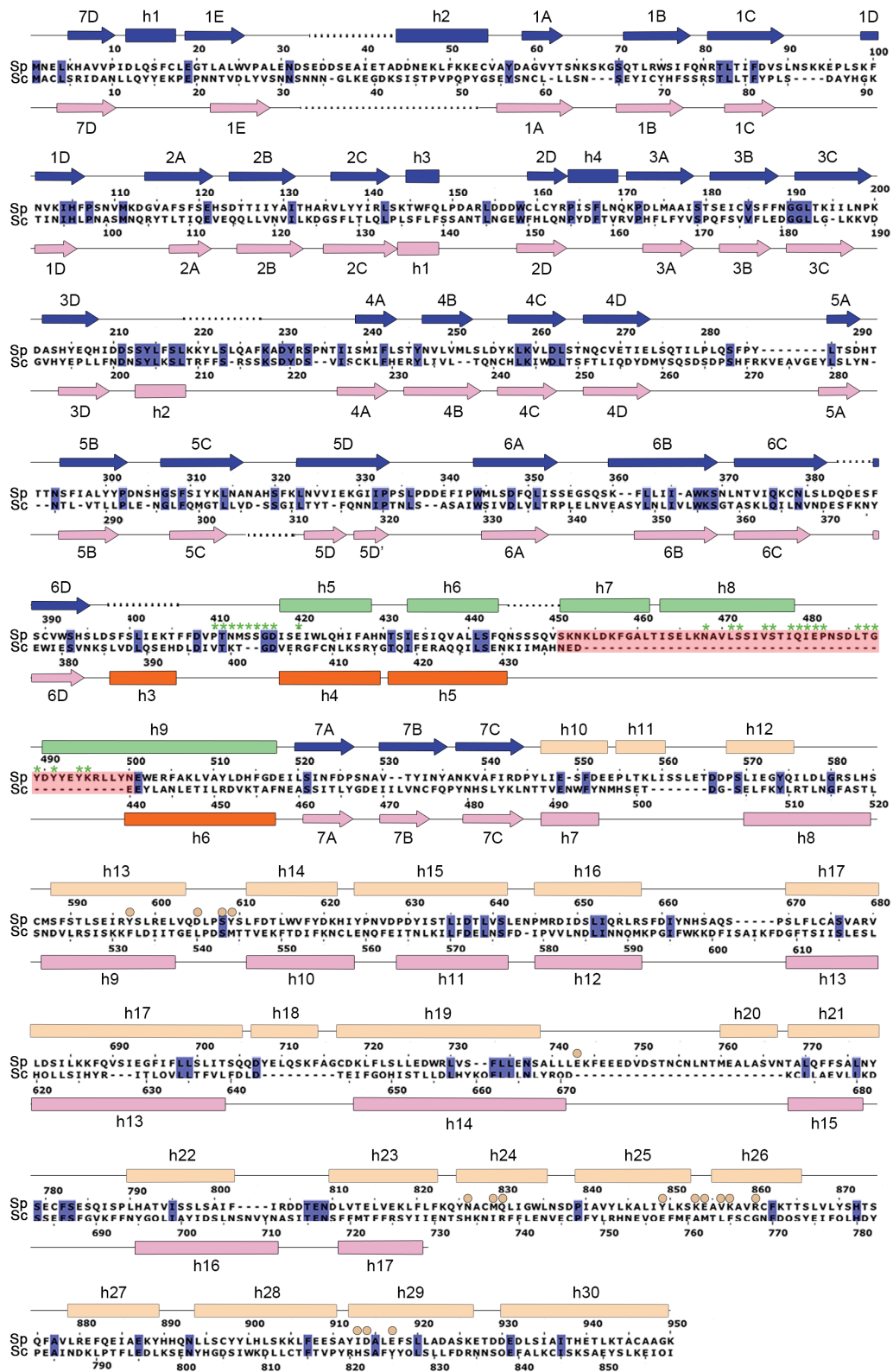


FIGURE 4-6 STRUCTURAL COMPARISON OF SP-NUP120¹⁻⁹⁵⁰ AND SC-NUP120¹⁻⁷²⁹.

4.2.6 STRUCTURE OF NUP120-BOUND NUP37

Upon Nup120 binding, while the overall structure of Nup37 remains largely the same (the two structures could be aligned with a R.M.S.D. of 0.5 Å for 371 C_α atoms), some disordered regions in non-liganded Nup37 adopt α -helical or loop structure (Figure 4-3A and 4-7). Specifically, on the bottom surface of Nup37, the 4CD and the 5CD loops are in close vicinity to the loop immediate ahead of helix h5 and the extended h8-h9 loop region of Nup120 6D-7A insert, respectively. On the top surface of Nup37, Ile251 of the 4D- 5A loop makes van der Waals contacts with Glu743 and Lys744 in the loop following h19 of the helical domain Nup120 (Figure 4-8). It should be noted that, the N-terminal 5 residues of Nup37, instead of forming an extended β -strand packed against the 6th blade of Nup37, become flexible upon Nup120 binding, possibly due to a lack of crystal packing contacts.

4.2.7 NUP120-NUP37 INTERFACE

Nup120 interacts with Nup37 through a concave surface contributed by the 6D-7A insert and α -helical domain of Nup120. The total buried surface area for the hetero-dimer is $\sim 4900 \text{ \AA}^2$, with $\sim 2100 \text{ \AA}^2$ of the buried surface area contributed by the 6D-7A insert-Nup37 interface (labeled as A and A' in Figure 4-9B) and the remaining $\sim 2800 \text{ \AA}^2$ contributed by α -helical domain-Nup37 interface (labeled as B and B' in Figure 4-9B). A detailed schematic view of the hetero-dimer interface is shown in Figure 4-8. Binding of Nup37 to the enlarged 6D-7A insert of Nup120 is primarily through hydrophobic

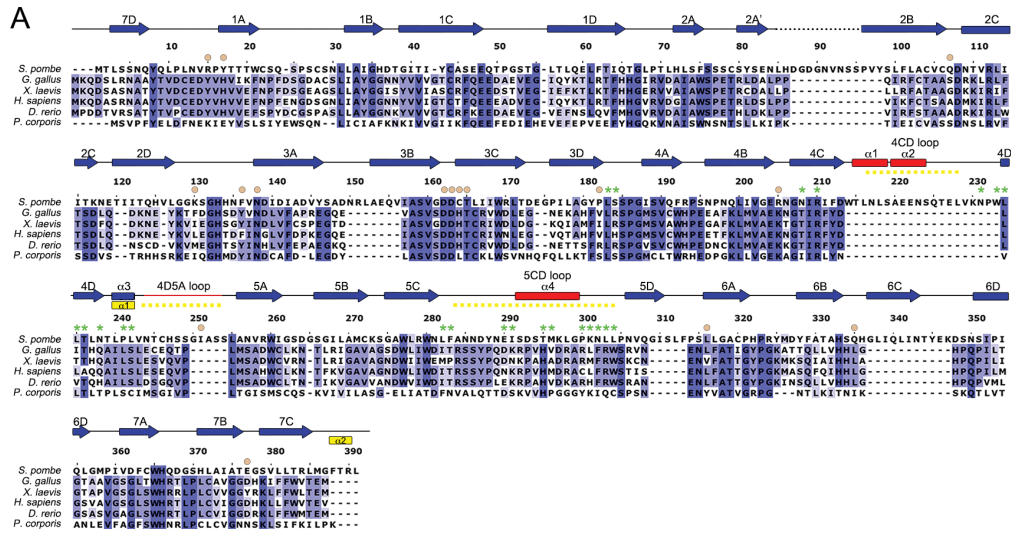


FIGURE 4-7 STRUCTURAL COMPARISON OF THE NONLIGANDED AND NUP120-BOUND FORMS OF NUP37.

(A) Sequences were aligned by ClustalW with residue numbers indicated for Nup37. Secondary structural elements are shown as follows: arrows indicate β -strands; boxes indicate α -helices; lines indicate loops; and dotted lines indicate disordered regions. Note that disordered regions (yellow dots) of non-liganded Nup37 assume ordered structures (three helices and one loop, indicated in red) in the Nup120-bound form. Green asterisks and wheat-colored circles indicate Nup37 residues interacting with residues of insert or helical regions of Nup120, respectively. (B) Cartoon presentation as in Figure 4-3A showing superimposition of the non-liganded and bound forms of Nup37 on the surface model of Nup120; structural changes upon binding to Nup120 are indicated in red.

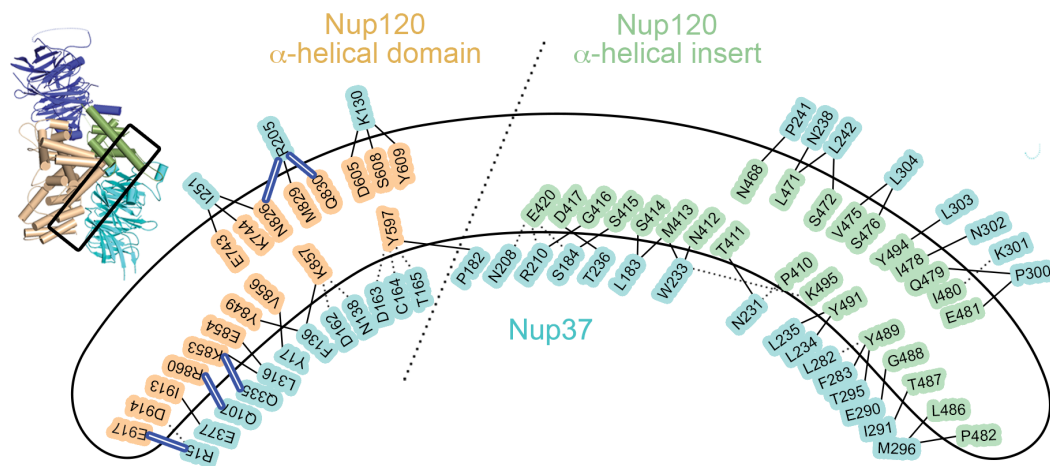


FIGURE 4-8 DETAILED ANALYSES OF THE NUP120¹⁻⁹⁵⁰-NUP37 INTERACTOME.

Interactions of specific residues by hydrogen bonds (dotted lines), van der Waals interaction (thin lines), and electrostatic interactions (blue lines) are indicated. For reference, a boxed region of the cartoon structure (a miniature equivalent of Figure 4-3A, right) is indicated on the left.

FIGURE 4-9 SURFACE PROPERTIES OF THE NUP120¹⁻⁹⁵⁰-NUP37 INTERFACE.

(A) The Nup120¹⁻⁹⁵⁰-Nup37 complex (center) was split and rotated +90° or -90° about the vertical axis. Nup120¹⁻⁹⁵⁰ alone is shown on the left, and Nup37 alone is shown on the right (colored as in Figure 4-1). (B) Nup120¹⁻⁹⁵⁰ and Nup37 surface representations with interacting regions bordered by black lines. “A” and “A” mark the interface of the Nup120 6D-7A insert and Nup37; “B” and “B” mark the interface of the helical domain and Nup37. (C) Surface models colored according to multispecies sequence alignments. Sequence conservation is shaded in a color gradient from yellow (diverged) to red (conserved). The hetero-dimer interface is outlined in black. Some prominent interacting residues are labeled. (D) Surface models colored according to electrostatic potential calculated by Adaptive Poisson-Boltzmann Solver (6) and illustrated (-4 to +4 kBT/e) with PyMOL.

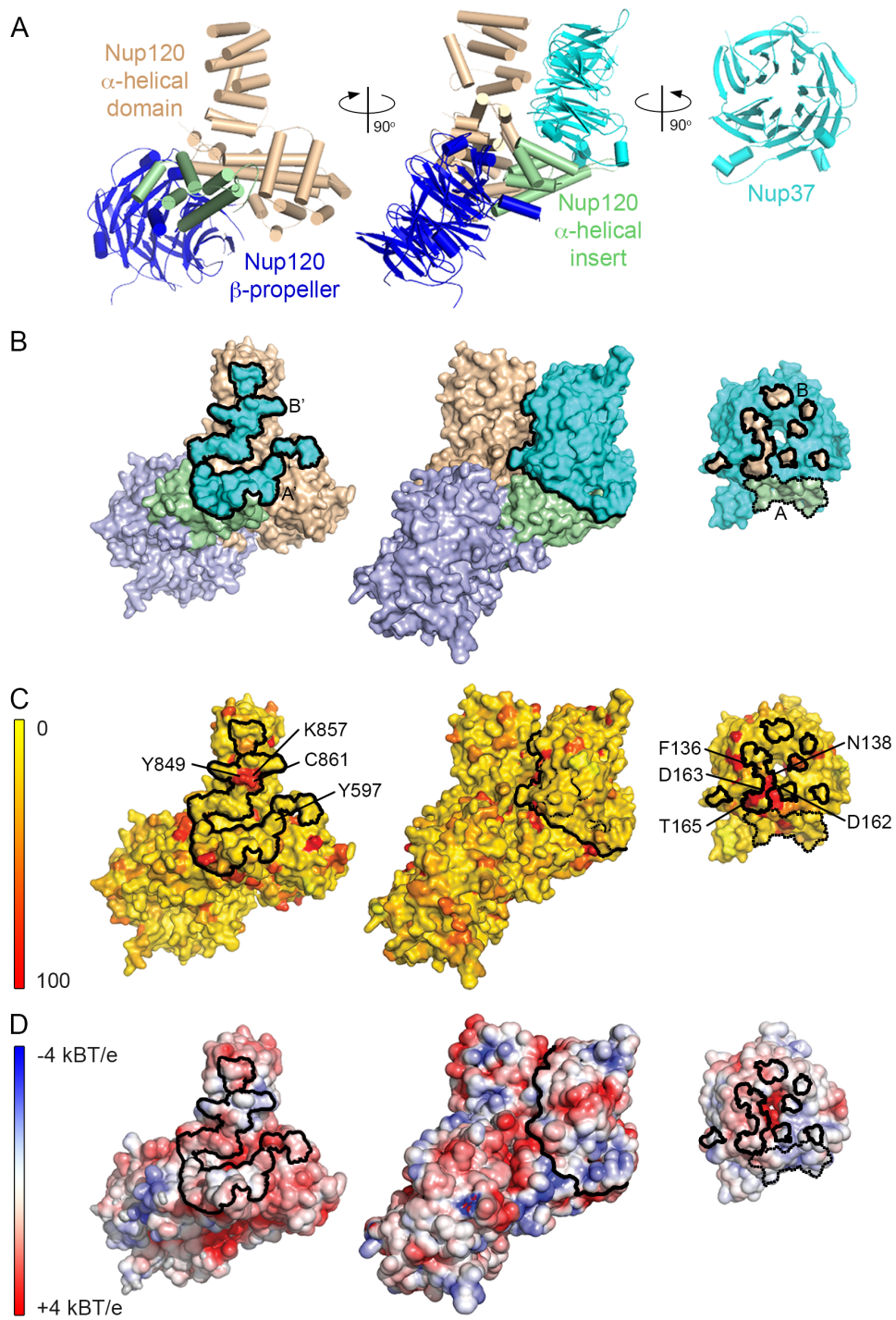


FIGURE 4-9 SURFACE PROPERTIES OF THE NUP120¹⁻⁹⁵⁰-NUP37 INTERFACE.

contacts and a few hydrogen bonds, whereas the interface between Nup37 and the helical domain of Nup120 involves, in addition, several electrostatic interactions (Figures 4-6, 4-8 and 4-9). Within this extensive interface, some prominent hydrophobic centers are highly conserved across species from Sp to human (Figure 4-9C). For example, in the α -helical region, Phe136 of Nup37 closely stacks with side chain of Lys857 from Nup120. Other residues from Nup120 (including Tyr849, Cys861) and those from Nup37 (e.g. Thr165, Asn138 Asp162 and Asp163) further strengthen the interaction. On the distal end of the curved interface of the helical bundle region, a prominent hydrophobic core is formed centering on residues Phe283, Ile291, and Leu282 (contributed by Nup37) and Tyr491, Tyr489, and Pro482 (contributed by Nup120). This extensive binding interface explains why the hetero-dimer resists high salt (1M NaCl, 1M urea) or low salt challenge.

4.2.8 STRUCTURAL COMPARISON OF SP-NUP120 AND SC-NUP120

Seven blades of Sc-Nup120 and Sp-Nup120 propellers and most of the prominent helices in α -helical regions in both structures can be well aligned. However, two key regions of Sp-Nup120 stand out as exceptions and ensnare Nup37: the enlarged 6D-7A insert of the Sp-Nup120 β -propeller (outlined by dotted lines in Figure 4-3C) and the expanded C-terminal helical domain (Figure 4-3B). Compared with the 70 residue-long 6D-7A insert in Sc-Nup120, Sp-Nup120s 6D-7A insert contains ~50 more amino acid residues. The enlargement of the helical insert of the Sp-Nup120 β -propeller

gives rise to two additional helices (h7 and h8) and $\sim 21 \text{ \AA}$ elongation of helix h9 (Figures 4-6 and 4-10). More importantly, helices h8, h9, and the loop connecting h8-h9 make extensive contacts with the 4th and 5th blades of the Nup37 propeller (Figures 4-3B and 4-8).

Comparison of the previously reported Sc-Nup120¹⁻⁷²⁹ structure (Leksa et al., 2009; Seo et al., 2009) with the Sp-Nup120¹⁻⁹⁵⁰ structure reveals seven additional α -helical at its C-terminus (Figure 4-6). This extended helical region of Sp-Nup120 harbors a series of residues distributed along helices h24-h26 and h29 that contact Nup37 (Figures 4-3, 4-6, 4-8, 4-10). The structure of the corresponding region of Sc-Nup120 has not been determined. Based on the observation that Sc-Nup120 alone is not sufficient to bind Nup37 (Figure 4-1C), we suggest that Nup120 orthologs of Sp and metazoa specifically utilize features of these C-terminal α -helical as a partial binding platform for Nup37. We also envisage that the remaining Nup37 binding sites within the Sp-Nup120 β -propeller evolved through the expansion of the 6D-7A insert (Figure 4-10B) by its increased contacts with Nup37. This expansion is conserved in Nup120 orthologs that are competent to bind Nup37 (Figure 4-11).

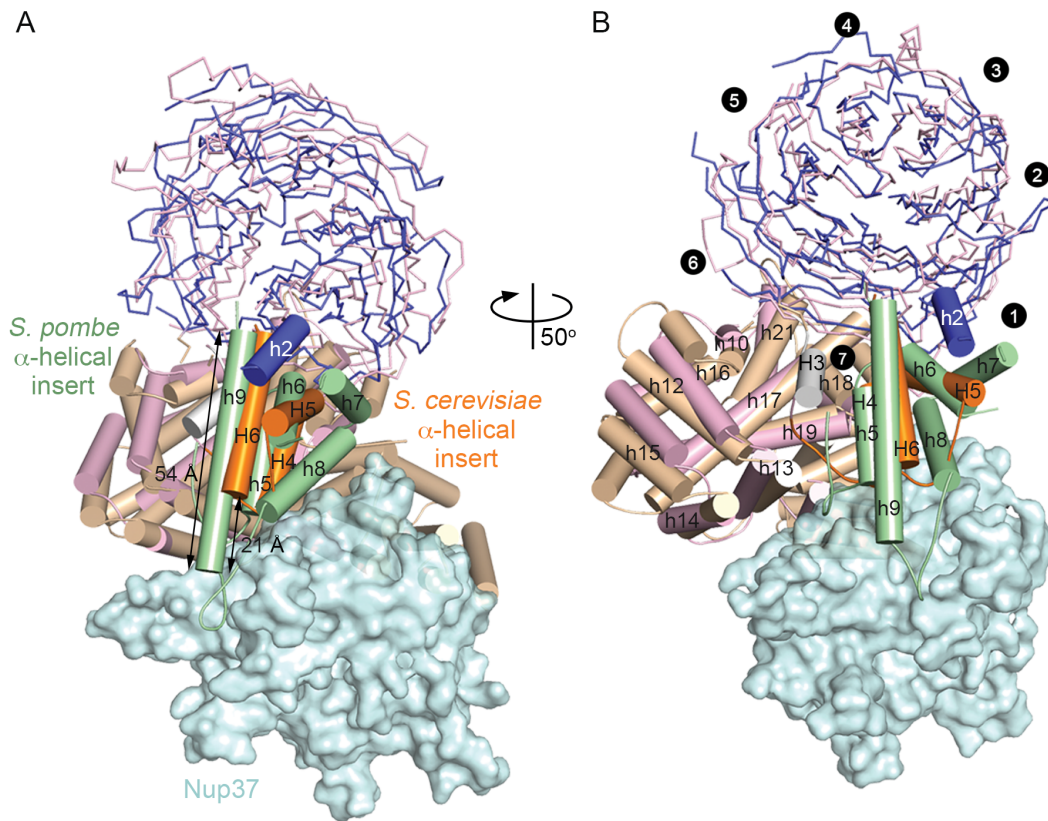


FIGURE 4-10 SUPERIMPOSED STRUCTURES OF SP-NUP120¹⁻⁹⁵⁰·NUP37 AND SC-NUP120¹⁻⁷²⁹.

(A) Overlay of the Sp-Nup120 and Sc-Nup120 structures. (B) A 50°-rotated view is shown. β -Propellers (pink for *S. cerevisiae* and blue for *S. Pombe*) are shown in the $C\alpha$ skeleton model except for cartoon representations for 1E-1A helix h2 (blue) and helices in the 6D-7A insert (orange for *S. cerevisiae* and green for *S. pombe*). Prominent helices are labeled for Sp-Nup120 (lower case) and Sc- Nup120 (upper case). Helical domains are depicted in cartoon model (wheat for *S. pombe* and pink for *S. cerevisiae*). Blades of both β -propellers and some helices of inserts and the helical domain are labeled. Nup37 is shown as surface model in light gray. An arrow indicates a 21-Å extension of h9 in Sp-Nup120.

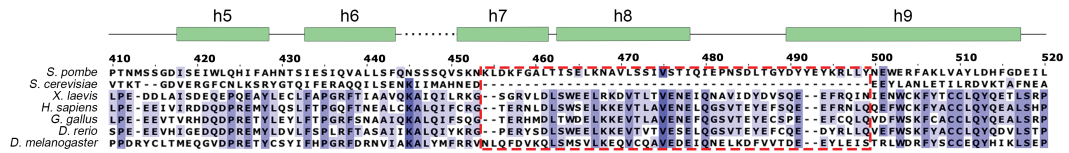


FIGURE 4-11 MULTIPLE SEQUENCE ALIGNMENT OF NUP120.

Multiple sequence alignment of Nup120 6D-7A insert regions with conserved residues shaded in blue. A red box identifies the expanded 6D-7A insert regions in *S. pombe* and metazoan cells.

4.3 DISCUSSION

We report the atomic structures of a complex of two nucleoporins from *S. pombe*, Nup120¹⁻⁹⁵⁰ and full length Nup37, as well as of non-liganded Nup37. These structures inform not only about the evolution of the coatomer module of the NPC, but also about structural changes that accompany the post-translational assembly of Nup120-Nup37 as part of a hetero-octameric coatomer module.

Localized adjacent to the cylindrical pore membrane with its distinct embedded Poms, the coatomer module of the NPC underwent evolution toward higher complexity: a hetero-heptamer in *S. cerevisiae* evolved into a hetero-octamer in *S. pombe* and into a hetero-nonamer in metazoa. The heptamer- to octamer- or to nonamer transition involves acquisition of Nup37 or of Nup37 and Nup43. Although most analyses have so far been carried out with the Sc hetero-heptamer, the constituent members of the coatomer module of other species are generally identifiable by sequence homologies (DeGrasse et al., 2009); most likely, all modules also share a similar, electron microscopically defined, Y-shaped structure.

Our biochemical studies together with structural analyses shed light onto the evolution of the Y-shaped complex. We first biochemically identified Nup120 as the binding partner for Nup37 (Figure 4-1). The structure of full length Nup37 further revealed that it folds into a canonical 7-bladed β -propeller that showed several unstructured regions on its surface. Some of these become structured upon binding to Nup120. Immediately after cellular

synthesis, these regions may temporarily be protected by chaperones to allow an ordered assembly with Nup120, as well as with other surrounding Nups or Poms. These unstructured regions increase surface entropy and pose problems for crystallization but are likely to endow the nucleoporin interactome with considerable plasticity to accommodate a huge size range of transport substrates.

The overall architecture of the Nup120¹⁻⁹⁵⁰-Nup37 complex resembles the shape of a bicycle, to which Nup37 only provides the “rear wheel”, whereas Nup120¹⁻⁹⁵⁰ contributes its main frame and the “front wheel” (Figure 4-3B left panel). However, the Nup120-derived front wheel, also a seven-bladed β -propeller, is distinguished from Sc-Nup120 by the presence of an extension of about 50 residues in its 6D-7A insert. Strikingly, this 50 residues extension provides numerous contact sites (Figures 4-6 and 4-8) to fasten the rear wheel and is conspicuously absent in Sc, but is present in Sp and metazoan cells (Neumann et al., 2010). Another noteworthy difference between the Sc- and Sp-Nup120 β -propellers is the presence in Sp of 1E-1A helix h2 (Figures 4-3, 4-4 and 4-6), which projects out from the β -propeller and stabilizes the adjacently located 50 residues extension. The equivalent region is disordered in the crystal structure of Sc-Nup120 (Leksa et al., 2009; Seo et al., 2009).

Other principal contact sites for the Nup37 β -propeller are contributed primarily by the C-terminal portion of the α -helical domain of Nup120¹⁻⁹⁵⁰ (Figures 4-6 and 4-8). Notably, the previously determined

crystal structure of Sc-Nup120¹⁻⁷²⁹ fragment lacked the equivalent region (Figures 4-1 and 4-6) (Leksa et al., 2009; Seo et al., 2009). Our finding that Sc-Nup120 does not bind to Nup37 *in vitro*, however, suggests that in Sc-Nup120, this region may have evolved to exert other, yet to be determined, functions.

As β -propellers are classical interaction platforms for other co-factors, the capture of Nup37 may facilitate a more extensive integration of the coatomer module of the NPC into the network of surrounding Nups and Poms. The addition of the Nup37 binding platform to the NPC is predicted to give rise to additional functional properties of the NPC not present in Sc. What these might be will have to await identification and characterization of other binding partners of Nup37. But as Sp, like Sc, undergoes closed mitosis, the Nup37 acquisition in Sp (or loss in Sc) is presumed not to relate to the reversible NPC disassembly into sub-complexes that occurs in open mitosis, where the coatomer, other disassembled Nups, and transport factors function in other capacities, such as the assemblies of kinetochores and spindles (Orjalo et al., 2006; Mishra et al., 2010).

**CHAPTER V: BIOCHEMICAL ANALYSES OF INTERACTIONS BETWEEN
THE NPC CORE SCAFFOLD AND PORE MEMBRANE DOMAIN**

5.1 OVERVIEW

Nups positioned in close proximity to the pore membrane domain (POM) of the NE play a critical role in the stabilization of membrane curvature and are essential for the assembly of the NPC within the NE. We investigated interactions between members of the membrane scaffolding Nup107-160 complex with surrounding transmembrane Nups (Poms) to determine the structural conservation of the NPC membrane coat. To investigate the molecular architecture of the mammalian NPC in the vicinity of the POM, we optimized the large-scale purification of fragments of key structural Nups and Poms, including Nup37, Nup160, and Pom121. We show that the interaction between the β -propeller/ α -solenoid Nup160 and the β -propeller Nup37 is conserved in both Sp and Hs. Compared to the interaction described for Sp Nup37 and Nup160 orthologues (Chapter IV), binding of human Nup37 to Nup160 requires the predicted 6D-7A α -helical insert of the Nup160 β -propeller domain in addition to a region of the Nup160 α -solenoid domain. Based on previously identified interactions of scaffold β -propellers with Pom121 (Chapter III), we extended our analyses to evaluate the binding of Pom121 to additional β -propellers of the core scaffold in an attempt to further characterize the pore membrane interactome. We optimized the large-scale purification of complexes of the Nup160 β -propeller domain with Pom121, and mapped the Nup160-binding domain of Pom121 to an N-terminal \sim 100 amino acid residue fragment. Using recombinant proteins, we uncovered novel interactions between Pom121 and the β -propeller domains

of Nup37 and Nup43. These data expand the repertoire of Pom121 interacting proteins to include the β -propeller domains of Nup37, Nup43, and Nup160 of the core scaffold, and the β -propeller domain of Nup155 of the adaptor scaffold. Based on these data, we envisage a model whereby Pom121 bridges the structural modules of the NPC as it extends from the POM towards the central channel. Oligomerization of Pom121 polypeptides bound to scaffolding Nups could facilitate the association of Nup subcomplexes into higher-order assemblies during NPC biogenesis. While the biochemical characteristics of the interactions between Pom121 and β -propeller domains are as yet undetermined, we suggest that promiscuity between these interactions contributes to the plasticity of Nup interactions that are required within the NPC to allow for circumferential adjustments of the transport channel in response to the metabolic demands of the cell.

5.2 RESULTS

5.2.1 BIOCHEMICAL CHARACTERIZATION OF NUP160 AND NUP37 INTERACTIONS

Our previous analyses revealed the hetero-dimerization of Nup120 (the yeast orthologue of Human Nup160) and Nup37 of the octameric membrane-coating module of the *S. pombe* NPC (Chapter IV). Here, we investigate the conservation of this interaction within the mammalian nonameric membrane scaffolding complex, with the goal of resolving the structure of the Human Nup160-Nup37 complex at the atomic level. To this end, we optimized purification conditions for Nup37 and fragments of Nup160. Experiments aimed towards the purification of recombinant proteins from insect cells and subsequent biochemical analyses of their interactions are discussed below.

5.2.1.1 PURIFICATION OF NUP37

We first purified recombinant Nup37 using the Bac-to-Bac® baculovirus expression system (Figure 5-1). Bacmids were constructed that contain the human cDNA of Nup37 under the control of the viral polyhedron promoter, which ensures high-level expression of recombinant proteins in insect cells. Recombinant baculovirus was produced and amplified to a high titer. Briefly, GST-tagged Nup37 was purified from High Five™ insect cells grown in suspension following cell disruption by sonication and lysate clarification by centrifugation (see section 2.11). Clarified lysate was

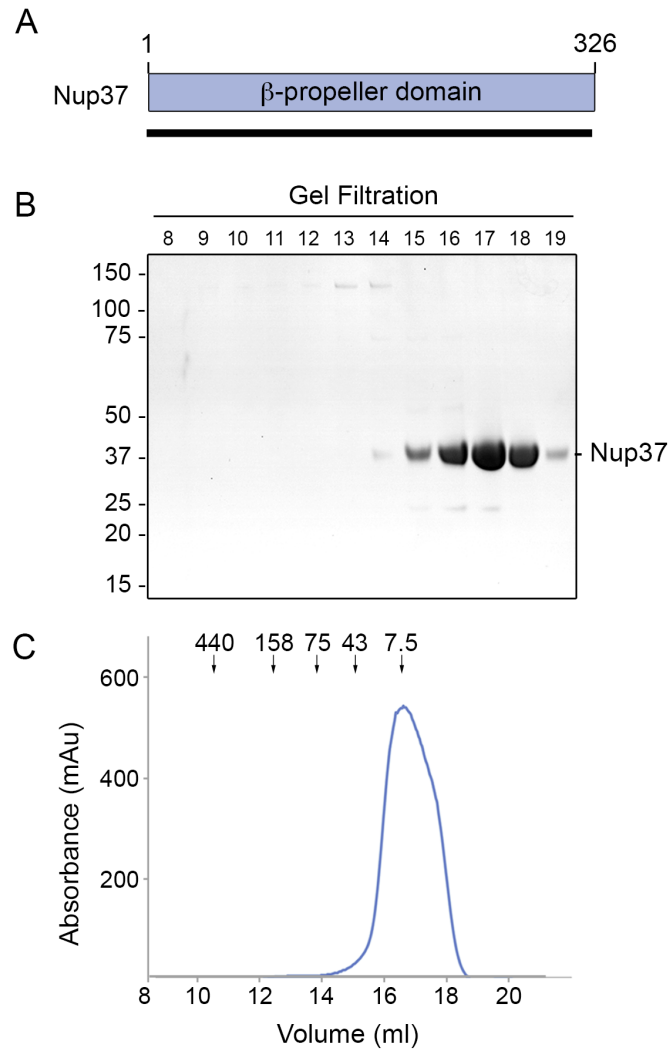


FIGURE 5-1 PURIFICATION OF HUMAN NUP37.

(A) Schematic of the domain organization of Human Nup37. Residue numbers indicate domain boundaries, and bar indicates the fragment used for purification. (B, C) Purification of Nup37 by size exclusion chromatography. (B) Fractions were sampled and proteins were resolved by SDS-PAGE and detected by Coomassie blue staining. The point at which Nup37 migrates is indicated to the right of the panel. (C) Chromatogram representing the elution profile of Nup37 using a Superdex 200 10/300 gel filtration column. The migration of molecular mass standards is indicated. Mass markers are in kilodaltons.

incubated with immobilized GSH Sepharose, and bound proteins were eluted using buffer containing 20 mM GSH. Eluate containing tagged protein was pooled and further purified by ion exchange chromatography using HiTrap® Q Sepharose. Proteolytic removal of the GST-affinity tag was achieved by the addition of TEV. Eluate containing Nup37 was further purified by size exclusion chromatography (Figure 5-1B and C). Notably, Nup37 was observed to elute relatively late during gel filtration, at a molecular mass corresponding to a protein of ~8 kDa (Figure 5-1C). This is consistent with the prediction that Nup37 is tightly folded into a compact β -propeller structure. In general, protein structure can significantly affect the elution of proteins during gel filtration (Erickson, 2009). Proteins with a small hydrodynamic radius may interact more readily with porous gel filtration media. Therefore, proteins with highly compact tertiary structures, such as the canonical β -propeller domain, are more likely to be retained during gel filtration compared to proteins of similar mass in alternative conformations. Furthermore, the degree of disorder within the structure of a protein, such as the exposure of unfolded loops and linker regions, markedly affects the behavior of proteins during gel filtration (Erickson, 2009). Together, a combination of molecular mass and tertiary structure contribute to the unique elution profiles of individual proteins observed during gel filtration.

Due to the high yield and purity of Nup37 obtained, we attempted to crystallize Nup37 using conditions that were similar to those used previously for crystallization of Sp-Nup37 (100 mM HEPES, pH 7.4, 0.5 M lithium sulfate,

10% (vol/vol) 1,4-Butanediol, and 10 mM DTT, 30 °C) (Chapter IV). While crystals failed to form initially, we found that the addition of 10% (wt/vol) PEG 3350 markedly improved crystallization conditions, and numerous crystals developed that were used for downstream structural analyses. X-ray diffraction data from these crystals were obtained to ~2.5 Å resolution, and a preliminary atomic structure has been determined (J. Fan, personal communication). The structure of Nup37 is particularly useful in that it will contribute to the structural determination of Nup37-containing complexes, including Nup160-Nup37, by molecular replacement.

5.2.1.2 PURIFICATION OF FRAGMENTS OF NUP160

Human Nup160 is comprised of a β -propeller domain connected to a long α -helical domain (Figure 5-2A). Our previous analysis of Nup160 expression from *E. coli* demonstrated that neither full-length recombinant Nup160 nor fragments thereof could be obtained in amounts sufficient for crystallographic analyses (Chapter III). For this reason, we sought to compare the solubility of numerous fragments of Nup160 expressed in insect cells (Figure 5-2B, C). We based the lengths of each Nup160 fragment on secondary structural predictions made using the protein structure prediction server PSIPRED (Figure 5-3)(McGuffin et al., 2000). The accuracy of PSIPRED was verified by comparing structural predictions of Sp-Nup120 to the

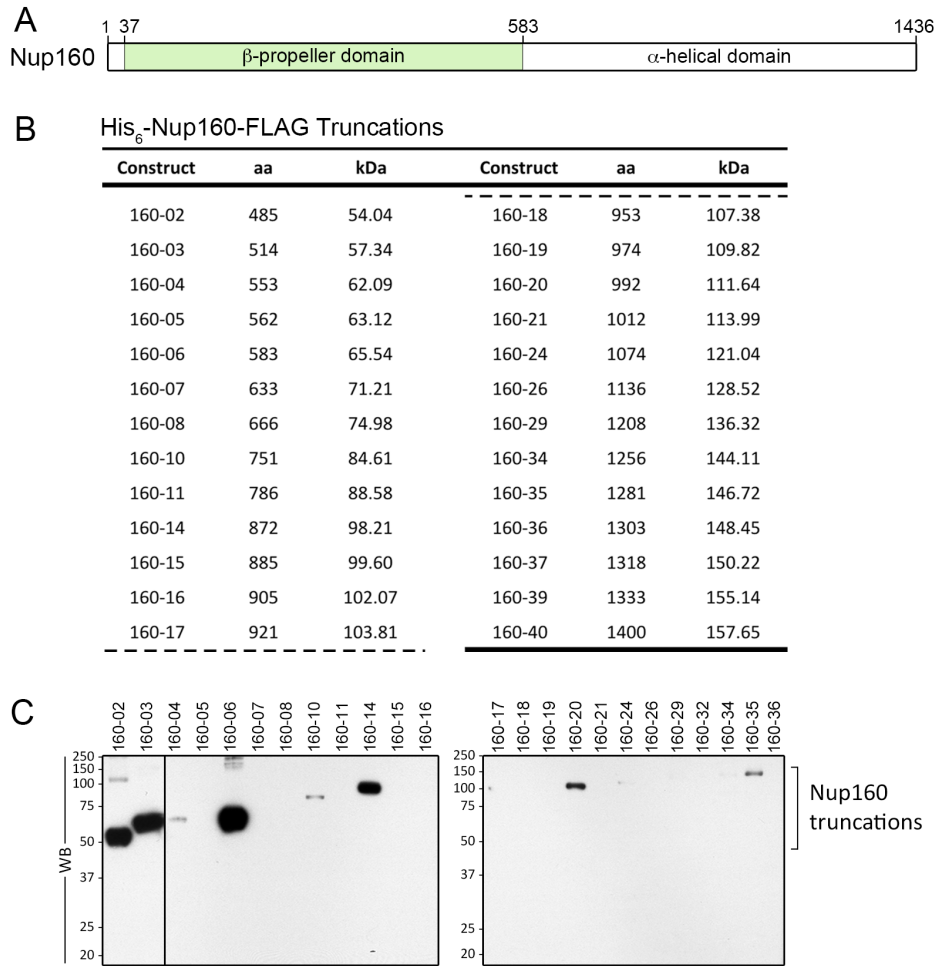


FIGURE 5-2 DESIGN AND EXPRESSION OF NUP160 TRUNCATIONS.

(A) Schematic of the domain organization of human Nup160. Residue numbers indicate domain boundaries, and bar indicates the fragment used for purification. (B) List of Nup160 truncations designed for expression in insect cells. Depicted for each truncation of Nup160 (Nup160-01 through Nup160-41) is the polypeptide length in amino acid residues (aa) and predicted molecular mass, in kilodaltons. All constructs begin with the first amino acid (aa) residue of Nup160 (ATG) and terminate with the residue designated in the 'aa' column of the table. Constructs are designed to express amino-terminal His₆ and carboxy-terminal FLAG affinity tags for purification and identification purposes. (C) Nup160 truncations were expressed in High Five™ insect cells and recombinant proteins were purified using Ni-NTA agarose affinity resin. Bound proteins were eluted using SDS-sample buffer, resolved by SDS-PAGE, and transferred to nitrocellulose for western blotting. Recombinant proteins were detected using an anti-FLAG-HRP monoclonal antibody. Mass markers are in kilodaltons (kDa). Nup160 truncations migrate in the range of ~50 and ~160 kDa.

structural organization that was determined experimentally (Chapter IV). Each fragment of Nup160 was designed to contain the predicted β -propeller domain of Nup160 followed by the sequential addition of each successive secondary structural motif. This required the construction of ~ 30 fragments of Nup160 (Figure 5-2B). Each construct contained an N-terminal His₆ tag for purification and a C-terminal FLAG tag for identification purposes. Recombinant bacmids constructed from each plasmid were transfected into Sf9 cells for viral amplification, and protein expression was elicited in High Five™ suspension insect cells. As demonstrated in Figure 5-2C, several Nup160 fragments expressed under these conditions were highly soluble. As expected, the solubility of Nup160 fragments decreased proportionately with their size. Presumably, these proteins contain numerous exposed hydrophobic regions that preclude their purification in the absence of a binding partner. Smaller fragments lacking these potential binding sites were expressed at relatively high levels. In particular, a fragment of Nup160 containing amino acid residues 1-583 (Nup160¹⁻⁵⁸³) was abundantly expressed and selected for subsequent analyses.

Based on alignment to Sp-Nup120, PSIPRED predictions of Hs-Nup160 suggest that Nup160¹⁻⁵⁸³ comprises the complete β -propeller domain (Figure 5-3). Importantly, this includes the conserved 6D-7A α -helical insert of Nup160 orthologues of *S. pombe* and metazoa. Notably, both the Nup120 6D-7A insert and its binding partner, Nup37, are absent from *S. cerevisiae*. The 6D-7A α -helical insert of Hs-Nup160 is predicted to contain

FIGURE 5-3 STRUCTURAL COMPARISON OF SP-NUP120¹⁻⁹⁵⁰ AND HS-NUP160³⁷⁻⁹⁵³.

Sequences of the indicated fragments of Nup120 from *Schizosaccharomyces pombe* (Sp) and Nup160 from *Homo sapiens* (Hs) were aligned according to their secondary structures; amino acid residue numbers are indicated. Identical residues are shaded in blue; an inserted stretch of about 50 residues unique to Nup120 orthologues of Sp and metazoan cells is shaded in pink. Indicated secondary structural elements for Sp-Nup120 are based on the crystal structure determined at 2.4 Å resolution (protein data bank ID 4GQ2; Liu et al., 2012). Secondary structural elements are indicated: Arrows indicate β-strands numbered according to their location in the seven-bladed β-propeller (Nup120: blue, Nup160: light blue); boxes indicate α-helices numbered in order from the N terminus to the C terminus (Nup120: orange, Nup160: light orange; green and light green for the α-helical insert region of Nup120 and Nup160, respectively); lines indicate loops, and dotted lines indicate disordered regions. The locations of residues of Sp-Nup120 interacting with Nup37 are indicated by green asterisks in the insert domain of the β-propeller and by orange circles in α-helical domain.

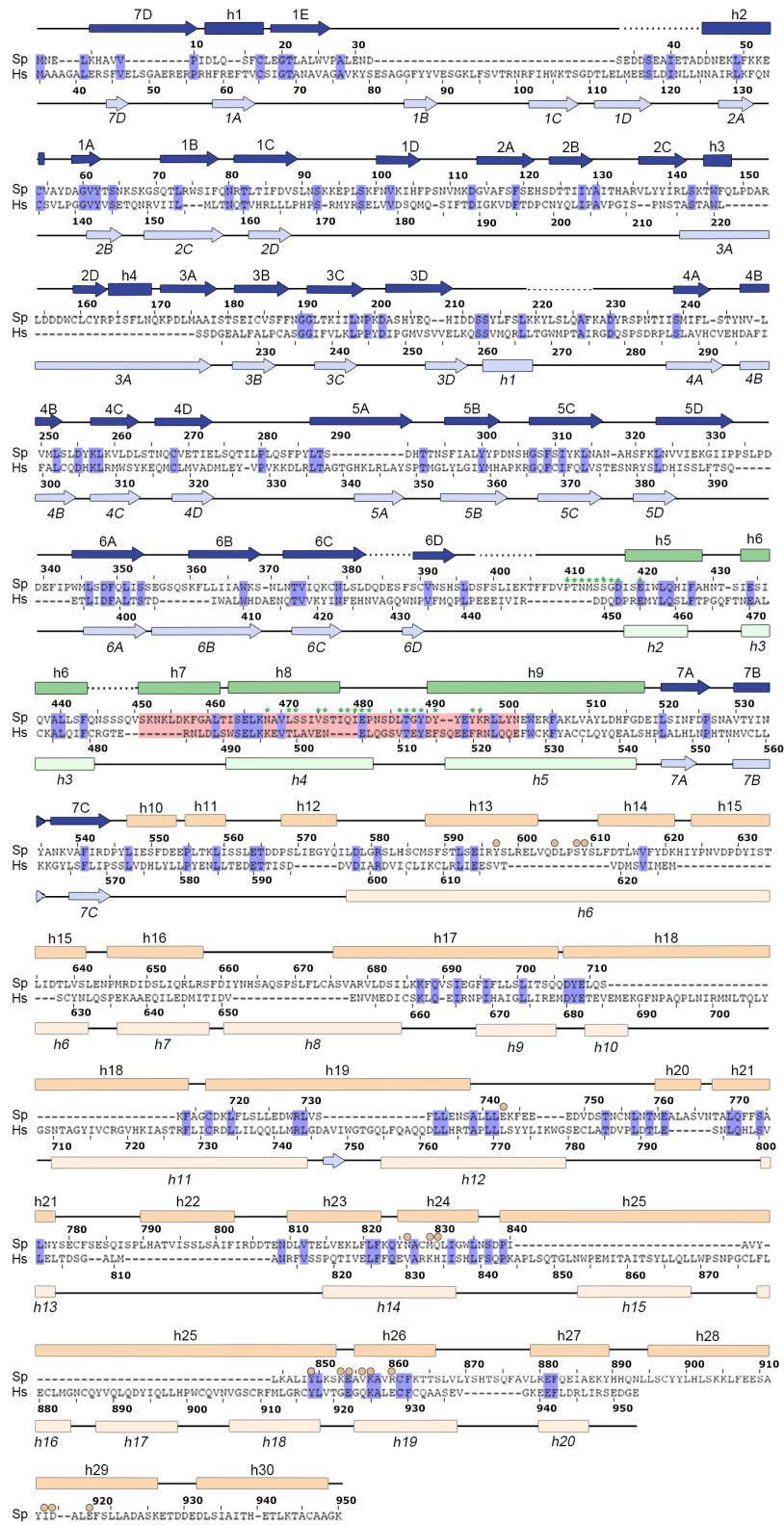


FIGURE 5-3 STRUCTURAL COMPARISON OF SP-NUP120¹⁻⁹⁵⁰ AND HS-NUP160³⁷⁻⁹⁵³.

four α -helices, as opposed to five α -helices observed in Sp-Nup120. Determining whether this represents limitations of the PSIPRED algorithm or accurately reflects the domain organization of Nup160 will await the resolution of Nup160 at the atomic level.

As expected, purification of Nup160¹⁻⁵⁸³ resulted in an extremely high yield of recombinant protein (~50-100 mg/L of cells) using a relatively simple purification protocol. Following protein production and initial purification by affinity and ion exchange chromatography, fractions containing Nup160¹⁻⁵⁸³ were pooled and purified by size exclusion chromatography (Figure 5-4B, C). Analysis of the gel filtration profile suggests that Nup160¹⁻⁵⁸³ is eluted in a single, monomeric peak (Figure 5-4C). Together, the stability of this fragment, coupled with the ease of purification prompted us to continue using Nup160¹⁻⁵⁸³ in subsequent analyses.

5.2.1.3 NUP160¹⁻⁵⁸³ DOES NOT DIRECTLY INTERACT WITH NUP37

We previously demonstrated that orthologues of Nup160 and Nup37 interact directly in *S. pombe* (Chapter IV). Thus, we evaluated the conservation of this interaction using purified Human Nup37 and Nup160¹⁻⁵⁸³, and evaluated their ability to form a complex *in vitro* using gel filtration (Figure 5-5). Two milligrams of each protein, alone or in combination were incubated on ice for 30 min. Each sample was subjected to size exclusion chromatography and the resulting fractions resolved by SDS-PAGE. The

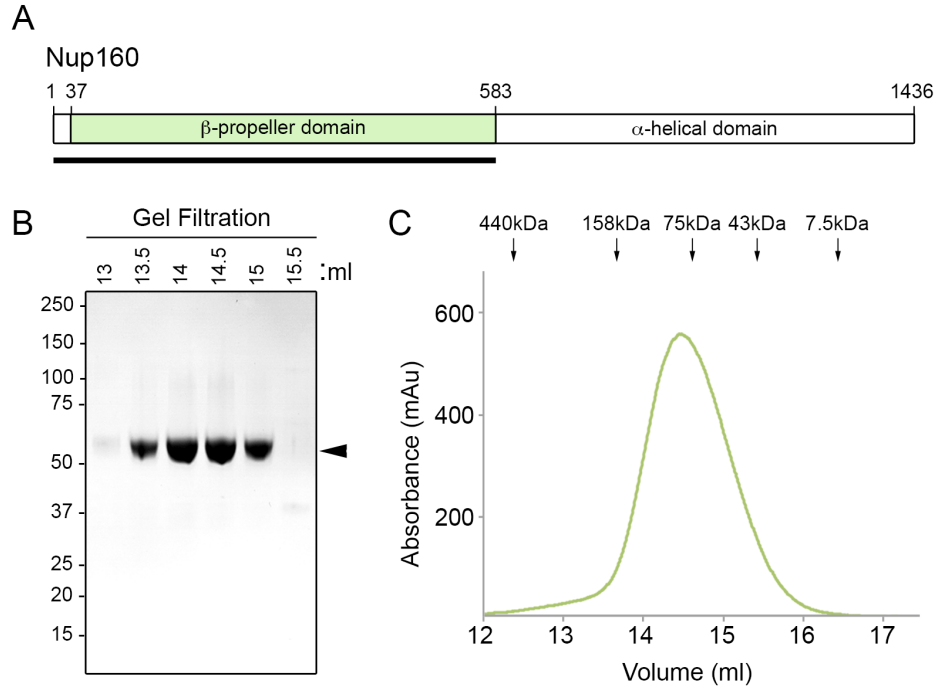


FIGURE 5-4 PURIFICATION OF NUP160¹⁻⁵⁸³.

(A) Schematic of the domain organization of Human Nup160. Residue numbers indicate domain boundaries, and bar indicates the fragment used for purification. (B, C) Purification of Nup160¹⁻⁵⁸³ by size exclusion chromatography. (B) Eluted fractions were sampled; proteins were resolved by SDS-PAGE and detected by Coomassie blue staining. The point at which Nup160¹⁻⁵⁸³ migrates is indicated by an arrowhead to the right of the panel. (C) Chromatogram representing the elution profile of Nup160¹⁻⁵⁸³ using a Superdex 200 10/300 gel filtration column. The migration of molecular mass standards is indicated. Mass markers are in kilodaltons.

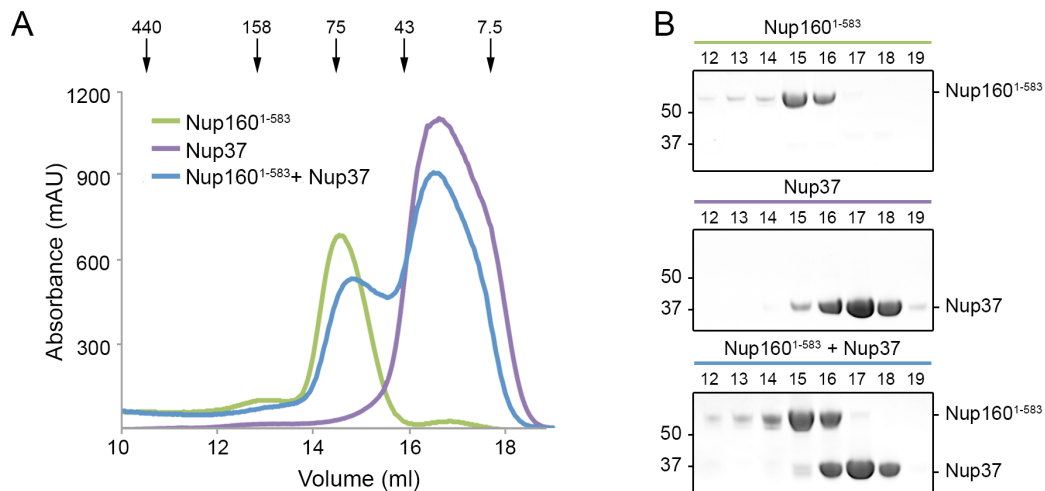


FIGURE 5-5 NUP37 AND NUP160¹⁻⁵⁸³ DO NOT INTERACT DIRECTLY.

Following incubation, Nup160¹⁻⁵⁸³, Nup37, or a mixture of purified Nup160¹⁻⁵⁸³ and Nup37 was subjected to size exclusion chromatography. (A) Representative chromatograms obtained after gel filtration of Nup160¹⁻⁵⁸³ (green), Nup37 (blue), or a mixture of both (red). The position at which mass markers migrate is indicated at the top of the panel. (B) Fractions were sampled and eluted proteins were resolved by SDS-PAGE. Gels were stained with Coomassie Blue stain. The point at which Nup160¹⁻⁵⁸³ and Nup37 migrate is indicated to the right of the panel. Mass markers are in kilodaltons.

absorbance profiles of Nup37 (Figure 5-5A, purple line) and Nup160¹⁻⁵⁸³ (Figure 5-5A, green line) each form distinct peaks when run individually. Following incubation, chromatographic analysis revealed that these peaks remain distinct (Figure 5-5A, blue line). SDS-PAGE analyses of the eluted fractions clearly demonstrate that despite pre-incubation, each protein elutes individually (Figure 5-5B). Taken together, these data strongly suggest that Nup37 and Nup160¹⁻⁵⁸³ do not form a complex *in vitro* under the conditions tested (20 mM HEPES, pH 7.5, 200 mM NaCl, 1 mM DTT).

Based on these results, we surmised that the β -propeller domain of Nup160, and by extension, the 6D-7A α -helical insert, is alone not sufficient to mediate an interaction with Nup37 (Chapter IV). Therefore, we referred to our previous expression analyses of Nup160 fragments to identify an alternative Nup160 fragment to use in further analyses (Figure 5-2). While none proved to express at levels sufficient for crystallographic analyses, we predicted that co-expression of longer fragments of Nup160 with Nup37 would improve their relative solubility. Furthermore, we modified the N-terminal residues of Nup160 used in subsequent analyses. Human Nup160 contains an N-terminal extension (NTE) of ~37 amino acid residues (Figure 5-6). The Nup160 NTE is unique to *H. sapiens*, and is notably absent from the proteomes of other metazoan species examined. While the structure of the Nup160 NTE is unknown, secondary structural predictions made using PSIPRED suggest that this region may be disordered (Figure 5-6). Therefore, we excluded the Nup160 NTE from our recombinant proteins on the basis

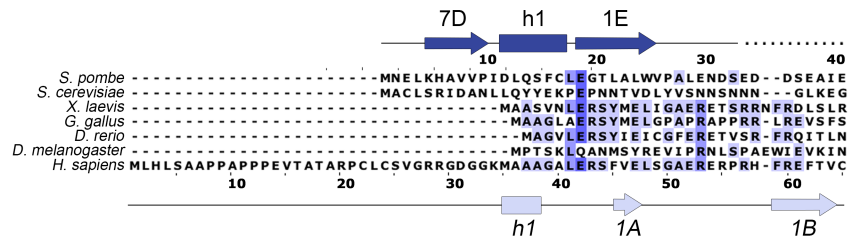


FIGURE 5-6 THE NUP160 NTE IS UNIQUE TO *H. SAPIENS*.

Multiple sequence alignment of the Nup160 NTE. Sequences are numbered according to *S. pombe* (top) or *H. Sapiens* (bottom). Alignment was generated using ClustalW. Conserved residues are shaded blue. Experimentally determined structural elements for *S. pombe* Nup120 are indicated in dark blue (top, based on pdb 4GQ2). Secondary structural predictions of *H. sapiens* Nup160 are indicated in light blue (bottom, generated using PSIPRED).

that disorder would negatively affect protein purification and crystallization (Oldfield et al., 2005). Using the structural alignment of Sp-Nup120 and Nup160 orthologues as a guide (Figure 5-3), we chose a fragment of Nup160 comprised of amino acid residues 37-953 (Nup160³⁷⁻⁹⁵³) to use in subsequent analyses. In addition to the 6D-7A α -helical insert, we predict that this fragment will contain an extended α -helical domain, similar to that of Sp-Nup120, which will facilitate binding to Nup37.

5.2.1.4 NUP160³⁷⁻⁹⁵³ INTERACTS DIRECTLY WITH NUP37

To purify large amounts of Nup160³⁷⁻⁹⁵³, we predicted that the exposure of potential hydrophobic patches on the surface of the recombinant polypeptide would preclude adequate solubilization in the absence of a binding partner. Thus, we modified our purification scheme, and co-infected insect cells with virus encoding Nup160³⁷⁻⁹⁵³ in addition to Nup37 (Figure 5-7). Briefly, recombinant viruses encoding His₆-tagged Nup160³⁷⁻⁹⁵³ or untagged Nup37 were individually amplified in Sf9 cells. To elicit protein production, High Five™ cells were co-infected with both viruses, and cells were harvested after 48 hours. Clarified lysates were incubated with Ni-NTA Agarose, and eluted proteins were further purified by ion exchange and size exclusion chromatography (Figure 5-7B, C). Results obtained from gel filtration suggest that Nup160³⁷⁻⁹⁵³-Nup37 co-elute as a complex, in a 1:1 molar ratio. SDS-PAGE analysis of eluted fractions clearly demonstrates co-elution of untagged Nup37 with His₆-Nup160³⁷⁻⁹⁵³, and chromatographic

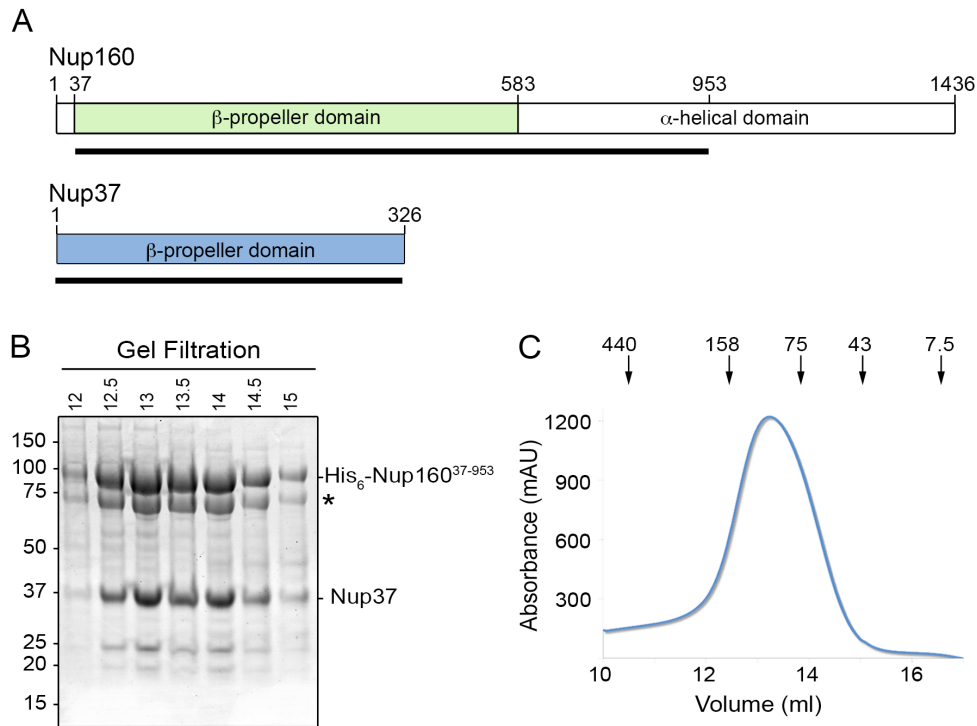


FIGURE 5-7 PURIFICATION OF NUP160³⁷⁻⁹⁵³-NUP37.

(A) Schematic of the domain organization of Nup160 and Nup37. Residue numbers indicate domain boundaries, and bars indicate the fragment used for purification. (B, C) Purification of Nup160³⁷⁻⁹⁵³-Nup37 by size exclusion chromatography. (B) Eluted fractions were sampled; proteins were resolved by SDS-PAGE and detected by Coomassie blue staining. The point at which Nup160³⁷⁻⁹⁵³ and Nup37 migrate is indicated to the right of the panel. An asterisk indicates a degradation product of Nup160. (C) Chromatogram representing the elution profile of Nup160³⁷⁻⁹⁵³-Nup37 using a Superdex 200 10/300 gel filtration column. The migration of molecular mass standards is indicated. Mass markers are in kilodaltons.

analysis revealed elution of the complex in a single peak. Of note, Nup160 was degraded during initial rounds of purification (degradation product indicated by an asterisk in Figure 5-7B). Degradation was completely inhibited during subsequent purifications by increasing the amounts of protease inhibitors used during cell lysis. In summary, these data strongly suggest that Nup160³⁷⁻⁹⁵³ and Nup37 directly interact, and that this interaction is conserved throughout the evolution of fungal and eukaryotic lineages.

Screening a variety of crystallization solutions revealed that crystals of Nup160³⁷⁻⁹⁵³-Nup37 formed readily under conditions of 0.1 M Bis-Tris, pH 6.5, 0.1 M NaCl and 1.5 M Ammonium Sulfate (Figure 5-8). In general, crystals range in size from ~20 to 40 μm . The vast majority of crystals form symmetrical hexagonal structures, with extremely sharp edges. Additionally, several other conditions tested allowed the formation of microcrystals. Combining information of various buffer conditions that support crystal growth will allow the optimization of crystallization conditions for Nup160³⁷⁻⁹⁵³-Nup37 complexes that will ultimately improve crystal growth and diffraction quality.

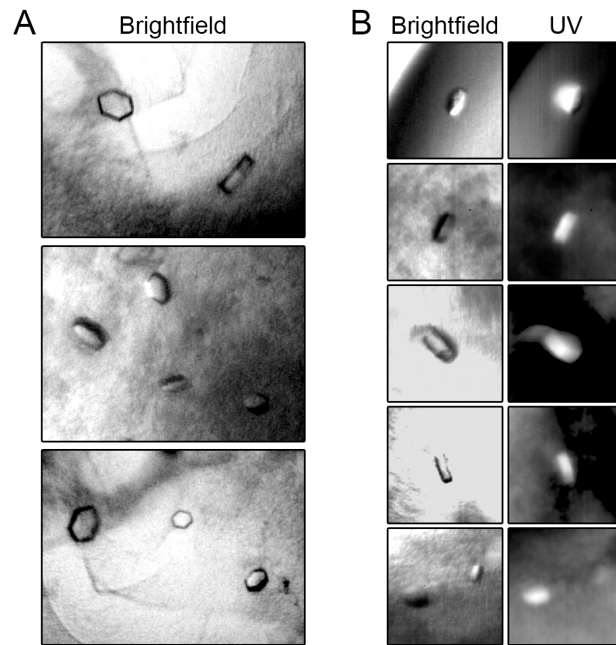


FIGURE 5-8 CRYSTALS OF THE NUP160³⁷⁻⁹⁵³-NUP37 COMPLEX.

Crystals of Nup160³⁷⁻⁹⁵³-Nup37 obtained in buffer containing 0.1M Bis-Tris, pH 6.5, 0.1 M NaCl and 1.5 M Ammonium Sulfate. Crystals were imaged using brightfield (A, B) and UV microscopy (B).

5.2.2 BIOCHEMICAL CHARACTERIZATION OF POM121 INTERACTIONS WITH β -PROPELLER PROTEINS OF THE NPC CORE SCAFFOLD

Our next goal was to investigate the molecular interactions between Nup160 and Nup37 of the nonameric membrane-scaffolding coat with the surrounding pore membrane. Mammalian NPCs are associated with three Poms, Pom121, NDC1 and gp210 (Gerace et al., 1982; Hallberg et al., 1993; Mansfeld et al., 2006; Stavru et al., 2006a). While the majority of gp210 resides in the NE luminal space, extensive regions of Pom121 and NDC1 emanate towards the NPC interior where they are exposed to various Nup subcomplexes (Wozniak et al., 1989; Hallberg et al., 1993; Soderqvist and Hallberg, 1994; Lau et al., 2006; Mansfeld et al., 2006; Stavru et al., 2006a). Indeed, we have previously observed direct interactions between Pom121 and NDC1 with Nups of the core and adaptor scaffolding complexes (Chapter III). One such interaction occurs between the N-terminus of Pom121 and the β -propeller domain of Nup160. The work below describes recent efforts directed at obtaining large amounts of Nup160-Pom121 complexes that may be used for crystallographic analysis. Resolving this structure will provide the first observation of interactions between the NPC core and surrounding pore membrane at the atomic level.

5.2.2.1 PURIFICATION OF POM121²¹⁵⁻⁵⁵⁷

Human Pom121 contains a single transmembrane domain at its N-terminus, with a large \sim 120 kDa domain residing within the NPC (Figure 5-

9A) (Hallberg et al., 1993; Funakoshi et al., 2007; Funakoshi et al., 2011). We have previously mapped the NPC-interacting domain of Pom121 to a fragment comprised of amino acid residues 215-557 (Pom121²¹⁵⁻⁵⁵⁷), and demonstrated that this fragment directly binds the β -propeller domain of Nup160 (Chapter III). To obtain high levels of recombinant protein, bacmids were engineered for expression of Pom121²¹⁵⁻⁵⁵⁷ in insect cells. Following infection, cells were harvested and disrupted by sonication. Following binding to Ni-NTA Agarose, beads were washed with buffer containing 20 mM imidazole, and bound proteins were eluted with buffer containing 200 mM imidazole. Eluate was further purified by ion exchange chromatography using HiTrap® Q Sepharose. Size exclusion chromatography was then used to purify Pom121²¹⁵⁻⁵⁵⁷ to homogeneity (Figure 5-9B, C).

Analysis of Pom121²¹⁵⁻⁵⁵⁷ by gel filtration revealed a striking elution profile (Figure 5-9C). With a molecular mass of ~37 kDa, the predicted elution volume for Pom121²¹⁵⁻⁵⁵⁷ is ~16 ml. However, the majority of Pom121²¹⁵⁻⁵⁵⁷ eluted at ~14 ml, a volume typically occupied by much larger proteins. One possibility for this apparent discrepancy is the oligomerization of Pom121²¹⁵⁻⁵⁵⁷ into higher-order multimers. Homo-oligomerization would markedly increase the mass of eluted Pom121²¹⁵⁻⁵⁵⁷, and explain the observed elution at a volume characteristic of larger proteins. Alternatively,

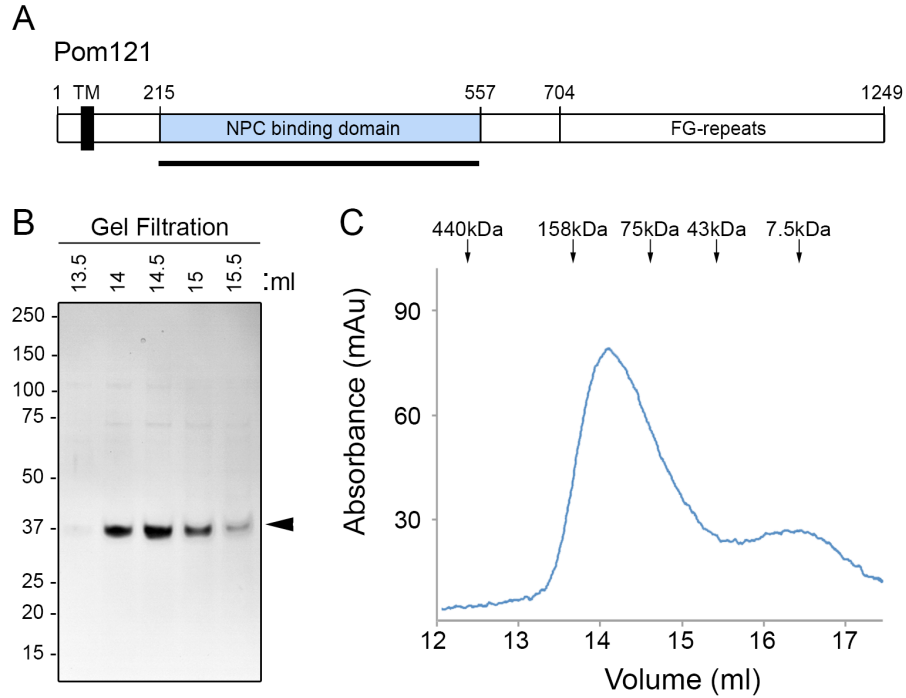


FIGURE 5-9 PURIFICATION OF POM121²¹⁵⁻⁵⁵⁷.

(A) Schematic of the domain organization of Pom121. Residue numbers indicate domain boundaries, and bar indicates the fragment used for purification. (B, C) Purification of Pom121²¹⁵⁻⁵⁵⁷ by size exclusion chromatography. (B) Eluted fractions were sampled; proteins were resolved by SDS-PAGE and detected by Coomassie blue staining. To the right of the panel, an arrowhead indicates the point at which Pom121²¹⁵⁻⁵⁵⁷ migrates. (C) Chromatogram representing the elution profile of Pom121²¹⁵⁻⁵⁵⁷ using a Superdex 200 10/300 gel filtration column. The migration of molecular mass standards is indicated. Mass markers are in kilodaltons.

the elution profile of Pom121²¹⁵⁻⁵⁵⁷ might be significantly affected by its tertiary structure. As mentioned previously, protein conformation directly affects the rate of migration during gel filtration (Erickson, 2009). While the tertiary structure of Pom121 is unknown, we used PSIPRED to predict secondary structural elements (Figure 5-10A). PSIPRED predictions suggest that the vast majority of Pom121²¹⁵⁻⁵⁵⁷ lacks defined structural motifs. The few structural elements predicted are restricted to the N- and C-termini of the Pom121²¹⁵⁻⁵⁵⁷ fragment. The lack of secondary structural motifs suggests that a significant portion of Pom121²¹⁵⁻⁵⁵⁷ may be natively unfolded. To further evaluate the structure of Pom121²¹⁵⁻⁵⁵⁷, we used the protein disorder prediction system PrDOS to estimate the probability that Pom121²¹⁵⁻⁵⁵⁷ contains natively unstructured regions (Figure 5-10B). In agreement with PSIPRED predictions, information obtained from PrDOS suggests that while the N- and C-termini of Pom121²¹⁵⁻⁵⁵⁷ are likely structured, the majority of Pom121²¹⁵⁻⁵⁵⁷ is unfolded. In summary, either homo-oligomerization or structural disorder of Pom121 polypeptides, or a combination of both, might contribute to the elution of Pom121²¹⁵⁻⁵⁵⁷ in a characteristic of a much larger protein.

5.2.2.2 PURIFICATION OF COMPLEXES OF NUP160¹⁻⁵⁸³-POM121²¹⁵⁻⁵⁵⁷

We next evaluated the ability of purified Pom121²¹⁵⁻⁵⁵⁷ to form a complex with the purified β -propeller domain of Nup160 (Nup160¹⁻⁵⁸³). Our previous analyses demonstrated that Pom121²¹⁵⁻⁵⁵⁷ can interact directly with

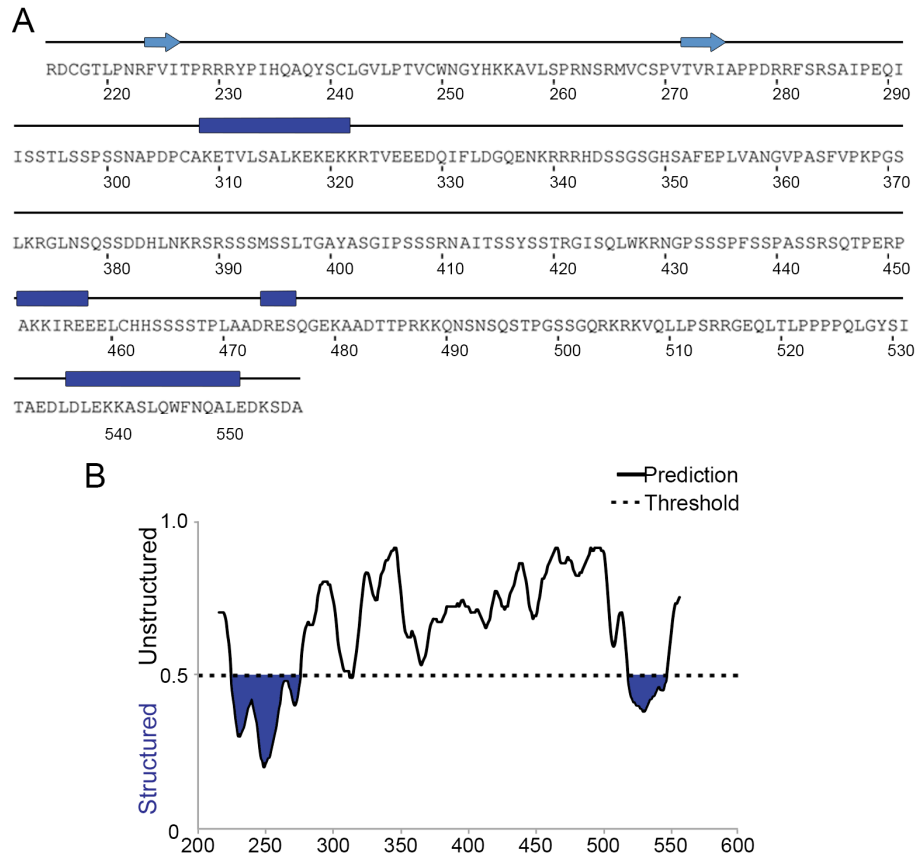


FIGURE 5-10 SECONDARY STRUCTURE PREDICTIONS FOR POM121²¹⁵⁻⁵⁵⁷.

(A) Secondary structures of a fragment of Pom121 containing amino acid residues 215-557 were predicted using the PSIPRED protein structure prediction server (McGuffin et al., 2000). β -sheets are represented as light blue arrows; α -helices as dark blue rectangles. (B) Predictions of natively unfolded regions of Pom121²¹⁵⁻⁵⁵⁷ were made using the PrDOS protein disorder prediction system (Ishida and Kinoshita, 2007). A threshold was set that assumed a false positive rate of no greater than 5%. Regions predicted to contain structural motifs are colored blue.

a fragment of Nup160 comprised of amino acid residues 37-490 (Chapter III). Therefore, we predicted that Pom121²¹⁵⁻⁵⁵⁷ would interact directly with Nup160¹⁻⁵⁸³. To analyze complex formation, purified proteins were incubated for 30 min at 4 °C. Complex formation was evaluated by comparison of gel filtration profiles of pre-incubated Pom121²¹⁵⁻⁵⁵⁷ and Nup160¹⁻⁵⁸³ to those of individual proteins alone (Figure 5-11). Individual proteins were resolved in fractions consistent with their previously determined elution profiles. However, pre-incubation of Pom121²¹⁵⁻⁵⁵⁷ with Nup160¹⁻⁵⁸³ significantly affected the migration of each protein during gel filtration (Figure 5-11A, green line). Analysis of eluted fractions by SDS-PAGE clearly demonstrated the appearance of a complex of Pom121²¹⁵⁻⁵⁵⁷ and Nup160¹⁻⁵⁸³ in the fraction eluted at 13.5 ml following pre-incubation (Figure 5-11B). Importantly, neither Pom121²¹⁵⁻⁵⁵⁷ nor Nup160¹⁻⁵⁸³ were detected in this fraction when run individually (Figure 5-11B, arrows). We used this complex to initiate crystallization trials. Amorphous crystals formed in buffer containing 0.1 M Bis-Tris, pH 8.5, 0.2 M NaCl, and 10 mM TCEP (Figure 5-11C). While the morphology of these crystals implies they may be of poor diffraction quality, we confirmed these crystals contained protein by examining their intrinsic fluorescence using UV microscopy. Optimizing crystallization conditions will ultimately improve crystal growth and diffraction quality.

As mentioned previously, we predict that the majority of Pom121²¹⁵⁻⁵⁵⁷ is natively unfolded. While disordered regions of proteins often have important functional roles, they can markedly interfere with crystallization

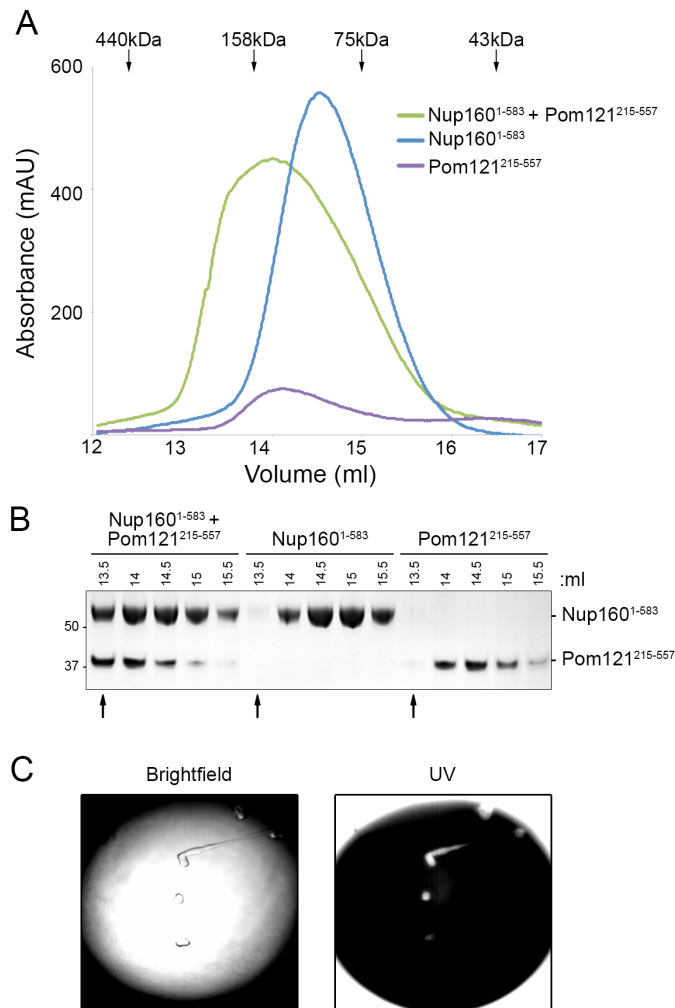


FIGURE 5-11 POM121²¹⁵⁻⁵⁵⁷ INTERACTS DIRECTLY WITH NUP160¹⁻⁵⁸³.

(A, B) Following incubation, a mixture of purified Nup160¹⁻⁵⁸³ and Pom121²¹⁵⁻⁵⁵⁷ was subjected to size exclusion chromatography. A) Representative chromatograms obtained after gel filtration of Nup160¹⁻⁵⁸³ (blue), Pom121²¹⁵⁻⁵⁵⁷ (purple), or a mixture of both (green). The position at which mass markers migrate is indicated at the top of the panel. (B) Fractions were sampled and eluted proteins were resolved by SDS-PAGE. Gels were stained with Coomassie Blue stain. The point at which Nup160¹⁻⁵⁸³ and Pom121²¹⁵⁻⁵⁵⁷ migrate is indicated to the right of the panel. Mass markers are in kilodaltons. An arrow indicates the fraction in which the Nup160¹⁻⁵⁸³-Pom121²¹⁵⁻⁵⁵⁷ complex elutes. (C) Complexes of Nup160¹⁻⁵⁸³-Pom121²¹⁵⁻⁵⁵⁷ were concentrated and used to screen a variety of solutions optimized for crystal growth by hanging drop vapor diffusion. Crystals were imaged using brightfield and UV microscopy.

and impede structural analysis (Ishida and Kinoshita, 2007). For this reason, we considered two alternative approaches to improve crystallization of Nup160-Pom121 complexes. First, we demonstrated that Nup160 interacts with an ~100 amino acid residue region of the Pom121 N-terminus (Pom121²¹⁵⁻³²²)(Figure 5-12). For these experiments, GST-tagged fragments of Pom121 were expressed in *E. coli* and purified using GSH Sepharose. Bead-bound proteins were incubated with purified His₆-Nup160¹⁻⁵⁸³-FLAG, and bound proteins were eluted using SDS sample buffer, resolved by SDS-PAGE, and visualized using Coomassie blue (CB) stain. The presence of Nup160 in eluates was confirmed by western blot using an anti-FLAG antibody. As expected, Nup160¹⁻⁵⁸³ interacted directly with GST-Pom121²¹⁵⁻⁵⁵⁷, and failed to bind GST alone. Intriguingly, binding of Nup160¹⁻⁵⁸³ occurs within a domain of Pom121 that is predicted to contain secondary structural motifs (Pom121²¹⁵⁻³²²; Figure 5-10A). Because this fragment lacks the majority of the predicted disordered region of Pom121, we predict that complexes of Nup160¹⁻⁵⁸³-Pom121²¹⁵⁻³²² will be more susceptible to crystallization.

Alternatively, it is possible that a portion of the Pom121 unstructured domain adopts an ordered conformation upon binding to interacting partners. Disorder-to-order transitions of natively unfolded proteins are commonly observed during ligand recognition, and are often critical for binding partner association (Dyson and Wright, 2005). In general, this type of binding-induced conformational change is characteristic of

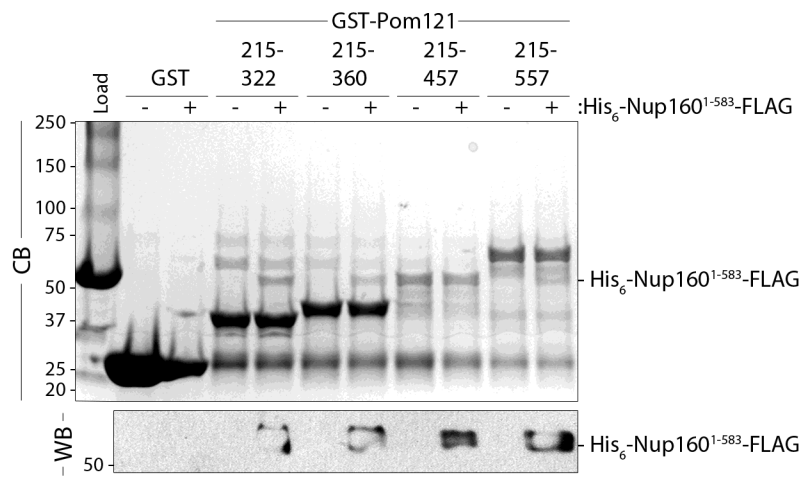


FIGURE 5-12 MAPPING THE NUP160 BINDING DOMAIN OF POM121.

Purified Nup160¹⁻⁵⁸³-FLAG was incubated with bead-bound fragments of GST-Pom121 or with GST alone. Bound proteins were eluted using SDS sample buffer, resolved by SDS-PAGE, and stained with Coomassie blue (CB) stain. To confirm the presence of bound Nup160¹⁻⁵⁸³-FLAG, western blot (WB) analysis was performed using an anti-FLAG monoclonal antibody.

proteins that interact with multiple binding partners (Dyson and Wright, 2005). As an additional approach to improve crystallization of Pom121-containing complexes, we hypothesized that, in addition to Nup160, the inclusion of additional Pom121 binding partners would occupy remaining disordered regions, allowing the formation of higher quality crystals.

5.2.2.3 POM121²¹⁵⁻⁵⁵⁷ INTERACTS WITH THE β -PROPELLER PROTEINS NUP37 AND NUP43

To identify binding partners of Pom121 in addition to Nup160, we focused on members of the Nup107-160 membrane scaffolding complex. Nups that comprise this complex are composed exclusively of β -propeller and α -solenoid domains. It has been suggested that the β -propellers of these Nups are critical mediators of inter-subcomplex interactions, while interactions between α -solenoid domains within the subcomplex provide structural rigidity to the membrane coat (see section 1.4.2.2) (Leksa and Schwartz, 2010). Therefore, we predicted that β -propeller proteins of the Nup107-160 complex would be among the additional Pom121 interactors. We have previously determined that Pom121 does not interact with the β -propellers Sec13 and Seh1 (Chapter III). Therefore, we narrowed our focus to include the β -propeller proteins Nup37 and Nup43. The acquisition of these proteins defines the evolutionary transition of the scaffolding core from hetero-heptamer of Sc to hetero-nonamer of metazoan cells. We reasoned

that, because Nup160 interacts directly with both Nup37 and Pom121, binding to Nup160 would position Pom121 and Nup37 in close proximity where they may potentially interact. We included Nup43 in our analyses, as interacting partners for this protein remain to be identified.

To evaluate binding, GST-tagged Nup37 and Nup43 were expressed in *E. coli* and purified using GSH Sepharose (Figure 5-13). A GST-tagged fragment of the Nup160 β -propeller domain (GST-Nup160³⁷⁻⁴⁹⁰) and GST alone were included as positive and negative controls for binding Pom121²¹⁵⁻⁵⁵⁷, respectively. Bead bound proteins were incubated with purified Pom121²¹⁵⁻⁵⁵⁷, and bound proteins were eluted using SDS sample buffer, resolved by SDS-PAGE, and visualized using Coomassie blue (CB) stain. As expected, Pom121²¹⁵⁻⁵⁵⁷ interacted directly with Nup160³⁷⁻⁴⁹⁰, and failed to bind GST alone. Strikingly, Pom121²¹⁵⁻⁵⁵⁷ was observed to directly bind both Nup37 and Nup43. We confirmed the presence of Pom121²¹⁵⁻⁵⁵⁷ in eluted samples by western blot using anti-Pom121 specific polyclonal antibodies. Together, these data demonstrate the direct association of Pom121 with three β -propeller proteins of the NPC core scaffold. In addition to data obtained previously (Chapter III), this extends the Pom121 interactome to include the β -propeller proteins Nup37, Nup43, and Nup160 with Nup155 of the adaptor scaffold. It will be important to determine the relative affinities of Pom121 for each of Nup37, Nup43 and Nup160, and to investigate the potential for combinations of these proteins to form higher-order complexes. We predict that the binding of additional β -propeller proteins to

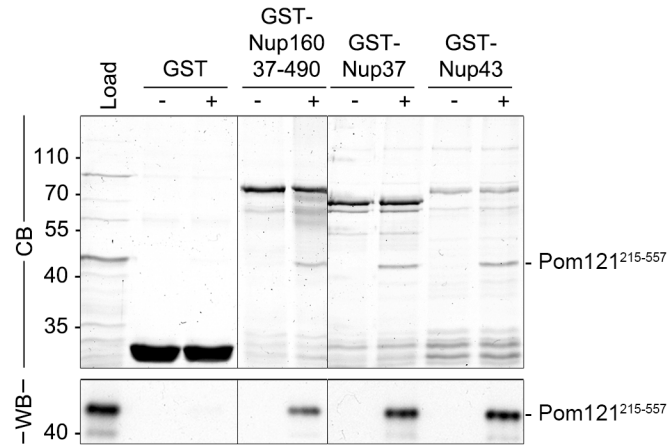


FIGURE 5-13 POM121²¹⁵⁻⁵⁵⁷ INTERACTS DIRECTLY WITH THE β -PROPELLERS OF NUP160, NUP37 AND NUP43.

Purified Pom121²¹⁵⁻⁵⁵⁷ was incubated with bead bound GST-Nup160³⁷⁻⁴⁹⁰, GST-Nup37, GST-Nup43, or GST alone. Bound proteins were eluted using SDS sample buffer, resolved by SDS-PAGE, and stained with Coomassie blue (CB) stain. To confirm the presence of bound Pom121²¹⁵⁻⁵⁵⁷, western blot (WB) analysis was performed using an anti-Pom121 specific polyclonal antibody. Approximately 10% of Pom121²¹⁵⁻⁵⁵⁷ used for binding is resolved in the lane marked Load.

Pom121²¹⁵⁻⁵⁵⁷ will minimize the exposure of Pom121 disordered regions, and allow for the formation of high quality crystals during forthcoming crystallization trials.

5.3 DISCUSSION

In an effort to further our understanding of the molecular architecture of the metazoan NPC membrane coat, we characterized complexes of the β -propeller/ α -solenoid Nup160 of the Nup107-160 core scaffolding complex with the β -propeller protein Nup37 and membrane-bound Pom121. We optimized conditions for the large-scale purification of Nup37, Pom121, and fragments of Nup160, and evaluated the formation of complexes between recombinant proteins. We demonstrated the evolutionary conservation of the interaction between Nup160 and Nup37, and show that this interaction requires the extended α -solenoid domain of Nup160 in addition to the 6D-7A α -helical insert of the Nup160 β -propeller. We extended previous analyses of the interaction of the Nup160 β -propeller with Pom121, and mapped the Nup160 binding domain of Pom121 to an ~100 amino acid residue fragment of its N-terminus. Finally, we uncovered novel interactions between Pom121 and the β -propeller proteins Nup37 and Nup43 of the scaffolding Nup107-160 complex. We predict that the ability of Pom121 to bind numerous β -propeller proteins, alone or in combination, could provide architecturally distinct structural conformations of the NPC

membrane scaffold in the vicinity of the pore membrane. Promiscuity of Pom121 interactions with β -propeller proteins could facilitate the circumferential adjustments of the membrane coat that are required to regulate the transport properties of the NPC.

5.3.1 THE INTERACTION BETWEEN NUP37 AND NUP160 IS CONSERVED IN METAZOAN CELLS

Our analyses of interactions between Nup160 and Nup37 suggest that this interaction is conserved in metazoan cells. Our previous work describes the co-evolution of Nup160 orthologues (termed Nup120 in yeast) with the acquisition of Nup37 within the membrane scaffolding complex (Chapter IV). Structural analyses of the Nup120-Nup37 complex of *Sp* revealed numerous Nup37 binding sites interspersed throughout an α -helical bundle that protrudes from the Nup120 β -propeller, termed the 6D-7A α -helical insert. Conspicuously, structural analyses of Nup120 orthologues revealed the conservation of the 6D-7A α -helical insert in species that contain Nup37. Importantly, the 6D-7A α -helical insert is absent from Nup120 of *Sc*, which lacks a Nup37 orthologue. As expected, *Sc*-Nup120 is unable to bind Nup37. Together, these results suggested that the *Sp*-Nup120 6D-7A α -helical insert is required for binding Nup37. The results presented here extend previous observations to suggest that the Human Nup160 6D-7A α -helical insert is alone insufficient to capture Nup37. Using

recombinant proteins *in vitro*, we demonstrated that purified Nup37 fails to interact with a fragment of Nup160 comprised of the β -propeller domain (Nup160¹⁻⁵⁸³) (Figure 5-5). Extending the length of Nup160 to include a portion of the α -solenoid domain (Nup160³⁷⁻⁹⁵³) restored binding of Nup37 (Figure 5-7). We conclude from these analyses that the hydrophobic interface of the Nup160 α -solenoid domain is required in conjunction with the 6D-7A α -helical insert to efficiently incorporate Nup37 within the NPC core scaffold.

5.3.2 INTERACTIONS BETWEEN POM121 AND β -PROPELLERS LINK THE CORE SCAFFOLD TO THE POM

We extended our biochemical analyses of the metazoan scaffolding complex to include interactions between members of the core scaffold with proteins of the POM. Our previous analyses revealed specific interactions between Pom121 and the β -propeller domains of Nup160 and Nup155 of the core and adaptor scaffolding complexes, respectively (Chapter III). We extended the Pom121 interactome to include two additional β -propellers of the core scaffold, Nup37 and Nup43 (Figure 5-13). At this time, it is unknown whether Pom121 interacts simultaneously with these Nups, or whether binding of specific Nups is mutually exclusive. Our previous analyses of Pom121 complexes suggest that binding of Pom121 to the β -propeller domain of Nup155 precludes the association of Pom121 with Nup160.

Whether a similar binding mechanism exists for interactions of Pom121 with Nup37 and Nup43 remains to be determined.

Several possible binding scenarios can be envisaged, each with important implications on NPC assembly. Simultaneous binding of Pom121 to β -propellers of neighboring core scaffolding complexes (including Nup37, Nup43, and Nup160) could facilitate the oligomerization of hetero-nonamers. As observed for interactions between Nup160 and Nup133 (see section 1.4.2.3), Pom121 interactions with β -propellers of adjacent hetero-nonamers could contribute the ring-like, head-to-tail arrangement of Y-shaped complexes (Seo et al., 2009). Alternatively, simultaneous interactions of Pom121 with β -propellers of the core and adaptor scaffolds (including Nup37, Nup43 and Nup155) might provide an essential linkage between the core and adaptor scaffold structural modules of the NPC. At this time, no such interactions have been reported (Bilokapic and Schwartz, 2012). The regulation of such inter-subcomplex interactions would be critical during NPC assembly. Finally, Pom121 might oscillate between binding conformations in response to the transport requirements of the cell. Plasticity of Nup interactions has recently emerged as a central theme that presumably allows for large circumferential adjustments to occur within the NPC central channel and core scaffold complex (Debler et al., 2008; Solmaz et al., 2011; Solmaz et al., 2013). Understanding the role of Pom121 in NPC assembly awaits the resolution of structures of Pom121-containing complexes. Comparing the structures of complexes of Pom121 with β -

propellers of the core and adaptor scaffolds will undoubtedly provide key insight into the molecular mechanisms governing both the assembly of the NPC as well as the structural adaptations required to accommodate the efficient transport of numerous macromolecules.

5.3.3 CONSEQUENCES OF THE UNSTRUCTURED NATURE OF POM121²¹⁵⁻⁵⁵⁷

Several secondary structural prediction programs have indicated that the majority of the Nup-binding domain of Pom121, Pom121²¹⁵⁻⁵⁵⁷, is natively unfolded (Figure 5-10). Natively unfolded proteins have been implicated in the regulation of numerous biological processes, including transcription, translation, cellular signaling and cell cycle progression (Wright and Dyson, 1999; Dunker et al., 2002; Iakoucheva et al., 2002; Uversky, 2002; Dyson and Wright, 2005; Uversky, 2011). Disordered proteins often undergo coupled folding and binding, alternatively termed ‘disorder-to-order’ transitions, during ligand recognition (for review, see Uversky, 2011). In this way, natively unstructured domains have been described as ‘molecular switches’, transitioning to an ordered conformation upon binding partner recognition. Intriguingly, coupled folding and binding of disordered regions has been described as a key regulatory mechanism in the self-assembly of large multi-protein complexes, such as the assembly of the ribosome (Namba, 2001; Gross et al., 2003).

We predict that a portion of Pom121 adopts specific structural conformations upon recognition of binding partners, such as Nup160. In

many cases, the intrinsic flexibility of disordered regions allows for numerous conformational changes to occur during the simultaneous binding of interacting partners (Dyson and Wright, 2005). As numerous binding partners for Pom121 have now been described (Chapter III; Figure 5-13), one can envisage such a mechanism might facilitate binding of Pom121 to numerous β -propeller proteins.

Intrinsically disordered regions have also been demonstrated to contribute to protein homo-oligomerization (Uversky, 2011). While we observed the oligomerization of Pom121²¹⁵⁻⁵⁵⁷ polypeptides during gel filtration, the tendency of Pom121 polypeptides to form higher-order multimers in the presence of interacting Nups within the context of the endogenous NPC remains unknown. It is conceivable that oligomerization of Pom121-contacting complexes contributes to NPC assembly. Oligomerization of Pom121 complexed with scaffolding Nups might trigger the higher-order assembly of NPC protomers around the symmetrical octad axis. A similar role in NPC assembly has been suggested for the dimerization of membrane-associated Nup53 (Handa et al., 2006).

Finally, disordered regions of proteins are often targets of post-translational modifications that significantly affect protein-protein interactions. As we predict Pom121 to be critical in linking Nup subcomplexes to the POM, it is intriguing to consider the regulation of such interactions by post-translational modifications, such as phosphorylation. By interacting with a diverse subset of Nups, Pom121 is an attractive potential

target of mitotic kinases that regulate NPC disassembly during mitosis. Indeed, phosphorylation of specific sites within the Nup-binding region of Pom121 has been identified by mass spectrometry in large-scale analyses of the mitotic phosphoproteome (Dephoure et al., 2008; Olsen et al., 2010; Rigbolt et al., 2011). Control of Pom121 complex formation with Nups of the core and adaptor scaffolds by the actions of mitotic kinases and phosphatases might represent a key regulatory step in the disassembly and reassembly of the NPC during mitosis. Understanding the molecular consequences of phosphorylation of Pom121-containing complexes will require the resolution of various Pom121-Nup complexes at the atomic level.

CHAPTER VI: **PERSPECTIVES**

6.1 SYNOPSIS

Evolutionary progression from prokaryote to eukaryote, and subsequent divergence of eukaryotic lineages, occasioned the development of an intricate endomembrane system that afforded cells the advantage of partitioning their metabolic activities (Blobel, 1980). This necessitated the adaptation of proteins to form a structural scaffold that stabilized the sharply curved edges of invaginated membrane sheets and tubules (Devos et al., 2004). Within the POM of the NE, these proteins comprise the cylindrical, lattice-like coat stabilizing the pore membrane that circumscribes the NPC. Interaction networks between neighboring Nup scaffold modules, including associations with surrounding Poms, have only recently begun to emerge and are likely to play key roles in the regulation of NPC assembly. Data presented in Chapters III and V identify Pom121 as a central player mediating the association of the NPC scaffold with the POM through interactions with core Nup complexes. In the following section, this information will be integrated into current architectural models of the NPC, and discussed within the context of our current understanding of NPC biogenesis.

6.2 CONSERVATION OF THE NPC-POM INTERFACE

Throughout the past decade, advances in computational and structural biology have significantly enhanced our understanding of the organization of structural modules within NPCs, and defined discrete,

biochemically distinct Nup subcomplexes. While interactions between Nups within individual subcomplexes have in many cases been well defined, interactions between subcomplexes, and importantly, interactions linking the NPC to the surrounding POM, have remained elusive (Grandi et al., 1995b; Guan et al., 1995; Siniosoglou et al., 1996; Marelli et al., 1998; Siniosoglou et al., 2000; Belgareh et al., 2001; Hawryluk-Gara et al., 2005; Alber et al., 2007b; Bilokapic and Schwartz, 2012).

Recent work has shed light how the NPC-POM interface is established in *Sc*. Data from two key studies revealed an elaborate interaction network between yeast Poms Ndc1p, Pom152p and Pom34p, and extended this network to include Nup53p/Nup59p and Nup170p/Nup157p of the NPC adaptor scaffold (Makio et al., 2009; Onischenko et al., 2009). Interactions between metazoan NDC1 and Nup53 could be recapitulated in pulldown experiments using RLNEs, suggesting this branch of the NPC-POM interaction network is likely conserved (Mansfeld et al., 2006; Hawryluk-Gara et al., 2008). Whether these interactions occur directly, or require additional binding partners remains to be investigated.

Establishing the conservation of Pom152p interactions with the NPC scaffold, however, is hindered by the lack of clear orthology between Poms of yeast and metazoan cells. In this respect, comparisons of primary amino acid sequences or tertiary structure predictions have failed to identify conservation between either Pom152p or Pom34p of *Sc* with Pom121 or gp210 of metazoan cells (Liu et al., 2009; Neumann et al., 2010). Topological

predictions suggest that Pom152p and gp210 share a similar domain architecture, where the vast majority of each protein resides within the NE lumen (Greber et al., 1990; Wozniak et al., 1994; Devos et al., 2004). Biochemical analyses, however, have failed to detect any significant functional conservation between these Poms. While a role for Pom152p in assembly of the yeast NPC has clearly been established, gp210 appears to be dispensable for this process in metazoan cells (Eriksson et al., 2004; Stavru et al., 2006b; Onischenko et al., 2009). Instead, alternative roles for gp210 have been proposed in regulating both cell differentiation and NEBD (Olsson et al., 1999; Galy et al., 2008; D'Angelo et al., 2012). Furthermore, the expression of gp210 is restricted to a subset of differentiated cells, suggesting that critical a role for this Pom in NPC assembly is unlikely (Olsson et al., 2004; Gomez-Cavazos and Hetzer, 2012).

Based on data presented here, we propose that Pom152p and Pom121 perform homologous functions in linking NPC scaffold complexes to the POM (Chapter III, Figure 6-1). Using tagged-Pom152p as bait in pulldown studies from RLNEs, we uncovered novel, cross-species interactions between Pom152p with Nup155 of the adaptor scaffold, and with members of the Nup107-160 core scaffold complex (Figure 3-16). We further demonstrated that interactions between Pom152p and Nup155 occur directly. These data are consistent with interactions observed between Pom152p and Nup170p (yeast orthologue of Nup155), and explain the integration of exogenously

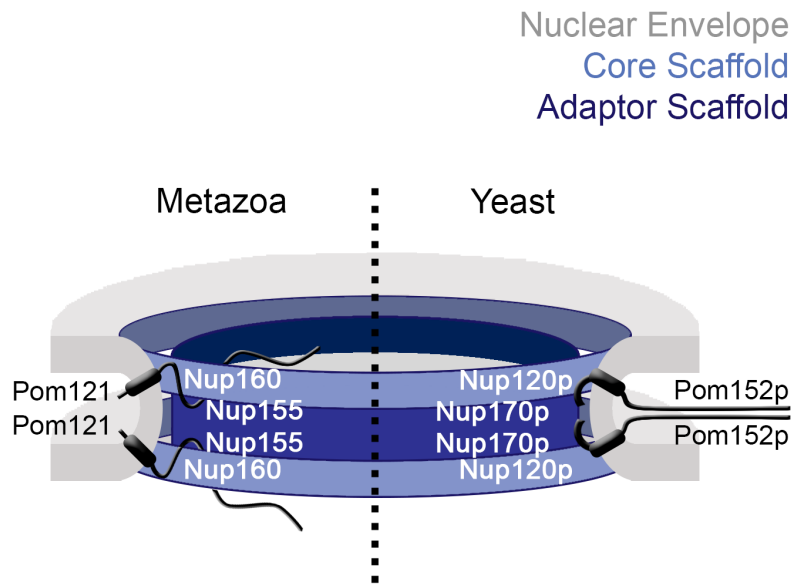


FIGURE 6-1 **MODEL FOR THE CONSERVATION OF THE NPC-POM INTERFACE IN YEAST AND METAZOA.**

In the yeast *S. cerevisiae* and *S. pombe*, interactions of the pore-membrane protein Pom152p with Nup120p and Nup170p of the core (blue) and adaptor (purple) scaffolds, respectively, link the NPC core to the nuclear envelope membrane (gray). A similar network of interactions is established in metazoan cells, where interactions of Pom121 with Nup160 and Nup155 define the NPC-POM interface. The transmembrane segments of Pom152p and Pom121 are indicated by black rectangles.

expressed GFP-Pom152p within the metazoan NPC (Wozniak et al., 1994; Makio et al., 2009). Importantly, comparison of interaction profiles of Pom152p and Pom121 from RLNE suggests they interact with a remarkably similar subset of Nups, including members of the core and adaptor scaffold complexes. Furthermore, both Poms interact directly with Nup155. Therefore, we propose that the fragment of Pom121 used in our studies (aa 215-557) is functionally orthologous to the NPC exposed domain of Pom152p (aa 1-111).

As an extension of this hypothesis, it can be envisaged that Pom152p links the yeast Nup84p core scaffold to the POM (orthologous to the Nup107-160 complex). Based on interactions observed between Pom152p and the Nup107-160 complex (Chapter III), the assumption that Pom152p and Pom121 are functional orthologues, and our analyses of Pom121-Nup160 complexes (Chapters III and V), we predict that parallel interactions might occur between yeast Pom152p and Nup120p (orthologue of Nup160). These interactions would be the first observed between the yeast POM and core scaffold. As the race towards achieving atomic resolution structures of the Nup84p heptamer continues, it is intriguing to consider that integrating information of the interactions between scaffold Nups with surrounding Poms may be pivotal in resolving architectural models of the NPC membrane coat.

Due to the marked discrepancy in the lengths of Pom152p and Pom121 polypeptides discussed above (i.e. ~110 aa vs. ~340 aa), it may be

difficult to envision a model whereby a small fragment of Pom152p establishes the same interaction network as a fragment of Pom121 nearly three times its size. This inconsistency might be reconciled either of two ways. First, a central tenet of our model describing the Pom121 interactome within the metazoan NPC is the plasticity of interactions between Pom121 and Nups (Chapter V). Transitioning between Pom152p/Pom121 binding partners might be achieved, in part, by competition for a similar binding domain. Therefore, residues of Pom152p/Pom121 that facilitate binding of multiple interactors might significantly overlap, and could conceivably be restricted to a relatively small domain. Second, simultaneous interactions between a small domain of Pom152p/Pom121 and Nups might occur if binding partners were localized in close proximity to one another. We suggest that this is likely for the organization of Pom121-binding Nups within the metazoan NPC, and that a similar arrangement may occur in yeast (see below).

Comparing structural predictions of Nup-interacting domains of Pom152p and Pom121 suggests that the mechanism in which they interact with the surrounding scaffold might be conserved. As discussed in Chapter V, Pom121²¹⁵⁻⁵⁵⁷ is comprised of a long, natively unfolded domain characterized by relatively few structural motifs. We suggest that association with binding partners allows Pom121²¹⁵⁻⁵⁵⁷ to adopt specific structural conformations, and that the unstructured domain architecture facilitates binding of Pom121²¹⁵⁻⁵⁵⁷ to multiple Nups. Intriguingly, structural predictions of the

Nup-binding domain of Pom152p¹⁻¹¹¹ suggest that it adopts a similar natively unfolded architecture (Figure 6-2). Secondary structure predictions made using PSIPRED identified a single α -helix (Figure 6-2A). These predictions were supported by analysis using the disorder prediction server PrDOS, which suggests that the majority of Pom152p¹⁻¹¹¹ is unfolded (Figure 6-2B). Together with data discussed above, it can be envisaged that Pom152p interacts with a repertoire of scaffold Nups, orthologous to those described for Pom121, through a similar mechanism involving the disorder-to-order transition of its natively unfolded binding domain. Whether these predictions hold true awaits the identification of additional Pom152p binding Nups, and evaluation of the atomic structures of Pom152p complexes.

6.3 CHARACTERIZING THE POM121 INTERACTOME

In the analyses presented within this thesis, we demonstrate direct interactions between Pom121²¹⁵⁻⁵⁵⁷ and five Nups: Nup37, Nup43, Nup98, Nup155 and Nup160 (Chapters III and V). Several lines of evidence suggest these Nups are positioned in close spatial proximity within the NPC. First, Nup37, Nup43 and Nup160 are *bone fide* members of the Nup107-160 complex (Loiodice et al., 2004). While the positioning of Nup43 within this complex is unknown, we demonstrated conserved, direct interactions between Nup160 and Nup37 (Chapters IV and V). Second, although initially isolated as part of peripherally localized Nup subcomplexes, structural analyses have demonstrated that Nup98 can be reconstituted into the

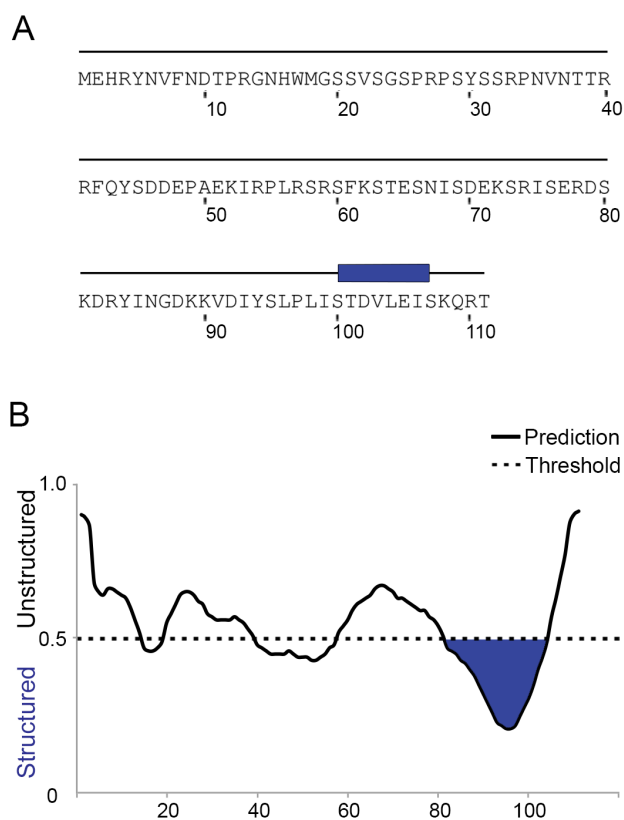


FIGURE 6-2 SECONDARY STRUCTURE PREDICTIONS FOR POM152P¹⁻¹¹¹.

(A) Secondary structure predictions of a fragment of Pom152p containing amino acid residues 1-111 were made using the PSIPRED protein structure prediction server (McGuffin et al., 2000). A single α -helix is represented as a dark blue rectangle. (B) Predictions of natively unfolded regions of Pom152p¹⁻¹¹¹ were made using the PrDOS protein disorder prediction system (Ishida and Kinoshita, 2007). A threshold was set that assumed a false positive rate of no greater than 5%. Regions predicted to contain structural motifs are shaded blue.

Nup170-160 core scaffold, through interactions with the α -solenoid Nup96 (Fontoura et al., 2001; Griffis et al., 2003; Stuwe et al., 2012). Finally, we demonstrate that, under certain conditions, Nup155 and Nup160 directly interact (Chapter III). While these proteins are components of biochemically distinct subcomplexes, and their interactions with Pom121 are mutually exclusive, this suggests that they may be localized within their respective subcomplexes in such a way as to potentially influence inter-subcomplex interactions. Together, these results suggest that all members of the Pom121 interactome identified thus far are potentially positioned in close proximity to one another in the context of overall NPC architecture. Whether a subset of interactions occurs simultaneously with Pom121, and the potential impact of these interactions on NPC function, architecture, and biogenesis, remains to be determined.

A similar arrangement of orthologous Pom121-binding Nups might occur within the Sc NPC. Elegant structural analyses of the Nup84p complex have demonstrated that orthologues of both Nup98 and Nup155 (yeast Nup145Np and Nup157p, respectively) can be reconstituted into the hetero-heptamer *in vitro* (Lutzmann et al., 2005). Intriguingly, it was revealed that Nup157p interacts with the core scaffold through a direct interaction with Nup120p. The degree to which this interaction reflects our observed interaction between Nup155 and Nup160 remains to be determined. As we speculate that Pom152p may interact directly with Nup120p, it will be important to determine the impact of Pom152p binding on the Nup157p-

Nup120p interaction. If the intricacies of the Pom121 interactome are conserved in yeast, binding of Nup157p and Nup120p to Pom152p may be mutually exclusive.

6.4 DEFINING A ROLE FOR POM121 IN NE AND NPC ASSEMBLY

The positioning of Nup155, Nup160 and Pom121 in close proximity to one another, and to the POM, has important implications for their roles in NE and NPC biogenesis. Essential roles for Nup155, Pom121 and the Nup107-160 complex have been defined in *X. laevis* NPC assembly assays *in vitro* (Walther et al., 2003; Antonin et al., 2005; Franz et al., 2005). We extend these observations to include an essential role for Nup155 and Pom121 in NPC assembly in mammalian cells (Chapter III). At the resolution of mitosis, the ordered, step-wise recruitment of Nups to sites of future NPC assembly initiates with chromatin association of the Nup107-160 complex and subsequent recruitment of Pom121 (Dultz et al., 2008). During NPC assembly *in vitro*, the roles of Pom121 and the Nup107-160 complex converge in the establishment of a NE assembly checkpoint, which monitors recruitment of soluble Nups and inhibits the premature fusion of NE membranes in their absence (see section 1.5.1.6) (Walther et al., 2003; Antonin et al., 2005). This model was extended to include essential roles for Nup53 and Nup155 of the adaptor scaffold (Franz et al., 2005; Hawryluk-Gara et al., 2008). Depletion of either Pom121 or adaptor scaffold Nups similarly inhibited membrane fusion, suggesting that they function in a temporarily related pathway during

checkpoint activation. Intriguingly, the function of Nup53 in checkpoint activation was mapped to its Nup155-binding domain, highlighting the importance of the Nup53-Nup155 complex in NPC assembly (Hawryluk-Gara et al., 2008).

How these proteins communicate during NPC assembly remains to be established. It was proposed that physical interactions between Pom121 with core and adaptor scaffold Nups were critical for the regulation of the NE assembly checkpoint, although interactions between scaffold Nups with the surrounding POM could not be established (Antonin et al., 2005; Franz et al., 2005). We suggest that the interactions presented here between Pom121, Nup155 and Nup160 are critical for establishing the NE assembly checkpoint and for the biogenesis of NPCs within the NE (Chapter III).

It is intriguing to consider the hierarchy of interactions we observed between Nup155 and Nup160 with Pom121, and to relate them to their temporally distinct recruitment kinetics during post-mitotic NPC assembly (Dultz et al., 2008). While Pom121 and Nup107-160 complex members are recruited early during NPC assembly, it is tempting to speculate that interactions among these proteins signal the initiation of the NE assembly checkpoint. Such a signal would be quenched by the recruitment of additional Nups that facilitate stabilization of membrane curvature, allowing for the fusion of NE membrane leaflets. In light of the observation that interactions between Nup155 and Nup160 with Pom121 are mutually exclusive, it is tempting to speculate that transitioning between Pom121

complexes participates in checkpoint abatement. One can envisage a model whereby interactions between Pom121 and Nup160 are established early during their recruitment to NPC assembly sites. Conformational changes within Pom121 induced by binding Nup160 would inhibit its participation in NE membrane fusion until further recruitment of membrane scaffold Nups, such as Nup155. Binding of Pom121 to Nup155 would satiate the checkpoint signal and allow NE fusion and subsequent incorporation of channel Nups. In this way, the release of Nup160 from Pom121, the occupation of Nup155 by Pom121, or a conformational change within Pom121 induced by either event, might satisfy the checkpoint and allow for NE/NPC assembly. These structural transitions may also facilitate activation of nuclear transport.

CHAPTER VII: REFERENCES

- Aaronson, R.P., and G. Blobel. 1974. On the attachment of the nuclear pore complex. *J Cell Biol.* 62:746-754.
- Abramoff, M.D., P.J. Magelhaes, and S.J. Ram. . 2004. Image processing with ImageJ. *Biophotonics International.* 11:36.
- Adams, P.D., P.V. Afonine, G. Bunkoczi, V.B. Chen, I.W. Davis, N. Echols, J.J. Headd, L.W. Hung, G.J. Kapral, R.W. Grosse-Kunstleve, A.J. McCoy, N.W. Moriarty, R. Oeffner, R.J. Read, D.C. Richardson, J.S. Richardson, T.C. Terwilliger, and P.H. Zwart. 2010. PHENIX: a comprehensive Python-based system for macromolecular structure solution. *Acta Crystallogr D Biol Crystallogr.* 66:213-221.
- Akey, C.W. 1989. Interactions and structure of the nuclear pore complex revealed by cryo-electron microscopy. *J Cell Biol.* 109:955-970.
- Akey, C.W., and M. Radermacher. 1993. Architecture of the *Xenopus* nuclear pore complex revealed by three-dimensional cryo-electron microscopy. *J Cell Biol.* 122:1-19.
- Alber, F., S. Dokudovskaya, L.M. Veenhoff, W. Zhang, J. Kipper, D. Devos, A. Suprpto, O. Karni-Schmidt, R. Williams, B.T. Chait, M.P. Rout, and A. Sali. 2007a. Determining the architectures of macromolecular assemblies. *Nature.* 450:683-694.
- Alber, F., S. Dokudovskaya, L.M. Veenhoff, W. Zhang, J. Kipper, D. Devos, A. Suprpto, O. Karni-Schmidt, R. Williams, B.T. Chait, A. Sali, and M.P. Rout. 2007b. The molecular architecture of the nuclear pore complex. *Nature.* 450:695-701.
- Anderson, D.J., and M.W. Hetzer. 2007. Nuclear envelope formation by chromatin-mediated reorganization of the endoplasmic reticulum. *Nat Cell Biol.* 9:1160-1166.
- Anderson, D.J., and M.W. Hetzer. 2008. Shaping the endoplasmic reticulum into the nuclear envelope. *J Cell Sci.* 121:137-142.
- Antonin, W., C. Franz, U. Haselmann, C. Antony, and I.W. Mattaj. 2005. The integral membrane nucleoporin pom121 functionally links nuclear pore complex assembly and nuclear envelope formation. *Mol Cell.* 17:83-92.
- Antonin, W., and I.W. Mattaj. 2005. Nuclear pore complexes: round the bend? *Nat Cell Biol.* 7:10-12.
- Bailer, S.M., C. Balduf, and E. Hurt. 2001. The Nsp1p carboxy-terminal domain is organized into functionally distinct coiled-coil regions required for

assembly of nucleoporin subcomplexes and nucleocytoplasmic transport. *Mol Cell Biol.* 21:7944-7955.

- Bastos, R., A. Lin, M. Enarson, and B. Burke. 1996. Targeting and function in mRNA export of nuclear pore complex protein Nup153. *J Cell Biol.* 134:1141-1156.
- Baur, T., K. Ramadan, A. Schlundt, J. Kartenbeck, and H.H. Meyer. 2007. NSF- and SNARE-mediated membrane fusion is required for nuclear envelope formation and completion of nuclear pore complex assembly in *Xenopus laevis* egg extracts. *J Cell Sci.* 120:2895-2903.
- Bayliss, R., H.M. Kent, A.H. Corbett, and M. Stewart. 2000a. Crystallization and initial X-ray diffraction characterization of complexes of FxFG nucleoporin repeats with nuclear transport factors. *J Struct Biol.* 131:240-247.
- Bayliss, R., T. Littlewood, and M. Stewart. 2000b. Structural basis for the interaction between FxFG nucleoporin repeats and importin-beta in nuclear trafficking. *Cell.* 102:99-108.
- Bayliss, R., T. Littlewood, L.A. Strawn, S.R. Wentz, and M. Stewart. 2002. GLFG and FxFG nucleoporins bind to overlapping sites on importin-beta. *J Biol Chem.* 277:50597-50606.
- Beaudouin, J., D. Gerlich, N. Daigle, R. Eils, and J. Ellenberg. 2002. Nuclear envelope breakdown proceeds by microtubule-induced tearing of the lamina. *Cell.* 108:83-96.
- Beck, M., F. Forster, M. Ecke, J.M. Plitzko, F. Melchior, G. Gerisch, W. Baumeister, and O. Medalia. 2004. Nuclear pore complex structure and dynamics revealed by cryoelectron tomography. *Science.* 306:1387-1390.
- Belgareh, N., G. Rabut, S.W. Bai, M. van Overbeek, J. Beaudouin, N. Daigle, O.V. Zatsepina, F. Pasteau, V. Labas, M. Fromont-Racine, J. Ellenberg, and V. Doye. 2001. An evolutionarily conserved NPC subcomplex, which redistributes in part to kinetochores in mammalian cells. *J Cell Biol.* 154:1147-1160.
- Berke, I.C., T. Boehmer, G. Blobel, and T.U. Schwartz. 2004. Structural and functional analysis of Nup133 domains reveals modular building blocks of the nuclear pore complex. *J Cell Biol.* 167:591-597.
- Bilokapic, S., and T.U. Schwartz. 2012. 3D ultrastructure of the nuclear pore complex. *Curr Opin Cell Biol.* 24:86-91.

- Bischoff, F.R., and D. Gorlich. 1997. RanBP1 is crucial for the release of RanGTP from importin beta-related nuclear transport factors. *FEBS Lett.* 419:249-254.
- Bischoff, F.R., and H. Ponstingl. 1991. Catalysis of guanine nucleotide exchange on Ran by the mitotic regulator RCC1. *Nature.* 354:80-82.
- Blethrow, J.D., J.S. Glavy, D.O. Morgan, and K.M. Shokat. 2008. Covalent capture of kinase-specific phosphopeptides reveals Cdk1-cyclin B substrates. *Proc Natl Acad Sci U S A.* 105:1442-1447.
- Blobel, G. 1980. Intracellular protein topogenesis. *Proc Natl Acad Sci U S A.* 77:1496-1500.
- Blobel, G., and V.R. Potter. 1966. Nuclei from rat liver: isolation method that combines purity with high yield. *Science.* 154:1662-1665.
- Bodoor, K., S. Shaikh, D. Salina, W.H. Raharjo, R. Bastos, M. Lohka, and B. Burke. 1999. Sequential recruitment of NPC proteins to the nuclear periphery at the end of mitosis. *J Cell Sci.* 112 (Pt 13):2253-2264.
- Boehmer, T., J. Enninga, S. Dales, G. Blobel, and H. Zhong. 2003. Depletion of a single nucleoporin, Nup107, prevents the assembly of a subset of nucleoporins into the nuclear pore complex. *Proc Natl Acad Sci U S A.* 100:981-985.
- Boehmer, T., S. Jeudy, I.C. Berke, and T.U. Schwartz. 2008. Structural and functional studies of Nup107/Nup133 interaction and its implications for the architecture of the nuclear pore complex. *Mol Cell.* 30:721-731.
- Brickner, D.G., I. Cajigas, Y. Fondufe-Mittendorf, S. Ahmed, P.C. Lee, J. Widom, and J.H. Brickner. 2007. H2A.Z-mediated localization of genes at the nuclear periphery confers epigenetic memory of previous transcriptional state. *PLoS Biol.* 5:e81.
- Brohawn, S.G., N.C. Leksa, E.D. Spear, K.R. Rajashankar, and T.U. Schwartz. 2008. Structural evidence for common ancestry of the nuclear pore complex and vesicle coats. *Science.* 322:1369-1373.
- Brohawn, S.G., J.R. Partridge, J.R. Whittle, and T.U. Schwartz. 2009. The nuclear pore complex has entered the atomic age. *Structure.* 17:1156-1168.
- Brohawn, S.G., and T.U. Schwartz. 2009a. A lattice model of the nuclear pore complex. *Commun Integr Biol.* 2:205-207.

- Brohawn, S.G., and T.U. Schwartz. 2009b. Molecular architecture of the Nup84-Nup145C-Sec13 edge element in the nuclear pore complex lattice. *Nat Struct Mol Biol.* 16:1173-1177.
- Buendia, B., and J.C. Courvalin. 1997. Domain-specific disassembly and reassembly of nuclear membranes during mitosis. *Exp Cell Res.* 230:133-144.
- Burke, B., and J. Ellenberg. 2002. Remodelling the walls of the nucleus. *Nat Rev Mol Cell Biol.* 3:487-497.
- Burke, B., and C.L. Stewart. 2012. The nuclear lamins: flexibility in function. *Nat Rev Mol Cell Biol.* 14:13-24.
- Cai, M., Y. Huang, R. Ghirlando, K.L. Wilson, R. Craigie, and G.M. Clore. 2001. Solution structure of the constant region of nuclear envelope protein LAP2 reveals two LEM-domain structures: one binds BAF and the other binds DNA. *EMBO J.* 20:4399-4407.
- Callan, H.G., and S.G. Tomlin. 1950. Experimental studies on amphibian oocyte nuclei. I. Investigation of the structure of the nuclear membrane by means of the electron microscope. *Proc R Soc Lond B Biol Sci.* 137:367-378.
- Capelson, M., C. Doucet, and M.W. Hetzer. 2010. Nuclear pore complexes: guardians of the nuclear genome. *Cold Spring Harb Symp Quant Biol.* 75:585-597.
- Chadrin, A., B. Hess, M. San Roman, X. Gatti, B. Lombard, D. Loew, Y. Barral, B. Palancade, and V. Doye. 2010. Pom33, a novel transmembrane nucleoporin required for proper nuclear pore complex distribution. *J Cell Biol.* 189:795-811.
- Chaudhary, N., and J.C. Courvalin. 1993. Stepwise reassembly of the nuclear envelope at the end of mitosis. *J Cell Biol.* 122:295-306.
- Chaudhuri, I., J. Soding, and A.N. Lupas. 2008. Evolution of the beta-propeller fold. *Proteins.* 71:795-803.
- Chook, Y.M., and G. Blobel. 1999. Structure of the nuclear transport complex karyopherin-beta2-Ran x GppNHp. *Nature.* 399:230-237.
- Chook, Y.M., and K.E. Suel. 2011. Nuclear import by karyopherin-betas: recognition and inhibition. *Biochim Biophys Acta.* 1813:1593-1606.

- Cingolani, G., C. Petosa, K. Weis, and C.W. Muller. 1999. Structure of importin-beta bound to the IBB domain of importin-alpha. *Nature*. 399:221-229.
- Cingolani, G., J. Bednenko, M.T. Gillespie, and L. Gerace. 2002. Molecular basis for the recognition of a nonclassical nuclear localization signal by importin beta. *Molecular cell*. 10:1345-1353.
- Collaborative Computational Project, N. 1994. The CCP4 suite: programs for protein crystallography. *Acta Crystallogr D Biol Crystallogr*. 50:760-763.
- Cook, A., F. Bono, M. Jinek, and E. Conti. 2007. Structural biology of nucleocytoplasmic transport. *Annu Rev Biochem*. 76:647-671.
- Cook, A., E. Fernandez, D. Lindner, J. Ebert, G. Schlenstedt, and E. Conti. 2005. The structure of the nuclear export receptor Cse1 in its cytosolic state reveals a closed conformation incompatible with cargo binding. *Mol Cell*. 18:355-367.
- Cook, A.G., and E. Conti. 2010. Nuclear export complexes in the frame. *Curr Opin Struct Biol*. 20:247-252.
- Crisp, M., Q. Liu, K. Roux, J.B. Rattner, C. Shanahan, B. Burke, P.D. Stahl, and D. Hodzic. 2006. Coupling of the nucleus and cytoplasm: role of the LINC complex. *J Cell Biol*. 172:41-53.
- Cronshaw, J.M., A.N. Krutchinsky, W. Zhang, B.T. Chait, and M.J. Matunis. 2002. Proteomic analysis of the mammalian nuclear pore complex. *J Cell Biol*. 158:915-927.
- D'Angelo, M.A., J.S. Gomez-Cavazos, A. Mei, D.H. Lackner, and M.W. Hetzer. 2012. A change in nuclear pore complex composition regulates cell differentiation. *Dev Cell*. 22:446-458.
- Dacks, J.B., and M.C. Field. 2007. Evolution of the eukaryotic membrane-trafficking system: origin, tempo and mode. *J Cell Sci*. 120:2977-2985.
- Daigle, N., J. Beaudouin, L. Hartnell, G. Imreh, E. Hallberg, J. Lippincott-Schwartz, and J. Ellenberg. 2001. Nuclear pore complexes form immobile networks and have a very low turnover in live mammalian cells. *J Cell Biol*. 154:71-84.
- Daub, H., J.V. Olsen, M. Bairlein, F. Gnad, F.S. Oppermann, R. Korner, Z. Greff, G. Keri, O. Stemmann, and M. Mann. 2008. Kinase-selective enrichment enables quantitative phosphoproteomics of the kinome across the cell cycle. *Mol Cell*. 31:438-448.

- De Souza, C.P., and S.A. Osmani. 2009. Double duty for nuclear proteins--the price of more open forms of mitosis. *Trends Genet.* 25:545-554.
- Debler, E.W., Y. Ma, H.S. Seo, K.C. Hsia, T.R. Noriega, G. Blobel, and A. Hoelz. 2008. A fence-like coat for the nuclear pore membrane. *Mol Cell.* 32:815-826.
- DeGrasse, J.A., K.N. DuBois, D. Devos, T.N. Siegel, A. Sali, M.C. Field, M.P. Rout, and B.T. Chait. 2009. Evidence for a shared nuclear pore complex architecture that is conserved from the last common eukaryotic ancestor. *Mol Cell Proteomics.* 8:2119-2130.
- Dephoure, N., C. Zhou, J. Villen, S.A. Beausoleil, C.E. Bakalarski, S.J. Elledge, and S.P. Gygi. 2008. A quantitative atlas of mitotic phosphorylation. *Proc Natl Acad Sci U S A.* 105:10762-10767.
- Devos, D., S. Dokudovskaya, F. Alber, R. Williams, B.T. Chait, A. Sali, and M.P. Rout. 2004. Components of coated vesicles and nuclear pore complexes share a common molecular architecture. *PLoS Biol.* 2:e380.
- Devos, D., S. Dokudovskaya, R. Williams, F. Alber, N. Eswar, B.T. Chait, M.P. Rout, and A. Sali. 2006. Simple fold composition and modular architecture of the nuclear pore complex. *Proc Natl Acad Sci U S A.* 103:2172-2177.
- Doucet, C.M., and M.W. Hetzer. 2010. Nuclear pore biogenesis into an intact nuclear envelope. *Chromosoma.* 119:469-477.
- Doucet, C.M., J.A. Talamas, and M.W. Hetzer. 2010. Cell cycle-dependent differences in nuclear pore complex assembly in metazoa. *Cell.* 141:1030-1041.
- Doye, V., and E.C. Hurt. 1995. Genetic approaches to nuclear pore structure and function. *Trends Genet.* 11:235-241.
- Drin, G., J.F. Casella, R. Gautier, T. Boehmer, T.U. Schwartz, and B. Antonny. 2007. A general amphipathic alpha-helical motif for sensing membrane curvature. *Nat Struct Mol Biol.* 14:138-146.
- Drummond, S.P., S.A. Rutherford, H.S. Sanderson, and T.D. Allen. 2006. High resolution analysis of mammalian nuclear structure throughout the cell cycle: implications for nuclear pore complex assembly during interphase and mitosis. *Can J Physiol Pharmacol.* 84:423-430.
- Dultz, E., and J. Ellenberg. 2010. Live imaging of single nuclear pores reveals unique assembly kinetics and mechanism in interphase. *J Cell Biol.* 191:15-22.

- Dultz, E., S. Huet, and J. Ellenberg. 2009. Formation of the nuclear envelope permeability barrier studied by sequential photoswitching and flux analysis. *Biophys J.* 97:1891-1897.
- Dultz, E., E. Zanin, C. Wurzenberger, M. Braun, G. Rabut, L. Sironi, and J. Ellenberg. 2008. Systematic kinetic analysis of mitotic dis- and reassembly of the nuclear pore in living cells. *J Cell Biol.* 180:857-865.
- Dunker, A.K., C.J. Brown, J.D. Lawson, L.M. Iakoucheva, and Z. Obradovic. 2002. Intrinsic disorder and protein function. *Biochemistry.* 41:6573-6582.
- Dwyer, N., and G. Blobel. 1976. A modified procedure for the isolation of a pore complex-lamina fraction from rat liver nuclei. *J Cell Biol.* 70:581-591.
- Dyson, H.J., and P.E. Wright. 2005. Intrinsically unstructured proteins and their functions. *Nat Rev Mol Cell Biol.* 6:197-208.
- Emsley, P., B. Lohkamp, W.G. Scott, and K. Cowtan. 2010. Features and development of Coot. *Acta Crystallogr D Biol Crystallogr.* 66:486-501.
- Erickson, H.P. 2009. Size and shape of protein molecules at the nanometer level determined by sedimentation, gel filtration, and electron microscopy. *Biol Proced Online.* 11:32-51.
- Eriksson, C., C. Rustum, and E. Hallberg. 2004. Dynamic properties of nuclear pore complex proteins in gp210 deficient cells. *FEBS Lett.* 572:261-265.
- Erkman, J.A., E.J. Wagner, J. Dong, Y. Zhang, U. Kutay, and W.F. Marzluff. 2005. Nuclear import of the stem-loop binding protein and localization during the cell cycle. *Mol Biol Cell.* 16:2960-2971.
- Fath, S., J.D. Mancias, X. Bi, and J. Goldberg. 2007. Structure and organization of coat proteins in the COPII cage. *Cell.* 129:1325-1336.
- Favreau, C., H.J. Worman, R.W. Wozniak, T. Frappier, and J.C. Courvalin. 1996. Cell cycle-dependent phosphorylation of nucleoporins and nuclear pore membrane protein Gp210. *Biochemistry.* 35:8035-8044.
- Feldherr, C., D. Akin, T. Littlewood, and M. Stewart. 2002. The molecular mechanism of translocation through the nuclear pore complex is highly conserved. *J Cell Sci.* 115:2997-3005.
- Feldherr, C.M. 1998. Macromolecular exchanges between the nucleus and cytoplasm. *J Cell Biochem Suppl.* 30-31:214-219.

- Finlay, D.R., E. Meier, P. Bradley, J. Horecka, and D.J. Forbes. 1991. A complex of nuclear pore proteins required for pore function. *J Cell Biol.* 114:169-183.
- Flemming, D., P. Sarges, P. Stelter, A. Hellwig, B. Bottcher, and E. Hurt. 2009. Two structurally distinct domains of the nucleoporin Nup170 cooperate to tether a subset of nucleoporins to nuclear pores. *J Cell Biol.* 185:387-395.
- Fontoura, B.M., G. Blobel, and M.J. Matunis. 1999. A conserved biogenesis pathway for nucleoporins: proteolytic processing of a 186-kilodalton precursor generates Nup98 and the novel nucleoporin, Nup96. *J Cell Biol.* 144:1097-1112.
- Fontoura, B.M., S. Dales, G. Blobel, and H. Zhong. 2001. The nucleoporin Nup98 associates with the intranuclear filamentous protein network of TPR. *Proc Natl Acad Sci U S A.* 98:3208-3213.
- Forster, F., O. Medalia, N. Zauberman, W. Baumeister, and D. Fass. 2005. Retrovirus envelope protein complex structure in situ studied by cryo-electron tomography. *Proc Natl Acad Sci U S A.* 102:4729-4734.
- Franz, C., P. Askjaer, W. Antonin, C.L. Iglesias, U. Haselmann, M. Schelder, A. de Marco, M. Wilm, C. Antony, and I.W. Mattaj. 2005. Nup155 regulates nuclear envelope and nuclear pore complex formation in nematodes and vertebrates. *EMBO J.* 24:3519-3531.
- Franz, C., R. Walczak, S. Yavuz, R. Santarella, M. Gentzel, P. Askjaer, V. Galy, M. Hetzer, I.W. Mattaj, and W. Antonin. 2007. MEL-28/ELYS is required for the recruitment of nucleoporins to chromatin and postmitotic nuclear pore complex assembly. *EMBO Rep.* 8:165-172.
- Frenkiel-Krispin, D., B. Maco, U. Aebi, and O. Medalia. 2010. Structural analysis of a metazoan nuclear pore complex reveals a fused concentric ring architecture. *J Mol Biol.* 395:578-586.
- Fried, H., and U. Kutay. 2003. Nucleocytoplasmic transport: taking an inventory. *Cell Mol Life Sci.* 60:1659-1688.
- Funakoshi, T., M. Clever, A. Watanabe, and N. Imamoto. 2011. Localization of Pom121 to the inner nuclear membrane is required for an early step of interphase nuclear pore complex assembly. *Mol Biol Cell.* 22:1058-1069.
- Funakoshi, T., K. Maeshima, K. Yahata, S. Sugano, F. Imamoto, and N. Imamoto. 2007. Two distinct human POM121 genes: requirement for the formation of nuclear pore complexes. *FEBS Lett.* 581:4910-4916.

- Gall, J.G. 1967. Octagonal nuclear pores. *J Cell Biol.* 32:391-399.
- Galy, V., W. Antonin, A. Jaedicke, M. Sachse, R. Santarella, U. Haselmann, and I. Mattaj. 2008. A role for gp210 in mitotic nuclear-envelope breakdown. *J Cell Sci.* 121:317-328.
- Gerace, L., and G. Blobel. 1980. The nuclear envelope lamina is reversibly depolymerized during mitosis. *Cell.* 19:277-287.
- Gerace, L., Y. Ottaviano, and C. Kondor-Koch. 1982. Identification of a major polypeptide of the nuclear pore complex. *J Cell Biol.* 95:826-837.
- Gilchrist, D., B. Mykytka, and M. Rexach. 2002. Accelerating the rate of disassembly of karyopherin.cargo complexes. *The Journal of biological chemistry.* 277:18161-18172.
- Gillespie, P.J., G.A. Khoudoli, G. Stewart, J.R. Swedlow, and J.J. Blow. 2007. ELYS/MEL-28 chromatin association coordinates nuclear pore complex assembly and replication licensing. *Curr Biol.* 17:1657-1662.
- Glavy, J.S., A.N. Krutchinsky, I.M. Cristea, I.C. Berke, T. Boehmer, G. Blobel, and B.T. Chait. 2007. Cell-cycle-dependent phosphorylation of the nuclear pore Nup107-160 subcomplex. *Proc Natl Acad Sci U S A.* 104:3811-3816.
- Gomez-Cavazos, J.S., and M.W. Hetzer. 2012. Outfits for different occasions: tissue-specific roles of Nuclear Envelope proteins. *Curr Opin Cell Biol.* 24:775-783.
- Gorlich, D., N. Pante, U. Kutay, U. Aebi, and F.R. Bischoff. 1996. Identification of different roles for RanGDP and RanGTP in nuclear protein import. *EMBO J.* 15:5584-5594.
- Gorlich, D., P. Henklein, R.A. Laskey, and E. Hartmann. 1996B. A 41 amino acid motif in importin-alpha confers binding to importin-beta and hence transit into the nucleus. *The EMBO journal.* 15:1810-1817.
- Grandi, P., T. Dang, N. Pane, A. Shevchenko, M. Mann, D. Forbes, and E. Hurt. 1997. Nup93, a vertebrate homologue of yeast Nic96p, forms a complex with a novel 205-kDa protein and is required for correct nuclear pore assembly. *Mol Biol Cell.* 8:2017-2038.
- Grandi, P., V. Doye, and E.C. Hurt. 1993. Purification of NSP1 reveals complex formation with 'GLFG' nucleoporins and a novel nuclear pore protein NIC96. *EMBO J.* 12:3061-3071.

- Grandi, P., S. Emig, C. Weise, F. Hucho, T. Pohl, and E.C. Hurt. 1995a. A novel nuclear pore protein Nup82p which specifically binds to a fraction of Nsp1p. *J Cell Biol.* 130:1263-1273.
- Grandi, P., N. Schlaich, H. Tekotte, and E.C. Hurt. 1995b. Functional interaction of Nic96p with a core nucleoporin complex consisting of Nsp1p, Nup49p and a novel protein Nup57p. *EMBO J.* 14:76-87.
- Greber, U.F., A. Senior, and L. Gerace. 1990. A major glycoprotein of the nuclear pore complex is a membrane-spanning polypeptide with a large luminal domain and a small cytoplasmic tail. *EMBO J.* 9:1495-1502.
- Griffis, E.R., S. Xu, and M.A. Powers. 2003. Nup98 localizes to both nuclear and cytoplasmic sides of the nuclear pore and binds to two distinct nucleoporin subcomplexes. *Mol Biol Cell.* 14:600-610.
- Gross, J.D., N.J. Moerke, T. von der Haar, A.A. Lugovskoy, A.B. Sachs, J.E. McCarthy, and G. Wagner. 2003. Ribosome loading onto the mRNA cap is driven by conformational coupling between eIF4G and eIF4E. *Cell.* 115:739-750.
- Grossman, E., O. Medalia, and M. Zwerger. 2012. Functional architecture of the nuclear pore complex. *Annu Rev Biophys.* 41:557-584.
- Guan, T., S. Muller, G. Klier, N. Pante, J.M. Blevitt, M. Haner, B. Paschal, U. Aebi, and L. Gerace. 1995. Structural analysis of the p62 complex, an assembly of O-linked glycoproteins that localizes near the central gated channel of the nuclear pore complex. *Mol Biol Cell.* 6:1591-1603.
- Gurkan, C., A.V. Koulov, and W.E. Balch. 2007. An evolutionary perspective on eukaryotic membrane trafficking. *Adv Exp Med Biol.* 607:73-83.
- Guttinger, S., E. Laurell, and U. Kutay. 2009. Orchestrating nuclear envelope disassembly and reassembly during mitosis. *Nat Rev Mol Cell Biol.* 10:178-191.
- Guttler, T., and D. Gorlich. 2011. Ran-dependent nuclear export mediators: a structural perspective. *EMBO J.* 30:3457-3474.
- Hallberg, E., R.W. Wozniak, and G. Blobel. 1993. An integral membrane protein of the pore membrane domain of the nuclear envelope contains a nucleoporin-like region. *J Cell Biol.* 122:513-521.
- Handa, N., M. Kukimoto-Niino, R. Akasaka, S. Kishishita, K. Murayama, T. Terada, M. Inoue, T. Kigawa, S. Kose, N. Imamoto, A. Tanaka, Y. Hayashizaki, M. Shirouzu, and S. Yokoyama. 2006. The crystal

- structure of mouse Nup35 reveals atypical RNP motifs and novel homodimerization of the RRM domain. *J Mol Biol.* 363:114-124.
- Haque, F., D. Mazzeo, J.T. Patel, D.T. Smallwood, J.A. Ellis, C.M. Shanahan, and S. Shackleton. 2010. Mammalian SUN protein interaction networks at the inner nuclear membrane and their role in laminopathy disease processes. *J Biol Chem.* 285:3487-3498.
- Harel, A., A.V. Orjalo, T. Vincent, A. Lachish-Zalait, S. Vasu, S. Shah, E. Zimmerman, M. Elbaum, and D.J. Forbes. 2003. Removal of a single pore subcomplex results in vertebrate nuclei devoid of nuclear pores. *Mol Cell.* 11:853-864.
- Hawryluk-Gara, L.A., M. Platani, R. Santarella, R.W. Wozniak, and I.W. Mattaj. 2008. Nup53 is required for nuclear envelope and nuclear pore complex assembly. *Mol Biol Cell.* 19:1753-1762.
- Hawryluk-Gara, L.A., E.K. Shibuya, and R.W. Wozniak. 2005. Vertebrate Nup53 interacts with the nuclear lamina and is required for the assembly of a Nup93-containing complex. *Mol Biol Cell.* 16:2382-2394.
- Heald, R., and F. McKeon. 1990. Mutations of phosphorylation sites in lamin A that prevent nuclear lamina disassembly in mitosis. *Cell.* 61:579-589.
- Heath, I.B. 1980. Variant mitoses in lower eukaryotes: indicators of the evolution of mitosis. *Int Rev Cytol.* 64:1-80.
- Hetzer, M., H.H. Meyer, T.C. Walther, D. Bilbao-Cortes, G. Warren, and I.W. Mattaj. 2001. Distinct AAA-ATPase p97 complexes function in discrete steps of nuclear assembly. *Nat Cell Biol.* 3:1086-1091.
- Hetzer, M.W. 2010. The nuclear envelope. *Cold Spring Harb Perspect Biol.* 2:a000539.
- Hetzer, M.W., T.C. Walther, and I.W. Mattaj. 2005. Pushing the envelope: structure, function, and dynamics of the nuclear periphery. *Annu Rev Cell Dev Biol.* 21:347-380.
- Hetzer, M.W., and S.R. Wenthe. 2009. Border control at the nucleus: biogenesis and organization of the nuclear membrane and pore complexes. *Dev Cell.* 17:606-616.
- Hinshaw, J.E., B.O. Carragher, and R.A. Milligan. 1992. Architecture and design of the nuclear pore complex. *Cell.* 69:1133-1141.
- Hocevar, B.A., D.J. Burns, and A.P. Fields. 1993. Identification of protein kinase C (PKC) phosphorylation sites on human lamin B. Potential role

- of PKC in nuclear lamina structural dynamics. *J Biol Chem.* 268:7545-7552.
- Hoelz, A., E.W. Debler, and G. Blobel. 2011. The structure of the nuclear pore complex. *Annu Rev Biochem.* 80:613-643.
- Hsia, K.C., P. Stavropoulos, G. Blobel, and A. Hoelz. 2007. Architecture of a coat for the nuclear pore membrane. *Cell.* 131:1313-1326.
- Hu, T., T. Guan, and L. Gerace. 1996. Molecular and functional characterization of the p62 complex, an assembly of nuclear pore complex glycoproteins. *J Cell Biol.* 134:589-601.
- Hudson, A.M., and L. Cooley. 2008. Phylogenetic, structural and functional relationships between WD- and Kelch-repeat proteins. *Subcell Biochem.* 48:6-19.
- Iakoucheva, L.M., C.J. Brown, J.D. Lawson, Z. Obradovic, and A.K. Dunker. 2002. Intrinsic disorder in cell-signaling and cancer-associated proteins. *J Mol Biol.* 323:573-584.
- Imamoto, N., and T. Funakoshi. 2012. Nuclear pore dynamics during the cell cycle. *Curr Opin Cell Biol.* 24:453-459.
- Ishida, T., and K. Kinoshita. 2007. PrDOS: prediction of disordered protein regions from amino acid sequence. *Nucleic Acids Res.* 35:W460-464.
- Izaurrealde, E., U. Kutay, C. von Kobbe, I.W. Mattaj, and D. Gorlich. 1997. The asymmetric distribution of the constituents of the Ran system is essential for transport into and out of the nucleus. *EMBO J.* 16:6535-6547.
- Jarnik, M., and U. Aebi. 1991. Toward a more complete 3-D structure of the nuclear pore complex. *J Struct Biol.* 107:291-308.
- Jeady, S., and T.U. Schwartz. 2007. Crystal structure of nucleoporin Nic96 reveals a novel, intricate helical domain architecture. *J Biol Chem.* 282:34904-34912.
- Johnson, L.N., and D. Barford. 1993. The effects of phosphorylation on the structure and function of proteins. *Annu Rev Biophys Biomol Struct.* 22:199-232.
- Joseph, J., S.H. Tan, T.S. Karpova, J.G. McNally, and M. Dasso. 2002. SUMO-1 targets RanGAP1 to kinetochores and mitotic spindles. *J Cell Biol.* 156:595-602.

- Kampmann, M., C.E. Atkinson, A.L. Mattheyses, and S.M. Simon. 2011. Mapping the orientation of nuclear pore proteins in living cells with polarized fluorescence microscopy. *Nat Struct Mol Biol.* 18:643-649.
- Kampmann, M., and G. Blobel. 2009. Three-dimensional structure and flexibility of a membrane-coating module of the nuclear pore complex. *Nat Struct Mol Biol.* 16:782-788.
- King, M.C., C.P. Lusk, and G. Blobel. 2006. Karyopherin-mediated import of integral inner nuclear membrane proteins. *Nature.* 442:1003-1007.
- Kiseleva, E., T.D. Allen, S. Rutherford, M. Bucci, S.R. Wente, and M.W. Goldberg. 2004. Yeast nuclear pore complexes have a cytoplasmic ring and internal filaments. *J Struct Biol.* 145:272-288.
- Kondo, H., K. Uchiyama, and T. Okiyoneda. 2004. [p97-mediated membrane fusion is required for Golgi and ER assembly]. *Tanpakushitsu Kakusan Koso.* 49:916-919.
- Krull, S., J. Dorries, B. Boysen, S. Reidenbach, L. Magnius, H. Norder, J. Thyberg, and V.C. Cordes. 2010. Protein Tpr is required for establishing nuclear pore-associated zones of heterochromatin exclusion. *EMBO J.* 29:1659-1673.
- Laskowski RA, M.M., Moss DS, Thornton JM. 1993. PROCHECK: A program to check the stereochemical quality of protein structures. *J Appl Cryst.* 26:283-291.
- Lau, C.K., V.A. Delmar, and D.J. Forbes. 2006. Topology of yeast Ndc1p: predictions for the human NDC1/NET3 homologue. *Anat Rec A Discov Mol Cell Evol Biol.* 288:681-694.
- Laurell, E., K. Beck, K. Krupina, G. Theerthagiri, B. Bodenmiller, P. Horvath, R. Aebersold, W. Antonin, and U. Kutay. 2011. Phosphorylation of Nup98 by multiple kinases is crucial for NPC disassembly during mitotic entry. *Cell.* 144:539-550.
- Laurell, E., and U. Kutay. 2011. Dismantling the NPC permeability barrier at the onset of mitosis. *Cell Cycle.* 10:2243-2245.
- Lange, A., R.E. Mills, C.J. Lange, M. Stewart, S.E. Devine, and A.H. Corbett. 2007. Classical nuclear localization signals: definition, function, and interaction with importin alpha. *The Journal of biological chemistry.* 282:5101-5105.
- Lee, S.J., N. Imamoto, H. Sakai, A. Nakagawa, S. Kose, M. Koike, M. Yamamoto, T. Kumasaka, Y. Yoneda, and T. Tsukihara. 2000. The adoption of a

twisted structure of importin-beta is essential for the protein-protein interaction required for nuclear transport. *J Mol Biol.* 302:251-264.

- Lee, S.J., T. Sekimoto, E. Yamashita, E. Nagoshi, A. Nakagawa, N. Imamoto, M. Yoshimura, H. Sakai, K.T. Chong, T. Tsukihara, and Y. Yoneda. 2003. The structure of importin-beta bound to SREBP-2: nuclear import of a transcription factor. *Science.* 302:1571-1575.
- Lee, S.J., Y. Matsuura, S.M. Liu, and M. Stewart. 2005. Structural basis for nuclear import complex dissociation by RanGTP. *Nature.* 435:693-696.
- Leksa, N.C., S.G. Brohawn, and T.U. Schwartz. 2009. The structure of the scaffold nucleoporin Nup120 reveals a new and unexpected domain architecture. *Structure.* 17:1082-1091.
- Leksa, N.C., and T.U. Schwartz. 2010. Membrane-coating lattice scaffolds in the nuclear pore and vesicle coats: commonalities, differences, challenges. *Nucleus.* 1:314-318.
- Liang, Y., and M.W. Hetzer. 2011. Functional interactions between nucleoporins and chromatin. *Curr Opin Cell Biol.* 23:65-70.
- Liu, H.L., C.P. De Souza, A.H. Osmani, and S.A. Osmani. 2009. The three fungal transmembrane nuclear pore complex proteins of *Aspergillus nidulans* are dispensable in the presence of an intact An-Nup84-120 complex. *Mol Biol Cell.* 20:616-630.
- Liu, X., J.M. Mitchell, R.W. Wozniak, G. Blobel, and J. Fan. 2012. Structural evolution of the membrane-coating module of the nuclear pore complex. *Proc Natl Acad Sci U S A.* 109:16498-16503.
- Loiodice, I., A. Alves, G. Rabut, M. Van Overbeek, J. Ellenberg, J.B. Sibarita, and V. Doye. 2004. The entire Nup107-160 complex, including three new members, is targeted as one entity to kinetochores in mitosis. *Mol Biol Cell.* 15:3333-3344.
- Lopez-Garcia, P., and D. Moreira. 1999. Metabolic symbiosis at the origin of eukaryotes. *Trends Biochem Sci.* 24:88-93.
- Lu, L., M.S. Ladinsky, and T. Kirchhausen. 2009. Cisternal organization of the endoplasmic reticulum during mitosis. *Mol Biol Cell.* 20:3471-3480.
- Lu, L., M.S. Ladinsky, and T. Kirchhausen. 2011. Formation of the postmitotic nuclear envelope from extended ER cisternae precedes nuclear pore assembly. *J Cell Biol.* 194:425-440.

- Lutzmann, M., R. Kunze, A. Buerer, U. Aebi, and E. Hurt. 2002. Modular self-assembly of a Y-shaped multiprotein complex from seven nucleoporins. *EMBO J.* 21:387-397.
- Lutzmann, M., R. Kunze, K. Stangl, P. Stelter, K.F. Toth, B. Bottcher, and E. Hurt. 2005. Reconstitution of Nup157 and Nup145N into the Nup84 complex. *J Biol Chem.* 280:18442-18451.
- Macaulay, C., E. Meier, and D.J. Forbes. 1995. Differential mitotic phosphorylation of proteins of the nuclear pore complex. *J Biol Chem.* 270:254-262.
- Madrid, A.S., J. Mancuso, W.Z. Cande, and K. Weis. 2006. The role of the integral membrane nucleoporins Ndc1p and Pom152p in nuclear pore complex assembly and function. *J Cell Biol.* 173:361-371.
- Mahajan, R., C. Delphin, T. Guan, L. Gerace, and F. Melchior. 1997. A small ubiquitin-related polypeptide involved in targeting RanGAP1 to nuclear pore complex protein RanBP2. *Cell.* 88:97-107.
- Maimon, T., N. Elad, I. Dahan, and O. Medalia. 2012. The human nuclear pore complex as revealed by cryo-electron tomography. *Structure.* 20:998-1006.
- Maimon, T., and O. Medalia. 2010. Perspective on the metazoan nuclear pore complex. *Nucleus.* 1:383-386.
- Makhnevych, T., C.P. Lusk, A.M. Anderson, J.D. Aitchison, and R.W. Wozniak. 2003. Cell cycle regulated transport controlled by alterations in the nuclear pore complex. *Cell.* 115:813-823.
- Makio, T., L.H. Stanton, C.C. Lin, D.S. Goldfarb, K. Weis, and R.W. Wozniak. 2009. The nucleoporins Nup170p and Nup157p are essential for nuclear pore complex assembly. *J Cell Biol.* 185:459-473.
- Mans, B.J., V. Anantharaman, L. Aravind, and E.V. Koonin. 2004. Comparative genomics, evolution and origins of the nuclear envelope and nuclear pore complex. *Cell Cycle.* 3:1612-1637.
- Mansfeld, J., S. Guttinger, L.A. Hawryluk-Gara, N. Pante, M. Mall, V. Galy, U. Haselmann, P. Muhlhauser, R.W. Wozniak, I.W. Mattaj, U. Kutay, and W. Antonin. 2006. The conserved transmembrane nucleoporin NDC1 is required for nuclear pore complex assembly in vertebrate cells. *Mol Cell.* 22:93-103.

- Marelli, M., J.D. Aitchison, and R.W. Wozniak. 1998. Specific binding of the karyopherin Kap121p to a subunit of the nuclear pore complex containing Nup53p, Nup59p, and Nup170p. *J Cell Biol.* 143:1813-1830.
- Marelli, M., C.P. Lusk, H. Chan, J.D. Aitchison, and R.W. Wozniak. 2001. A link between the synthesis of nucleoporins and the biogenesis of the nuclear envelope. *J Cell Biol.* 153:709-724.
- Matsuura, Y., and M. Stewart. 2004. Structural basis for the assembly of a nuclear export complex. *Nature.* 432:872-877.
- Matunis, M.J., E. Coutavas, and G. Blobel. 1996. A novel ubiquitin-like modification modulates the partitioning of the Ran-GTPase-activating protein RanGAP1 between the cytosol and the nuclear pore complex. *J Cell Biol.* 135:1457-1470.
- Maul, G.G. 1971. On the octagonality of the nuclear pore complex. *J Cell Biol.* 51:558-563.
- Maul, G.G. 1977. The nuclear and the cytoplasmic pore complex: structure, dynamics, distribution, and evolution. *Int Rev Cytol Suppl:*75-186.
- Maul, G.G., H.M. Maul, J.E. Scogna, M.W. Lieberman, G.S. Stein, B.Y. Hsu, and T.W. Borun. 1972. Time sequence of nuclear pore formation in phytohemagglutinin-stimulated lymphocytes and in HeLa cells during the cell cycle. *J Cell Biol.* 55:433-447.
- Maul, G.G., J.W. Price, and M.W. Lieberman. 1971. Formation and distribution of nuclear pore complexes in interphase. *J Cell Biol.* 51:405-418.
- McGuffin, L.J., K. Bryson, and D.T. Jones. 2000. The PSIPRED protein structure prediction server. *Bioinformatics.* 16:404-405.
- Meinke, P., T.D. Nguyen, and M.S. Wehnert. 2011. The LINC complex and human disease. *Biochem Soc Trans.* 39:1693-1697.
- Mejat, A., and T. Misteli. 2010. LINC complexes in health and disease. *Nucleus.* 1:40-52.
- Melcak, I., A. Hoelz, and G. Blobel. 2007. Structure of Nup58/45 suggests flexible nuclear pore diameter by intermolecular sliding. *Science.* 315:1729-1732.
- Miller, B.R., and D.J. Forbes. 2000. Purification of the vertebrate nuclear pore complex by biochemical criteria. *Traffic.* 1:941-951.

- Mishra, R.K., P. Chakraborty, A. Arnaoutov, B.M. Fontoura, and M. Dasso. 2010. The Nup107-160 complex and gamma-TuRC regulate microtubule polymerization at kinetochores. *Nat Cell Biol.* 12:164-169.
- Mosammaparast, N., and L.F. Pemberton. 2004. Karyopherins: from nuclear-transport mediators to nuclear-function regulators. *Trends Cell Biol.* 14:547-556.
- Muhlhauser, P., and U. Kutay. 2007. An in vitro nuclear disassembly system reveals a role for the RanGTPase system and microtubule-dependent steps in nuclear envelope breakdown. *J Cell Biol.* 178:595-610.
- Nagy, V., K.C. Hsia, E.W. Debler, M. Kampmann, A.M. Davenport, G. Blobel, and A. Hoelz. 2009. Structure of a trimeric nucleoporin complex reveals alternate oligomerization states. *Proc Natl Acad Sci U S A.* 106:17693-17698.
- Namba, K. 2001. Roles of partly unfolded conformations in macromolecular self-assembly. *Genes Cells.* 6:1-12.
- Nemergut, M.E., C.A. Mizzen, T. Stukenberg, C.D. Allis, and I.G. Macara. 2001. Chromatin docking and exchange activity enhancement of RCC1 by histones H2A and H2B. *Science.* 292:1540-1543.
- Neumann, N., D. Lundin, and A.M. Poole. 2010. Comparative genomic evidence for a complete nuclear pore complex in the last eukaryotic common ancestor. *PLoS One.* 5:e13241.
- Nigg, E.A. 1992. Assembly and cell cycle dynamics of the nuclear lamina. *Semin Cell Biol.* 3:245-253.
- Nousiainen, M., H.H. Sillje, G. Sauer, E.A. Nigg, and R. Korner. 2006. Phosphoproteome analysis of the human mitotic spindle. *Proc Natl Acad Sci U S A.* 103:5391-5396.
- Ohtsubo, M., H. Okazaki, and T. Nishimoto. 1989. The RCC1 protein, a regulator for the onset of chromosome condensation locates in the nucleus and binds to DNA. *J Cell Biol.* 109:1389-1397.
- Oldfield, C.J., E.L. Ulrich, Y. Cheng, A.K. Dunker, and J.L. Markley. 2005. Addressing the intrinsic disorder bottleneck in structural proteomics. *Proteins.* 59:444-453.
- Olsen, J.V., M. Vermeulen, A. Santamaria, C. Kumar, M.L. Miller, L.J. Jensen, F. Gnad, J. Cox, T.S. Jensen, E.A. Nigg, S. Brunak, and M. Mann. 2010.

Quantitative phosphoproteomics reveals widespread full phosphorylation site occupancy during mitosis. *Sci Signal.* 3:ra3.

- Olsson, M., M. Ekblom, L. Fecker, M. Kurkinen, and P. Ekblom. 1999. cDNA cloning and embryonic expression of mouse nuclear pore membrane glycoprotein 210 mRNA. *Kidney Int.* 56:827-838.
- Olsson, M., S. Scheele, and P. Ekblom. 2004. Limited expression of nuclear pore membrane glycoprotein 210 in cell lines and tissues suggests cell-type specific nuclear pores in metazoans. *Exp Cell Res.* 292:359-370.
- Onischenko, E., L.H. Stanton, A.S. Madrid, T. Kieselbach, and K. Weis. 2009. Role of the Ndc1 interaction network in yeast nuclear pore complex assembly and maintenance. *J Cell Biol.* 185:475-491.
- Onischenko, E., and K. Weis. 2011. Nuclear pore complex-a coat specifically tailored for the nuclear envelope. *Curr Opin Cell Biol.* 23:293-301.
- Orjalo, A.V., A. Arnaoutov, Z. Shen, Y. Boyarchuk, S.G. Zeitlin, B. Fontoura, S. Briggs, M. Dasso, and D.J. Forbes. 2006. The Nup107-160 nucleoporin complex is required for correct bipolar spindle assembly. *Mol Biol Cell.* 17:3806-3818.
- Otwinowski Z, M.W. 1997. Processing of X-ray diffraction data collected in oscillation mode. *Methods in Enzymology.* 276:307-326.
- Partridge, J.R., and T.U. Schwartz. 2009. Crystallographic and biochemical analysis of the Ran-binding zinc finger domain. *J Mol Biol.* 391:375-389.
- Pucadyil, T.J., and S.L. Schmid. 2009. Conserved functions of membrane active GTPases in coated vesicle formation. *Science.* 325:1217-1220.
- Rabut, G., V. Doye, and J. Ellenberg. 2004. Mapping the dynamic organization of the nuclear pore complex inside single living cells. *Nat Cell Biol.* 6:1114-1121.
- Radu, A., G. Blobel, and R.W. Wozniak. 1993. Nup155 is a novel nuclear pore complex protein that contains neither repetitive sequence motifs nor reacts with WGA. *J Cell Biol.* 121:1-9.
- Rasala, B.A., A.V. Orjalo, Z. Shen, S. Briggs, and D.J. Forbes. 2006. ELYS is a dual nucleoporin/kinetochore protein required for nuclear pore assembly and proper cell division. *Proc Natl Acad Sci U S A.* 103:17801-17806.

- Rasala, B.A., C. Ramos, A. Harel, and D.J. Forbes. 2008. Capture of AT-rich chromatin by ELYS recruits POM121 and NDC1 to initiate nuclear pore assembly. *Mol Biol Cell*. 19:3982-3996.
- Reichelt, R., A. Holzenburg, E.L. Buhle, Jr., M. Jarnik, A. Engel, and U. Aebi. 1990. Correlation between structure and mass distribution of the nuclear pore complex and of distinct pore complex components. *J Cell Biol*. 110:883-894.
- Rexach, M. 2009. Piecing together nuclear pore complex assembly during interphase. *J Cell Biol*. 185:377-379.
- Rexach, M., and G. Blobel. 1995. Protein import into nuclei: association and dissociation reactions involving transport substrate, transport factors, and nucleoporins. *Cell*. 83:683-692.
- Ribbeck, K., and D. Gorlich. 2001. Kinetic analysis of translocation through nuclear pore complexes. *EMBO J*. 20:1320-1330.
- Ribbeck, K., G. Lipowsky, H.M. Kent, M. Stewart, and D. Gorlich. 1998. NTF2 mediates nuclear import of Ran. *EMBO J*. 17:6587-6598.
- Rigbolt, K.T., T.A. Prokhorova, V. Akimov, J. Henningsen, P.T. Johansen, I. Kratchmarova, M. Kassem, M. Mann, J.V. Olsen, and B. Blagoev. 2011. System-wide temporal characterization of the proteome and phosphoproteome of human embryonic stem cell differentiation. *Sci Signal*. 4:rs3.
- Rotem, A., R. Gruber, H. Shorer, L. Shaulov, E. Klein, and A. Harel. 2009. Importin beta regulates the seeding of chromatin with initiation sites for nuclear pore assembly. *Mol Biol Cell*. 20:4031-4042.
- Rothballer, A., and U. Kutay. 2012a. SnapShot: The nuclear envelope I. *Cell*. 150:868-868 e861.
- Rothballer, A., and U. Kutay. 2012b. SnapShot: the nuclear envelope II. *Cell*. 150:1084-1084 e1081.
- Rothballer, A., T.U. Schwartz, and U. Kutay. 2013. LINCing complex functions at the nuclear envelope: What the molecular architecture of the LINC complex can reveal about its function. *Nucleus*. 4:29-36.
- Rout, M.P., J.D. Aitchison, A. Suprapto, K. Hjertaas, Y. Zhao, and B.T. Chait. 2000. The yeast nuclear pore complex: composition, architecture, and transport mechanism. *J Cell Biol*. 148:635-651.

- Rout, M.P., and G. Blobel. 1993. Isolation of the yeast nuclear pore complex. *J Cell Biol.* 123:771-783.
- Saitoh, H., R. Pu, M. Cavenagh, and M. Dasso. 1997. RanBP2 associates with Ubc9p and a modified form of RanGAP1. *Proc Natl Acad Sci U S A.* 94:3736-3741.
- Salina, D., K. Bodoor, D.M. Eckley, T.A. Schroer, J.B. Rattner, and B. Burke. 2002. Cytoplasmic dynein as a facilitator of nuclear envelope breakdown. *Cell.* 108:97-107.
- Schirmer, E.C., L. Florens, T. Guan, J.R. Yates, 3rd, and L. Gerace. 2003. Nuclear membrane proteins with potential disease links found by subtractive proteomics. *Science.* 301:1380-1382.
- Schirmer, E.C., and L. Gerace. 2005. The nuclear membrane proteome: extending the envelope. *Trends Biochem Sci.* 30:551-558.
- Schooley, A., B. Vollmer, and W. Antonin. 2012. Building a nuclear envelope at the end of mitosis: coordinating membrane reorganization, nuclear pore complex assembly, and chromatin de-condensation. *Chromosoma.*
- Schrader, N., P. Stelter, D. Flemming, R. Kunze, E. Hurt, and I.R. Vetter. 2008. Structural basis of the nic96 subcomplex organization in the nuclear pore channel. *Mol Cell.* 29:46-55.
- Schwartz, T.U. 2005. Modularity within the architecture of the nuclear pore complex. *Curr Opin Struct Biol.* 15:221-226.
- Seo, H.S., Y. Ma, E.W. Debler, D. Wacker, S. Kutik, G. Blobel, and A. Hoelz. 2009. Structural and functional analysis of Nup120 suggests ring formation of the Nup84 complex. *Proc Natl Acad Sci U S A.* 106:14281-14286.
- Shaulov, L., R. Gruber, I. Cohen, and A. Harel. 2011. A dominant-negative form of POM121 binds chromatin and disrupts the two separate modes of nuclear pore assembly. *J Cell Sci.* 124:3822-3834.
- Sheehan, M.A., A.D. Mills, A.M. Sleeman, R.A. Laskey, and J.J. Blow. 1988. Steps in the assembly of replication-competent nuclei in a cell-free system from *Xenopus* eggs. *J Cell Biol.* 106:1-12.
- Siniosoglou, S., M. Lutzmann, H. Santos-Rosa, K. Leonard, S. Mueller, U. Aebi, and E. Hurt. 2000. Structure and assembly of the Nup84p complex. *J Cell Biol.* 149:41-54.

- Siniooglou, S., C. Wimmer, M. Rieger, V. Doye, H. Tekotte, C. Weise, S. Emig, A. Segref, and E.C. Hurt. 1996. A novel complex of nucleoporins, which includes Sec13p and a Sec13p homolog, is essential for normal nuclear pores. *Cell*. 84:265-275.
- Smith, A., A. Brownawell, and I.G. Macara. 1998. Nuclear import of Ran is mediated by the transport factor NTF2. *Curr Biol*. 8:1403-1406.
- Soderqvist, H., and E. Hallberg. 1994. The large C-terminal region of the integral pore membrane protein, POM121, is facing the nuclear pore complex. *Eur J Cell Biol*. 64:186-191.
- Solmaz, S.R., G. Blobel, and I. Melcak. 2013. Ring cycle for dilating and constricting the nuclear pore. *Proc Natl Acad Sci U S A*.
- Solmaz, S.R., R. Chauhan, G. Blobel, and I. Melcak. 2011. Molecular architecture of the transport channel of the nuclear pore complex. *Cell*. 147:590-602.
- Stagg, S.M., P. LaPointe, and W.E. Balch. 2007. Structural design of cage and coat scaffolds that direct membrane traffic. *Curr Opin Struct Biol*. 17:221-228.
- Stavru, F., B.B. Hulsmann, A. Spang, E. Hartmann, V.C. Cordes, and D. Gorlich. 2006a. NDC1: a crucial membrane-integral nucleoporin of metazoan nuclear pore complexes. *J Cell Biol*. 173:509-519.
- Stavru, F., G. Nautrup-Pedersen, V.C. Cordes, and D. Gorlich. 2006b. Nuclear pore complex assembly and maintenance in POM121- and gp210-deficient cells. *J Cell Biol*. 173:477-483.
- Stewart, M. 2007. Molecular mechanism of the nuclear protein import cycle. *Nat Rev Mol Cell Biol*. 8:195-208.
- Stoffler, D., B. Feja, B. Fahrenkrog, J. Walz, D. Typke, and U. Aebi. 2003. Cryo-electron tomography provides novel insights into nuclear pore architecture: implications for nucleocytoplasmic transport. *J Mol Biol*. 328:119-130.
- Strambio-De-Castillia, C., M. Niepel, and M.P. Rout. 2010. The nuclear pore complex: bridging nuclear transport and gene regulation. *Nat Rev Mol Cell Biol*. 11:490-501.
- Strawn, L.A., T. Shen, N. Shulga, D.S. Goldfarb, and S.R. Wentz. 2004. Minimal nuclear pore complexes define FG repeat domains essential for transport. *Nat Cell Biol*. 6:197-206.

- Strom, A.C., and K. Weis. 2001. Importin-beta-like nuclear transport receptors. *Genome Biol.* 2:REVIEWS3008.
- Stuwe, T., L.S. von Borzyskowski, A.M. Davenport, and A. Hoelz. 2012. Molecular basis for the anchoring of proto-oncoprotein Nup98 to the cytoplasmic face of the nuclear pore complex. *J Mol Biol.* 419:330-346.
- Suntharalingam, M., and S.R. Wentz. 2003. Peering through the pore: nuclear pore complex structure, assembly, and function. *Dev Cell.* 4:775-789.
- Talamas, J.A., and M.W. Hetzer. 2011. POM121 and Sun1 play a role in early steps of interphase NPC assembly. *J Cell Biol.* 194:27-37.
- Tcheperegine, S.E., M. Marelli, and R.W. Wozniak. 1999. Topology and functional domains of the yeast pore membrane protein Pom152p. *J Biol Chem.* 274:5252-5258.
- Tetenbaum-Novatt, J., and M.P. Rout. 2010. The mechanism of nucleocytoplasmic transport through the nuclear pore complex. *Cold Spring Harb Symp Quant Biol.* 75:567-584.
- Theerthagiri, G., N. Eisenhardt, H. Schwarz, and W. Antonin. 2010. The nucleoporin Nup188 controls passage of membrane proteins across the nuclear pore complex. *J Cell Biol.* 189:1129-1142.
- Therizols, P., C. Fairhead, G.G. Cabal, A. Genovesio, J.C. Olivo-Marin, B. Dujon, and E. Fabre. 2006. Telomere tethering at the nuclear periphery is essential for efficient DNA double strand break repair in subtelomeric region. *J Cell Biol.* 172:189-199.
- Timney, B.L., J. Tetenbaum-Novatt, D.S. Agate, R. Williams, W. Zhang, B.T. Chait, and M.P. Rout. 2006. Simple kinetic relationships and nonspecific competition govern nuclear import rates in vivo. *The Journal of cell biology.* 175:579-593.
- Tran, E.J., and S.R. Wentz. 2006. Dynamic nuclear pore complexes: life on the edge. *Cell.* 125:1041-1053.
- Ulbert, S., W. Antonin, M. Platani, and I.W. Mattaj. 2006a. The inner nuclear membrane protein Lem2 is critical for normal nuclear envelope morphology. *FEBS Lett.* 580:6435-6441.
- Ulbert, S., M. Platani, S. Boue, and I.W. Mattaj. 2006b. Direct membrane protein-DNA interactions required early in nuclear envelope assembly. *J Cell Biol.* 173:469-476.

- Unwin, P.N., and R.A. Milligan. 1982. A large particle associated with the perimeter of the nuclear pore complex. *J Cell Biol.* 93:63-75.
- Uversky, V.N. 2002. Natively unfolded proteins: a point where biology waits for physics. *Protein Sci.* 11:739-756.
- Uversky, V.N. 2011. Intrinsically disordered proteins from A to Z. *Int J Biochem Cell Biol.* 43:1090-1103.
- Van de Vosse, D.W., Y. Wan, R.W. Wozniak, and J.D. Aitchison. 2011. Role of the nuclear envelope in genome organization and gene expression. *Wiley Interdiscip Rev Syst Biol Med.* 3:147-166.
- van der Voorn, L., and H.L. Ploegh. 1992. The WD-40 repeat. *FEBS Lett.* 307:131-134.
- Vasu, S., S. Shah, A. Orjalo, M. Park, W.H. Fischer, and D.J. Forbes. 2001. Novel vertebrate nucleoporins Nup133 and Nup160 play a role in mRNA export. *J Cell Biol.* 155:339-354.
- Vollmer, B., A. Schooley, R. Sachdev, N. Eisenhardt, A.M. Schneider, C. Sieverding, J. Madlung, U. Gerken, B. Macek, and W. Antonin. 2012. Dimerization and direct membrane interaction of Nup53 contribute to nuclear pore complex assembly. *EMBO J.* 31:4072-4084.
- Walde, S., and R.H. Kehlenbach. 2010. The Part and the Whole: functions of nucleoporins in nucleocytoplasmic transport. *Trends Cell Biol.* 20:461-469.
- Walther, T.C., A. Alves, H. Pickersgill, I. Loiodice, M. Hetzer, V. Galy, B.B. Hulsmann, T. Kocher, M. Wilm, T. Allen, I.W. Mattaj, and V. Doye. 2003. The conserved Nup107-160 complex is critical for nuclear pore complex assembly. *Cell.* 113:195-206.
- Weis, K. 2007. The nuclear pore complex: oily spaghetti or gummy bear? *Cell.* 130:405-407.
- Wente, S.R., and M.P. Rout. 2010. The nuclear pore complex and nuclear transport. *Cold Spring Harb Perspect Biol.* 2:a000562.
- Whittle, J.R., and T.U. Schwartz. 2009. Architectural nucleoporins Nup157/170 and Nup133 are structurally related and descend from a second ancestral element. *J Biol Chem.* 284:28442-28452.
- Whittle, J.R., and T.U. Schwartz. 2010. Structure of the Sec13-Sec16 edge element, a template for assembly of the COPII vesicle coat. *J Cell Biol.* 190:347-361.

- Winey, M., D. Yarar, T.H. Giddings, Jr., and D.N. Mastronarde. 1997. Nuclear pore complex number and distribution throughout the *Saccharomyces cerevisiae* cell cycle by three-dimensional reconstruction from electron micrographs of nuclear envelopes. *Mol Biol Cell*. 8:2119-2132.
- Wool, I.G., Y.L. Chan, and A. Gluck. 1995. Structure and evolution of mammalian ribosomal proteins. *Biochem Cell Biol*. 73:933-947.
- Worman, H.J., and J.C. Courvalin. 2000. The inner nuclear membrane. *J Membr Biol*. 177:1-11.
- Wozniak, R., B. Burke, and V. Doye. 2010. Nuclear transport and the mitotic apparatus: an evolving relationship. *Cell Mol Life Sci*. 67:2215-2230.
- Wozniak, R.W., E. Bartnik, and G. Blobel. 1989. Primary structure analysis of an integral membrane glycoprotein of the nuclear pore. *J Cell Biol*. 108:2083-2092.
- Wozniak, R.W., G. Blobel, and M.P. Rout. 1994. POM152 is an integral protein of the pore membrane domain of the yeast nuclear envelope. *J Cell Biol*. 125:31-42.
- Wright, P.E., and H.J. Dyson. 1999. Intrinsically unstructured proteins: re-assessing the protein structure-function paradigm. *J Mol Biol*. 293:321-331.
- Yahav, T., T. Maimon, E. Grossman, I. Dahan, and O. Medalia. 2011. Cryo-electron tomography: gaining insight into cellular processes by structural approaches. *Curr Opin Struct Biol*. 21:670-677.
- Yang, L., T. Guan, and L. Gerace. 1997. Integral membrane proteins of the nuclear envelope are dispersed throughout the endoplasmic reticulum during mitosis. *J Cell Biol*. 137:1199-1210.
- Yang, Q., M.P. Rout, and C.W. Akey. 1998. Three-dimensional architecture of the isolated yeast nuclear pore complex: functional and evolutionary implications. *Mol Cell*. 1:223-234.
- Yavuz, S., R. Santarella-Mellwig, B. Koch, A. Jaedicke, I.W. Mattaj, and W. Antonin. 2010. NLS-mediated NPC functions of the nucleoporin Pom121. *FEBS letters*. 584:3292-3298.
- Zeitler, B., and K. Weis. 2004. The FG-repeat asymmetry of the nuclear pore complex is dispensable for bulk nucleocytoplasmic transport in vivo. *J Cell Biol*. 167:583-590.

Zuleger, N., M.I. Robson, and E.C. Schirmer. 2011. The nuclear envelope as a chromatin organizer. *Nucleus*. 2:339-349.